POLYTECHNIQUE MONTRÉAL

affiliée à l'Université de Montréal

Synthesis and Characterization of Nanothermites for Energetic Applications

AHMED EMAM

Département de génie chimique

Thèse présentée en vue de l'obtention du diplôme de *Philosophiæ Doctor*

Génie chimique

Septembre 2021

© Ahmed Emam, 2021.

POLYTECHNIQUE MONTRÉAL

affiliée à l'Université de Montréal

Cette thèse intitulée :

Synthesis and Characterization of Nanothermites for Energetic Applications

présentée par **Ahmed EMAM**

en vue de l'obtention du diplôme de *Philosophiæ Doctor*

a été dûment acceptée par le jury d'examen constitué de :

Gregory PATIENCE, président
Charles DUBOIS, membre et directeur de recherche
Jamal CHAOUKI, membre et codirecteur de recherche
John WEN, membre et codirecteur de recherche
Jean-Philippe HARVEY, membre
Fiona KELLY, membre externe

DEDICATION

To God, my beloved parents, sisters and my beloved wife and beautiful son,

ACKNOWLEDGEMENTS

This work would never have been completed without the support of several people, to whom I wish to express my sincere gratitude for all the help they gave me during the last three years.

Professor Charles Dubois, thank you for your guidance, helpful suggestions, encouragement, and for the trust you have placed in me throughout this project. Also, I am deeply grateful for all valuable comments on this thesis.

Prof. Jamal Chaouki, my co-supervisor: thank you for supporting this project, and for all the efforts for improving the quality of the papers.

I would like to thank Dr. John Wen, my co-supervisor for his help in carrying out the characterization analysis at Laboratory for Emerging Energy Research (LEER) at Waterloo University, as well as his important and relevant comments on the articles.

Besides my supervisors, I would like to thank the rest of my thesis committee, namely Professor Gregory Patience, Professor Fiona Kelly and Professor Jean Philippe Harvey for accepting to evaluate my thesis.

I also thank the invaluable financial support from The Egyptian Ministry of Defense.

Several members of the chemical engineering department of Polytechnique offered technical assistance for this work, including Mr. Matthieu Gauthier, Mr. Robert Delisle, Ms. Martine Lamarche, Ms. Claire Cerclé, and Mr. Gino Robin. My sincere thanks to all.

I would also like to thank important friends that were beside me during the development of this work: Dr. Amr Elnady, Dr. Hatem Belal, Ramy Sadek, Dr. Ragee Rateb, Dr. Sherief Elbasuiney, Moustafa Ossman, Mahmoud Youssry, Dr. Hesham Tantawy and Dr. Ehab Youssef.

I also wish to thank Mr. Alex Baranovsky for laser ignition measurements, Mr. Matthieu Gauthier for his assistance with the morphological characterizations.

A special thanks to my family: father, mother and my sisters, for their love and encouragement, as well as for the invaluable support during this endeavour. My lovely wife and my son, Fahd, thank you for your love and support. Dad and mother love you.

RÉSUMÉ

Une grande attention a été accordée au développement de nouveaux matériaux énergétiques pour atteindre les performances de plus en plus exigeantes des systèmes de propulsion à grande vitesse. La nanothermite est l'une des principales approches pour le développement de nouveaux matériaux énergétiques en intégrant intentionnellement des combustibles et oxydants métalliques nanométriques. Par rapport aux poudres de thermite traditionnelles à l'échelle du micron, les nanothermites offrent des améliorations de la vitesse de réaction, du dégagement de chaleur, de la pression et de la puissance de poussée en tirant parti: d'une grande surface spécifique, d'une diminution de l'énergie d'activation, d'une libération d'énergie rapide et d'une densité d'énergie élevée. Malgré leurs avantages par rapport aux microthermites, les nanothermites souffrent toujours d'une couche d'oxyde plus épaisse, de retards d'allumage relativement longs, d'une cinétique de combustion lente, d'un frittage des nano-réactifs avant l'allumage et d'une combustion incomplète, qui ont limité leur applicabilité.

Les travaux de recherche actuels sont consacrés à la synthèse et à la caractérisation des nanothermites en tant que matériaux énergétiques. On vise à obttenir des caractéristiques de combustion améliorées pour des applications énergétiques, tel des micropropulseurs et des propulsifs solides modifiés. Le projet de recherche s'est déroulé en quatre phases. La première phase traite de l'évaluation approfondie de l'impact potentiel de différents nanomatériaux de carbone (oxyde de graphène, oxyde de graphène réduit, nanotubes de carbone et nanofibres de carbone) sur les caractéristiques de combustion des nanothermites. Les nanothermites furent préparée avec des oxydants à base d’oxygène comme réactif alternative aux oxydants métalliques, représentée par le perchlorate de potassium et la poudre de nano aluminium.

La seconde phase a consisté en l'étude comparative entre différentes nanothermites tertiaires de sels métalliques et oxygéné (oxydants oxygénés) pour identifier l'impact potentiel de chaque oxydant sur les performances de la nanothermite. En bref, cette partie du travail visait à comparer et analyser le comportement thermique de différentes compositions tertiaires de nanothermite pour identifier le mécanisme de réaction et l’énergie d’activation à partir d’analyse calorimétrique différentielle. De plus, il était aussi souhaité de préciser soigneusement le rôle de chaque composite de nanothermite et son application possible (chaleur ou poussée).

La troisième phase portait sur des mélanges de nanothermites avec une combustion contrôlable et des paramètres de performance adaptés pour les applications de propulsion à petite échelle. Précisément, j'ai développé des nanothermites quaternaires à base de n-Al, de perchlorate de potassium, d'oxyde de graphène et de quantités variables de nitrocellulose (NC) en utilisant une technique d'électrofilage simple.

Enfin, dans la quatrième phase, j'ai présenté de nouvelles thermites énergétiques vertes avec des températures d'allumage basses, une puissance de poussée stable et une bonne réactivité. Ces thermites sont basés sur le [Cu4Na (Mtta) 5 (CH3CN)] n (Mtta = 5-méthyl-1H-tétrazole) armature métal-organique énergétique (EMOF-1) comme combustible en remplacement de l'aluminium, et de divers types de oxydants oxygénés.

Les nanothermites à l'exception de celles avec NC ont été préparées par sonication conventionnelle comme une voie rapide et directe. MOF-1 a été synthétisé via la technique assistée par micro-ondes comme une technique plus rapide, économe en énergie et plus verte. Une caractérisation cohérente des nanothermites s'est produite dans deux directions nécessaires. Tout d'abord, les techniques de microscopie représentées par SEM couplé à EDX ont effectué des caractérisations morphologiques et chimiques pour les mélanges de nanothermites. La spectroscopie de diffraction des rayons X a évalué de manière adéquate la structure cristalline des nanoparticules de combustible et d'oxydant. La spectroscopie infrarouge à transformée de Fourier (FTIR) a été réalisée pour confirmer qu'il n'y avait pas de réaction entre les réactifs de la nanothermite pendant le processus de préparation. La spectromètrie Raman a confirmé spécifiquement la préparation réussie de graphène et d'oxyde de graphène réduit. D'autre part, l'analyse thermogravimétrique, la calorimétrie différentielle à balayage et la bombe calorimétrique ont évalué la réactivité et le comportement thermique des nanothermites en termes de température d'allumage, de température de décomposition de l'oxydant, de chaleur de combustion et d'identifier leurs mécanismes de réaction. Les approches de Kissinger et Ozawa ont calculé les paramètres cinétiques apparents (énergie d'activation et facteur de fréquence) pour les nanothermites préparées. Le comportement de combustion des composites a été évalué en allumant les échantillons à différentes densités de chargement dans des tubes acryliques ouverts à l'aide d'un laser à onde continue de 3,5 W et une imagerie à haute vitesse a capturé la propagation de la flamme. Enfin, pour les applications de propulsion, un moteur d'essai à petite échelle (STM)

avec une buse convergente / divergente a évalué les performances de poussée des échantillons préparés.

Les résultats ont démontré que l'ajout de nanomatériaux de carbone et en particulier d'oxyde de graphène augmentait la chaleur dégagée et diminuait à la fois la température d'inflammation et l'énergie d'activation. En effet, seulement un ajout de 5% d'oxyde de graphène a augmenté la chaleur de combustion de 3553 ± 209 à 9614 ± 418, réduit la température d'inflammation et l'énergie d'activation de 545,1 à 508,7 ° C et de 145 à 135 kJ / mol respectivement. En général, les nanothermites à base de sels oxygéné sont plus réactives que celles contenant des oxydes métalliques et une réaction de diffusion gaz-solide est le mécanisme de réaction dominant et dominant. En outre, le comportement de combustion des nanothermites avec des nanomatériaux de carbone a révélé deux régimes de réaction distincts (lent et rapide) à des densités de remplissage faibles et élevées (20 et 50% de TMD). Les impulsions totales et spécifiques (IFT et ISP) ont atteint un pic à 5% GO / Al / KClO4 pour les régimes de réaction lents et rapides. Précisément, IFT et ISP ont enregistré respectivement 10,1 mN.s et 147,2 s à ~ 50% TMD et ce sont des améliorations de plus de 95% par rapport à l'échantillon de référence sans GO (6,6 mN.s et 96,2 s). En outre, l'ajout de NC à la nanothermite tertiaire GO / Al / KClO4 a introduit une autre étape dans la réaction de décomposition de la thermite pour être une réaction de diffusion en phase gaz-solide et en phase liquide-liquide et la dernière étape (phase liquide-liquide) a augmenté avec l'augmentation du pourcentage de NC . Cependant, le temps de retard à l'allumage et la puissance nécessaire pour allumer le mélange enrichi en NC ont augmenté et améliorent ainsi la sécurité des échantillons, tout en maintenant une réponse suffisamment rapide pour des applications pratiques. IFT et ISP ont culminé avec l'ajout de 5% de nitrocellulose à ~ 50% de TMD, avec IFT de 19,9 mN.s et ISP de 203,2 s. Il s'agit d'améliorations de plus de 50% par rapport à l'échantillon de référence sans NC (13,4 mN.s & 137,4 s). Les nouveaux mélanges de thermite à base d'EMOF-1 ont présenté des caractéristiques de combustion supérieures de deux à trois fois la chaleur de combustion moyenne par rapport aux mélanges à base d'aluminium, à près de la moitié de la température d'allumage. Parmi eux, la thermite EMOF-1 / KIO4 a affiché le dégagement de chaleur le plus élevé (5,1 kJ / g), tandis que la thermite EMOF-1 / NH4NO3 affiche la température de début la plus basse (259 ^{o}C) suivie de EMOF-1 / KIO4 avec (314 ^{o}C). En outre, les thermites à base d'EMOF-1 ont obtenu un temps de combustion plus long et une

poussée moyenne stable qui facilitent la production d'une force de propulsion soutenue contrairement aux thermites à base d'aluminium comme carburant. Compte tenu de la remarquable diversité des performances de combustion observées pour les nanothermites préparés, ce travail est d'une grande importance au regard des nombreuses applications énergétiques possibles, comme dans les micropropulseurs, les propulseurs avancés et les explosifs primaires verts.

ABSTRACT

Development of new energetic materials has captured much interest to as demands increase for microscale energetic devices and miniature propulsion systems. Nanothermite is one of the main approaches in the development of new energetic materials by intentionally integrating nanoscale metallic fuels and oxidisers. They are leveraging their large specific surface area, reduced activation energy, fast energy release and high energy density in enhancing the reaction rate, heat release, pressure and thrust output. Despite their advantages over microthermites, nanothermites still suffer from proportionally thicker oxide layer shell, relatively long ignition delays, slow combustion kinetics, sintering of nano-reactants before ignition, and incomplete combustion, which have limited their applicability.

The current research work is devoted to the synthesis and characterization of nanothermites as nano scale energetic materials with enhanced combustion characteristics for energetic applications, specifically microthrusters and modified propellants. The research project is conducted in four phases: the first phase deals with an extensive evaluation of the potential impact of different carbon nano materials (GO, RGO, CNTs and CNF) on the combustion characteristics of nanothermites. Prepared nanothermites are based on oxygenated salts as a reactive alternative to metallic ones, most notably potassium perchlorate and nano aluminum powder.

The second phase consists of a comparative study between different metallic and oxygenated salt-based tertiary nanothermites to identify the effects of each oxidiser on the performance of nanothermite. This part of the work compares and analyzes the thermal behaviour of different nanothermite tertiary compositions to identify the thermite reaction mechanism through correlations with the activation energy and differential scanning calorimetry results. In addition, the results are used to suggest roles for each nanothermite composite and their possible applications (heat or thrust).

The third phase introduces nanothermite mixtures with controllable combustion and tailored performance parameters for small-scale propulsion applications. Quaternary nanothermites based on n-Al, potassium perchlorate, graphene oxide and varying quantities of nitrocellulose (NC) were developed using facile electrospinning technique.

Finally, in the fourth phase, I presented new green energetic thermites with low ignition temperatures, long stable thrust output, and reactivity. These thermites are based on the $[Cu_4Na(Mtta)_5(CH_3CN)]_n$ (Mtta = 5-Methyl-1H-tetrazole) energetic metal-organic framework (EMOF-1) as a fuel instead of aluminum metal fuel and various types of oxygenated salts.

Nanothermites, except those with nitrocellulose, were prepared via conventional sonication as a quick, direct route. EMOF-1 was synthesised via the microwave-assisted technique as a more rapid, energy-efficient and greener technique. Consistent characterization of nanothermites occurred in two directions. First, microscopy techniques, such as SEM coupled with EDX, were used for morphological and chemical characterization of the nanothermite mixtures. X-ray diffraction spectroscopy assessed crystalline structure of fuel and oxidizer nanoparticles. Fourier Transform Infrared Spectroscopy was carried out to confirm that there is no chemical reaction between nanothermite reactants during the preparation process. Raman spectrometer evaluated the successful preparation of graphene and reduced graphene oxide. The second direction included use of thermogravimetric analysis, differential scanning calorimetry and oxygen bomb calorimetry to assess reactivity and thermal behaviour of nanothermites in terms of onset ignition temperature, oxidizer's decomposition temperature, heat of combustion and reaction mechanisms. Kissinger and Ozawa approaches calculated the apparent kinetic parameters (activation energy & frequency factor) for the prepared nanothermites. The nanothermite mixtures are packed with different densities and ignited using a 3.5 W continuous wave laser to observe combustion phenomena and thrust production. High-speed camera recorded the combustion propagation process. Finally, small-scale test motor (STM) determined thrust performance and combustion propagation processes within small nozzles to explore the applicability of prepared nanothermites in compact-energetic systems.

Results demonstrated that addition of carbon nanomaterials and particularly graphene oxide increased heat released and decreased both ignition temperature and activation energy. Indeed, only a 5 % addition of graphene oxide increased the heat of combustion from 3553 ± 209 J/g to 9614 ± 418 J/g, reduced ignition temperature and activation energy from 545.1 to 508.7 $^{\circ}$C and 145 to 135 kJ/mol respectively. In general, nanothermites based on oxygenated salts are more reactive than those with metallic oxides and a gas-solid diffusion reaction is the controlling and dominant reaction mechanism. Furthermore, combustion behaviour of nanothermites with

carbon nanomaterials revealed two distinct reaction regimes (slow and fast) at low and high packing densities (20 and 50 % TMD), respectively. Total and specific impulses (I_{FT} and I_{SP}) peaked at 5% GO/Al/$KClO_4$ for both slow and fast reaction regimes. Precisely, I_{FT} and I_{SP} recorded 10.1 mN.s and 147.2 s respectively at ~ 50% TMD and these are improvements of over 95 % compared to the reference sample without GO (6.6 mN.s & 96.2 s). Thermal decomposition of NC/GO/Al/$KClO_4$ quaternary nanothermites occurred in two steps (gas−solid phase and liquid−liquid phase diffusion reaction) compared to the only gas−solid reaction in tertiary mixture without NC. The liquid−liquid step in quaternary mixtures increased with increasing NC percentage. Although the ignition delay time increased, the power required to ignite the NC-enriched mixture also increased and thus improving safety of the samples while still maintain a sufficiently fast response for practical applications. I_{FT} and I_{SP} reached a maximum when 5% NC/GO/Al/$KClO_4$ at ~ 50% TMD is used. More specifically, I_{FT} and I_{SP} were recorded as 19.9 mN.s and 203.2 s respectively, which indicated an improvement of over 50 % in comparison to the reference sample without GO (13.4 mN.s and 137.4 s). New thermite mixtures based on EMOF-1 exhibited superior combustion characteristics of two to three-folds the average heat of combustion compared to aluminum-based ones, at almost half the ignition temperature. Among them, EMOF-1/KIO_4 thermite displayed the highest heat release (5.1 kJ/g), while EMOF-1/NH_4NO_3 thermite shows the lowest onset temperature (259 $^{\circ}$C) followed by EMOF-1/KIO_4 with (314 $^{\circ}$C). Also, EMOF-1 based thermites achieved longer combustion time and stable average thrust which facilitate the production of sustained propulsive force contrasted to thermites based on aluminum as a fuel. Given the remarkable and diverse combustion performances observed for prepared nanothermites, this work is of great importance with respect to the many possible energetic applications, such as in microthrusters, advanced propellants and green initiating explosives.

TABLE OF CONTENTS

DEDICATION III

ACKNOWLEDGEMENTS IV

RÉSUMÉ V

ABSTRACT V

TABLE OF CONTENTS XII

LIST OF TABLES XVII

LIST OF FIGURES XIX

LIST OF SYMBOLS AND ABBREVIATIONS XXIV

LIST OF APPENDICES XXIX

CHAPTER 1 INTRODUCTION 1

CHAPTER 2 LITERATURE REVIEW 5

2.1 Overview 5

2.2 Nanothermite fuels 5

2.3 Aluminum Nanopowder: A key fuel for Nanothermites 9

2.3.1 Nanometric aluminum 10

2.3.2 Characterization of nanometric aluminum 11

2.3.3 Combustion mechanisms of nanometric aluminum 12

2.4 Nanothermite oxidisers 17

2.4.1 Metallic oxidisers 18

2.4.2 Oxidizing salts 20

2.5 Carbon nanomaterials and energetic compositions 23

2.5.1 Preparation methods of GO 24

2.5.2 EMs based on GO and RGO 25

2.5.3 EMs based on CNTs 26

2.6 High-energy metal–organic frameworks 28

2.6.1 One-dimensional EMOFs 29

2.6.2 Two-dimensional EMOFs 30

2.6.3 Three dimensional EMOFs 32

2.7 Synthesis of Nanothermites 34

2.7.1 Ultrasonic nanopowder mixing 35

2.7.2 Characterization of nanothermites 36

2.8 Applications of nanothermites 37

2.9 Problematic 38

CHAPTER 3 OBJECTIVES 40

3.1 Objective 40

3.2 Specific objectives 40

CHAPTER 4 ORGANIZATION OF THE ARTICLES 41

CHAPTER 5 ARTICLE 1: SYNTHESIS AND CHARACTERIZATION OF TERTIARY NANOTHERMITE CNMS/AL/$KCLO_4$ WITH ENHANCED COMBUSTION CHARACTERISTICS 43

5.1 Abstract 43

5.2 Introduction 44

5.3 Experimental Section 47

5.3.1 Reagents and Materials 47

5.3.2 Synthesis of GO 48

5.3.3 Preparation of nanothermites 49

5.4 Nanothermite characterization 50

5.5 Calculation of the heat of combustion....51

5.6 Results and Discussion....51

5.6.1 Structural and chemical characterization....51

5.6.2 Thermal Performance....57

5.7 Conclusion....64

5.8 References....64

CHAPTER 6 ARTICLE 2: COMBUSTION BEHAVIOR AND REACTION KINETICS OF GO/AL/OXIDIZING SALTS TERNARY NANOTHERMITES....70

6.1 Abstract....70

6.2 Introduction....71

6.3 Materials and methods....73

6.3.1 Materials....73

6.3.2 Synthesis of GO....73

6.3.3 Preparation of nanothermite compositions....74

6.3.4 Homogeneity of nanothermites....75

6.3.5 Thermal analysis and reaction calorimetry....75

6.4 Results and discussion....75

6.4.1 Structure and chemical characterization....75

6.4.2 Thermal behaviour....76

6.4.3 Heat of combustion of nanothermites....85

6.4.4 Nanothermite reaction kinetics....87

6.4.5 Nanothermite reaction mechanism....90

6.5 Conclusions....93

6.6 References....93

CHAPTER 7 ARTICLE 3: SUPERIOR PERFORMANCE OF QUATERNARY NC/GO/AL/$KCLO_4$ NANOTHERMITE FOR HIGH SPEED IMPULSE SMALL-SCALE PROPULSION APPLICATIONS……99

7.1 Abstract 99

7.2 INTRODUCTION.....100

7.3 Materials and methods 103

7.3.1 Materials.....103

7.3.2 Synthesis of GO 103

7.3.3 Preparation of nanothermite compositions.....104

7.3.4 Nanothermite characterization 105

7.4 Results and Discussion.....107

7.4.1 Thermal behaviour and combustion mechanism.....108

7.4.2 Thrust performance of quaternary nanothermites 112

7.4.3 Effect of 5 % NC/GO/Al/KClO4 Bulk Density 120

7.4.4 Performance of the nanothermites integrated in STM with a nozzle.....122

7.5 Conclusion.....126

7.6 Acknowledgement.....126

7.7 References 127

CHAPTER 8 ARTICLE 4: COMBUSTION CHARACTERISTICS OF EMOF/OXYGENATED SALTS NOVEL THERMITES FOR GREEN ENERGETIC APPLICATIONS 133

8.1 Abstract 133

8.2 Introduction 134

8.3 Materials and methods 137

8.3.1 Materials.....137

8.3.2 Synthesis of EMOF-1 138

8.3.3 Preparation of thermite compositions 139

8.3.4 Instrumentation 141

8.4 Results and discussions 141

8.4.1 Structural and chemical characterization 141

8.4.2 Thermal analysis 145

8.4.3 Reaction Kinetics 150

8.4.4 Combustion characteristics 153

8.5 Conclusions 156

8.6 Acknowledgement 157

8.7 References 157

8.8 Supporting Information 162

CHAPTER 9 GENERAL DISCUSSION 168

CHAPTER 10 CONCLUSIONS AND RECOMMENDATIONS 172

10.1 Conclusions 172

10.2 Recommendations 175

BIBLIOGRAPHY 177

APPENDICES 192

LIST OF TABLES

Table 2-1 Different applications and preparation methods for energetic materials based on graphene, GO and RGO 26

Table 2-2 Different applications and preparation methods for energetic materials based on CNTs 28

Table 2-3 Common used solvents for nanothermite preparation 35

Table 5-1 Chemical composition of different nanothermite samples 50

Table 5-2 Total heat released and maximum decomposition temperature calculated from DSC 61

Table 5-3 Heat of combustion calculated from the bomb calorimeter 62

Table 6-1 Nanothermite compositions based on salt and metallic oxidisers 74

Table 6-2 Heat of combustion calculated from bomb calorimeter 86

Table 6-3 Kinetic parameters of nanothermite mixtures 89

Table 7-1 Elemental composition of prepared GO samples expressed in mass fraction 107

Table 7-2 Combustion characteristics of nanothermite samples 114

Table 7-3 Ignition properties of nanothermite composites 118

Table 7-4 Combustion characteristics of nanothermites within CD nozzle STM at 20 and 50 % TMD 123

Table 8-1 Sensitivity and combustion characteristics of ATRZ-1/thermite mixtures [36, 37] 136

Table 8-2 Chemical composition and reaction of different nanothermite samples 140

Table 8-3 Relative percentage for EMOF-1 elemental analysis 143

Table 8-4 Thermal characteristics of thermite samples 148

Table 8-5 Kinetic parameters of EMOF-1 based thermite compositions 152

Table A1 Elemental analysis and heat of combustion of CNMs 196

Table A2 Chemical composition of different nanothermite samples 197

Table A3 Modeling parameters at the inlet of the nozzle based on ICT calculation 200

Table A4 Combustion characteristics of nanothermite samples at 20 %TMD 203

Table A5 Ignition properties of nanothermite composites.....206

Table A6 Combustion characteristics of nanothermite samples at 55 %TMD 210

Table A7 Thrust performance of GO/nanothermites within CD nozzle STM at 20 & 55 %TMD 212

LIST OF FIGURES

Figure 2-1 Nanothermites fuels and oxidizers 6

Figure 2-2 Gravimetric and volumetric heats of combustion for common metal fuels 6

Figure 2-3 Mass content in alumina of spherical aluminum nanoparticles.....11

Figure 2-4 Diffusion oxidation mechanism 15

Figure 2-5 Explosion mechanism of n-Al oxidation.....16

Figure 2-6 Melt dispersion mechanism.....17

Figure 2-7 Schematic diagram of reaction mechanism of Al/AgIO3 nanothermite 22

Figure 2-8 Preparation steps of GO.....24

Figure 2-9 Schematic diagram of formation SWCNTs and MWCNTs from graphene.....27

Figure 2-10 Zigzag chain of compound 1 29

Figure 2-11 Structure of compound 2-1D EMOF.....30

Figure 2-12 Compound 14 2D EMOF 30

Figure 2-13 Two zigzag chains linked by azido ligands form $[Cd(DAT)_2(N_3)_2]n$ 31

Figure 2-14 Structure of [Cu(Htztr)]n 2D EMOF.....31

Figure 2-15 Structure of (A) compound 31 and (B) compound 32 3D EMOFs 32

Figure 2-16 Structure of compound 35 3D EMOFs.....33

Figure 2-17 Bar chart of heat of detonation of EMOFs and general explosives.....33

Figure 2-18 Classification of nanothermite synthesis methods 34

Figure 2-19 Some applications of nanothermites.....37

Figure 5-1 GO and RGO preparation process.....48

Figure 5-2 SEM micrographs of 5 % GO nanothermite composition.....52

Figure 5-3 EDS images of the 5% GO/Al/$KClO_4$ nanothermite.....53

Figure 5-4 Raman spectra of neat GO and RGO powder and 5 % GO/Al/$KClO_4$ 53

Figure 5-5 FTIR spectra of Al, $KClO_4$, GO and 5%GO/Al/$KClO_4$ 55

Figure 5-6 XRD patterns of GO and RGO.....56

Figure 5-7 XRD patterns of thermite samples 57

Figure 5-8 TGA thermogram for different percentages of GO over Al/$KClO_4$ nanothermites 58

Figure 5-9 DSC plots of (A) reference sample (Al/KClO4) and (B) nanothermite of 5% GO/Al/KClO4 59

Figure 5-10 DSC thermograms percentages of different % of GO nanothermites 60

Figure 5-11 Energy release of 5% GO/Al/KClO4 as a function of equivalence ratio 63

Figure 6-1 A scheme of GO preparation.....74

Figure 6-2 EDS images of the 5% GO/Al/KIO_4 nanothermite 76

Figure 6-3 TGA/DSC curves of GO 77

Figure 6-4 TGA/DSC curves for 5 % GO/Al/$KClO_4$ and reference nanothermites 78

Figure 6-5 Thermal analysis of 5 % GO over Al/$K_2S_2O_8$ and reference nanothermites.....79

Figure 6-6 TGA/DSC curves for 5 % GO over Al/KIO_4 and reference nanothermites.....80

Figure 6-7 TGA/DSC curves for 5 % GO over Al/$KMnO_4$ and reference nanothermites.....81

Figure 6-8 TGA/DSC curves for GO/Al/ NH_4NO_3 and its reference nanothermites.....82

Figure 6-9 DSC (a) curve of GO/Al/Fe_2O_3, (b) GO/Al/CuO and (c) GO/Al/ WO_3.....84

Figure 6-10 Data correlation line of ln (β/T_p^2) against ($1/T_p$) for nanothermite samples 88

Figure 6-11 Relation between oxygen release temperature of different oxidizers and onset temperature of their nanothermites 91

Figure 6-12 Suggested reaction mechanism of tertiary nanothermites 92

Figure 7-1 Schematic of electrospinning formation of quaternary NC/GO/Al/$KClO_4$ nanothermites 105

Figure 7-2 (A) Laser ignition and high-speed imaging set up (B) nozzle configuration (C) Dimension of open STM (D) Dimension of CD STM.....106

Figure 7-3 SEM image and EDX analysis of 5 % NC/GO/Al/KClO4 nanothermite 108

Figure 7-4 DSC curves of nanothermites with different NC content.....109

Figure 7-5 Suggested reaction mechanism of quaternary nanothermites 111

Figure 7-6 Thrust profiles for different NC/nanothermite samples at 20%TMD 112

Figure 7-7 Snapshots of different nanothermite composites in open tube test engine.....116

Figure 7-8 (A) Optical emissions of different nanothermite samples. (B) Combined optical signal and thrust curve for the 5% NC sample 117

Figure 7-9 Normalized photodiode signal of different nanothermite samples.....119

Figure 7-10 AlO photodiode signal of different nanothermite samples.....120

Figure 7-11 Specific and volumetric impulses of 5 % NC/GO/Al/KP with different %TMD 121

Figure 7-12 (A-F) Thrust/time curves for reference, 2.5 and 5 % NC nanothermites at 20 and 50 % TMD with and without nozzle, respectively.....122

Figure 7-13 Snapshot at the end of combustion for 5 % NC sample at (A) low packing density and (B) high packing density 125

Figure 8-1 3D structure of (a) ATRZ-1 and (b) EMOF-1 viewed along the a-axis. (recreated from CCDC files “DIXNUV” and “TOXRIJ”, respectively) 135

Figure 8-2 Stepwise synthesis of the energetic MOF (EMOF-1). a) Click reaction for the formation of the Mtta-linker, b) Coordination of the formed linker to the metal ions present in the reaction medium and the formation of the energetic MOF (EMOF-1).....138

Figure 8-3 The detailed structure of EMOF-1, revealing a) Na azolate chains, b) Cu beetle-like chains, c) unit cell of EMOF-1, d) distorted hexagonal geometry of Na(I) centres, and e) tetrahedral geometry Cu(I) centres (according to the color code). [reproduced from CCDC file “*TOXRIJ”*] 142

Figure 8-4 SEM images of the block-like crystals of EMOF-1. Side cross-section showing the built-up layers within the crystal (inset).....143

Figure 8-5 FTIR spectrum of EMOF-1 144

Figure 8-6 SEM images and EDX analysis of EMOF-1 and KIO4 thermite.....145

Figure 8-7 TGA/DSC curves of EMOF-1 based composites.....147

Figure 8-8 Data correlation line of ln ln(βTp2) against (1000/Tp) for nanothermite samples, error bars are taken as the uncertainties from linear fitting.....151

Figure 8-9 Force profiles for different EMOF-1 thermite samples.....153

Figure 8-10 Comparison between pressure and pressurization rate for different EMOF-1 based energetic mixtures 155

Figure S1 Synthesis scheme for EMOF-1 via the microwave-assisted technique.....163

Figure S2 The initial pulse within the heating step of EMOF-1 preparation.....163

Figure S3 The whole microwave synthesis process for EMOF-1.....164

Figure S4 Block diagram of laser ignition and high-speed imaging set up 164

Figure S5 PXRD pattern for EMOF-1 compared to the simulated pattern.....165

Figure S6 Temperature output of bomb calorimeter.....166

Figure S7 Snapshots for different EMOF-1 thermite samples.....167

Figure 10-1 Map of combustion properties and applications of different thermite mixtures 175

Figure A1 Schematic diagram of experimental setup showing: laser ignition and high-speed imaging set up (A), no-nozzle STM configuration (B), CD nozzle STM configuration (C), and converging diverging nozzle geometry (D).....198

Figure A2 Schematic diagram of 2D-axisymmetric domain used for modelling showing: A) reservoir boundary conditions, and B) nozzle-area boundary and initial conditions.....199

Figure A3 Comparative plots for nanothermites based on: (A) Al/KClO4 with various CNM additives (B) Al based mixtures with different oxidizers; all enriched with 5%GO content 201

Figure A4 Thrust profiles for different GO/nanothermite samples at 20 %TMD 202

Figure A5 Optical emissions of different GO/nanothermite samples.....205

Figure A6 AlO photodiode signal of different nanothermite samples 207

Figure A7 Specific impulse plotted against powdered sample density (%TMD) for Al/KClO4 based nanothermites 208

Figure A8 Peak thrust and combustion duration of 5% GO/Al/KClO4 with different %TMD showing fast reaction regime (yellow), transitional regime (green), and slow reaction regime (gray) 208

Figure A9 Thrust profiles for different GO/nanothermite samples at 55 %TMD 209

Figure A10 Thrust-time curves for different GO/nanothermite samples at (A) 20 %TMD (B) 55 %TMD with and without CD nozzle.....211

Figure A11 Snapshots of different GO/nanothermite composites in CD STM at 20 %TMD 214

Figure A12 Velocity profile at different moments for the reference sample with 20 %TMD.....215

Figure A13 Temperature profile at different moments for the reference sample with 20 %TMD 216

Figure A14 Temperature and velocity profiles of the plume from the open tube at different moments for the reference sample with 20 %TMD: a) - c): temperature; d) - f): velocity..217

Figure A15 Simulated thrust-time profiles of the Al/KClO4 nanothermite (reference) sample with different nozzle geometries: A) 20%TMD; B) 55%TMD and C): the CD nozzle with varying TMDs 219

LIST OF SYMBOLS AND ABBREVIATIONS

E	Activation energy
Al	Aluminum
Al_2O_3	Aluminium oxide
NH_4ClO_4	Ammonium perchlorate
Be	Beryllium
Bi_2O_3	Bismuth oxide
B	Boron
CNMs	Carbon nanomaterials
CNTs	Carbon nanotubes
CNFs	Carbon nanofibers
CHP	Cobalt hydrazine perchlorate
CuO	Copper oxide
DSC	Differential scanning calorimetry
EMs	Energetic materials
EMOFs	Energetic metal–organic frameworks
EDS	Energy dispersive spectroscopy
t_e	Ending burning time
EG	Expanded graphite

n	Exponent
FTIR	Fourier Transform Infrared Spectroscopy
GO	Graphene oxide
Q	Heat of combustion
HE-MOFs	High energy metal-organic frameworks
HTPB	Hydroxyl-terminated polybutadiene
Fe_2O_3	Iron oxide
t_i	Initial burning time
LIBS	Laser-induced breakdown spectroscopy
Mg	Magnesium
M	Metal fuel
MO	Metal oxide
MICs	Metastable intermolecular composite
MDM	Melt dispersion mechanism
MoO_3	Molybdenum oxide
MOFs	Metal-organic frameworks
MWCNTs	Multi-walled carbon nano tubes
n-Al	Nano aluminum
NSTEX	Nanostructured thermite explosive

W_t	Nanothermite charge weight
m	Nanothermite mass charge
NC	Nitrocellulose
HNO_3	Nitric acid
NHP	Nickel hydrazine perchlorate
n	Number of measured samples
E	Photodiode signal
H_3PO_4	Phosphoric acid
$KClO_4$	Potassium perchlorate
KMnO4	Potassium permanganate
KIO_4	Potassium periodates
K_2SO_4	Potassium sulphate
$K_2S_2O_8$	Potassium persulphate
K	Pre-exponential factor
C_{ox}^{m}	Ratio between oxidiser concentration and pressure at the particle surface
RGO	Reduced graphene oxide
red-P	Red phosphorus
m	Reaction order
T	Reaction temperature

SEM	Scanning electron microscope
Si	Silicon
Ag_2O	Silver oxide
$AgIO_3$	Silver iodate
SWCNTs	Single wall carbon nano tubes
STM	Small-scale test motor
$NaNO_3$	Sodium nitrate
$NaIO_4$	Sodium periodates
Cp	Specific heat capacity
I_{SP}	Specific impulse
σ	Standard deviation
U	Standard uncertainty
H_2SO_4	Sulphuric acid
ΔT	Temperature difference
TGA	Thermal gravimetric analysis
TMD	Theoretical maximum density
t_{oxide}	Thickness of alumina layer
Ti	Titanium
t	Time of combustion

I_{FT}	Total impulse
TEM	Transmission electron microscope
WO_3	Tungsten oxide
R	Universal gas constant
I_{SV}	Volumetric impulses
V_t	Volume of the nanothermite charge
XRD	X-ray diffraction

LIST OF APPENDICES

Appendix A ARTICLE 5: THRUST CHARACTERISTICS OF NANO-CARBON/AL/OXYGENATED SALT NANOTHERMITES FOR MICRO-ENERGETIC APPLICATIONS 192

CHAPTER 1 INTRODUCTION

Energetic materials (EMs) have captured much attention due to their uses in many applications serving both the civilian and military fields. They have been used in micro- and nano-welding, material synthesis, ejection seats, safety air cushion, and power generation as civilian applications. On the other hand, regarding the military purposes, their use is being considered in pyrotechnics, micro-igniters, micro-thruster, course correction of small caliber ammunitions, propulsion, and hydrogen generation [1-4]. Developments in the field of micro electro mechanical systems (MEMS) increase the interest in the synthesis and development of new EMs to sufficiently meet the increasing demands in microscale energetic devices and miniature propulsion systems [5].

In broad terms, Energetic Materials (EMs) can be defined as materials that store chemical energy and are classified into propellants, explosives, and pyrotechnics. The primary difference between these three categories is the rate of energy release. While rocket propellants and pyrotechnics are characterized by a relatively slow combustion process (several seconds), explosives release their energy through a fast detonation process (microsecond timescale) [6]. According to molecular structure, EMs can be divided into monomolecular EMs (MEMs), composite materials or metastable intermolecular compounds (MIC). On the one hand, MEMs contain fuel and oxidizing components within the same type of molecules (such as nitrocellulose, nitroglycerine, and trinitrotoluene). On the other hand, MICs are made of a mixture of fuels (aluminum, sulfur, carbon, etc.) and oxidants (iron oxide, cupper oxide, potassium perchlorate, etc.), such as Al/Fe_2O_3 or Al/CuO mixtures [7].

Thermites are classified as a type of MICs. Compared to MEMs, thermites offer a high energy density owing to the higher enthalpies of metallic fuels [8]. Slow rate of energy release and relatively long ignition delays are the main drawbacks of using thermites [9, 10]. Moreover, the high electrostatic sensitivity, in addition to the relatively elevated ignition temperature (~ 800 $^{\circ}$C), are considered, to this day, as problematic issues associated with thermites [11-13]. Moreover, lower peak pressures and excessive oxidation of nano-Al before combustion represent potential problems linked with thermites [14, 15]. Therefore, the thrust output by micro-scale devices would be limited because of the apparent lack of C-H-O-N elements in the thermite constituents and the decrease of the active Al content [16, 17]. In practice, the importance of green thermites

increases significantly because the inherent drawbacks with traditional thermite compositions. Hyper toxicity, hydrolytic instability, and other environmental severe pollution hazards result from using some of the primary components integrated into thermite mixtures such as NaN_3, and NH_4ClO_4 [12, 18]. As a result of the dangers these materials pose to environmental and human health, their military and civilian uses are limited [19, 20].

Nanothermites are solid-phase EM mixtures traditionally composed of metal and metal-oxide components at nanometric scale. They are distinguished from microthermites by high reaction rate, heat release, pressure and thrust. The higher performance of nanothermites results from their large specific surface area, reduced activation energy and fast energy release [21, 22]. On the other side, nanothermites have limited applicability because their particle agglomeration before ignition, relatively long ignition delays and slow combustion kinetics which lead to incomplete combustion [9, 22-25]. In addition, difficult ignition and propagation process within small tubes and slots are one of the important problems that decrease the applicability of EMs in micro-energetic systems [26].

A common family of nanothermites are those based on nano aluminum (n-Al) powders, traditionally mixed with metallic oxides. Aluminum is the most used metal fuel in nanothermites due to its high heat of formation, high density, low melting temperature, low toxicity, and compatibility with other reactants. For novel nanothermites, this definition is extended to include alternative oxidizers to metallic ones such as oxygenated or fluorinated oxidisers which have the ability to exchange their high electronegative atoms (O, S, F…) with Al during reaction and enhance gas generation [24, 27-30].

The main objective required in the development of nanothermites is increasing the gas generation to emulate the behaviour of organic EMs and overcome the low gas production problems associated with Al-based thermites. Oxygenated salts (oxygenated oxidisers) could be an excellent alternative to metallic oxidisers in the preparation of nanothermites with high reactivity and better combustion performance. [31, 32]. They have higher atomic oxygen content compared to metal oxides or oxysalts and so are more suitable for gas generation and high burn rate applications [28, 33]. Moreover, the lower dissociation energies of non-metal-oxygen bonds (Cl-O, I-O, etc.) in oxygenated salts offer higher oxygen mobility that can lead to decomposition and oxygen release at lower temperatures when compared to metal-oxygen bonds (Cu-O, Fe-O, Bi-O,

etc.) [34, 35]. Oxygenated salts produce intermediate radicals (e.g. hydroxyl radical ($OH^{\cdot}$)) upon decomposition which in turn are able to produce other subsequent radicals and oxidants by initiating a chain of degradation reactions. As such, oxygenated salts have higher oxidation ability than oxidizers which undergo an electron capture based oxidation mechanism [36, 37].

Recently, carbon nanomaterials (CNMs), such as carbon nanotubes (CNTs), carbon nanofibers (CNFs), graphene and its derivatives (graphene oxide (GO), reduced graphene oxide (RGO)) have been active fields of research in the improvement of nanothermites due to their large specific areas and unique thermal, electrical and mechanical properties [38]. In particular, GO is an appropriate candidate for introduction into nanothermites due to its catalytic properties as well as relatively simple preparation methods. GO itself is considered to be a potential EM because it liberates oxygen stored on its basal plane and long edges functional groups through violent exothermic reaction [39].

NC, as an EM can be used to reduce the oxidation process of Al powders during storage by taking advantage of increasing its chemical activity and gas production. Moreover, the beneficial use of NC arises from its easy dissolving in organic solvent to form collodion solution and excellent interaction with the raw particles at the solid/liquid interface. Besides, it might provide a way to enhance mechanical properties such as resilience [40, 41].

In order to overcome the problems associated with the commonly used Al-based nanothermites and prepare green thermites with improved gas generation, energetic metal-organic frameworks (EMOFs) will be investigated as alternatives to the Al fuel to prepare new, improved thermite compositions [42, 43]. The superiority of EMOFs results from their high detonation heat due to the involvement of nitrogen-containing organic ligands like imidazoles, triazoles, tetrazoles, triazines, tetrazines, and their substituted derivatives. This is due to their high nitrogen content and energy density [44]. Also, EMOFs are bimetallic MOFs with an immense amount of released gases, fairly good stability, high surface area, controllable structure, and uniform pore size [45].

Since new EMs are the key to advances in micro scale energy demanding systems as actuation parts, igniters, propulsion units, and power, nanothermite is one of the main approaches to achieve the development of new EMs. The present research focuses on the synthesis and characterization of new nanothermites as nano-scale energetic materials for energetic applications (microthrusters and gas generation applications). In order to develop new thermite compositions,

it is important to know more about the thermite materials and their reaction mechanism. In addition, we need to investigate the possible effect of the new components on improving of combustion properties of nanothermites to suit future energetic applications. So, for facilitating the interpretation of the findings presented in this PhD thesis, a literature review is presented in Chapter 2. It concerns the review of the characteristics of n-Al powder, its reaction mechanisms, and the difference between metallic and oxygenated salts' properties. In addition, it reviews energetic compositions based on CNMs and EMOF, synthesis, characterization methods and applications of nanothermites. Chapter 3 summarizes four journal articles concerning the findings of this work. Chapter 4 focuses on the evaluation of impact of different CNMs (GO, RGO, CNTs and CNFs) on the thermal performance of nanothermite compositions based on n-Al and oxygenated salts (primarily $KClO_4$). In addition, chapter 4 describes investigation of various equivalence ratios between the fuel and oxidiser in the preparation of new nanothermite compositions with a high-energy output, burning rate, gas generation and propulsive force. Chapter 5 compares the effect of GO on the thermal behaviour and reaction characteristics of tertiary nanothermites based on n-Al and different types of oxygenated salts and metallic oxidizers. The controlling mechanisms of different nanothermite compositions are discussed based on the measured kinetic parameters. Chapter 6 is devoted to evaluating the influence of chemical composition and packing density on combustion process and thrust generating characteristcs of the previously prepared nanothermites. Chapter 7 discusses production of quaternary NC/GO/Al/$KClO_4$ nanothermite using facile electrospinning technique with controllable combustion and tailored performance parameters for small-scale propulsion applications. Chapter 8 presents a novel type of thermite energetic materials based on a powerful 3D EMOF and different types of oxygenated salts. A critical review of the findings of this PhD thesis, focusing on the uses of prepared nanothermites on energetic applications, is presented in chapter 9. Finally, the most important conclusions are given in chapter 10, as well as the perspectives and recommendations for new research in the field of nanothermites for impactful applications.

CHAPTER 2 LITERATURE REVIEW

2.1 Overview

Thermite reaction is defined as a highly exothermic oxidation – reduction reaction that typically comprises metallic or non-metallic oxidisers (oxygen donor) and metal fuel or metalloid (oxygen acceptor or reducing agent). This reaction yields stable metal oxide and pure metal or metal salt of the corresponding oxidiser according to equation (1) [46].

$$M + AO \rightarrow MO + A + \Delta H \quad (1)$$

Where M and MO represent metal fuel and its equivalent oxide respectively. AO and A are metallic or non-metallic oxidizers (oxygenated salts) and its corresponding pure metal or metal salt and ΔH is the enthalpy of reaction (heat of reaction) in cal/g, J/g or J/cm^3.

The Initiation rate of thermite reaction depends on the amount of energy transferred to thermite sample as compared to the its activation energy. In addition, consecutive mass transfer of active components to the interface, and through any protective oxide layers is required. Thus, controlling heat and mass transfer can improve ignition process of thermite reaction [47].

Recently nanothermites are considered as one of the most promising energetic compositions due to their broad range of possible application in both civilian and military fields [48-51]. Nanothermites distinguish themselves by having at least one of their components at the nanometer scale. Because of their growing uses in several applications, it is essential to promptly acquire an in-depth understanding of nanothermite materials and as well as properly explore their physical and chemical characteristics

2.2 Nanothermite fuels

Materials used as a fuel in nanothermites must have high reducing properties; importantly, they should have high affinity to react with oxygen liberated from the oxidiser to form product oxide and heat [52]. Therefore, most oxophilic metals and corresponding oxides used in thermite reaction locate on the left side of Mendeleev's periodic table and depicted in Figure 2-1.

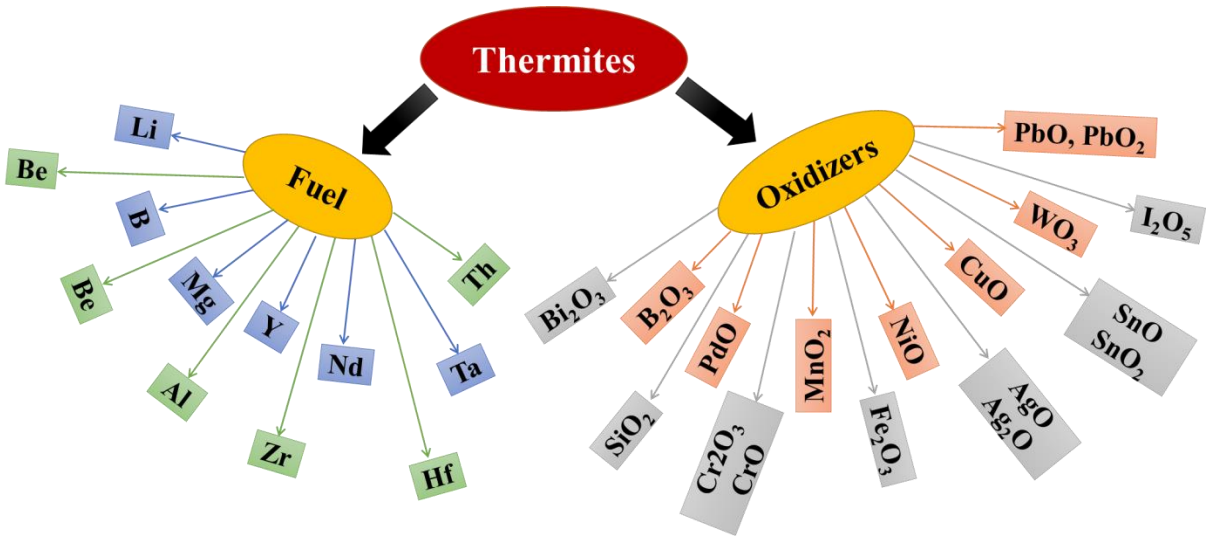

Figure 2-1 Nanothermites fuels and oxidizers

Energetic fuels should fulfil some requirements such as high density, high heat of formation, moderate amount of gases released, low melting point, stability, compatibility with other ingredients and low toxicity. Fischer and Grubelich calculated thermochemical performances of the most interesting metals for thermite composites as illustrated in Figure 2-2 [53, 54].

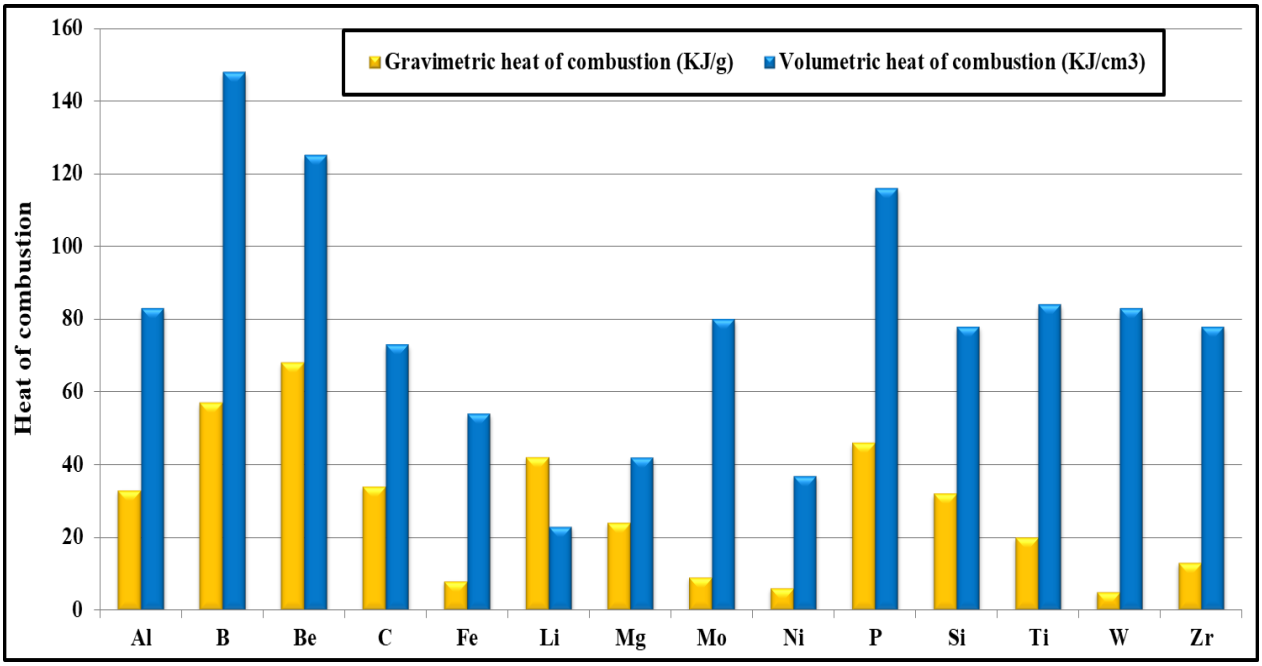

Figure 2-2 Gravimetric and volumetric heats of combustion for common metal fuels

Less stability and difficult passivation of several oxidizing elements reduce suitability of many elements as fuels for nanothermites compositions. So, based on thermochemical calculations, the best fuels for nanothermites are boron (B), beryllium (Be), aluminium (Al) and titanium (Ti). Spherical morphology remains the most abundant state of nano-metric fuels used for nanothermites and the platelet morphology is very rare [55].

Although, Be is one of the highest heat of combustion among all other metals used in nanothermite reactions, it is not often used in the preparation of nanothermites due to its high toxicity, carcinogenicity, and fine particle reaction products which spread out in the form of fumes [32].

At first sight, Boron nanopowder (n-B) would appear to be the ideal fuel for nanothermites due its low molecular weight, high enthalpy (58 kJ/g) and good chemical and physical stability. Despite these intrinsic qualities, Al is more reactive and efficient fuel for nanothermites than n-B. This outcome is in contradiction with what we naturally expect from materials like B when taking in our account its superior theoretical properties. Boron, compared with Al, is less reactive due to its refractory nature, high melting and evaporation temperature, which are 2075 $^{\circ}$C and 4000 $^{\circ}$C respectively. In addition, B requires significant quantity of heat for its phase change (5.2 and 480 kJ/g) and the oxide layer on B particles is more difficult to break than alumina [32, 55].

Sullivan et al. investigated the benefits of addition n-B (62 nm) on the combustion behaviour of CuO/Al nanothermite. They found that adding of n-B (not more than 50 % fuel percentage) decreases the ignition delay time and progressively increased the pressurization rate of combustion and the converse is true when adding more than 50 % B [56]. Martirosyan and co-workers noted that addition of 2.53 % (mass fraction) of 50 nm B to MoO_3/Al nanothermite enhanced the produced pressure from 0.48 to 1.3 MPa [57]. A group of researchers from China in 2009 investigated the combustion time of n-B and concluded that neither diffusion nor chemical kinetics limited or controlled the combustion of n-B. Furthermore, combustion of micro sized B should occur at high temperature due to its high melting point because of dissipation of heat that occurs during the combustion process [58]. So, in order to get the largest heat output of n-B, it should be used within high flame temperature EMs to be able to evaporate the oxide layer and melt the B core. More simply put, n-B as a secondary fuel is more useful than as the primary one.

Magnesium (Mg) is distinguished by its highly reducing nature, reactivity and wide availability. These characteristics make Mg an excellent fuel if it is employed under the right conditions. Though it has approximately the same melting point of Al (660 $^{\circ}$C), its boiling point (1090 $^{\circ}$C) is very low compared with that of Al (2470 $^{\circ}$C) and other metals. The relatively low boiling point of Mg increases its reactivity in magnesiothermic formations through raising the initial pressure of the composition by vaporization of Mg and hence, positively enhancing the combustion process [55, 59]. The highly oxidizing nature of Mg in powder form represents its major shortcoming. Zhou et al. studied the oxidation process of Mg with air in a dry cabinet and found that Mg instantaneously oxidized with just a small contact with air and after one month, the proportion of Mg to oxygen reached the oxide stoichiometric ratio [60]. Generally, the Mg nanopowder reacts actively with any oxygen containing materials, including carbon dioxide and hence it is very susceptible to self-ignite with spontaneous oxidation. Furthermore, Zhou et al. performed thermal properties characterization of Mg and copper oxide (CuO) energetic mixture using differential scanning calorimetry (DSC). They deduced that Mg/CuO released about 3.4 kJ/g without melting of Mg [60]. As one of nanothermite practical applications, G. Singla et al. synthesised nanometric B and tungsten through a mechanosynthesis process where Mg reacts with boron oxide and tungsten trioxide respectively [61, 62].

According to Fischer and Grubelich, nanometric Ti is one of the best fuels for nanothermite use because of its high reactivity and the presence of a protective oxide layer which passivates its surface and makes it less sensitive to its environment [53, 63]. It is commercially available in the spherical powder form with a wide range of diameter (30-300 nm). However, while oxidation of Ti starts early at temperatures between (100-200 $^{\circ}$C), its complete oxidation does not occur until the temperature reaches 1000 $^{\circ}$C [55]. Particularly low ignition temperature of Ti leads to unsafe handling of it in large amounts [32]. Billy and his research group reported that chemical properties of Ti are similar to those of silicon (Si). It reacts in a violent way with CuO, lead oxide and permanganate while it has a moderate reaction behaviour with sodium carbonate, potassium nitrate and chlorate [64]. Based on the previous mentioned characteristics, Ti is considered a promising fuel with curious pyrotechnic properties for n-EMs.

Red phosphorus (red-P) is a metalloid of interest as a fuel for nanothermites however it is not mentioned in Fischer's standard classification [32]. Hale et al. discovered thermite compositions

based on red phosphorus and metallic oxides [65]. Marc Comet pioneered an integration of nano oxides with red phosphorus to properly form nanothermites [66]. Red-P oxidizes to phosphorus trioxide or phosphorus pentoxide according to the amount of the present oxygen and releases a high amount of energy (18.2 kJ/g to 24.3 kJ/g). The direct reaction between red-P and oxygenated salts yields EMs with explosive properties [67]. Nanometric red-P cannot be produced because it is not soluble in a liquid and cannot be prepared by traditional methods used in nanomaterial manufacturing. Thermite mixtures based on red-P and nickel oxide is one of the most reactive mixtures followed by those with iron trioxide, bismuth trioxide, copper oxide and lead oxide respectively [55]. Generally, mixtures based on red-P and metallic oxides give high combustible compositions with exciting properties. Red phosphorus in sub-micrometer size could undoubtedly enhance the reactivity of these compositions [68].

Silicon (Si) is another type of metalloid used as a fuel for energetic compositions. Porous nano-Si has been used in some energetic formulations with high oxygenated salts like perchlorates and reported in a review by Zhou et al. [69]. Heat of combustion of EMs based on Si as a fuel with sodium and calcium perchlorate individually as oxidisers were measured at 9.2 kJ/g and 8.6 kJ/g respective using a bomb calorimeter [70]. In addition, Becker et al. investigated the combustion behaviour of porous Si with a surface area 840 m^2/g mixed with sodium perchlorate. They found the propagation velocity of this composition was 3050 m/s [71]. Although these EMs typically based on Si and red-P have high energy output, they are typically not classified as thermite because of they are not strictly metal elements. It is preferable to use Si as an additive like B and not as a primary fuel to improve the combustion properties of Al based nanothermites [72].

2.3 Aluminum nanopowder: A key fuel for nanothermites

Fischer and Grubelich theoretically tabulated heat of combustion of thermite compositions. They concluded that thermites based on Mg and boron trioxide, Be and lead oxide have the highest heat released per unit mass and volume, recording 8.92 kJ/g, 26.72 kJ/cm^3 respectively. These values of heat released are smaller than that of oxidation of pure fuel. Hence, heat released from the oxidation reaction of the fuel along with reaction kinetics are equally important in accurately determining the fuel performance [73].

Widespread availability and the tremendous development in industrial production of Al led to the discovery of new aluminothermic compositions. High enthalpy of combustion (1646 kJ/mol), low melting point (660 $^{\circ}$C) and consequently low ignition temperature are the natural distinctive characteristics making Al the best fuel choice for thermites. In addition, Al is also very thermally conductive which enhances the combustion velocity of nanothermite, has low vapour pressure, and develops an oxide layer that covers and protects pure Al from spontaneous combustion [74]. Thus, based on the previous mentioned characteristics, n-Al has a more favourable use in nanothermites as a fuel than other nanostructured materials like B and diamond in spite of their better thermodynamic properties [73].

2.3.1 Nanometric aluminum

In terms of energy release, n-Al powder is the best candidate fuel for modern nanothermite formulations. To deeply understand n-Al, we will further investigate n-Al forms, characterization methods, and oxidation mechanisms. The main structure of n-Al is a crystalline Al core surrounded by an amorphous aluminium oxide (Al_2O_3) shell. The alumina layer protects the Al core from further oxidation by atmospheric oxygen; consequently preventing Al ignition and its accompanied hazards. Pesiri et al. stated that the thickness of Al_2O_3 layer is usually in the range of 2-5 nm. Al with alumina thickness less than 2 nm can be pyrophoric and susceptible to spontaneous ignition [55, 75]. Passivating n-Al by a sufficient thickness of Al_2O_3 layer and not storing it in large quantities control risks associated with pyrophoric behaviour of n-Al. Figure 2-3 illustrates the direct relation between the alumina content and the effective diameter of n-Al. It appears that content of n-Al decreases greatly with decreasing particle diameter.

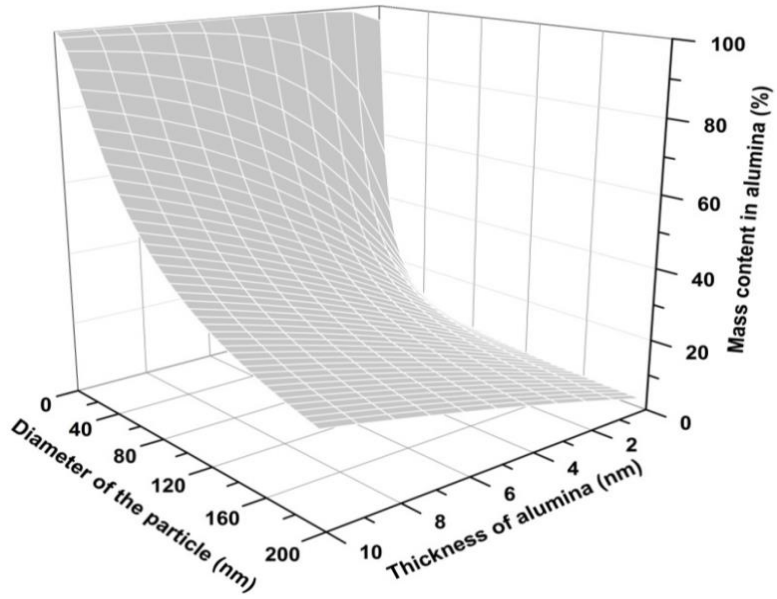

Figure 2-3 Mass content in alumina of spherical aluminum nanoparticles

Because of the inert nature of the alumina layer, the specific heat released by n-Al with smaller particle size and high content of alumina will typically decrease compared to its initial mass. Hence, we will add more of n-Al to achieve the stoichiometric ratio between necessary fuel and oxidiser in nanothermite mixture. As a conclusion, from a practical point of view of nanothermite preparation, Al particles size should not be neither too small nor large to gain the benefits of their small size. So, the most suitable particle size for n-Al as a fuel for nanothermite compositions between 40-120 nm [32].

Researchers published many studies on the passivation process of n-Al. They found that a controlled oxidation is be the most efficient way to passivate n-Al and properly protect its core. Other passivation methods may lead to the reaction between n-Al and the coating materials and consequent formation of impurities and unexpected oxidation may naturally occur. Pre-oxidation of n-Al spheres directly after their production is necessary to prevent the formation of necks between more n-Al spheres through cold welding [75-78].

2.3.2 Characterization of nanometric aluminum

Precise determination of the metallic content of n-Al powder is imperative for successful nanothermite preparation. Puszynski et al. reported four methods to measure metallic content of

n-Al powder [79]. Before all else, TGA is used to determine the mass ratio between Al/Al_2O_3 in the n-Al sample. It additionally provides us with essential information about the combustion behaviour of n-Al such as surface moisture content, steps of oxidation process and the rate of each step. Generally, oxidation of n-Al occurs in 2-3 steps starting from 350 – 400 $^{\circ}$C and ends at approximately 1200 $^{\circ}$C. In addition, oxidation rate after melting of n-Al at 660 $^{\circ}$C is lower than in solid phase due to the clogging flows paths by molten Al. Hence, the oxidation process of internal Al particles will be difficult after melting. Furthermore, an oxidation step between 450 – 600 $^{\circ}$C disappears in n-Al with particle sizes between (40 – 100 nm) [55].

Volumetric method or gas evolution technique is the second method to measure metallic content of n-Al. The advantage of employing a volumetric method comes from its simplicity and the small sample size required to carry it out. In this method, volume of hydrogen released from the reaction between n-Al and potassium hydroxide determines metallic content of n-Al.

The third method to evaluate metallic content of n-Al is the calorimetric method. We calculate heat released from the combustion of n-Al and compare it with that of pure Al to determine the mass ratio between Al/Al_2O_3 in the sample. This method assumes that the heat released by oxidation of micro Al and n-Al is the same.

Laser-induced breakdown spectroscopy (LIBS) is the fourth method used to determine the metallic content of n-Al. In this method, a concentrated laser pulse vaporizes a small sample of n-Al, then the vapour expands, cooling of micro plasma occurs, and finally each element is identified according to its atomic emission line. Despite the considerable merits of LIBS technique, it is not used a lot determine the metallic content of n-Al powder.

2.3.3 Combustion mechanisms of nanometric aluminum

Much considerable attention has been directed towards properly understanding the reaction behaviour of n-Al in order to use it effectively in energetic applications. Since the combustion of n-Al is a disputed topic, much research has been conducted to identify mechanisms which can describe this reaction. Neglecting the effect of the surrounding n-Al particle environment is the main shortcoming in almost all previous theoretical and practical studies which describe the behaviour of an isolated aluminum nanoparticle. Three different mechanisms suggested by

Sundaram and his research group can be used to describe the combustion process of n-Al particles, which are the diffusion of material in the gaseous phase, the diffusion of material through the alumina protective layer and chemical reaction kinetics [80]. There are also other alternative mechanisms that were suggested to illustrate the combustion of n-Al, like the explosion mechanism introduced by Levitas [81]. In fact, three proposed processes characterized the combustion of n-Al: the diffusion of the material, the explosion and its kinetics. Generally, the experimental conditions in which a combustion reaction is carried out will specify the combustion mechanism of n-Al metal.

2.3.3.1 Fixed ignition temperature model

Fixed ignition temperature model is the first and simple combustion mechanism demonstrated that large Al particles cannot ignite until the temperature reaches the melting point of Al_2O_3 layer (2042 $^{\circ}$C). Hence, Al_2O_3 protective layer on the surface of Al particles will prevent the ignition process before starting in melting. After melting of alumina layer, formation of separate islands of Al_2O_3 instead of the continuous one will occur and hence, the surface of Al will be exposed to the oxidisers and ignition takes place. This specific mode is suitable and provides satisfactory results for large Al particles and will not be a good choice to sufficiently illustrate the ignition mechanism of n-Al [82, 83].

2.3.3.2 Stress in the oxide layer model

Rozenband and his research group introduced stress in the oxide layer model to illustrate the combustion mechanism of n-Al. First, the increase in mechanical stresses through the heating and melting of Al core will break up the outer alumina shell. Then the oxidisers will be in direct contact with Al, and ignition can occur. Because there is not enough information about the mechanical properties of the heated Al, there are many arguments regarding this model. The effect of the mechanical stress on the alumina layer does not appear before the melting of the pure Al shell (i.e. 660 $^{\circ}$C). At high temperature (1100 $^{\circ}$C), the mechanical stress of the alumina layer can be relaxed preventing a rupture from occurring. This model even so has many considerable discussions in its ability to properly describe the ignition process of n-Al at low temperature (500-600 $^{\circ}$C) [84].

2.3.3.3 Oxidation growth modeling

In this model, a parabolic regime describes the oxidation of Al adequately. In addition, the chemical reactions between oxidizing species of the gaseous environment control the initial oxidation increase of Al. Fedorov et al. properly described the overall oxidation growth as illustrated in equation (2) [85].

$$\frac{dt_{oxide}}{dt} = K\ (t_{oxide}) - n\ C_{ox}^{m} \exp(-\ \frac{E}{RT}) \qquad (2)$$

Where K, t_{oxide}, t,C_{ox}^{m}, m, R, n, E and T are pre-exponential factor, thickness of alumina layer, time of combustion, ratio between oxidiser concentration and pressure at the particle surface, reaction order, universal gas constant, exponent describing the relation between the oxidation rate and alumina layer thickness, activation energy, and reaction temperature respectively.

Heat released from the oxidation process can be precisely calculated based on the experimental results collected for different oxidation temperatures and compared to heat losses. In doing so, ignition of Al can be predicted by heat transfer model with enthalpy of oxidation.

2.3.3.4 Diffusion of chemical species mechanism

Wagner is the pioneer in theorizing the possible effect of alumina shell on the essential characteristics of Al [86]. Mott classified metals according to the thickness of their oxides layer into two diverse groups. Firstly, metals such as copper or iron whose oxide layer thicknesses proportionally increase with the square root of time. Secondly, metals like Al, chromium, or zinc, whose protective oxide layer, once formed, remains constant in thickness without any increase. According to Mott NF, oxidation mechanism is usually carried out by the diffusion of dissociated metal ions and electrons through alumina layer [87]. Precisely, the diffusion takes place through the motion of a vacant lattice point where positive holes will be resulted from the dissociation of the oxidizer and missing electrons, and then the positive holes will move through vacant lattice by a replacement process. Catalytic oxidation of Al occurs at the alumina/gas interface between the migrated Al atoms from the core and oxygen. This process requires a sufficient amount of energy to transfer Al ions and electrons to alumina/gas interface. Cabrera et al. assessed the possible effect of temperature on the rate of oxidation of Al. The developed model is scientifically based on the theory presented by Mott. They deduced that the rate of oxidation

increases with temperature, starting from 200 °C and reaching the maximum point at 400 °C [88, 89].

After many studies, Henz et al. found that n-Al's oxidation reaction occurs at alumina/atmosphere interface. The electric field has more effect on the diffusion process of n-Al towards the Al_2O_3 protective layer than the effect of oxide anions to the core of n-Al. They also observed that combustion of n-Al occurred if the diffused oxygen through core/shell interface reached the n-Al core [90]. Rai and his group evaluated the possible effect of temperature on the n-Al oxidation process using TEM. They discovered that above 800 °C, hollow n-Al_2O_3 instantaneously formed. Finally, Rai et al. reported that the catalytic oxidation of n-Al occurs in two steps, starting with diffusion of oxygen into solid Al and then diffusion of both oxygen and Al melts. They also introduced a relation between n-Al's oxidation time and its radius in what is called power law. This law takes into account the potential effect of pressure exerted by the n-Al core on the alumina layer [91]. Figure 2-4 demonstrates the behaviour of diffusion oxidation mechanism.

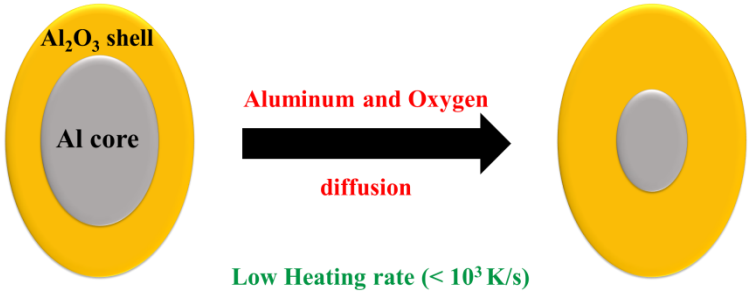

Figure 2-4 Diffusion oxidation mechanism [92]

2.3.3.5 Explosion mechanism of n-Al oxidation

Wang et al. illustrated the dynamic effect of the alumina layer on the combustion mechanism of n-Al. They used in their extensive investigation n-Al with average particle size of 60 nm and effective Al_2O_3 thickness of 3-6 nm. They proved that there is a linear relationship between the distance at which the effect of n-Al reaction is observed and the amount of absorbed energy. They also noted that the Al_2O_3 layer has an important role in the explosion mechanism of n-Al, if the effective temperature is sufficiently high to burst the core/shell structure [93]. Levitas and his group studied the oxidation mechanism through the dispersion of molten Al to illustrate

properties of nanothermite compositions. They believed that diffusion of Al and oxygen through the alumina layer is preferable due to the high increase in temperature and pressure of the reaction front of nanothermites. They also noticed, for n-Al with particle size less than 40-50 nm, the flame propagation velocity and the ignition delay time of nanothermites will be independent on the size of Al particles[81]. This conclusion led to the development of the mechanochemical model which accurately describes the possible reaction of n-Al at high heating rates [94]. Figure 2-5 clarifies how the explosion mechanism of n-Al occurs.

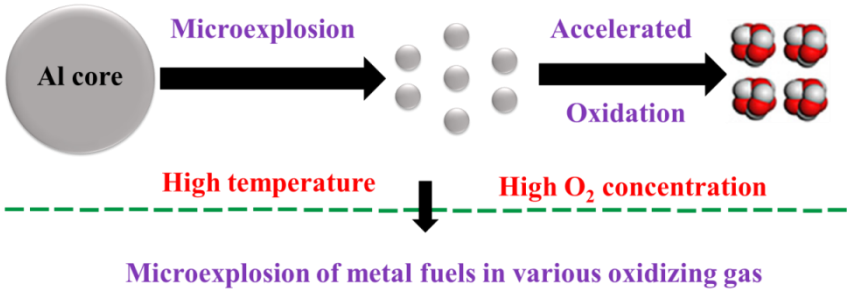

Figure 2-5 Explosion mechanism of n-Al oxidation [92]

2.3.3.6 Melt dispersion mechanism

Melt dispersion mechanism (MDM) currently represents the most suitable mechanism to illustrate the reactivity of n-Al compositions, especially nanothermites. First, Al core melts at fast heating rate (10^7–10^8 °C/s) and the melting process is accompanied by a 6% of volume expansion which produces very significant pressure (0.1–4 GPa) leads to dynamic spallation and breaking the alumina layer. Then, the Al_2O_3 layer is cracked and ejected in the form of fragments is accompanied by pressure drop (10 MPa) on the surface of liquid Al. After that, the pressure difference on the Al surface will yield a shock wave that propagates to the core of the n-Al particle. Finally, Al particle will divide into smaller particle which propagate with a velocity of 100–250 m/s and the oxidation reaction will not be affected by the diffusion process [95]. Campbell et al. simulated the oxidation process of n-Al (20 nm) in an oxygen environment and temperature of 300 K through molecular dynamic simulation. They found that final thickness of the alumina layer reached 3.3 nm within 0.1 ns [96]. Bazyn et al. investigated the combustion process of n-Al with average particle of 80 nm. They calculated the combustion time of n-Al caused by reflecting shock waves in a shock tube by measuring the intensity of light of the

reacting materials. They also found that the combustion time of n-Al in a mixture of oxygen and nitrogen with equal ratio decreases with proportionately increasing both temperature and pressure of gas. At elevated temperature (~ 1600 K), the effect of pressure on the combustion time was negligible compared with temperature. Bazyn et al. applied MDM under their experimental conditions and they found that applied conditions affected the distance travelled by n-Al (10^{-7} - 10^{-3} m) before its complete oxidation [97]. Figure 2-6 illustrates the sequence of MDM combustion mechanism.

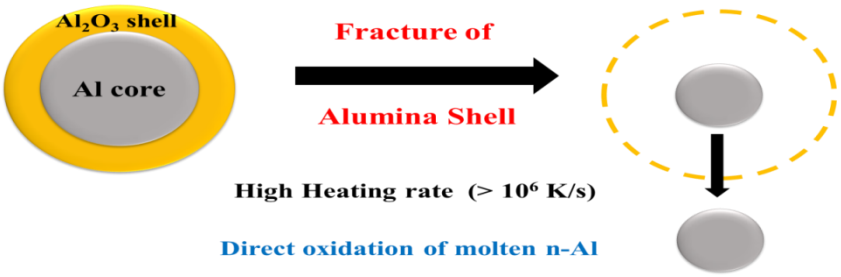

Figure 2-6 Melt dispersion mechanism [92]

In nanothermite compositions, the n-Al is typically covered by the alumina layer and surrounded by the air filling the pores in the composite structure. While catalytic oxidation of 1 cm^3 of n-Al under normal pressure and temperature requires about 1.2 L of air, at the reaction temperature of nanothermite, the volume of air increases approximately 10 fold. Hence, the air in nanothermite pores will produce a slight effect on the overall reaction and Prentice et al. clarified this behaviour in n-Al and tungsten oxide nanothermite composition [98].

Water also plays an important role in nanothermite reaction, which simply comes from the atmospheric humidity. Tappan et al. studied the combustion velocity of mixtures of n-Al with different particle sizes and water. They concluded that n-Al and water mixture reacts at the gas phase and the elimination of the proton of water is the limiting step in the reaction kinetics [99]. Given the finding by Tappan and Risha, MDM cannot be applied on n-Al and water compositions.

2.4 Nanothermite oxidisers

Metallic oxidizer and, conventionally, n-Al fuel are the main components of nanothermites. Earlier research on nanothermite field focused on metallic oxides like iron oxide (Fe_2O_3, FeO),

copper oxide (CuO), silver oxide (Ag_2O) and bismuth oxide (Bi_2O_3). Recently, studies have shifted towards oxygenated salts or oxygenated metal salts in order to develop nanothermites with superior reactivity. Oxidisers can be used either in micro or nano scale particles. The main oxidation-reduction reaction of nanothermite occurs between the metal fuel and generated oxygen from the decomposition of oxygenated salts or metal oxides, which are reduced to original metal or metal salt. Although, metal sulphide and fluoride can be used theoretically as oxidiser, it has not been utilized in the form of nano-structured oxidiser in nanothermites preparation.

Oxidizing agents for nanothermite preparation are usually oxygen-rich ionic solids, which at elevated temperature decompose and release their oxygen. There are some consideration in selecting the employed oxidizers such as being in suitable pure form, availability of different particle sizes, and cost. Moreover, they should be stable over a broad range of temperature, not react with humidity, and easily decompose to liberate their oxygen [59].

2.4.1 Metallic oxidisers

When we consider inorganic chemistry, we find a wide variety of metal oxides. However, can any metal oxide be properly used in the preparation of nanothermite composition? The direct answer is no, because highly reducing metal such as alkaline or alkaline earth elements can easily form oxides. These oxides are extremely stable in normal conditions and consequently they do not apply in the preparation of nanothermites. Electronegativity of the metals classifies those suitable for nanothermite formulations. Therefore, metals with electronegativity between 1.5 and 2.5 on the Pauling scale are the best choices for nanothermite mixtures. Fischer and his group arranged thermites and energetic compositions based on their thermochemical characteristics [100].

As we mentioned before, the most commonly used metallic oxidisers for nanothermite compositions are Bi_2O_3, CuO, Fe_2O_3, MoO_3 and WO_3. Here, we will highlight general properties of some nanothermite mixtures based on these oxides.

Weismiller et al. properly investigated the influence of particle dimensions of nanothermites constituents (Al/CuO and Al/MoO3) on their performance. They concluded that nanothermites contain both fuel and oxidiser in nanostructure form offered high combustion rate. Moreover, the

effect of nanostructured metallic oxidant causes the more significant outcome on the combustion performance than n-Al. The reduction of nanothermite performance is ascribed to the significant amount of Al_2O_3 cover on n-Al surface and cause the dilution of the overall mixture that yields incomplete combustion. On the other hand, nanostructured oxidizer leads to the liberation of its oxygen easily through oxide sublimation in MoO_3 or decomposition in CuO. In addition to the easy liberation of oxygen, the diffusion distance of gaseous products will decrease and totally enhanced the nanothermite reactivity [101].

Puszynski summarized and reviewed the combustion characteristics of nanothermite compositions based on different metallic oxidizers like Bi_2O_3, CuO, MoO_3 and WO_3 and various n-Al particles. He found that the highest combustion rate of nanothermite compositions were achieved with n-Al particle size in the range of 50-80 nm [102].

Puszynski et al. examined the combustion performance of nanothermites based on n-Al (40 nm) and metallic oxidizers (Bi_2O_3, CuO, and MoO_3) with analogous particle size using pressure cell and DSC. Direct results from pressure cell analysis demonstrated that Al/Bi_2O_3 sustains higher dynamic pressure than Al/MoO_3 and Al/CuO respectively [103]. Recently, Glavier and his research group looked at the maximum pressure and the pressurization rate for the same nanothermite compositions studied previously by Puszynski et al. In their investigation, they used pressure cell analysis and compressed nanothermite pellets at different percentages (10, 30 and 50 %) of their theoretical maximum density (TMD). Nanothermites based on Al/CuO and Al/Bi_2O_3 compressed at 30 and 50 % exhibited the maximum pressure and pressurization rate respectively [104].

Sanders et al. reported that burning rate of metallic oxide was enhanced greatly in closed environment compared to an open one. They found that combustion of loose powder Al/Bi_2O_3 and Al/MoO_3 is more rapid than pellets [105]. Trebs et al. examined theoretically the possible effect of humidity on the pressure output of aluminothermic compositions reported by Sanders et al. They concluded that water content changed pressure signals produced by these nanothermites significantly due to their acute sensitivity to humidity [106].

Jian et al. examined the ignition behaviour of metallic oxide nanothermite mixtures and classified it into three groups. First, compositions which ignite before release of oxygen from oxidizers

such as Al/Bi_2O_3 and Al/SnO_2. Second, mixtures that react after the liberation of oxygen like composition based on Al and Co_3O_4. Third, nanothermites that ignite without release of oxygen for example Al/WO_3 and Al/MoO_3. The reason behind the ignition of compositions in the first and the third case can be reasonably related to the direct contact between the fuel and oxidizer [23].

2.4.2 Oxidizing salts

Goldschmidt, a pioneer in the field of thermites, initially used metal oxides and Al as a fuel [107]. Research in the field of EMs is now directed at oxygenated salts as oxidizers for nanothermite compositions to enhance their performance. EMs based on oxidizing salts have a variety of practical uses in the field of solid propulsion and micro energetic systems. For example, a mixture of Al and ammonium perchlorate (NH_4ClO_4) propels the booster stage of the Ariane V rocket. Though developed over a century ago, ammonal is still employed as an explosive with little sensitivity to priming [108]. There are limited investigations in the field of nanothermites based on oxidizing salts, so further examination is warranted.

Oxidizing salts are more useful than metallic oxides due to their significant content of oxygen, ease of decomposition, readily release of oxygen, and low oxidation state which increases their reactivity [28]. The most used oxygenated oxidisers in nanothermites formulations are chlorates, perchlorates, nitrates, iodates, periodates, bromates, permanganates, peroxides, superoxides and persulphates [55].

Armstrong was one of the first to study the combustion velocity of aluminothermic compositions based on n-Al and NH_4ClO_4 using pressure cell analysis. He found that combustion velocity and pressure, respectively, increased from 25 mm/s at 0.14 MPa to 600 mm/s at 15 MPa as Al particle size decreased from 200 nm to 40 nm [109].

Potassium permanganate (KMnO4) is one of the best oxidizing agents for pyrotechnic compositions. Because of its high oxidising power and low toxicity, it can be reliably used in the development of nanothermites with superior performance without significant environmental harm. Prakash et al. explored the pressurization rate of n-$Al/KMnO_4$ nanothermite using pressure cell, demonstrating that $Al/KMnO_4$ has a pressurization rate double that of CuO/Al and MoO_3/Al

nanothermites [110]. The main drawback of $KMnO_4$ compositions is the instability in contact with humidity, acids and organic materials. Aging of energetic compositions based on $KMnO_4$ occurs in the presence of humidity due to the rapid transformation of $KMnO_4$ to manganese dioxide (MnO_2). Moreover, self-ignition may naturally occur to these compositions when unintentionally in contact with organic materials, like glycerine or oxalic acid. Prakash and his research group succeeded to solve the instability of Al/$KMnO_4$ nanothermite by coating $KMnO_4$ with ferric oxide (Fe_2O_3). They concluded the reactivity of the new composition can be adjusted by varying the percentage of Fe_2O_3 [111].

Wu et al. encapsulated potassium perchlorate ($KClO_4$) by Fe_2O_3 and CuO individually using the same method described in [111]. Firstly, Fe_2O_3 successfully coated $KClO_4$ with excellent core-shell structure. CuO, which is supposed to be only in the shell, mixed with some $KClO_4$ that in turn disturbed its crystallization. Finally, Wu and his research group succeeded to coat $KClO_4$ with Fe_2O_3 and the successful product was in the form of hollow particles; the composition of the shell comprised a mixture between $KClO_4$ and Fe_2O_3. Nanothermite based on $KClO_4$/Fe_2O_3 and n-Al (50 nm) has higher performance and energy output than Al/CuO and Al/Fe_2O_3 alone. In general, nanothermite based on perchlorates typically has higher pressurization rate and maximum pressure compared to those with metallic oxides alone. The previous behaviour can be justly attributed to lower decomposition temperature for $KClO_4$ than Fe_2O_3 and CuO and hence earlier oxygen release, resulting in enhanced reactivity of the exothermic reaction [24].

Coating of perchlorate with metal oxides decreases its susceptibility to humidity and consequently limits its adverse effect on the surrounding environment. Despite this, (ClO_4^-) anions affect endocrine glands even in very small quantities. National Academy of Sciences reported that maximum daily safe absorbed amount of (ClO_4^-) is 0.7μg/kg. The potential danger of the (ClO_4^-) comes from its toxicity, which can be easily fixed, on a glycoprotein. The essential role of glycoprotein is transporting iodine across the basolateral membrane of the thyroid cells and consequently disturbs the production of hormones in the thyroid [112]. Subsequently, many published studies have been directed towards the replacement of perchlorates by periodates as a friendly environment oxidizer [31, 33].

The replacement of perchlorate salts by periodates in nanothermites was studied by Sullivan et al., who compared between the performance of nanothermite based on silver iodate ($AgIO_3$) and

those based on CuO. The reactivity of periodate compositions was higher than compositions based on metallic oxides. While Al/$AgIO_3$ achieved 57 psi/µs in a combustion time of 172 µs, Al/CuO attained 9.0 psi/µs in 192 µs. More gas release in the case of $AgIO_3$ than CuO is the reason in the elevation of Al/$AgIO_3$ pressure. The reaction mechanism of Al/$AgIO_3$ is clarified in Figure 2-7 [31].

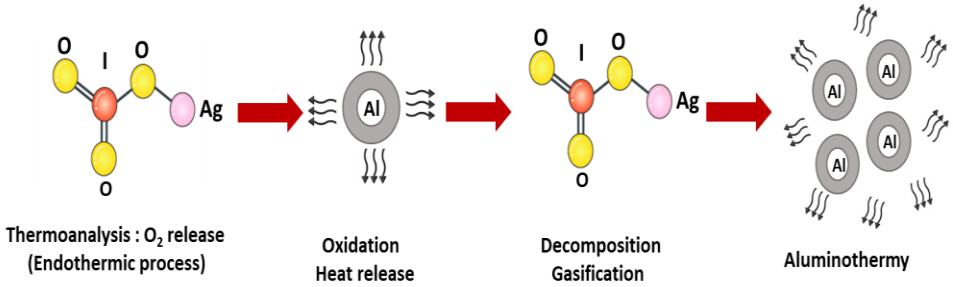

Figure 2-7 Schematic diagram of reaction mechanism of Al/$AgIO_3$ nanothermite

Also, they reported that heating rate affects the decomposition behaviour of $AgIO_3$. First, at a small heating rate (5 K/min), $AgIO_3$ melts at 692 K, then it decomposes into silver iodide (AgI) and oxygen releases at 740 K, finally AgI melts at 827 K and evaporates. Second, at a high heating rate ($5*10^5$ K/s), the gaseous species were detected at higher temperature (1150 K) than in the first case (740 K); AgI and Ag are unnoticed in the gaseous phase. Lastly, they concluded that ignition of Al/$AgIO_3$ nanothermite in the case of high heating rate occurs approximately at 1245 K which is merely above the $AgIO_3$ evaporation temperature. Based on the previous results, researchers hypothesised that ignition of Al is greatly dependent on oxygen partial pressure [31].

Jian et al. studied the combustion behaviour of nanothermites based on n-Al, sodium and potassium periodates ($NaIO_4$ & KIO_4) individually, using pressure cell analysis. Results demonstrated that rate of pressurization of these compositions greatly increased and reached to 2.4 - 2.6 MPa/µs compared with 0.06 MPa/µs for Al/CuO. Ignition temperature recorded at 880 K, 950 K and 1040 K for Al/$NaIO_4$, Al/KIO_4 and Al/CuO respectively. Furthermore, they detected that decomposition of KIO_4 occurs in two stages. Initially, KIO_4 decomposes exothermically to KIO_3 and oxygen. Next, KIO_3 is reduced at higher temperature to potassium iodide (KI) and oxygen. While nanothermite based on KIO_4 reacts strongly in both air and argon environment, KIO_4 decomposes without reacting with Al in a vacuum chamber at high heating

rate (106 K/s). Based on these results, it was concluded that oxygen has a crucial role on ignition and combustion of periodate nanothermites [33].

Recently, Zhou and their research group compared between the combustion performance of nanothermites based on n-Al (50 nm), potassium sulphate (K_2SO_4), potassium persulphate ($K_2S_2O_8$) and KIO_4 individually. Al/$K_2S_2O_8$ introduced the highest maximum pressure and pressurization rate on the pressure cell analysis. Moreover, they illustrated that $K_2S_2O_8$ decomposition occurs in three stages. At the first stage, $K_2S_2O_8$ converted to pyrosulfate ($K_2S_2O_7$) and released oxygen, followed by decomposition of $K_2S_2O_7$ into K_2SO_4, oxygen and sulphur dioxide (SO_2) with increasing the temperature. Finally, at higher temperature, K_2SO_4 decomposes into oxygen and SO_2. At the end, Zhou et al. found that $K_2S_2O_8$ and K_2SO_4 exhibit diverse behaviour. First, ignition of Al/$K_2S_2O_8$ happens between Al and oxygen released from $K_2S_2O_8$ decomposition. Second, ignition of Al/K_2SO_4 takes place by the condensed phase reaction between Al and K_2SO_4 like most nanothermites based on metal oxides [28].

In conclusion, nanothermites based on oxidizing salts reveal improved performance over those with metallic oxides. The significant reactivity of these aluminothermic compositions is ascribed to the fast release of high amount of oxygen at the early stage of oxidizer decomposition reaction.

2.5 Carbon nanomaterials and energetic compositions

Lately, carbon nanomaterials (CNMs) are being used as enhancement additives in EMs. CNMs have caught attention due to superior optical, hardness, electrical conductivity, radiation, high surface area, and interface properties. In addition, they can be adequately prepared in various shapes, crystal forms, and sizes. Graphene oxide (GO), reduced graphene oxide (RGO), and carbon nanotubes (CNTs) are considered the most promising candidates for EMs like nanothermites, solid propellants, and gas generators. The preference of GO and CNTs results from their significant catalytic properties in addition to simple preparation methods. Here, we will briefly review the potential effect of CNMs, especially GO and CNTs on combustion properties of EMs.

2.5.1 Preparation methods of GO

Several approaches can be taken to prepare graphene oxide. Generally, the preparation of GO occurs in two steps, starting by oxidation of graphite followed by removal of impurities from oxidizing material as illustrated in Figure 2-8.

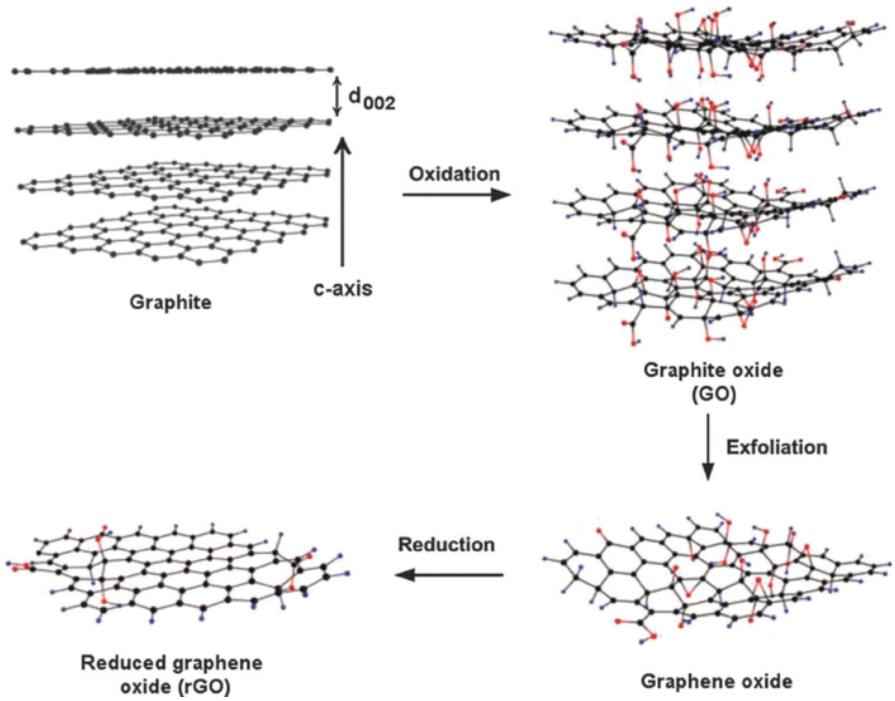

Figure 2-8 Preparation steps of GO [113]

The first preparation method of GO was described over a century ago by Brodie where he used potassium chlorate ($KClO_3$) and fuming nitric acid (HNO_3) as an oxidising agent [114]. Brodie's approach has many disadvantages such as long reaction times and production of toxic fumes. Hummers and Offeman in 1958 successfully developed another preparation process of GO where they used sulphuric acid (H_2SO_4), sodium nitrate ($NaNO_3$) to activate graphite and $KMnO_4$ as an oxidiser [115]. Lately, Tour's research group improved Hummers' method through decreasing the amount of $NaNO_3$, substituted by increasing the quantity of $KMnO_4$. They performed the reaction using a molar ratio of 9:1 of H_2SO_4 to phosphoric acid (H_3PO_4) instead of H_2SO_4 alone [116, 117]. The colour of GO gradually turns darker under normal storing condition and this is an indication of its transformation to reduced graphene oxide (RGO). In general, Hummers' method is the most widely used in the preparation of GO.

2.5.2 EMs based on GO and RGO

Compared to other CNMs, GO is considered the worthiest candidate to be integrated in EMs due its energetic nature. GO decomposes exothermically because of the oxygenic functional group on its structure accompanied by liberation of oxygen. GO and RGO are typically used to enhance the combustion properties of EMs. For example, Zhang et al. evaluated the effect of doping NC by GO at different percentages (0.1, 0.5, 1 and 2 wt. %) on its ignition characteristics. They found the addition of GO increased the burning rate of NC and decreased the laser ignition temperature. GO is not only used in enhancing the burning rate of EMs, but also to decrease sensitivity of the energetic crystals as in the case of HMX desensitization [118].

Nasir and his colleagues investigated the potential effect of nanocomposite material based on AP and GO on the combustion of composite propellant. They used a recrystallization method to synthesis AP/GO, then integrated with hydroxyl-terminated polybutadiene (HTPB) composite propellant and as a result burning rate increased by 15 % [119].

Functionalized graphene sheets (FGS) were successfully used to prepare GO/Al/Bi_2O_3 nanothermite in a self-assembly method. GO was added with different quantities from 1 wt. % to 10 wt. %. Self-assembled GO/Al/Bi_2O_3 achieved higher energy output than those of randomly mixed. Addition of GO increased the energy released from 739 to 1421 J/g. This energy enhancement can be reasonably attributed to the active role of GO as energetic reactant and the benefits from FGS method [120].

Ning et al. introduced RGO with different percentages on Al/Fe_2O_3 nanothermite using an atomic layer deposition method. They found that 4.8 wt. % of RGO improved heat release of Al/ Fe_2O_3 by 130 %. This enhancement in the energy can be ascribed to the increase in interfacial contact between the fuel and oxidiser and enhancement of reactant mass diffusion [121].

Ping et al. successfully prepared nanocomposite materials based on different metallic oxides (CoO, CuO and Fe_2O_3) and graphene. Graphene based composite materials showed good catalytic activity on thermal decomposition of $KClO_4$, with the best performance achieved by CoO/graphene. This enhancement is due to the catalytic effect of graphene, good electrical and thermal conductivity and large specific area. Those properties of graphene improve the adsorption and reaction between products and catalytic active sites and as a result enhance

thermal decomposition of $KClO_4$ [122]. Table 2-1 summarizes some applications of graphene, GO and RGO based energetic materials and their preparation methods.

Table 2-1 Different applications and preparation methods for energetic materials based on graphene, GO and RGO

Compositions	**Synthesis method**	**Applications**	**Reference**
Graphene/ Fe_2O_3/NH_4ClO_4	Sol–gel method and supercritical carbon dioxide drying technique	Propellants	[123]
Graphene/ NH_4NO_3	Sol–gel and supercritical CO_2 drying method	Propellants Nanothermite	[124]
CL-20/GL/RGO	emulsion polymerization and mixing methods	Energetic compositions	[125]
$Al/Bi_2O_3/GO$	Formed in a colloidal suspension phase that ultimately condenses into ultra-dense macrostructures	Nanothermite	[120]
NH_4NO_3/Graphene	Sol–gel method	Propellants	[123]
HMX/GO	Solvent– non solvent method	Propellants and explosives	[118]
GO/NC	Mixing pure NC– acetone solution and various weight ratios of GO water solution	Propellants	[126]
GO/FOX-7	Self-assembly impregnation in N-methyl-2-pyrrolidone at 100–110 °C	Explosives and propellants	[127]

2.5.3 EMs based on CNTs

Carbon nanotubes are typically a rolled sheet of graphene. CNTs can be found either in the form of single wall (SWCNTs) or in multi-walled (MWCNTs). While SWCNTs have a diameter in the

range of 0.4 nm, MWCNTs form with approximately 2-30 concentric tubes, positioned one inside another and have an outer diameter around 5-100 nm [38]. A schematic diagram illustrates the formation of both SWCNTs, and MWCNTs from an individual layer of honeycomb-like carbon is shown in Figure 2-9.

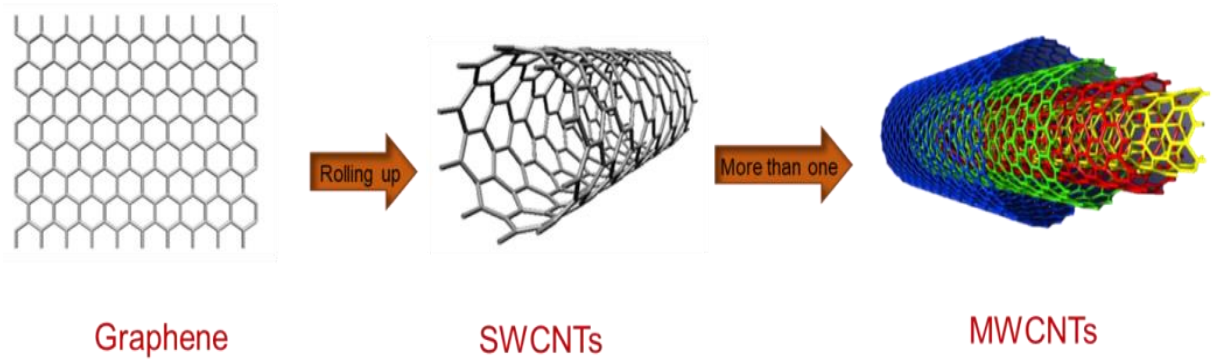

Figure 2-9 Schematic diagram of formation SWCNTs and MWCNTs from graphene

Carbon nanotubes integrate with EMs through functionalized polymer binder or combined directly with pyrotechnic compositions and metal fuels. They are used as a combustion catalyst carrier and recently have been functionalized with energetic groups. CNTs can be used as an analogue of GO in enhancing the combustion properties of energetic compositions and increase their heat generation. Qian et al. were the pioneer in combining CNTs with pyrotechnic formulations based on $KClO_4$ and KNO_3 in an attempt to increase burning rate of these compositions. They succeeded in their objective, and CNTs quadrupled the reaction rate of $KClO_4$ [128]. Also, CNTs were used to improve the radiation energy of $Zr/KClO_4$ and it was found that with only 0.5 wt. %, the energy release of the pyrotechnic composition increased to 1830 J/g [129]. Moreover, Sylvain et al. developed flash ignitable EMs with superior combustion characteristics by integrating CNTs with metal fuels such as (Al, Zn, Fe, Ni and Cu) [130]. Manjula Sharma and Vimal Sharma studied the beneficial effect of CNTs on the thermite reaction of Al/CuO. They observed a remarkable decrease in ignition temperature and activation energy where both of them lowered by 71 $^{\circ}$C and 23 % respectively. Also the reaction enthalpy became 13 times higher than reference with addition of 15 wt. % CNTs [131]. Table 2-2 summarizes the practical application and preparation method of EMs based on CNTs.

Table 2-2 Different applications and preparation methods for energetic materials based on CNTs

Materials	Preparation method	Applications	Reference
KNO_3/CNTs	mechanically mixing and grinding to nano size	Energetic initiator	[132]
Zr/$KClO_4$/CNTs	By grinding a mixture of Zr and $KCIO_4$ for 20 min	Pyrotechnic reagent	[129]
CNT/BAMO-AMMO	Using CNT-OH as a crosslinking agent, covalently modified BAMO-AMMO	Energetic binder	[133]
Fe_2O_3/MWCNTs	By mild and superior physical absorption method using molten $Fe(NO_3)_3 \cdot 9H_2O$ as the precursor	Thermites and pyrophoric substrates	[134]
GAP/CNTs binder films	Using hydroxylation CNTs as crosslinking agent, GAP as prepolymer, TDI as curing agent	Propellants, PBXs	[135]
Al/CNT composites	Al/CNT mixture was engineered by mechanical pulverization	Thermites and propellants	[136]
CuO/CNTs	Using sol-infusion method under normal pressure and low temperature (at 100 °C)	Catalyst for propellants	[137]
HMX/CNTs	Prepared with an ultrasonic compositing method	Energetic compositions	[138]
Al/Teflon/CNTs	By blending of Al with Teflon and CNTs	Explosives and propellants	[139]

2.6 High-energy metal–organic frameworks

Although many extensive works have been performed to develop and enhance the performance of nanothermites, some potential problems like the incomplete combustion of n-Al still exist.

Incomplete combustion of n-Al is due to the excessive oxidation of Al before combustion, which in turn decreases the active Al content. In addition to the incomplete combustion of Al, nanothermites have toxicity problems as they release dangerous products from some of their primary components. Recently, researchers have directed much effort to prepare new thermite compositions free of Al to overcome these problems and produce more sustainable products.

In order to achieve this objective, high-energy metal–organic frameworks (EMOFs) will be an important alternative fuel to Al in preparing new thermite compositions with superior combustion properties. Superiority of EMOFs resulted from their great detonation heat due to organic ligands with high energy density. In addition EMOFs produce large amount of gas, have good stability, high surface area, controllable structure and uniform pore size [140]. There are three distinct types of EMOFs (1D, 2D and 3D); each of them has its own energetic behaviour where 3D EMOF maintains the best performance.

2.6.1 One-dimensional EMOFs

There are many types of one-dimensional EMOFs (1D EMOFs); here, some will be discussed. Thomas M. Klapötke was the first researcher to report 1D EMOF (1D zig-zag chains linked through the bta^{-2} ligands) (compound 1) based on (H_2bta = bis(tetrazolyl)amine),$Cu(bta)(NH_3)_2 \cdot H_2O$ ligand with high nitrogen content (N% = 61.66 %), and density (1.9882 g/cm^3) as shown in Figure 2-1. He used ICT thermodynamic code to calculate thermochemical properties of this 1D EMOF such as enthalpy of formation, free activation energy, entropy of activation, among others. Furthermore, sensitivity tests have been performed such as impact and friction tests [141].

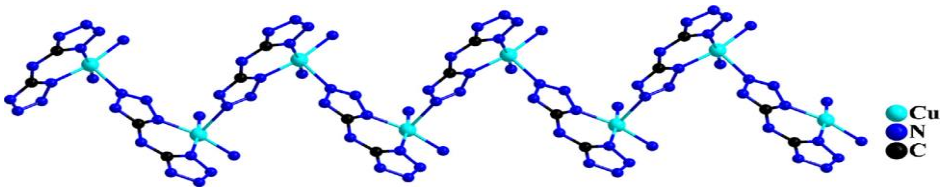

Figure 2-10 Zigzag chain of compound 1

Also, Shreeve adequately prepared [[Ag(MHT)].H_2O] (compound 2). Structure of compound 2 which has density of 2.47 g/cm^3, enthalpy of formation (−263 kJ/mol), (N% = 73.65 %) and impact sensitivity > 40 J is illustrated in Figure 2-11[142].

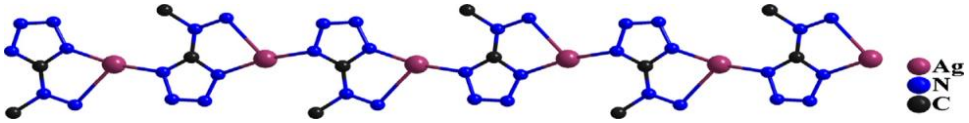

Figure 2-11 Structure of compound 2-1D EMOF

Oleksandr S. Bushuyev and his research group reported three distinct types of 1D EMOFs based on hydrazine complexes and non-coordinating anions like perchlorate or nitrate. Those 1D EMOFs based on (ClO_4^-) are nickel or cobalt hydrazine perchlorate (NHP & CHP), while those based on (NO_3^-) are nickel hydrazine nitrate (NHN). However, while these 1D EMOFs retain high heat of detonation comparable to explosive materials such as CL-20, PETN, RDX, MF and lead azide, they suffer from highly sensitivity to flame, spark, and impact, which decrease their commercial use.

2.6.2 Two-dimensional EMOFs

The considerable increase of energetic applications led to exploration of advanced 2D EMOFs. B.D. Wu et al. prepared two dimensional EMOFs (2D EMOFs) based on Cu and 1,2-diaminopropane (pn) azide ($[Cu(pn)(N_3)_2]_n$ or compound 14) as demonstrated in Figure 2-12.

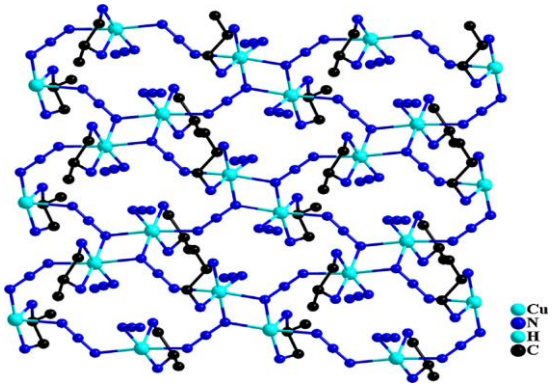

Figure 2-12 Compound 14 2D EMOF

Nitrogen content, density and heat of combustion of Compound 14 are 50.54 %, 1.762 g/cm^3 and -4.43 MJ/kg respectively. Also, compound 14 is insensitive to external stimuli [143].

Two-dimensional Cd^{II} EMOF (compound 16) with high nitrogen content and density (N% = 63.42%, 2.144 g/cm^3) was prepared by Z. Tang et al. Cadmium is the metal base of compound 16 and 1,5-diaminotetrazole (DAT) is its ligand.

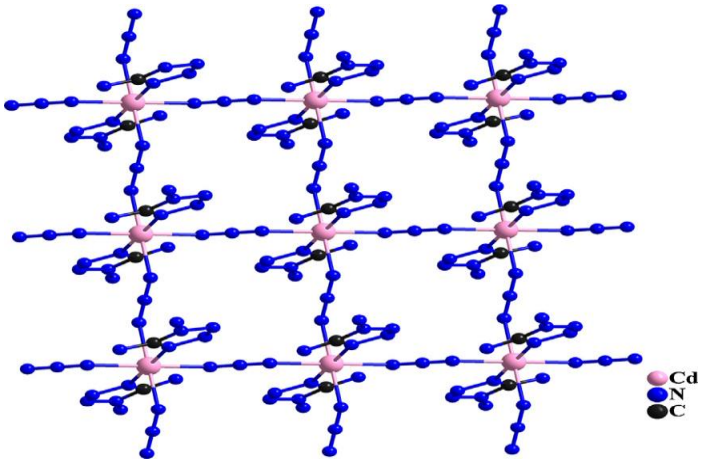

Figure 2-13 Two zigzag chains linked by azido ligands form $[Cd(DAT)_2(N_3)_2]n$

Recently, X. Liu and collaborators prepared high energetic 2D EMOF (compound 24). It was prepared by hydrothermal reaction between high nitrogen content ligand, 3-(1H-tetrazol-5-yl)-1H-triazole (H_2tztr) and Cu(II)/Cu(I) as clarified in Figure 2-14.

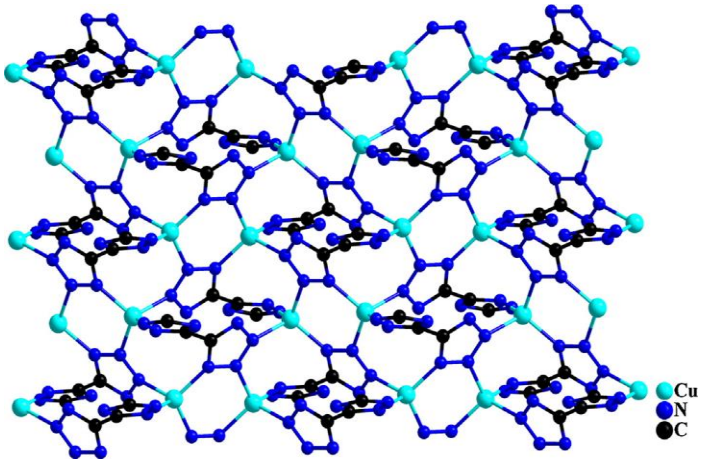

Figure 2-14 Structure of [Cu(Htztr)]n 2D EMOF

Compound 24 has nitrogen content (% N = 49.08 %), density (2.435 g/cm^3) and exhibits heat of detonation (3.9582 kcal/g), detonation velocity (10.4 km/s) and thermal stability (355 $^{\circ}$C). The high nitrogen content and rigid structural framework of compound 24 2D EMOF results in greater heat of detonation than even that of explosives like CL-20 and ONC.

2.6.3 Three dimensional EMOFs

Structural reinforcement and complicated connection modes are the characteristics distinguish three-dimensional EMOFs (3D EMOFs). S. Li et al. properly prepared the most recent two 3D EMOFs with superior heat of detonation. They used 4,4'-azo-1,2,4-triazole (atrz) as organic framework ligand and either Cu or Ag as a metal base. While compound 31 (ATRZ-1) prepared by hydrothermal reaction between artz and Cu, compound 32 (ATRZ-2) used Ag instead of Cu with the same ligand. Figure 2-15 illustrates porous structure of compound 31 and 32 respectively.

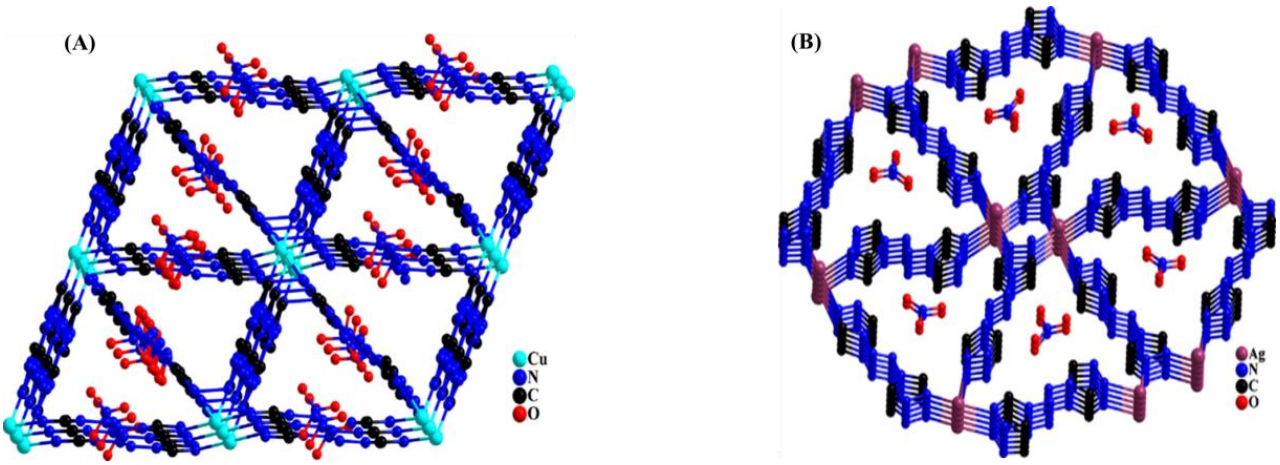

Figure 2-15 Structure of (A) compound 31 and (B) compound 32 3D EMOFs

Compound 31 and 32 are distinguished by their porous structure, high density (1.68 and 2.16 g/cm^3) and superior thermal stability (243 and 257 $^{\circ}$C). Furthermore, they exhibit lower sensitivity toward different stimuli than 1D and 2D EMOFs. Heat of detonation of compound 31 is 3.62 kcal/g, which is the highest heat of detonation of all prepared EMOFs, even higher than of those explosives (CL-20, ONC….etc.) [144].

The unprecedented 3D EMOF $[Cu_4Na(Mtta)_5(CH_3CN)]_n$ (compound 35) has the second highest heat of detonation after compound 31. It has been synthesized by the reaction between 5-methyl tetrazole (Mtta) as ligand and Cu (I) as a metal as shown in Figure 2-16.

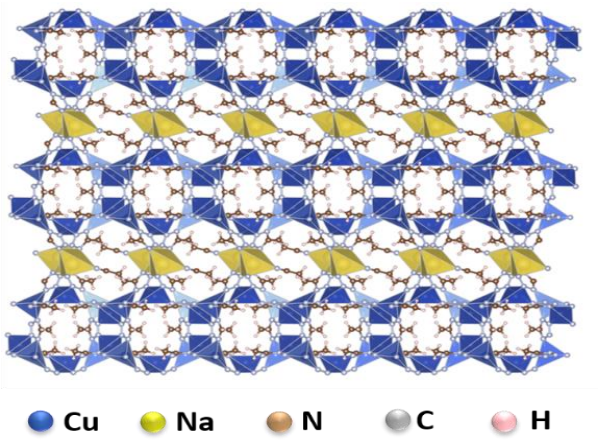

Figure 2-16 Structure of compound 35 3D EMOFs

Compound 35 typically has high nitrogen content (% N = 40.08 %), with impact and friction sensitivity lower than TNT and RDX. It retains heat of detonation (2.3657 kcal/g) and classified as the second best performing EMOF after $[Cu(atrz)_3(NO_3)_2]_n$. In addition to its excessive heat of detonation, it has high explosion velocity 7.225 km/s, comparable to those of TNT and PETN (6.881 km/s and 8.564 km/s respectively). Direct comparison between heat of detonation of different EMOFs and general explosives is illustrated in Figure 2-17 [145].

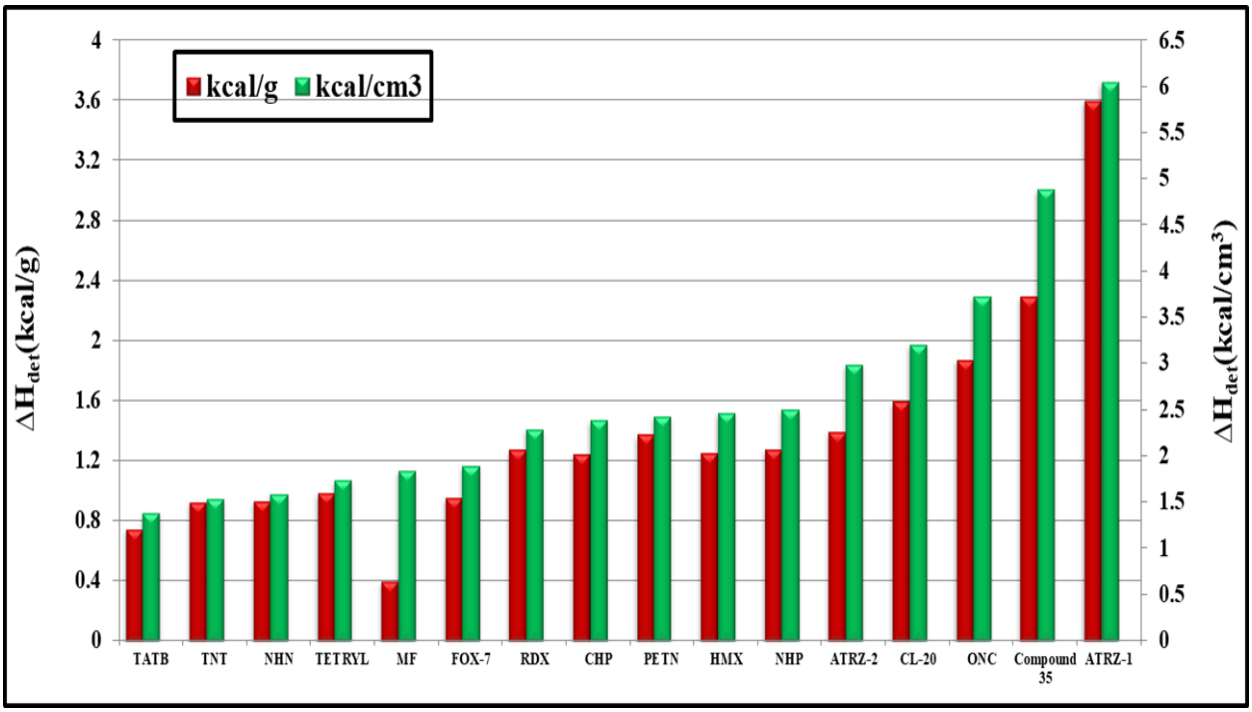

Figure 2-17 Bar chart of heat of detonation of EMOFs and general explosives

Literature in the field of nanothermite based on EMOFs is not very extensive. Shenghua Li and his research group reported new thermite material depended on ATRZ-1 EMOF as an effective fuel instead of Al and both NH_4ClO_4 and $KClO_4$ as oxidizers individually. This specific type of thermite exhibited good results in both sensitivity and performance tests [146]. Furthermore, this research group investigated the beneficial effect of periodate salts like KIO_4 and $NaIO_4$ as oxidizing agents instead of perchlorates with ATRZ-1 EMOF on thermite behaviour. They found thermite based on EMOFs and periodates salts revealed considerable potential as a green secondary gas generator in future applications with preferable combustion and sensitivity characteristics [147].

2.7 Synthesis of Nanothermites

Nanothermites can be synthesized by different preparation techniques. Preparation methods of nanothermites are divided into two main classifications. The first category is called bottom-up technique, where the fuel and oxidiser in nanometer scale are used as a building block for nanothermite compositions. Second, top-down approach, is based on breakdown of relatively coarse fuel and oxidizer to a smaller size. Figure 2-18 clarifies the general methods used to prepare nanothermites[73].

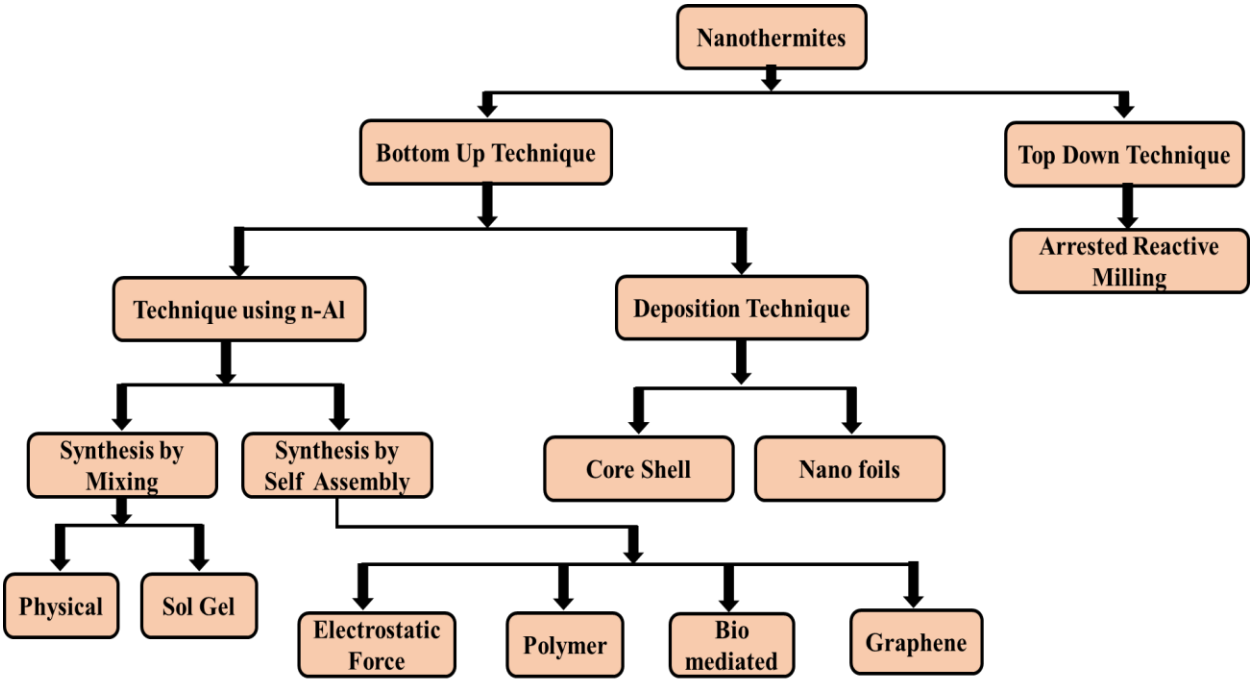

Figure 2-18 Classification of nanothermite synthesis methods

We will focus on the ultrasonic nanopowder mixing because it is the most common and simplest method to prepare nanothermite.

2.7.1 Ultrasonic nanopowder mixing

The most essential characteristic of the ultrasonic preparation method of nanothermite is its exceptional ability to fabricate nanothermite in large quantities (on order of kilograms) and hence achieve a variety of application demands. In this method, components of nanothermite are dispersed in a liquid by ultrasonic agitation for a certain period, and then the solvent is removed by drying under reduced pressure or in an oven for several hours. The intended target from ultrasonic mixing with a liquid is to prevent the aggregation of nanoparticles by decreasing or cancelling the surface forces between the nanoparticles. For this reason, separation of the particles from each other will occur and achieve a homogeneous mixing as much as possible. There are some attributes that need to be met for the dispersive liquid medium such as compatibility with nanothermite components, non-toxic, low boiling point for fast evaporation after mixing and proper dispersing properties. Table 2-3summarizes the properties of the most commonly used solvents in nanothermite preparation [32].

Table 2-3 Common used solvents for nanothermite preparation

Solvents	**Boiling Point**	**Dipolar Moment**	**Main Drawbacks**
Diethyl ether	34.5	1.14	Formation of explosive organic peroxides
Petroleum ether	42–62	~ 0	Poor dispersing properties
Acetone	56	2.7	No drawbacks
Hexane	68.7	0.00	Poor dispersing properties
Acetonitrile	81.6	3.90	Toxicity
2-Propanol	82.3	1.65	Can react with aluminum
Water	100	1.86	React with aluminum / Additives are needed
Dimethylformamide	153	3.81	High toxicity and high boiling point

Malichi et al. prepared nanothermite (n-Al/CuO) using sonication method with hexane as a dispersion medium, and then evaporated hexane on a hot plate at 48 $^{\circ}$C for 10 minutes [148]. In addition, tertiary nanothermite based on Al (50 nm), B (62 nm) and CuO was fabricated by Sullivan et al. by mixing the powders by ultrasonication in hexane. After that, the composition was dried in a furnace at 100 $^{\circ}$C for several minutes. Finally, the aggregations of the composition were broken by a spatula [56]. Isopropanol was used as a dispersion medium by Perry et al. to properly prepare nanothermite based on n-Al and WO_3 [149]. Thiruvengadathan used isopropanol as a medium to integrate Al/CuO nanothermite with explosive materials such as CL-20 or RDX [150]. Bouma et al. prepared Al/MoO_3 nanothermite in acetone. The choice of acetone depended on the possibility to incorporate other additives like Viton or graphite based materials. Thermite compositions prepared in batches of 0.5 g in 10 ml acetone [151].

In our work, we used acetone as a dispersion medium for the preparation of nanothermite compositions because it is compatible with the employed raw materials.

2.7.2 Characterization of nanothermites

Characterization of nanothermites should be performed in two directions: morphology and reactivity tests. Morphology characterization includes microscopic techniques (SEM-EDX, TEM, AFM…etc.), X-ray diffraction (XRD) and specific surface area measurements. Reactivity characterization can make use of thermal analysis (DSC and TGA), laser ignition tests, open tray burn tests, burn tube experiments, bomb calorimetry test, combustion micro tests (T-jump technique), impact tests, isothermal micro calorimetry and batch reactor tests.

Not all of these characterization techniques employed in the thesis. Based on the available instruments in Polytechnique, Research Center for High Performance Polymer and Composite Systems (CREPEC) and the UW Laboratory for Emerging Energy Research (LEER) at the University of Waterloo, characterization of the prepared nanothermites is efficiently performed. Picture of nanothermites from morphological and reactivity point of view will be fully illustrated in the next chapters.

2.8 Applications of nanothermites

Nanothermites are being studied for many potential applications in both civilian and military fields. From a civilian perspective, nanothermites can be employed in micro and nano welding, material synthesis, ejection seats, safety air cushions, and power generation. For military applications, nanothermites have captured much attention due to their use in pyrotechnics, micro igniters, microthruster, bullets, propulsion and hydrogen generation. Figure 2-19 illustrates some of nanothermites practical applications.

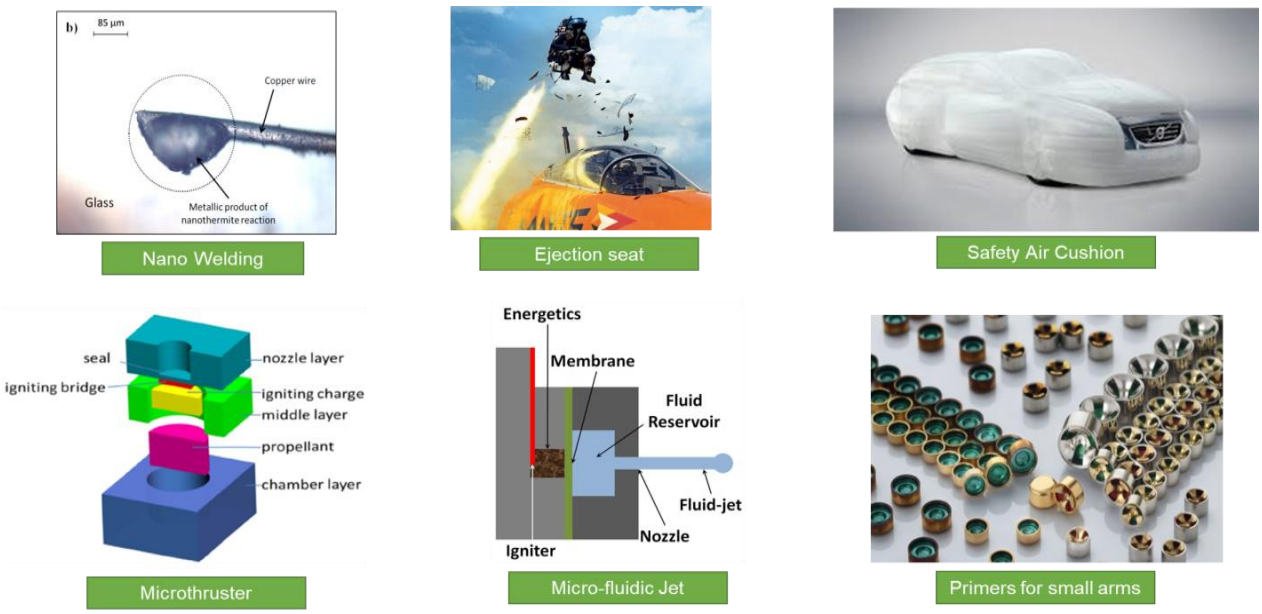

Figure 2-19 Some applications of nanothermites

Al/CuO nanothermite was pressed at various densities from 20 % to 80 % and used in microthruster. At high packing density, thrust had a value of 3-5 N at 1.5-3 ms, at low packing density; it had 75 N at 50 µs. Specific impulse in both cases was 20-25 s [152]. These microthrusters with precise thrust impulses can be properly used in space applications to control the altitude of small satellites.

Sourgen et al. used MIC based on RDX and Cr_2O_3/nano-Al to shift a 40 mm projectile. The experiment was performed in a wind tunnel under a supersonic airflow at Mach 3. Only 0.16 g of the hybrid compositions (representing just 0.051 % of the 315 g projectile mass) was being able to shift the projectile by 3 degrees from its initial attitude [153].

Moreover, nanothermites can be used in micro-fluidic jet injector applications. In this application, gases will be produced by the ignition of nanothermite composition, which stretches an elastic membrane, creating a fluid jet through a converging nozzle. Controlled flow of gases produced by these smooth actuators can be usefully used in devices that include multiple laboratory functions on a single chip.

Thin-deposited nanothermite film on glass substrate is used to fabricate micro igniters with glowing heat and pressure. Micro igniters can be used in both military and civilian applications such as missiles, rockets and automobile airbags [154].

Due to the toxicity problems accompanying primary initiating explosives, which contain lead or chromium, regulations, will strongly limit or even prohibit the utilization of these compounds. For this reason, one of the most promising and important applications of nanothermite is hybrid compositions like nanostructured thermite explosive (NSTEX). NSTEX is intend to be as the possible replacement of existing unsustainable initiators [155].

2.9 Problematic issues

Nanothermite is one of the main approaches to the key development of new EMs to achieve the increasing demands in high energy density propulsion systems. They are characterized by large specific surface area, high reactivity, energy density and fast energy release which leads to higher reaction rate, heat release, pressure and thrust output than microthermite [21, 22]. Despite the advantages of nanothermites over microthermites, the core problems of thermites generally are their slow rate of energy release, elevated ignition temperatures (> 800 $^{\circ}$C), particle agglomeration before ignition, and incomplete combustion compared to MEMs [9, 22-25]. Relatively long ignition delay of metallic fuels is usually accompanied by an interruption in the diffusion of oxidizer and/or fuel through the protective Al_2O_3 layer. As a result, a large portion of Al powders often remains unreacted [9, 22].

Another shortcoming of nanothermites are their lower peak pressures and excessive oxidation of n-Al under oxygen environment [25, 156]. Although the passivation layer covering n-Al is useful in decreasing the possibility of self-ignition of the material, it reduces the active Al content that will contribute in the combustion process. Therefore, the thrust output by micro-scale devices

will be limited because of the apparent lack of C-H-O-N elements in nanothermite constituents and the decrease of the active Al content [157, 158]. Moreover, high electrostatic sensitivity in addition to relatively elevated ignition temperatures (~ 800 $^{\circ}$C) are still considered significant issues associated with nanothermites [23, 24, 27].

In another direction, difficult ignition and propagation process within small tubes and slots are one of the important problems that decrease the applicability of EMs in micro-energetic systems [26]. In addition, the practical importance of green primary explosives increases because of the inherent drawbacks associated with traditional initiating explosives. Hyper-toxicity and hydrolytic instability are the hazards from using mercury fulminate, lead azide, or lead styphnate. As a direct result of environmental and human dangers posed by these materials, their military and civilian uses are limited [159, 160]. Therefore, NSTEX may be better alternatives to primary explosives, but the challenge is how to overcome the low combustion velocity or pressurization of nanothermites and consequently improve their deflagration to detonation transition (DDT) process.

Accordingly, developing and characterizing new nanothermites that could overcome the above-mentioned problems while improving their combustion properties would be a real asset for the future use of these materials in high energy density applications.

CHAPTER 3 OBJECTIVES

3.1 Objective

According to the literature review presented in Chapter 2, oxygenated oxidizers are promising alternatives to metallic oxides for the formulation of new nanothermites for high energy density and propulsion applications. However, the combustion properties of nanothermites based on n-Al, oxygenated salts and CNMs have not been addressed. On the other hand, investigating the combustion performance of propellants integrating nanothermite with NC as energetic polymers in small tubes for microthruster application is still lacking. Furthermore, using EMOFs as substitutes to Al is considered as one of the new directions for the preparation of friendly environmental nanothermites (free of Al) to overcome Al problems and positively enhance the overall performance. The main goal of this research is:

"To develop new nanothermite mixtures with controllable combustion and tailored performance parameters for small-scale energetic applications"

3.2 Specific objectives

The specific objectives of the current research work are:

i. Synthesis and characterization of tertiary nanothermite CNMs/Al/$KClO_4$ with superior combustion characteristics.

ii. Assess and compare between the effect of different metallic and oxygenated oxidizers on thermal behaviour, reaction kinetics and combustion mechanism of tertiary nanothermites.

iii. Exploring the ballistic performance of quaternary NC/GO/Al/$KClO_4$ nanothermite for high-speed impulse small-scale propulsion applications.

iv. Synthesis and characterization of environmental friendly thermite composition based on EMOFs as a fuel (free of aluminum).

CHAPTER 4 ORGANIZATION OF THE ARTICLES

The following four chapters comprise the articles corresponding to the main findings of this research work and represent the core of the thesis. Each chapter is presented as a separate peer-reviewed journal paper.

Chapter 5 presents the results of the first manuscript "*Synthesis and Characterization of Tertiary Nanothermite CNMs/Al/KClO4 with Enhanced Combustion Characteristics*" that has been published in *Propellants, Explosives, Pyrotechnics* (VOL. 46, P. 1-12, 2021). This work examined the influence of different types of CNMs (GO, RGO, CNTs and CNFs) on the thermal performance of tertiary nanothermites based on n-Al and oxygenated salts represented by $KClO_4$. Furthermore, optimization of GO percentage and equivalence ratios (ϕ) between the fuel and oxidiser were investigated. The results shown that the CNMs, especially GO, clearly enhanced the performance of prepared nanothermites. The maximum value of the heat of combustion was achieved at 5 % GO and for the ϕ value of 1.4. This systematic study was important to deepen our comprehensive understanding of CNMs action on nanothermite performance and to broaden their activity and applicability.

Chapter 6 presents the results of the second paper "*Combustion behavior and reaction kinetics of GO/Al/oxidizing salts ternary nanothermites*" that has been submitted to *Journal of Thermal Analysis and Calorimetry*. Following the investigation of the effect of CNMs on the thermal properties of Al/$KClO_4$ nanothermite and optimizing the best percentage of GO presented in the first article; this work assesses the effect of GO on the thermal behaviour and reactivity of tertiary nanothermites based on n-Al and different types of oxygenated salts and metallic oxidizers. The controlling mechanisms of different nanothermite compositions are discussed based on the measured kinetic parameters.

Chapter 7 encloses the results of the third article "*Superior performance of quaternary NC/GO/Al/KClO4 nanothermite for high speed impulse small-scale propulsion applications*" that has been published in *Combustion and Flame journal* (VOL. 232, NO. 111527, 1-13, 2021). This article discusses the preparation of quaternary NC/GO/Al/$KClO_4$ nanothermites using facile electrospinning technique with controllable combustion and tailored performance parameters. Thermal behaviour of the mixtures is analysed and a mechanism for the effect of NC in the

quaternary nanothermites is proposed. The prepared nanothermites ignited and self-propagated inside millimeter-scale STMs, which is contrary to classical EMs that has problems with ignition under the same conditions. This study was of great importance regarding the many possible energetic applications, such as in microscale energetic devices and miniature propulsion systems.

The fourth paper is found in Chapter 8 "*Combustion Characteristics of EMOFs/oxygenated salts Novel Thermite for Green Energetic Applications*" that has been published to *Thermochimica Acta journal* (VOL. 232, NO. 111527, 1-13, 2021). This article introduces a novel type of thermite energetic materials based on a powerful 3D EMOF-1 as alternative energetic fuel of Al and different types of oxygenated salts. EMOF-1 was prepared using microwaves instead of the solvothermal method reported before. Multiple characterization instruments are involved to ensure the morphology and the structure of EMOF-1 and the developed systems such as SEM-EDX, FTIR, and XRD. TGA, DSC, bomb calorimetry and laser ignition evaluated the combustion behavior of the achieved composites. Additionally, the apparent kinetic parameters (activation energy & frequency factor) were calculated using Kissinger and Ozawa approaches.

Additionally, Appendix A presents the results of a fifth paper "*Laser ignition of CNMs/Al/Peroxy salts nanothermites for micro thruster applications*" in the final stages to be submitted to *Journal of Applied Thermal Engineering.* This manuscript is devoted to evaluating the influence of chemical composition and packing density on combustion process and thrust generating characteristcs of the previously prepared tertiary nanothermites in chapters 6 and 7. This paper shaded the light that nanothermite mixtures with tailored combustion performance can be developed via addition small quantity of GO and using oxidizing salts instead of metallic ones and opens the route for more micro-energetic applications in the future.

CHAPTER 5 ARTICLE 1: SYNTHESIS AND CHARACTERIZATION OF TERTIARY NANOTHERMITE CNMS/AL/$KCLO_4$ WITH ENHANCED COMBUSTION CHARACTERISTICS

Ahmed Fahd [a], Charles Dubois*[a], Jamal Chaouki [a], John Z. Wen [b], Ehab Youssef [c]

[a] Chemical Engineering Department Polytechnique Montréal, Montréal, H3C3A7 (Canada),

*e-mail: charles.dubois@polymtl.ca

[b] Department of Mechanical and Mechatronics Engineering, University of Waterloo, Waterloo, Ontario, N2L3G1 (Canada)

[c] Chemical Engineering Department, Military Technical College, Cairo, Egypt

(This work was published online in Propellants, Explosives, Pyrotechnics on March 16th, 2021)

(Note: Ahmad Fahd is the name I always use instead of Ahmad Emam in my all publications)

5.1 Abstract

Much attention has been directed toward the development of new energetic materials to achieve the increasingly demanding performance of high-speed propulsion systems. Nanothermite is one of the main approaches for the development of new energetic materials by the close integration of oxidizer and metal fuel. This study is devoted to evaluating the impact of different carbon nanomaterials (graphene oxide, reduced graphene oxide, carbon nanotubes, and carbon nanofibers) on the thermal behavior of nanothermites based on potassium perchlorate and nano aluminium powder. Nanothermite compositions were prepared using a conventional sonication method. The morphology of nanothermites was characterized by a scanning electron microscope (SEM) coupled with energy dispersive spectroscopy (EDS), which confirmed that the nanoparticles are homogeneously dispersed without agglomeration. The structure of nanothermite was also characterized by Fourier Transform Infrared Spectroscopy (FTIR), X-ray diffraction (XRD), and Raman spectroscopy. The impact of carbon nanomaterials on the combustion behavior of nanothermite was evaluated by thermal gravimetric analysis (TGA), differential scanning calorimetry (DSC), and bomb calorimetry. There was good agreement between results

from DSC and bomb calorimetry. In general, the total heat released improved with the addition of carbon nanomaterials and particularly graphene oxide, which generated the highest increase in the heat of combustion. In addition, the maximum decomposition temperature shifted to a lower temperature, which indicates enhanced ignition characteristics. This is the first time reporting on the synthesis and characterization of tertiary nanothermites based on nano-aluminum, potassium perchlorate, and carbon nanosize materials. It can be concluded that these novel nanothermite compositions exhibit dramatically improved properties as demonstrated by a 200% increase in the heat of combustion with only a 5% addition of graphene oxide. Moreover, the ignition temperature decreased from 545.1 $^{\circ}$C to 508.7 $^{\circ}$C enhancing the overall combustion characteristics.

5.2 Introduction

For more than a decade now nanotechnology has been increasingly used in the fields of the environment, medicine, ceramics, and defence applications. In the latter case, significant progress has led to the development of nano energetic materials incorporating nanosize particles or showing nanoscale structural features. The essence of nanotechnology lies in the ability to modify and tune the material properties at the nanometric scale [1]. In light of recent significant advances in microscale energy systems, such as micro thrusters, igniters, initiators, propulsion units, and power, there is now considerable interest in the synthesis and development of new energetic materials to meet the increasing demand in high energy density propulsion systems [2].

In broad terms, Energetic Materials (EMs) can be defined as materials that store chemical energy and are classified into propellants, explosives, and pyrotechnics. The primary difference between propellants, pyrotechnics, and explosives is the rate of energy release. While propellants and pyrotechnics are characterized by a relatively slow combustion process (several seconds), explosives release their energy through a fast detonation process (microsecond timescale) [3]. Another way of classifying EMs is through their production process, such as monomolecular EMs (MEMs), composite or metastable intermolecular composite (MICs) materials. On the one hand, MEMs have the fuel and oxidiser components in the same molecular species (for example, nitrocellulose, nitroglycerine, and trinitrotoluene), while on the other hand, MICs are produced

from mixing fuel (aluminum, sulphur, carbon, etc.) and oxidisers (iron oxide, cupper oxide, potassium perchlorate, etc.), like in the case of Al/Fe_2O_3 or Al/CuO mixtures [4].

The advantage of using thermites, which are a special type of MIC, comes from their higher energy density as compared to MEMs due to the enthalpies of combustion of the metallic fuels they contain [5]. The disadvantage of thermites is their slow rate of energy release in contrast with MEMs. A problematic characteristic of thermites is the relatively long delay before ignition of the metallic fuels, which is usually accompanied by a further limitation in their burning rate due to the diffusion of the reactive species throughout the protective layer of metal oxides.

Thermites are, as per their traditional definition, mixtures of aluminum powder with metallic oxides. This definition can be extended to include mixtures in which atoms with high electronegativity (O, S, F, etc.) are exchanged between an oxidizer and a fuel, like in the case of $Al/KClO_4$ or $Al/K_2S_2O_8$ [6-8].

Nanothermite production is one of the most recent approaches for the development of new energetic materials by the integration of a potential oxidizer and metal fuel at the nanoscale. Aluminum (Al) nanopowder is the key material in nanothermite fuel due to its formation under high heat, high density, low melting temperature, low toxicity, and compatibility with other ingredients [9]. New nanothermite compositions are designed to increase the generation of decomposition gases to simulate the behavior of organic explosives. Hence, oxygenated oxidizers could be the ideal alternative to metallic oxidisers to prepare nanothermites for high reactivity and performance [8, 10-12]. Recently, carbon nanomaterials (CNMs), such as fullerenes, carbon nanotubes (CNTs), graphene, graphene oxide (GO), reduced graphene oxide (RGO), expanded graphite (EG), and carbon nanofibers (CNFs), have been widely used to enhance the performance of EMs. In particular, graphene and its derivatives will be promising candidates to enhance the ignition and combustion properties of nanothermites due to their large specific area and unique thermal, electrical and mechanical properties [13].

A growing body of literature can be found on novel nanothermite compositions and the effect of CNMs on their combustion performance. For instance, Kwon et al. studied the thermal characteristics of thermite composition based on copper oxide (CuO) and Al, a high-performance energetic material used in many applications, such as thermal batteries, decoy flares, and green

primers [14]. In his seminal article on the effect of CNTs on the CuO/Al thermite reaction, Sharma [15] shows that the enthalpy of the CuO/Al/CNT thermite reaction increased with the percentage of CNTs until becoming thirteen times (with 15 % CNTs) higher than the reference composition while the ignition temperature shifted to a lower temperature. A comparative study on the effect of graphene nano platelets on the combustion behaviour of nitromethane was carried out in 2009 by J.L. Sabourin and his research group at the Mechanical and Nuclear Engineering Department at Pennsylvania State University and they emphasized how graphene plays an important role in enhancing the burning rate of the propellant [16]. In [17] the authors prepared high performance nano energetic composites based on Bismuth trioxide (Bi_2O_3) and Al using functionalized graphene sheets (FGS) and studied the effect of GO on their combustion properties. For the FGS self-assembled nanocomposites, they found that an enhancement in energy release from 739±18 to 1421±12 J/g was measured using DSC. In a major advance in 2017, Fan Yang et al. tried to enhance the reactivity of Al/CuO thermite by coating it with potassium perchlorate ($KClO_4$) using a solvent/antisolvent method and they succeeded in preparing new MIC formulations of $KClO_4$@Al/CuO. They found that the novel composition reacts more vigorously than Al/CuO, with a higher burning rate and energy release [18].

The misuse of the term graphitic oxide and RGO instead of GO in the literature creates significant confusion. This confusion is caused by the misuse of the main fundamental concepts, and by oversimplification and misinterpretation of GO chemistry [19]. Graphitic oxide and RGO are different from GO because the final product of the oxidation process of graphite is commonly known as graphite oxide which is multi-layered and appeared in brownish. Exfoliation converts graphite into highly stabilized individual layers known as graphene oxide. Simply graphene oxide is the exfoliated product of graphite oxide as illustrated in Figure 5-1.

The main difference between GO and RGO is the C/O ratio in their structure. While the C/O ratio is very low in GO structures, it is significantly higher in RGO structures approaching almost zero oxygen content. Generally, there is a lot of superfluous analytics on graphitic oxide and RGO effect on classical thermite compositions (Al + metallic oxide) and thermite behavior may be varying according to the entire composition. In case of Al/MnO_2 thermite mixtures, addition of graphitic oxide hindered the thermite reaction and energy output and in other mixtures like Al/Bi_2O_3 and Al/Fe_2O_3, addition of graphitic oxide or RGO improved the energy output [17, 20,

21]. As a result, each thermite composition needs to be studied individually. No previous data had ever been recorded on the effect of CNMs on nanothermites based on oxygenated salts (KClO4); this made this investigation even more important specifically for small propulsion applications.

This work presents an investigation of the effect of different CNMs (GO, RGO, CNTs, and CNFs) on the thermal performance of nanothermite compositions based on n-Al and oxygenated oxidisers represented by $KClO_4$. Moreover, different equivalence ratios between the fuel and oxidiser will be investigated to prepare new nanothermite compositions with high energy output, burning rate, and gas generation. $KClO_4$ selected for this study was chosen as the oxidiser due to its high oxygen content, strong oxidizing nature, and slightly exothermic decomposition reaction. In addition, CNMs were used based on their large surface area, rich pore structure, and unique electrical, thermal, chemical, and mechanical properties. In particular, GO is considered to be a potential EM by itself, whereupon heating, it can readily undergo violent exothermic decomposition due to the extensive oxygenic functional groups on the basal plane (phenol, hydroxyl, and epoxide) and at the edges (carboxylic) [13, 22].

5.3 Experimental Section

5.3.1 Reagents and Materials

Graphite flakes, phosphoric acid (H_3PO_4), sulphuric acid (H_2SO_4), potassium permanganate ($KMnO_4$), hydrogen peroxide (H_2O_2), ascorbic acid and acetone used in the preparation of GO and thermite compositions were purchased from Sigma-Aldrich. $KClO_4$ was brought from Defence Research and Development Canada. The as-purchased Al spherical nanoparticles from US Research Nanomaterials Inc. have an average number particle size of 40 nm, a purity of more than 99.9 % metal basis, active Al content of 80 wt. % (mass fraction), a surface area of 30-50 m^2/g and a bulk density of 2.7 g/cm^3 as specified by the manufacturer. GO and RGO are prepared and characterized through XRD, Raman spectroscopy and FTIR. MWCNT and CNF were purchased from Sigma-Aldrich. MWCNT has >98 % carbon basis, O.D. × L 6-13 nm × 2.5-20 μm and specific surface area of 216 m^2/g. CNF which is graphitized, platelets (conical) has >98 % carbon basis, D×L 100 nm × 20-200 μm. The composition of CNMs used in the experiment

was checked by an CHNSO Elemental Analyzer EA3000 (EuroVector); the mass fraction (w) of C, H, N, S and O was as follows: for GO, w(C) = 0.5013 ± 0.0062, w(O) = 0.4681 ± 0.0046, w(H) = 0.0174 ± 0.0011, w(S) = 0.0205 ± 0.0015, for RGO, w(C) = 0.9139 ± 0.0118, w(O) = 0.0458 ± 0.0036, w(H) = 0.0189 ± 0.0011, w(S) = 0.0224 ± 0.0017, for MWCNT, w(C) = 0.9819 ± 0.0042, w(H) = 0.0013 ± 0.0011, w(N) = 0.0074 ± 0.0017, w(O) = 0.0031 ± 0.0014, w(Ni) = 0.0074 ± 0.0028 and for CNF, w(C) = 0.9816 ± 0.0037, w(H) = 0.0009 ± 0.0013, w(N) = 0.0039 ± 0.0026, w(O) = 0.0044 ± 0.0016, w(Ni) = 0.0094 ± 0.0023. Furthermore, Heat of combustion of CNMs was measured by oxygen bomb calorimeter and recorded 34.35 ± 0.32, 32.73 ± 0.36, 33.14 ± 0.42, and 32.88 ± 0.29 kJ/g for GO, RGO, MWCNT and CNF respectively.

5.3.2 Synthesis of GO

Reduced graphene oxide was prepared by the reduction of GO synthesised in the previous step. Ten grams of ascorbic acid dissolved in 50-100 ml DI and added to the GO solution was mixed and heated at 60-70 $^{\circ}$C for 1 h. The mixture was then left to cool down and decanted for 24 h. Finally, the black RGO product was filtered and washed with hot DI, cold DI, and acetone and at the end left to dry at room temperature for 24-48 h. A schematic diagram of GO and RGO preparation is illustrated in Figure 1.

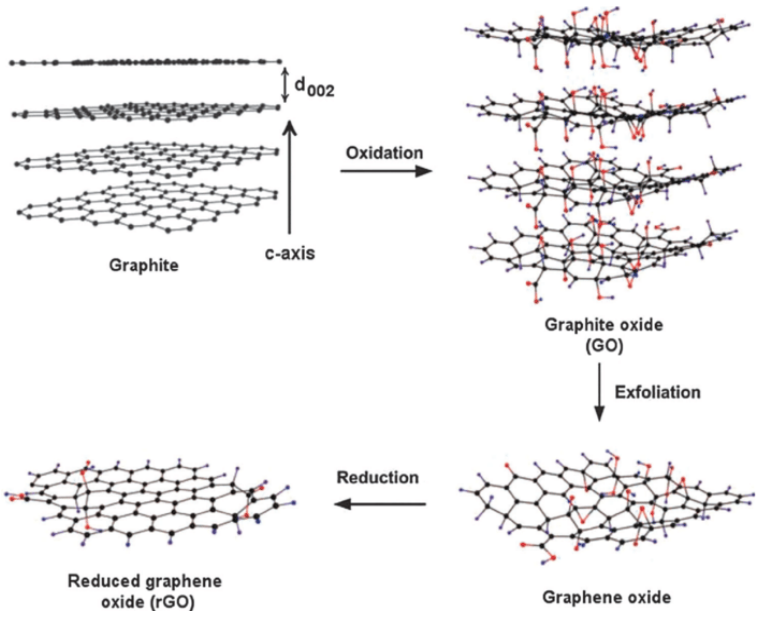

Figure 5-1 GO and RGO preparation process [24]

5.3.3 Preparation of nanothermites

Nanothermite compositions were prepared by weighing the fuel (n-Al) and oxidizer components ($KClO_4$) in a stoichiometric ratio (34.2 % Al and 65.8 % $KClO_4$) according to equation (1).

$$8Al + 3\ KClO_4 \rightarrow 4Al_2O_3 + 3KCl \quad (1)$$

The dispersion of n-Al, $KClO_4$ and GO (2.5, 5.0, 7.5, and 10 w/w %) was conducted in acetone. The samples were then processed in a sonic bath for 30 min to ensure proper mixing. Acetone was allowed to evaporate at 80 $^{\circ}$C for 1 hour with simultaneous mechanical stirring to prevent the reagglomeration of nanoparticles. The wet particles were then fully dried in a vacuum desiccator for 12h to remove any remaining solvent. Finally, the dried powder was gently broken up with a spatula to remove large clumps until the consistency was that of a loose powder. For comparison purposes, other CNMs (RGO, CNTs and CNFs) were used as alternatives to GO. Moreover, different equivalence ratios (Φ) (0.8, 0.9, 1.2, 1.4 and 1.6) of GO/Al/$KClO_4$ were prepared to determine the optimum fuel/oxidiser ratio. As our goal here is optimising and clarifying the effect of CNMs additives on the combustion performance of the prepared nanothermites, GO has approximately 50% carbon and 50% oxygen as a result of CHONS elemental analysis and they were not included in the composition with high percentage and limited to 5 %, hence they were not have a big influence or change Φ value and we neglected their effects on Φ calculations. Moreover, in the definition of Φ, Fuel/Oxidizer ratio refers to the molar ratio of oxygen actually present in $KClO_4$ to the oxygen necessary for the oxidation of Al to Al_2O_3. Previously, neglect the effect of CNMs on stoichiometric ratio was considered in many references due to their small amount and as they used as additives and we are looking for clarifying the effect of this additives [25, 26]. The various sample compositions are listed in Table 1.

Table 5-1 Chemical composition of different nanothermite samples

Sample Name	Al (wt %)	$KClO_4$ (wt %)	GO (wt %)	RGO (wt %)	CNT (wt %)	CNF (wt %)	Φ
S_0 (Ref. sample)	34.200	65.800	0	0	0	0	1
S_1 (5 % GO)	33.345	64.155	2.5	0	0	0	1
S_2 (5 % GO)	32.490	62.510	5	0	0	0	1
S_3 (7.5% GO)	31.635	60.865	7.5	0	0	0	1
S_4 (10 % GO)	30.780	59.220	10	0	0	0	1
S_5 (5 % GO)	27.902	67.098	5	0	0	0	0.8
S_6 (5 % GO)	30.278	64.722	5	0	0	0	0.9
S_7 (5 % GO)	36.494	58.506	5	0	0	0	1.2
S_8 (5 % GO)	40.014	54.986	5	0	0	0	1.4
S_9 (5 % GO)	43.135	51.865	5	0	0	0	1.6
S_{10} (5 % RGO)	32.490	62.510	0	5	0	0	1
S_{11} (5 % CNT)	32.490	62.510	0	0	5	0	1
S_{12} (5 % CNF)	32.490	62.510	0	0	0	5	1

5.4 Nanothermite characterization

Graphene oxide and reduced graphene oxide were characterized by Micro-Raman spectroscopy at room temperature with a WITec spectrometer system equipped with an argon ion laser (20 mW) excitation at 532 nm. The FTIR spectra were recorded using a PerkinElmer (spectrum 65) FTIR spectrometer in an attenuated total reflectance (Miracle ATR) mode and XRD patterns were recorded on a Panalytical 3050/60 Xpert-PRO using CuKα radiation.

The morphology of nanothermite samples was studied by a FEI Quanta FEG 450 SEM operated at 15 kV coupled with EDS measurements. FTIR spectra were acquired in the IR region of 400–4000 cm^{-1} with the help of Perkin Elmer SP-65. The crystalline structure was determined by XRD. Simultaneous TGA/DSC was performed to measure the weight loss and heat flow characteristics as a function of temperature using an SDT Q600 thermal analyzer (TA Instruments). The measurements on all of the samples prepared in this work were carried out in

argon under identical experimental conditions (heating rate of 10 °C/min and argon flow rate of 100 ml/min). The heat of combustion of nanothermite samples were measured by an oxygen bomb calorimeter (model: Parr™ 1341 Plain Jacket Calorimeter).

5.5 Calculation of the heat of combustion

The heat of combustion of all nanothermite samples was measured using a bomb calorimeter. Each test was performed twice and the average value of the heat of combustion was calculated. The energy of combustion was calculated according to the following equations (3) & (4) [27].

$$Q = (Q_{System} - Q_{Fuse\ wire})/m \tag{3}$$

$$Q_{System} = M * C_p * \Delta T \tag{4}$$

where Q represents the heat of combustion of each nanothermite sample in (J/g), Q_{System} is the total heat of combustion (heat of combustion of the sample + heat of combustion of fuse wire) in (J), $Q_{Fuse\ wire}$ is the heat of combustion of the fuse wire (J), (calculated according to the length used in the test), m demonstrates mass of the test sample (g), M identifies the mass of used water (usually 2000 ml = 2000 g), C_p is the specific heat capacity of water (J/g.°C) and ΔT specifies the temperature difference before and after combustion (°C).

5.6 Results and Discussion

5.6.1 Structural and chemical characterization

The morphology, physical and microstructure of nanothermite compositions were characterized by SEM coupled with EDS. SEM images were collected at different magnification powers to reflect the shape and distribution of the particles in the mixture. A typical SEM image of a 5 % GO sample is shown in Figure 5-2.

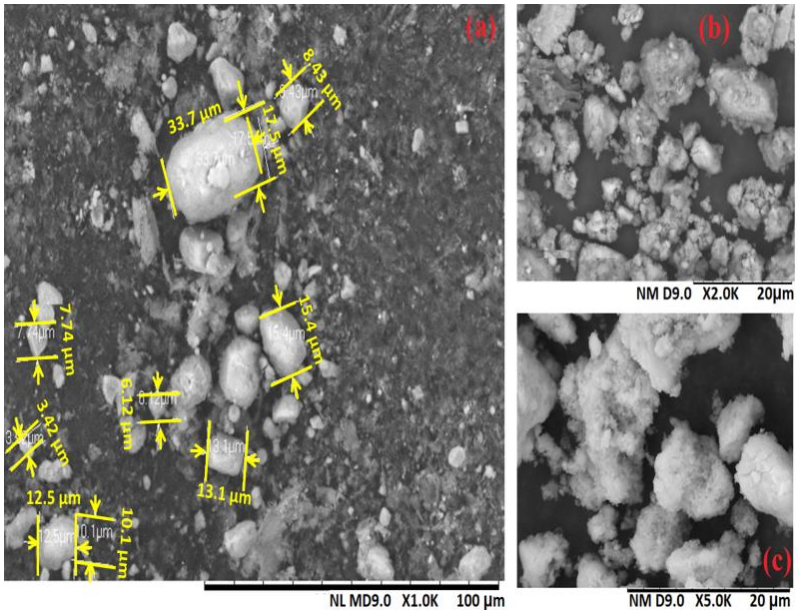

Figure 5-2 SEM micrographs of 5 % GO nanothermite composition

A SEM image with less magnification power (1K) is represented in (Figure 2a) to conclude the average particle size of the nanothermite mixture, which is recorded as 8-10 µm (number average). There are two modes governing the orientation of GO/Al/$KClO_4$ nanostructure within the larger macrostructure. On one hand, the smaller size and less planar GO/Al/$KClO_4$ particles tended to disperse according to a random macrostructure. On the other hand, the larger size and more planar GO/Al/KClO4 tend to form a layered macrostructure that may be attributed to the weak van der Waals interaction, which favoured the alignment of larger size particles with one another [17]. Figures (2b & 2c) clarify SEMs of the ultra-dense macro structures of GO/Al/$KClO_4$. They reveal that random macrostructure is the predominant mode for the entire sample.

The spatial homogeneity of the elemental composition of GO/Al/$KClO_4$ nanothermites is confirmed by EDS data reported in (Figure 5-3). It reveals a good mixing and distribution of the particles, thus validating the nanothermite preparation method. The presence of GO is indicated by the peak appearing at ~ 0.23 keV and characteristic of the emission line of carbon. The peak appearing at ~ 0.52 keV is representative of the emission line of oxygen. The thin layer of aluminum oxide over the Al particles, GO and KClO4 are the source of this element. Peaks

observed at 1.5, 2.6 and 3.4 keV in the EDS spectrum relate to the emission lines of Al, chlorine, and potassium, respectively.

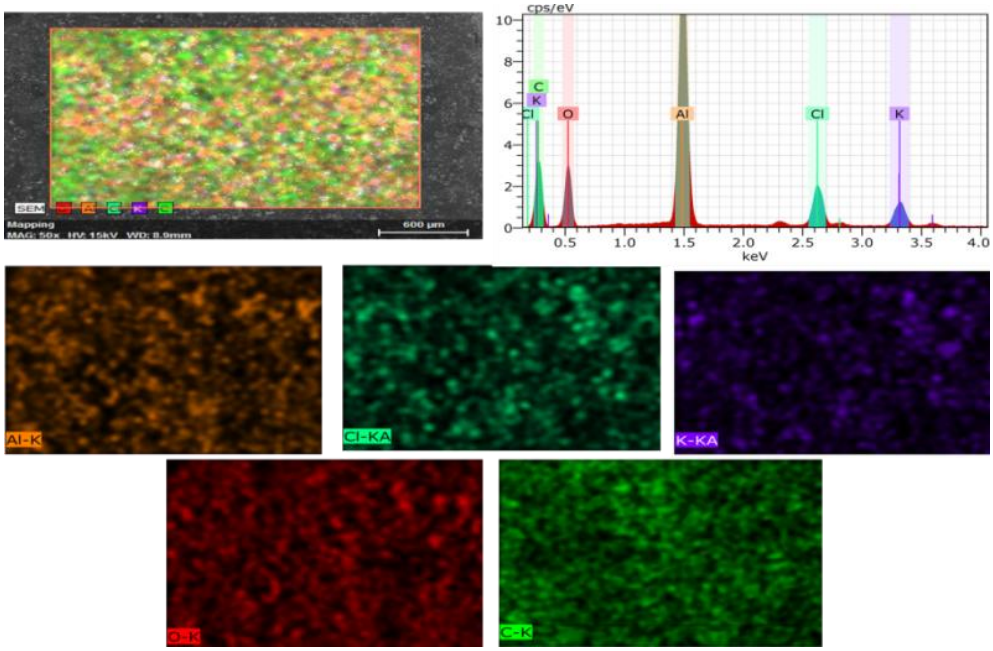

Figure 5-3 EDS images of the 5% GO/Al/$KClO_4$ nanothermite

Raman spectra of GO and RGO are differentiated by two fundamental peaks as found in Figure 5-4.

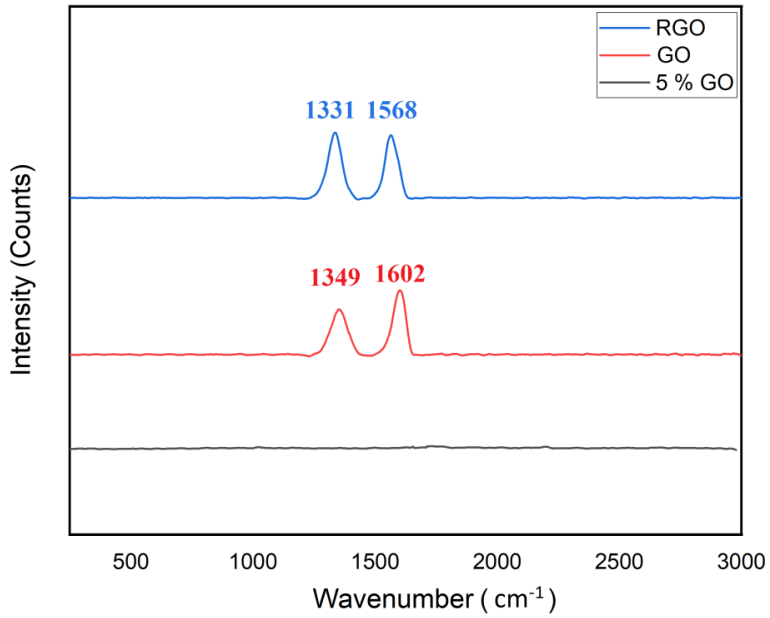

Figure 5-4 Raman spectra of neat GO and RGO powder and 5 % GO/Al/$KClO_4$

Two characteristic vibrational bands of any graphene materials are D and G bands and appear at 1330 and 1560 cm^{-1} respectively [28]. Firstly, the D band, which is commonly known as the defect band, is ascribed to carbon hybridization within plane sp^2 domains, inferring the presence of disordering carbon and defects. While the D band corresponds to disordered carbon, the G band is correlated to the vibration of ordered sp^2 hybridized carbon and identified as the E_{2g} vibrational mode. The ratio between the D and G band intensity (ID/IG) gives an indication of the defects and disordering level [29].

More defective structures corresponding to lower (ID/IG) exhibit higher positive enthalpy of reaction and this confirm the high heat of combustion of GO compared to other CNMs. This correlation between enthalpy of reaction and (ID/IG) is rather obvious as an introduction of defects into an ideal crystal structure leads to a breakage of bonds and thus increasing energy of the system, this behaviour is confirmed by many other studies of heat of combustion of CNMs [30 – 32].

As can be seen, the two main features for GO shifted upon oxidation and recorded 1349 and 1602 cm^{-1} for the D and G bands, respectively. Upon the reduction of GO, the two characteristic peaks shifted back to the position of graphite (1560 cm^{-1}) indicating the removal of oxygenated functional groups. The small shift in RGO peaks after the reduction can be explained by the existence of traces of oxygenated groups [33].

It would seem that both characteristic peaks of GO disappeared in the Raman spectra of 5 % GO due to the increase in ID/IG and consequently removed the defects developed in the structure of GO. This result confirms the excellent homogeneity and the deposition of $KClO_4$ over Al and highlights the role of GO in enhancing mixing intimacy and decreasing the contact distance between the fuel and oxidiser, which is expected to improve the performance of nanothermites.

To further investigate the spatial distribution of components in the nanothermite, the FTIR spectra of $KClO_4$, Al, GO and their mixtures are shown in Figure 5-5.

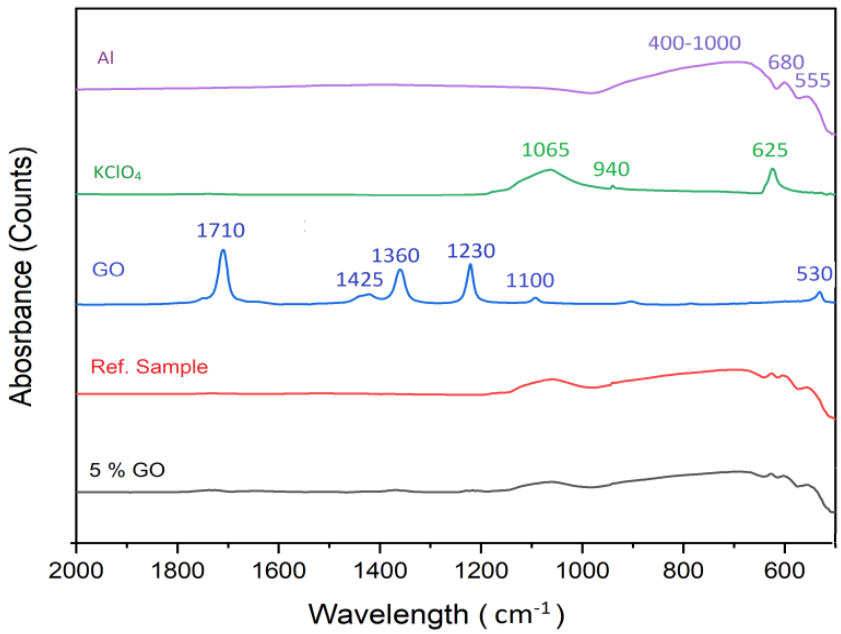

Figure 5-5 FTIR spectra of Al, $KClO_4$, GO and 5%GO/Al/$KClO_4$

Aluminum powder is represented by a broad peak at 400-1000 cm^{-1}, which is ascribed to the Al-O-Al stretching vibration resulting from the distribution of alumina between the octahedral and tetrahedral sites [34]. Peaks found at 555 and 680 cm^{-1} result from the vibration of the Al-O bonds of the pseudo-boehmite structure [35]. Perchlorate salts are distinguished by four primary Cl-O vibration modes, which are symmetric and anti-symmetric stretching appearing in the range of (900-1200 cm^{-1}), and symmetric and anti-symmetric deformation vibration modes (400-650 cm^{-1}) [36]. Potassium perchlorate is characterized by an anti-symmetric stretching vibration peak due to a Cl-O bond and it clearly appears at 1065 cm^{-1}. The symmetric stretching vibration is observed by a weak absorption peak at 940 cm^{-1} because it is an inactive IR [37]. The moderate intensity peak at 625 cm^{-1} is attributed to the Cl-O anti-symmetric deformation mode, while the symmetric deformation mode disappears in the spectrum because of its inactive IR [38]. The IR spectrum of GO clarifies the presence of different functional groups in GO. Stretching the carboxyl group (C=O) is identified by a peak at 1710 cm^{-1} [39]. Peaks specified at 1425 and 1360 cm^{-1} are allocated to the chemisorbed or physisorbed H_2O and CO_2 molecules on the surface of GO [15]. The alkoxy (C-O) stretching peak is clarified at 1100 cm^{-1} [40].

A comparison between the IR spectra for Al and $KClO_4$ with the reference sample shows the existence of the same peaks, which confirms that physical mixing took place without a chemical

reaction. However, peaks characterizing the IR spectrum of GO appear at low intensity at 5% GO/Al/KClO4, but they still reveal the presence of the same peaks from the reference sample as those in GO, thus van der Waals coherence proves all components have no chemical change to them.

Atomic structures and interlayer spacing of GO and RGO samples were further examined by XRD. The powder XRD patterns of GO and RGO are shown in (Figure 5-6).

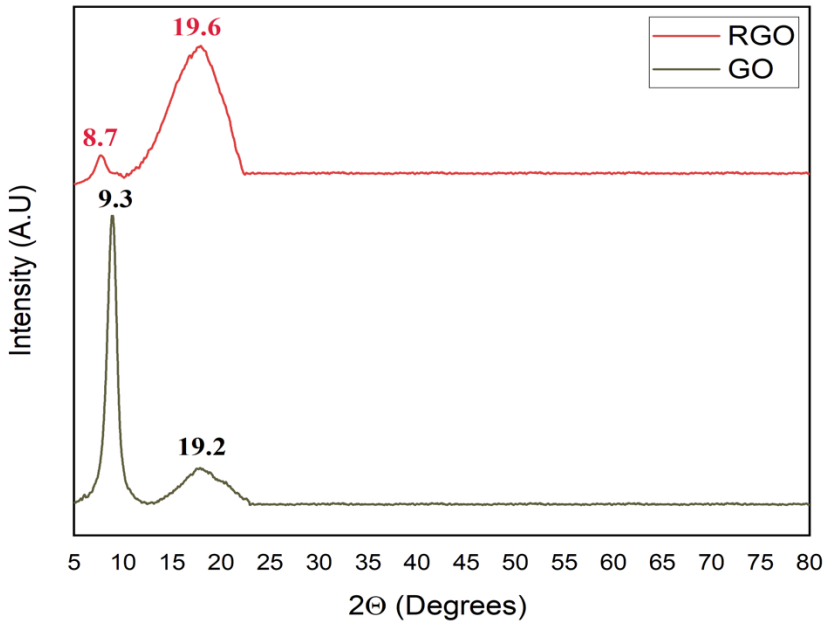

Figure 5-6 XRD patterns of GO and RGO

Graphene oxide exhibits a sharp peak at around (2Θ = 9.3°) corresponding to the (001) basal plane with d-spacing (d_{001} = 0.84 nm). The high d-spacing of GO results from the functional groups bearing oxygen atoms (hydroxyl, carboxyl, etc.) on the outer surface of thin graphene layers [41, 42]. In the case of RGO, a large intensity peak appears at (2Θ = 9.3°) in the case of GO, shrinks to a small peak at (2Θ = 8.7°) and a broad peak at (2Θ = 19.6°) corresponding to a d-spacing of 0.359 nm that is easily observed. The decreasing d-spacing of RGO can be ascribed to the removal of an oxygen-containing functional group of GO and the formation of RGO [43]. XRD patterns of different thermite compositions are illustrated in Figure 5-7.

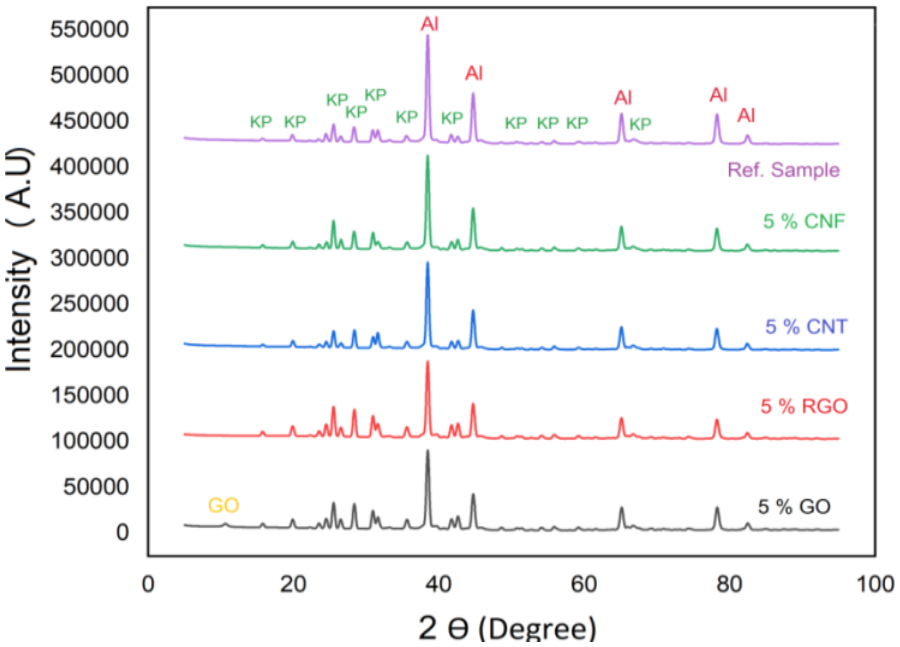

Figure 5-7 XRD patterns of thermite samples

The main diffraction peaks of Al and $KClO_4$ are clearly identified in all thermite compositions, indicating that their nanocrystalline structure was not lost during the preparation process [44]. In addition, a small diffraction peak revealing the presence of GO was found. Its low intensity is consistent with the low GO concentration in the samples with the lesser quantity in the thermite composition. Characteristic peaks of other CNMs are not revealed in the XRD patterns, probably because of the peaks' infusion with the background or may be due to their low scattering coefficient [15].

5.6.2 Thermal Performance

Simultaneous DSC/TGA analysis was performed for several nanothermites and the corresponding results of TGA are found in Figure 5-8.

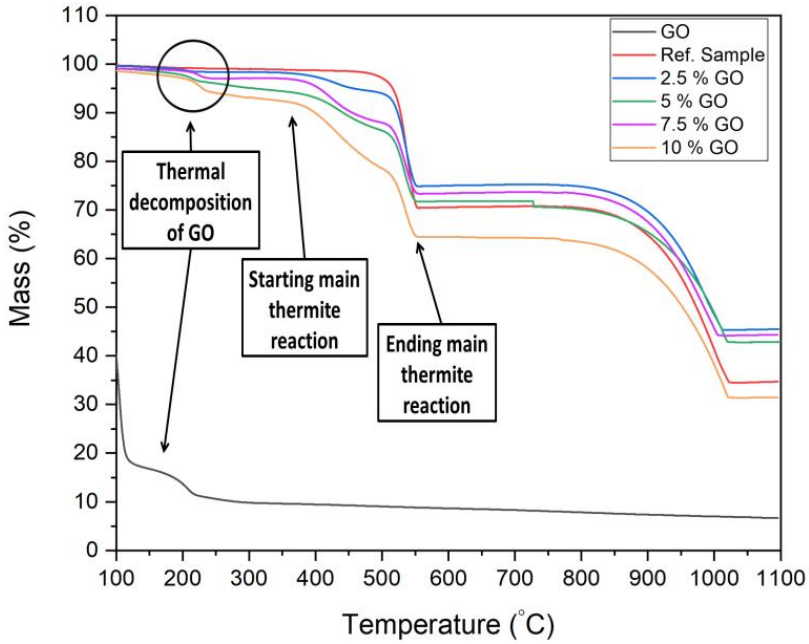

Figure 5-8 TGA thermogram for different percentages of GO over Al/$KClO_4$ nanothermites

The nanothermites containing GO decomposes in three stages. A first steep weight loss (~ 5%) is observed slightly above 200 °C. It is attributed to thermal decomposition of oxygenated functional groups of GO and the formation of graphite (C). A second weight loss from 400 to 550 °C contains two sub steps, corresponding to the reaction of C-$KClO_4$ (C formed from GO decomposition) and the major thermite reaction in GO/Al/$KClO_4$ [45]. The third weight loss is assigned to the melting of unreacted Al and potassium chloride (KCl) formed from the decomposition process.

DSC results are reported in Figure 5-9. Thermal decomposition of $KClO_4$ is characterized by three endothermic and one exothermic events. A first endothermic peak is displayed at approximately 302 °C and ascribed to the phase change of $KClO_4$ from a rhombic to cubic structure [46]. A second endothermic peak appears at 575 °C from the melting of $KClO_4$ and the last endothermic peak attributed to the melting of KCl is found at 770 °C. Only one sharp exothermic peak followed the melting of $KClO_4$ shown at ~ 600 °C. Clearly, Al is indicated by the single endothermic peak at 660 °C, which is the melting point of Al [46]. In addition to the

above mentioned peaks, Al/$KClO_4$ is characterized by an exothermic peak at 545.1 °C, which represents the main thermite reaction between Al and $KClO_4$.

The DSC trace of GO decomposition shows a remarkable exothermic peak at 200 °C, suggesting the removal of the oxygenated group in GO and thus confirming TGA findings [47]. Nanothermite of 5% GO/Al/$KClO_4$ had an exothermic peak at ~ 508 °C suggesting a thermite reaction occurrence and resulting in more heat being released than the reference sample. An increase of the energy output and a shift towards a lower decomposition temperature illustrate the effect of GO on the increasing energy released from nanothermite composition.

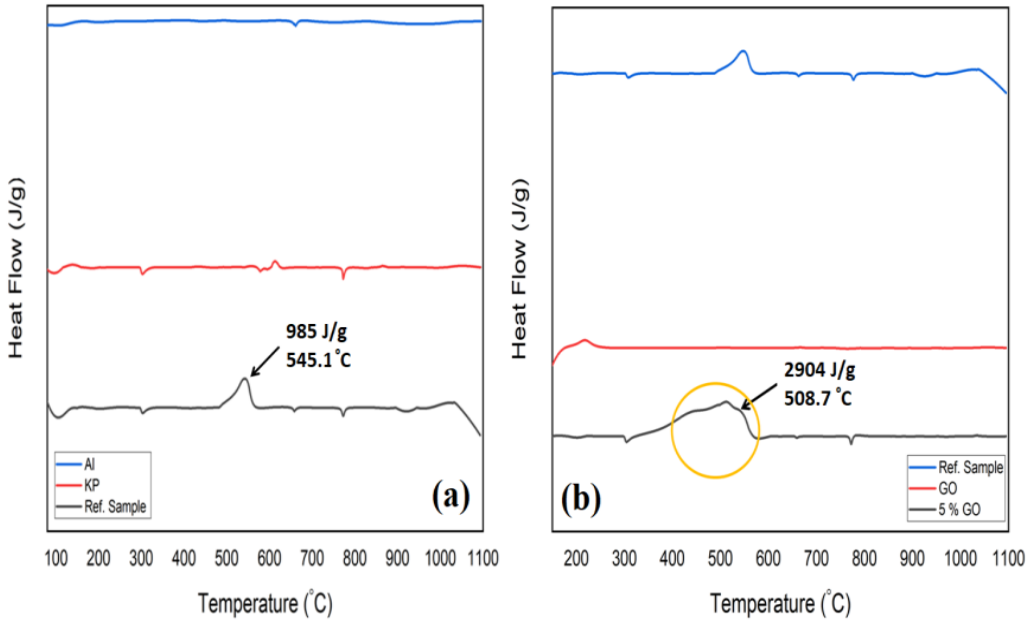

Figure 5-9 DSC plots of (A) reference sample (Al/$KClO_4$) and (B) nanothermite of 5% GO/Al/$KClO_4$

A comparison between the effect of different percentages of GO on the performance of nanothermite is clarified in the DSC plot as shown in Figure 5-10.

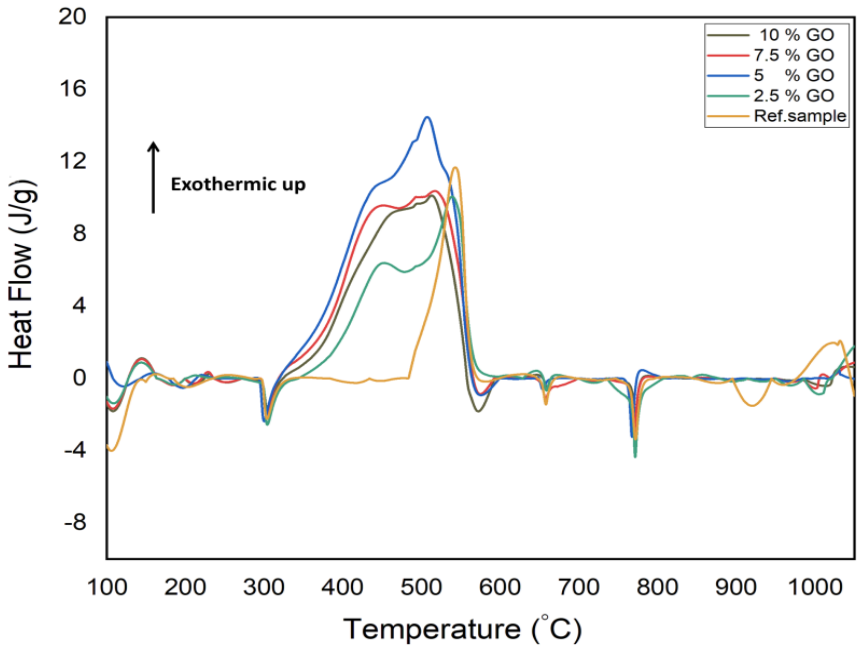

Figure 5-10 DSC thermograms percentages of different % of GO nanothermites

It is clear from Figure 10 that the exothermic energy released from the thermite reaction in the GO/Al/$KClO_4$ sample increased and the ignition temperature decreased due to the addition of GO. Enhancing the energy released can be explained by the effect of GO in improving both the fuel-oxidizer contact and the reactants mass diffusion. GO plays the role of substrate, hence increasing the dispersion of n-Al particles and effectively reducing their aggregation during the course of $KClO_4$. As a consequence, uniform mixing of n-Al metal fuel and $KClO_4$ oxidant will occur. Furthermore, reactions between C formed in the early stages through the decomposition of GO and nanothermite reactants (C-O, C-$KClO_4$ and C-Al) enable reaction pathways that help in accelerating the occurrence of main thermite reactions (Al-$KClO_4$ and Al-O) and play the role of pre-ignition reaction. On the other side, the higher content of GO (more than 5%) on nanothermites gives $KClO_4$ the chance to grow directly on GO nano sheets. The separation of the oxidant and the metal fuel will then occur causing the reduction of energy released in the thermite reaction [17, 40, 48].

A comparison between the effect of different CNMs on thermal decomposition and the energy release of the thermite reaction is demonstrated in Table 2.

Table 5-2 Total heat released and maximum decomposition temperature calculated from DSC

Sample Name	DSC results		
	Total Heat released (J/g)	**Maximum decomposition temperature (°C)**	**The increase in total heat released (%)**
S_0 (Ref. sample)	985.2	545.1	-----
S_1 (2.5 % GO)	1452	540.8	47
S_2 (5 % GO)	2904	508.7	195
S_3 (7.5% GO)	2334	513.3	135
S_4 (10 % GO	2035	520.6	107
S_5 (5 % RGO)	1396	522.2	42
S_6 (5 % CNT)	1488	516.2	51
S_6 (5 % CNF)	1407	537.0	43

Results illustrated in Table 2 show that CNMs have a great impact on increasing the energy release of nanothermites. The significant increase in energy release achieved through the incorporation of CNMs in nanothermites is a direct result of the intimate self-assembly of Al and $KClO_4$ and the introduction of carbon as a tertiary reactant [49]. The highest energy released was achieved by nanothermite composition with 5 % GO. The increase in the heat released was approximately 200 % greater than the initial value of the reference sample. This high energy release achieved by the new nanothermite composition has many advantages in developing micro scale propulsion systems.

Average values of the heat of combustion of all nanothermite compositions measured by the oxygen bomb calorimeter are tabulated in Table 3.

Table 5-3 Heat of combustion calculated from the bomb calorimeter

Sample Name	**Test No. 1 Heat of combustion (J/g)**	**Test No. 2 Heat of combustion (J/g)**	**Average Heat of combustion (J/g)**	**Φ**
S_0 (Ref. sample)	3762	3344	3553 ± 209	1
S_1 (2.5 % GO)	4265	3870	4068 ± 197	1
S_2 (5 % GO)	9196	10032	9614 ± 418	1
S_3 (7.5% GO)	6772	5573	6173 ± 550	1
S_4 (10 % GO)	6137	5413	5775 ± 362	1
S_5 (5 % GO)	6186	5685	5936 ± 250	0.8
S_6 (5 % GO)	6019	6939	6480 ± 460	0.9
S_7 (5 % GO)	11286	11704	11486 ± 209	1.2
S_8 (5 % GO)	12540	12958	12749 ± 209	1.4
S_9 (5 % GO)	12122	11871	11997 ± 125	1.6
S_{10} (5 % RGO)	6173	7042	6608 ± 435	1
S_{11} (5 % CNT)	8038	7190	7614 ± 424	1
S_{12} (5 % CNF)	7092	6371	6732 ± 361	1

Results demonstrated in Table 3 point out that the energy of combustion increased with the addition of GO and reached a maximum value at 5 % GO and after that started to drop. Furthermore, the addition of different types of CNMs enhances the heat of combustion of all nanothermites due to the previous mentioned reasons and as they generally act as secondary fuel which adds more energy to the system, help in the completion of n-Al combustion and

compensate the reduction of the active Al content due to the covering Al_2O_3 shell and this illustrates the increase in the energy output compared to the theoretical value. These results confirm and strongly agree with the findings of DSC that CNMs have a great influence on improving the performance of nanothermites and, consequently, its role in developing micro energetic applications. Nevertheless, there is improvement in the heat released with addition of CNMs; there is a difference between theoretical and experimental values of heat of reaction. Furthermore, our measured value of heat of combustion for the reference sample ($Al/KClO_4$) come with a great agreement with the literatured one which recorded 3620 ± 160 kJ/g [50, 51]. Alteration in heat of reaction attributed to the theoretical value is always calculated for Al metal, rather than Al nanoparticle which is totally different. Also, theoretical calculations don't simulate the real condition of the combustion process such inert Al_2O_3 passivation layer around the Al nanoparticles which act as diffusion barrier, heat sink and inhibiting oxygen from reacting with unreacted Al in the core of n-Al reducing the total energy liberated. Moreover, theoretical heat of reaction is calculated without taking into account the heats of the phase transitions (solid-solid. solid-liquid. or liquid-gas) occur over that temperature range and this leads to erroneously high heat of reaction. Finally, errors that may be occurred during the measurements such as thermometer reading errors and small amount of the samples (0.1 g) used can yield difference between theoretical and experimental heat of reaction. A plot of energy release of nanothermite composition based on 5 % GO at different equivalence ratios is presented in Figure 5-11.

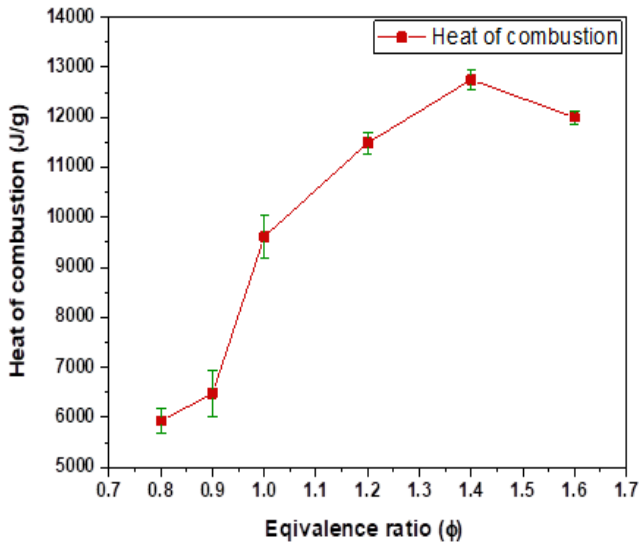

Figure 5-11 Energy release of 5% GO/Al/KClO4 as a function of equivalence ratio

Figure 11 shows that the energy release increased with φ value (fuel rich, φ > 1) and peaked at φ = 1.4. This can be attributed to the almost complete reaction between $KClO_4$ and n-Al (i.e., balanced reaction stoichiometry). This result confirms the findings in the literature that the optimum φ with respect to energy release and reactivity is generally fuel rich for nanocomposite energetic systems [52, 53].

5.7 Conclusion

This paper has examined the effect of different CNMs on the performance of nanothermites based on n-Al as the metal fuel and $KClO_4$ as the oxidizer. We successfully integrated several CNMs on nanothermite compositions using a simple sonication process. The CNMs, especially GO, clearly enhanced their performance. Compared to the reference sample, a significant improvement in energy release of up to 200 % was observed in nanothermites with only 5 % of GO (9.6 kJ/g). The maximum value of the heat of combustion (12.75 kJ/g) was achieved for the φ value of 1.4. The higher energy release of the GO/Al/KClO4 composition highlights the role of GO as an energetic reactant. In addition, the large surface area of GO facilitates the uniform mixing of n-Al and $KClO_4$. High performance nanothermites that were synthesized and characterized in this work bring new opportunities to fabricate novel micro energetic systems. Future work will focus on investigating the effect of GO on the performance of nanothermites based on n-Al and different oxygenated oxidisers.

5.8 References

[1] H. Singh, S. Banerjee, Nanostructured Energetic Composites: An Emerging Paradigm, in: S. Bhattacharya, A. Agarwal, T. Rajagopalan, V. Patel (Eds.) Nano-Energetic Materials, 2019, Springer Nature Singapore Pte Ltd. p. 37–81.

[2] C. Rossi, K. Zhang, D. Estève, P. Alphonse, P. Tailhades, C. Vahlas, Nanoenergetic Materials for MEMS: A Review, Journal of Microeletromechanical systems 2007, 16, p. 919–931.

[3] Y. Gan, L. Qiao, Combustion characteristics of fuel droplets with addition of nano and micron-sized aluminum particles, Combust. Flame. 2011, 158, 354–368.

[4] L. Zhou, N. Piekiel, S. Chowdhury, M. R. Zachariah, Time-resolved mass spectrometry of the exothermic reaction between nanoaluminum and metal oxides: the role of oxygen release, J Phys Chem C 2010, 114, 14269–14275.

[5] M. A. Trunov, M. Schoenitz, X. Zhu, E. L. Dreizin, Effect of polymorphic phase transformations in Al2O3 film on oxidation kinetics of aluminum powders, Combust. Flame 2005, 140, 310– 318.

[6] M. Comet, C. Martin, F. Schnell, D. Spitzer, Nanothermites: A short Review. Factsheet for Experimenters, Present and Future Challenges, Propellants Explos. Pyrotech 2019, 44, 18–36.

[7] C. Wu, K. Sullivan, S. Chowdhury, G. Jian, L. Zhou, M. R. Zachariah, Encapsulation of Perchlorate Salts within Metal Oxides for Application as Nanoenergetic Oxidizers, Adv. Funct. Mater. 2012, 22, 78–85.

[8] W. Zhou, J. B. DeLisio, X. Li, L. Liu, M. R. Zachariah, Persulfate salt as an oxidizer for biocidal energetic nanothermites, J. Mater. Chem. A 2015, 3, 11838–11846.

[9] K. Park, D. Lee, A. Rai, D. Mukherjee, M. R. Zachariah, Size-resolved kinetic measurements of aluminium nanoparticle oxidation with single particle mass spectrometry, J Phys Chem B 2005, 109, 7290–7299.

[10] G. Jian, J. Feng, R. J. Jacob, G. C. Egan, M. R. Zachariah, Superreactive Nanoenergetic Gas Generators Based on Periodate Salts, Angew. Chem. Int 2013, 52, 9743–9746.

[11] W. Zhou, J. B. DeLisio, X. Wang, M. R. Zachariah, Reaction mechanisms of potassium oxysalts based energetic composites, Combust. Flame 2017, 177, 1–9.

[12] X. Hu, J. B. DeLisio, X. Li, W. Zhou, M. R. Zachariah, Direct Deposit of Highly Reactive $Bi(IO_3)_3$ – Polyvinylidene Fluoride Biocidal Energetic Composite and its Reactive Properties, Adv.Eng. Mater. 2017, 19, 1–9.

[13] Q.-L. Yan, M. Gozin, F.-Q. Zhao, A. Cohena, S.-P. Pang, Highly energetic compositions based on functionalized carbon nanomaterials, The Royal Society of Chemistry, Nanoscale 2016, 8, 4799–4851.

[14] J. Kwon, J. M. Ducere, P. Alphonse, M. Bahrami, M. Petrantoni, J. F. Veyan, C. Tenailleau, A. Estève, C. Rossi, Y. J. Chabal, Interfacial chemistry in Al/CuO reactive nanomaterial and its role in exothermic reactio, ACS Appl. Mater. Interfaces 2013, 5, 605– 613.

[15] M. Sharma, V. Sharma, Effect of carbon nanotube addition on the thermite reaction in the Al/CuO energetic nanocomposite, Philosophical Magazine 2017, 97, 1921–1938.

[16] J. L. Sabourin, D. M. Dabbs, R. A. Yetter, F. L. Dryer, I. A. Aksay, Functionalized graphene sheet colloids for enhanced fuel/propellant combustion, ACS Nano 2009, 3, 3945–3954.

[17] R. Thiruvengadathan, S. W. Chung, S. Basuray, B. Balasubramanian, C. S. Staley, K. Gangopadhyay, S. Gangopadhyay, A Versatile Self-Assembly Approach toward High Performance Nanoenergetic Composite Using Functionalized Graphene, Langmuir 2014, 30, 6556–6564.

[18] F. Yang, X. Kang, J. Luo, Z. Yi, Y. Tang, Preparation of core-shell structure $KClO_4$@Al/CuO Nanoenergetic material and enhancement of thermal behavior, Scientific Reports 2017, 7, 3730.

[19] A. M. Dimiev, S. Eigler, Graphene Oxide, Fundamentals and Applications, 2017, John Wiley & Sons, Ltd. p. 455.

[20] J. Song, T. Guo, Miao Yao, J. Chen, W. Ding, X. Zhang, F. Bei, J. Huang, Hindering effect of graphene oxide on reaction performance of Al/MnO2 nanothermite system. Colloid and Interface Science Communications 2020, 37, 100271.

[21] N. F. Vilardi, Graphitic and graphene as enhancer for combustible mixtures, Mechanical engineering, Thesis, 2014, Naval postgraduate school, Monterey, California, USA, p. 158.

[22] X. Zhang, W. M. Hikal, Y. Zhang, S. K. Bhattacharia, L. Li, S. Panditrao, S. Wang, B. L. Weeks, Direct laser initiation and improved thermal stability of nitrocellulose/graphene oxide nanocomposites, Appl. Phys.Lett. 2013, 102, 141905.

[23] D. C. Marcano, D. V. Kosynkin, J. M. Berlin, A. Sinitskii, Z. Sun, A. Slesarev, L. B. Alemany, W. Lu, J. M. Tour, Improved synthesis of graphene oxide, ACS Nano 2010, 4, 4806–4814.

[24] S. Kumar, A. Kumar, A. Bahuguna, V. Sharma, V. Krishnan, Twodimensional carbon-based nanocomposites for photocatalytic energy generation and environmental remediation applications, Beilstein J. Nanotechnol. 2017, 1571–1600.

[25] J. J. Granier, M. L. Pantoya, Laser ignition of nanocomposite thermites, Combust. Flame 2004. 138, 373–383.

[26] E. Lafontaine, M. Comet, Nanothermites, 2016, 111 River Street, Hoboken, NJ 07030, USA: John Wiley & Sons, Inc. 1–323.

[27] D. P. Shoemaker, C. W. Garland, J. I. Steinfeld, J. W. Nibler, Experiment 7, in Experiments in Physical Chemistry, 1981, McGraw-Hill: New York, NY. p. 125–138.

[28] S. Stankovich, D. A. Dikin, R. D. Piner, K. A. Kohlhaas, A. Kleinhammes, Y. Y. Jia, Y. Wu, S. B. T. Nguyen, R. S. Ruoff, Synthesis of graphene based nanosheets viachemical reduction of exfoliated graphite oxide, Carbon 2007, 45, 1558–1565.

[29] S. Perumbilavil, P. Sankar, T. P. Rose, R. Philip, White light Zscanmeasurements of ultrafast optical nonlinearity in reduced graphene oxidenanosheets in the 400–700 nm region, Appl. Phys. Lett. 2005, 107, 051104.

[30] J.-C. Charlier, T. W. Ebbesen, P. Lambin, Structural and electronic properties of pentagon–heptagon pair defects in carbon nanotubes, Phys Rev B 1996, 53, 11108–11113.

[31] P. V. Lakshminarayanan, H. Toghiani, C. U. Pittman, Nitric acid oxidation of vapor grown carbon nanofibers, Carbon 2004, 42, 2433–2442.

[32] B. Nikolay, S. V. Cherkasov, S. V. Savilov, A. S. Ivanov, V. V. Lunin, Bomb calorimetry as a bulk characterization tool for carbon nanostructures, Carbon 2013, 63, 324–329.

[33] L. J. Brennan, P. K. Surolia, L. Rovelli, A. Loudon, S. P. Torsney, S. Roche, K. Ravindranathan Thampi, Y. K. Gun'ko Electrophoretic separation and deposition of metal-graphene nanocomposites and their application as electrodes in solar cells, Electronic Supplementary Material (ESI) for RSC Advances 2016, 6, 64097– 64109.

[34] J. Y.Ying, Mechanical properties and deformation behavior of materials having ultra-fine microstructure, Kluwer Academic Publishers: Netherlands, 1993, p. 565–570.

[35] H. Knözinger, P. Ratnasamy, Catalytic aluminas: Surface models and characterization of surface sites, Catalysis Reviews 1978, 17, 31–70.

[36] N. He, Y. Ni, J. Teng, H. Li, L. Yao, P. Zhao, Identification of inorganic oxidizing salts in homemade explosives using Fourier transform infrared spectroscopy, Spectrochimica Acta Part A: Molecular and Biomolecular Spectroscopy 2019, 221, 117164.

[37] F. Zapata, C. GarcÍa-Ruiz, The discrimination of 72 nitrate, chlorate and perchlorate salts using IR and Raman spectroscopy, Spectrochim. Acta A Mol. Biomol. Spectrosc. 2018, 189, 535–542.

[38] K. Nakamoto, Infrared and Raman Spectra of Inorganic and Coordination Compounds, Part A. Theory and Applications in Inorganic Chemistry, 6th edition ed. 2009, New York: John Wiley and Sons Inc.

[39] A. Hussein, S. Sarkar, D. Oh, K. Lee, B. Kim, Epoxy/p-phenylenediamine functionalized graphene oxide composites and evaluation of their fracture toughness and tensile properties, J. Appl. Polym. Sci. 2016, 133, https://doi.org/10.1002/app.43821.

[40] N. Yan, L. Qin, H. Hao, L. Hui, F. Zhao, H. Feng, Iron oxide/aluminum/ graphene energetic nanocomposites synthesized by atomic layer deposition: Enhanced energy release and reduced electrostatic ignition hazard, Applied Surface Science 2017, 408, 51–59.

[41] A. H. Mady, M. L. Baynosa, D. Tuma, J.-J. Shim, Facile microwave- assisted green synthesis of Ag-ZnFe2O4@rGO nanocomposites for efficient removal of organic dyes under UVand visible-light irradiation, Applied Catalysis B: Environmental 2017, 203,416–427.

[42] R. Krishna, E. Titus, O. Okhay, J. Campos Gil, J. Ventura, E. Venkata Ramana, J. J. A. Gracio, Rapid Electrochemical Synthesis of Hydrogenated Graphene Oxide Using Ni Nanoparticles, Int. J. Electrochem. Sci. 2014, 9, 4054–4069.

[43] Z. Bo, X. Shuai, S. Mao, H. Yan, J. Qian, J. Chen, J. Yan, K. Cen, Green preparation of reduced graphene oxide for sensing and energy storage applications, scientific reports 2014, 4, 4684.

[44] K. Gao, G. Li, Y. Luo, L. Wang, L. Shen, G. Wang, Preparation and characterization of the AP/Al/Fe_2O_3 ternary nanothermites, Journal of Thermal Analysis and Calorimetry 2014, 118, 43–49.

[45] P.-G. Ren, D.-X. Yan, X. Ji, T. Chen, Z.-M. Li, Temperature dependence of graphene oxide reduced by hydrazine hydrate, Nanotechnology 2011, 22, 055705.

[46] M. Fathollahi, H. Behnejad, A comparative study of thermal behaviors and kinetics analysis of the pyrotechnic compositions containing Mg and Al, J Therm Anal Calorim. 2015, 120, 1483–1492.

[47] K. Yin, H. Li, Y. Xia, H. Bi, J. Sun, Z. Liu, L. Sun, Thermodynamic and Kinetic Analysis of Low-temperature Thermal Reduction of Graphene Oxide Nano-Micro Lett. 2011, 3, 51–55.

[48] N. Piekiel, K. Sullivan, S. Chowdhury, M. R. Zachariah, The role of metal oxides in nanothermite reactions: Evidence of condensed phase initiation, DTIC Document, University of Maryland, 2010.

[49] F. Séverac, P. Alphonse, A. Estève, A. Bancaud, C. Rossi, Highenergy Al/CuO nanocomposites obtained by DNA-directed assembly, Adv. Funct. Mater 2012, 22,323–329.

[50] C. Farley, Reactions of Aluminum with Halogen Containing Oxides, in Mechanical Engineering, May 2013, Texas Tech University: USA. p. 74.

[51] C. W. Farley, M. L. Pantoya, M. Losada, S. Chaudhuri, Linking molecular level chemistry to macroscopic combustion behavior for nano-energetic materials with halogen containing oxides, The Journal of Chemical Physics 2013, 074701.

[52] R. Shende, S. Submaranian, S. Hasan, S. Apperson, R. Thiruvengadathan, K. Gangopadhyay, S. Gangopadhyay, P. Redner, D. Kapoor, S. Nicolich, W. Balas Nanoenergetic composites of CuO nanorods, nanowires, and Al-nanoparticles Propellants, Explos., Pyrotech., 33 2008, 122–130.

[53] A. Bezmelnitsyn, R. Thiruvengadathan, S. Barizuddin, D. Tappmeyer, S. Apperson, K. Gangopadhyay, S. Gangopadhyay, P. Redner, M. Donadio, D. Kapoor, S. Nicolich, Modified nanoenergetic composites with tunable combustion characteristics for propellant applications, Propellants, Explos. Pyrotech. 2010, 35, 384–394.

CHAPTER 6 ARTICLE 2: COMBUSTION BEHAVIOR AND REACTION KINETICS OF GO/AL/OXIDIZING SALTS TERNARY NANOTHERMITES

Ahmed Fahd [a,b], Charles Dubois [a, *], Jamal Chaouki [a], John Z. Wen [c]

[a] Chemical Engineering Department, École Polytechnique de Montréal, Montréal, H3C 3A7 (Canada)

[b] Chemical Engineering Department, Military Technical College, Cairo, 11646 (Egypt)

[c] Mechanical and Mechatronics Engineering Department, University of Waterloo, Ontario, N2L 3G1 (Canada)

(This work has been submitted to Journal of Thermal Analysis and Calorimetry)

(Note: Ahmad Fahd is the name I always use instead of Ahmad Emam in my all publications)

6.1 Abstract

In light of recent advances in micro-scale energy systems, such as microthruster and igniters among others, there is now considerable interest in using tertiary nanothermites to meet the increasing demand in high energy density propulsion systems. The first objective of this research is to compare and analyze the thermal behaviour of different nanothermite tertiary compositions based on nano-aluminum (n-Al), graphene oxide (GO), various salt and metallic oxidizers. The second objective is to identify the thermite reaction mechanism through correlations with the activation energy and exothermic peaks. Thermogravimetry analysis coupled with a differential scanning calorimeter (TGA/DSC) was employed to elucidate the reaction process of these nanothermite compositions, while bomb calorimetry was used to measure their heat of combustion. The apparent kinetics parameters were calculated using Kissinger and Ozawa approaches. The results demonstrate that the addition of GO enhances the reactivity of nanothermites with both salt and metallic oxidizers by reducing the reaction onset temperature, activation energy and increasing the heat release. For nanothermites with oxidizing salts, the heterogeneous solid-gas reaction mechanism plays a more important role than the condensed phase reactions. In general, nanothermites based on oxidizing salts are more reactive than those

with metallic ones, as indicated in both theoretical and experimental data. Among them, the GO/Al/$KClO_4$ nanothermite exhibits the highest heat release (9614 J/g), while the GO/Al/$K_2S_2O_8$ nanothermite shows the lowest onset temperature and activation energy (380 $^{\circ}$C and 105 kJ/mol). This study provides benchmark information for optimizing the tertiary nanothermites design, use, storage and handling.

6.2 Introduction

Thermal properties of nanothermite, such as ignition temperature and specific heat released, are important criteria that form part of the practical nanothermite usage as well as a key to exploring the reaction mechanism. Based on this, many studies have been carried out to improve their efficient combustion and ignition characteristics [1-6].

Nanothermites are solid-phase energetic mixtures traditionally composed of metal and metal-oxide components at nanometric scale. Compared with the traditional micron-level termite powder, nanothermites have the advantages of large surface area, a decrease in the needed activation energy, fast energy release and high energy density, and consequently it has improved reaction speed, heat release, pressure and force output [7, 8]. Despite their benefits over microthermites, nanothermites nonetheless go through from extraordinarily lengthy ignition delays, sluggish combustion kinetics, particle agglomeration earlier than ignition, and incomplete combustion, which have restricted their applicability [8-12]. A growing body of literature can be found on the thermal behaviour and combustion mechanism of nanothermite compositions. A solid-state reaction is the most common initiating reaction for thermite compositions, followed by the movement of the resulting reactive species toward each other [13]. The way and nature of movement of the species is still being debated [1-5]. Granier et al. assessed the ignition process and thermal properties of nanothermite based on n-Al and molybdenum oxide (MoO_3) and they found that n-Al reduced the ignition time significantly. In addition, they reported that the combustion of Al/MoO_3 will not occur until the temperature reaches the melting point of either Al or MoO_3 followed by a diffusion-controlled reaction [13]. Based on what was reported in [8,13], nanothermites will ignite around the melting temperature of Al (660 $^{\circ}$C). In [10] the authors investigated the thermal properties of nanothermites based on a wide range of oxidizers, which release oxygen at a widely different range of temperatures to find the relationship between

the oxidizer oxygen release temperature and nanothermite ignition temperature. They concluded that the presence of free oxygen is not necessary to initiate many types of Al based nanothermites. They also suggested a condensed phase reaction mechanism, which does not depend on free oxygen or melted Al. A condensed phase reaction mechanism is confirmed by many studies to be the governing mechanism for nanothermite combustion [14-17].

Recently, graphene and its derivatives have been attracting much attention for improving ignition and the combustion characteristics of nanothermite due to a large specific area and unique thermal, electrical and mechanical properties [18-21]. In particular, graphene oxide (GO) is one of the most appropriate candidate for components in nanothermites due to its superior catalytic properties as well as facile preparation methods [22]. Moreover, GO is considered to be a potential energetic material (EM) by itself, where upon heating, it can readily undergo violent exothermic decomposition due to the extensive oxygenic functional groups on the basal plane (phenol, hydroxyl, and epoxide) and at the edges (carboxylic) [23].

To this day, discussions of the effect of graphene and its derivatives, particularly GO, on the combustion properties and thermal behaviour of nanothermites have been limited to those based on certain types of metallic oxidizers, like Fe_2O_3 and Bi_2O_3 [24, 25]. On the other side the effect of GO on the thermal behaviour of nanothermites based on oxidizing salts and some types of metallic ones has not been explicitly studied from a thermal and mechanistic point of view. Hence, given the importance of gaining a more in-depth understanding of thermite materials for the development of new thermite compositions, it is vital to explore how physical and chemical characteristics of the new components affect the thermite reaction. Additionally, it is important to determine the reaction mechanism and understand the thermal behaviour of these new nanothermites to know how they can be used to adapt to future applications from a performance standpoint and practical safety concerns related to large-scale industrial use.

In the present work, we investigate the thermal behaviour and reaction characteristics of tertiary nanothermites based on n-Al, GO and different types of salt and metallic oxidizers. Experimental and theoretical investigations were performed on eight nanothermite compositions containing five oxidizing salts and three metallic oxides, respectively. Five controlled (reference) samples were prepared and analyzed with oxidizing salts for comparison purposes. All compositions were

characterized using TGA/DSC and a bomb calorimeter. The controlling mechanisms of different nanothermite compositions are discussed based on the measured kinetic parameters.

6.3 Materials and methods

6.3.1 Materials

Graphite flakes, phosphoric acid (H_3PO_4), sulphuric acid (H_2SO_4), hydrogen peroxide (H_2O_2), and acetone used in the preparation of GO were purchased from Sigma-Aldrich. Oxidizing salts, such as potassium perchlorate ($KClO_4$) and ammonium nitrate (NH_4NO_3), were brought from Defence Research and Development Canada. All other salts and metallic oxidizers, namely potassium periodate (KIO_4), potassium persulfate ($K_2S_2O_8$), potassium permanganate ($KMnO_4$), iron oxide (Fe_2O_3), cupper oxide (CuO) and tungsten oxide (WO_3) were purchased from Sigma-Aldrich. The as-purchased Al nanoparticles from Us Research Nanomaterials Inc. have a spherical shape with an average particle size of 40 nm, a purity of more than 99.9 % metal basis, an active Al content of 80 wt. % (mass fraction), a surface area of 30-50 m^2/g and a density 2.7 g/cm^3 as specified by the manufacturer.

6.3.2 Synthesis of GO

Graphene oxide was synthesized using an improved Hummer method with graphite powder as the starting material.[26] Graphite (1 g) was mixed with 13 ml of 85 % H_3PO_4 and 120 ml of concentrated H_2SO_4 (98 %) in a 300 ml beaker, followed by the slow addition of 6 g of $KMnO_4$ in portions while mixing manually with a glass rod to inhibit any severe reaction that might happen. After that, the mixture was left to cool down and then mixed slowly with a suitable overhead mechanical stirrer with a paddle rod (SS316L/PTFE) for 1-3 days until the mixture turned as viscous as honey and formed a mirror on the beaker's wall. After 3 days, the obtained products were slowly added in portions to 1.5 l of deionized water (DI) in a 2 l beaker with a stirrer mixing over an ice bath (~ 5 $^{\circ}$C). After one hour of mixing, hydrogen peroxide (~ 10 %) was added dropwise to the mixture with continuous mixing until the colour of the mixture turned to yellow/orange. GO dispersion was washed by decantation 2-3 times with DI acidified with hydrochloric acid (HCl) and minimizing the amount of liquid as much as possible to remove

most of the ionic impurities. Finally, GO was separated with centrifugation and washed with acetone. The flow sheet of GO preparation is illustrated in Figure 6-1.

Figure 6-1 A scheme of GO preparation

6.3.3 Preparation of nanothermite compositions

Nanothermite compositions were prepared by weighing the fuel (n-Al) and different oxidizers individually based on the stoichiometric ratio in Table 1. The dispersion of n-Al with each oxidizer and 5 % GO was conducted in acetone. The samples were then put in an ultrasonic bath for 30 min to ensure proper dispersion. Acetone was allowed to evaporate at 60 °C for 1 hour with simultaneous mechanical stirring to prevent the reagglomeration of nanoparticles. Wet particles were then fully dried in a vacuum desiccator for 12h to drive off any remaining acetone. Finally, the dried powder was gently broken up with a spatula to remove any large clumps and until the consistency was that of a loose powder. Table 1 illustrates different nanothermite compositions and their reactions.

Table 6-1 Nanothermite compositions based on salt and metallic oxidisers

Samples	Oxidizer type	Oxidizer (wt. %)	Al (wt. %)	GO (wt. %)	Thermite reactions
S_1	$KClO_4$	62.51	32.49	5	$8Al + 3KClO_4 \rightarrow 4Al_2O_3 + 3KCl$
S_2	$K_2S_2O_8$	83.84	11.16	5	$4Al + 3K_2S_2O_8 \rightarrow 2Al_2O_3 + 3K_2SO_4 + 3SO_2$
S_3	KIO_4	72.35	22.65	5	$8Al + 3KIO_4 \rightarrow 4Al_2O_3 + 3KI$
S_4	$KMnO_4$	81.14	13.86	5	$2Al + 2KMnO_4 \rightarrow 5Al_2O_3 + 3K_2O + 6MnO$
S_5	NH_4NO_3	77.56	17.44	5	$2Al + 3NH_4NO_3 \rightarrow Al_2O_3 + 3N_2 + 6H_2O$
S_6	CuO	77.47	17.53	5	$2Al + 3CuO \rightarrow Al_2O_3 + 3Cu$
S_7	Fe_2O_3	70.99	24.01	5	$2Al + Fe_2O_3 \rightarrow Al_2O_3 + 3Fe$
S_8	WO_3	77.05	17.95	5	$2Al + WO_3 \rightarrow Al_2O_3 + W$

6.3.4 Homogeneity of nanothermites

Morphology and homogeneity of nanothermite samples were studied by FEI Quanta FEG 450 SEM operated at 15 kV coupled with EDS measurements.

6.3.5 Thermal analysis and reaction calorimetry

Simultaneous TGA/DSC (Mettler Toledo, DSC1) was performed to assess the thermal characteristics of nanothermite compositions. Approximately 5 mg of nanothermite sample was placed into an alumina crucible and heated from 30 $^{\circ}$C to 1100 $^{\circ}$C with different heating rates (2, 5, 8, 10 $^{\circ}$C/min). All TGA/DSC measurements were performed under argon atmosphere with a flow rate of 100 ml/min. The heat of combustion of nanothermite samples was measured by an oxygen bomb calorimeter (model: Parr™ 1341 Plain Jacket Calorimeter). Each test was performed five times and the average value of heat of combustion was calculated and compared with the theoretical one.

6.4 Results and discussion

6.4.1 Structure and chemical characterization

The chemical composition of prepared GO was checked by an CHNSO Elemental Analyzer EA3000 (EuroVector); the mass fraction (w) of C, H, N, S and O was as follows: for GO, w(C) = 0.5013 ± 0.0062, w(O) = 0.4681 ± 0.0046, w(H) = 0.0174 ± 0.0011, w(S) = 0.0205 ± 0.0015. Furthermore, Heat of combustion of GO was measured by oxygen bomb calorimeter and recorded at 34.35 ± 0.32 KJ/g.

The homogenous distribution of each component throughout the thermite samples is an important performance factor. The quality of dispersion in the samples was evaluated using SEM-EDS analysis, as shown in Figure 6-2, in which the GO/Al/KIO_4 was selected as a representative for all of the samples.

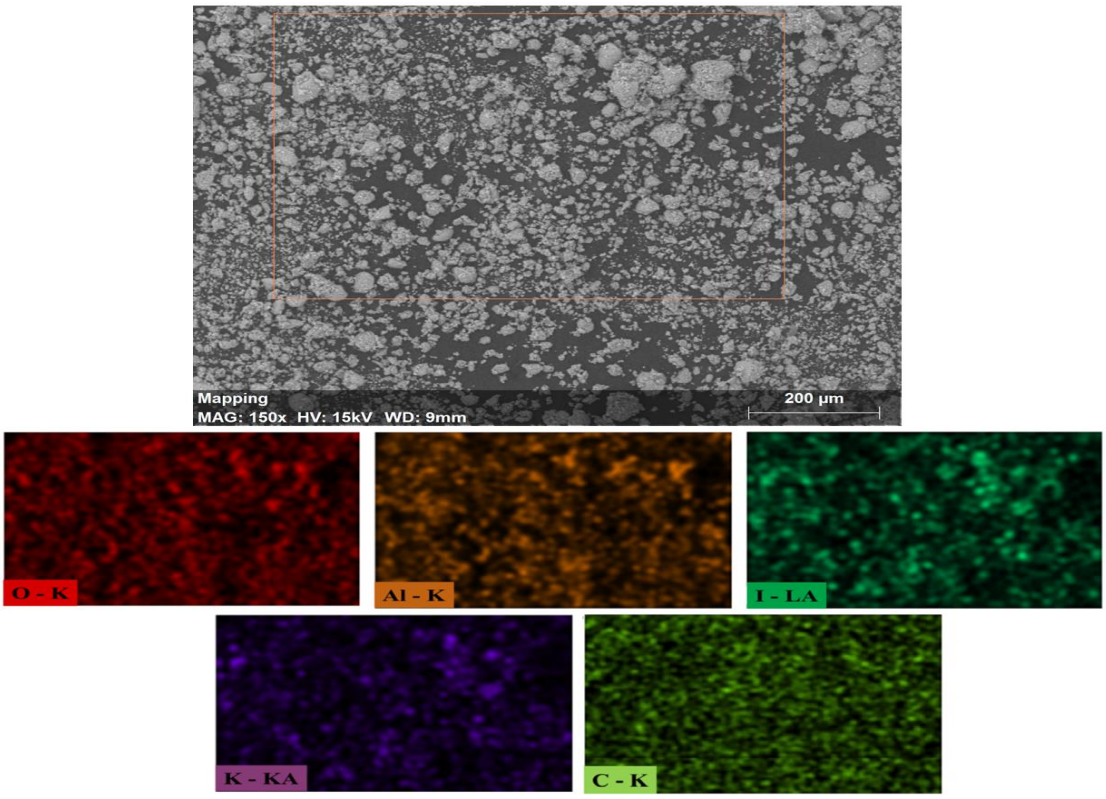

Figure 6-2 EDS images of the 5% GO/Al/KIO_4 nanothermite

The spatial homogeneity of the elemental composition of GO/Al/KIO_4 nanothermites is confirmed by the EDS data reported in Figure 2. As it can be seen, no agglomerations of the fuel or the oxidizer were noticed, which confirms the good mixing and distribution of the particles and thus validates the preparation method. Furthermore, this good homogeneity paves the way for the next step of thermal characterization.

6.4.2 Thermal behaviour

Simultaneous DSC/TGA was performed for prepared GO and different nanothermite formulations. Thermal behaviour of GO is illustrated in Figure 6-3.

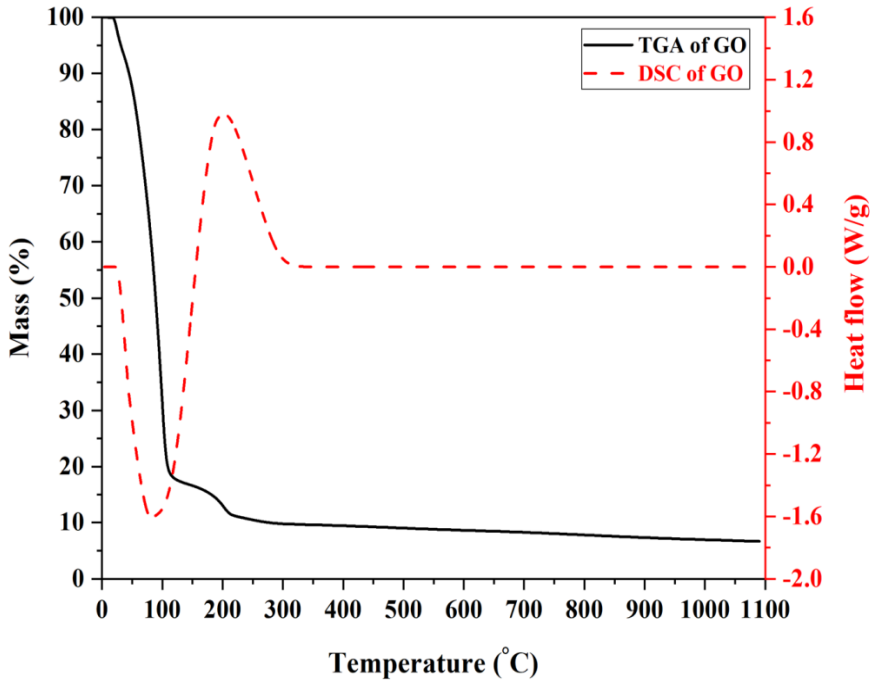

Figure 6-3 TGA/DSC curves of GO

TGA curve shows that the mass loss of GO happens in three stages. First mass loss of up to 100 °C can be attributed to the evaporation of the interstitial water entrapped inside GO and corresponding to the endothermic in DSC curve. Second mass loss from 100-250 °C is ascribed to thermal decomposition of oxygenated functional groups (acidic and hydroxyl groups) of GO and the formation of graphite (C). The second mass loss is consistent with the exothermic peak observed slightly above 200 °C in DSC curve. Third mass loss up to 1100 °C yields from the decomposition of carbonyl groups that was formed on the surface of GO during the oxidation process [27, 28]. The thermal decomposition of GO/Al/$KClO_4$ nanothermite is illustrated in Figure 6-4.

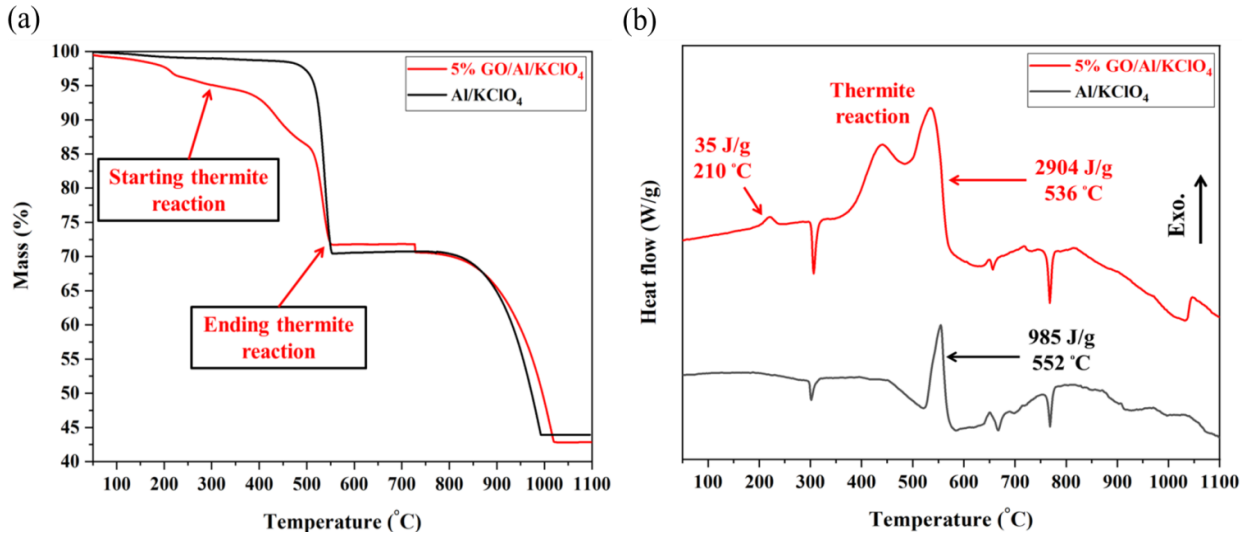

Figure 6-4 TGA/DSC curves for 5 % GO/Al/$KClO_4$ and reference nanothermites

The GO/Al/$KClO_4$ nanothermite decomposes in two stages as demonstrated in Fig. 4a. A first and steep weight loss is observed slightly above 200 °C. It is attributed to the thermal decomposition of the oxygenated functional groups of GO, the formation of graphite (C) and the liberation of oxygen. A second weight loss from 400 to 550 °C is assigned to the major thermite reaction in GO/Al/$KClO_4$ [29].

Figure 4b shows that thermal decomposition of Al/$KClO_4$ is characterized by three endothermic and one exothermic event. A first endothermic peak is displayed at approximately 302 °C and ascribed to the phase change of $KClO_4$ from a rhombic to a cubic structure [30]. A second peak is exothermic and represents the main thermite reaction between Al and $KClO_4$ and is accompanied by a large mass loss between 500-560 °C. The third and fourth endothermic peaks are assigned to the melting of the unreacted Al and KCl reaction product at 660 and 770 °C, respectively [30].

In the case of GO/Al/$KClO_4$, there was a new exothermic peak at 210 °C, corresponding to the decomposition of GO, which suggests the removal of the oxygenated group in GO and confirms TGA findings [31]. The main thermite reaction peak is divided into two consecutive overlapping peaks. First, a decreased and broadened thermite reaction peak indicates staged reaction pathways between C (formed in the early stages through the decomposition of GO) and nanothermite reactants (i.e., C-O, C-$KClO_4$ reactions). These reactions effectively help accelerate the occurrence of the subsequent main thermite reactions (Al- $KClO_4$ and Al-O). Moreover, C-O and

C-$KClO_4$ reactions clarify the increase in energy released from the thermite reaction in the GO/Al/$KClO_4$ and the decrease in its reaction onset temperature. The thermal decomposition of GO/Al/ $K_2S_2O_8$ nanothermite is illustrated Figure 6-5.

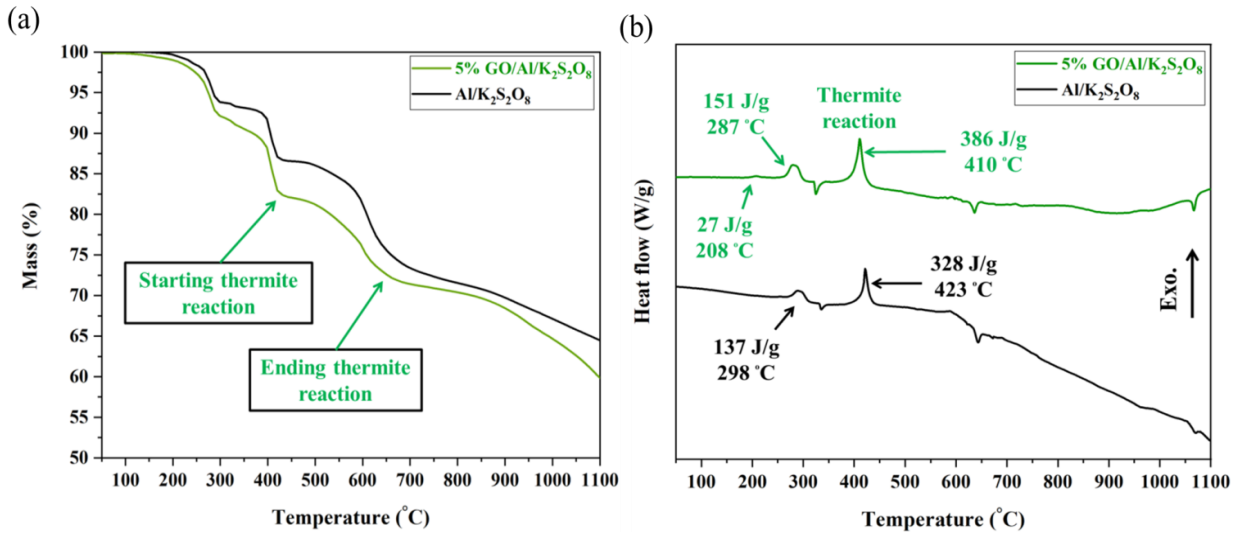

Figure 6-5 Thermal analysis of 5 % GO over Al/$K_2S_2O_8$ and reference nanothermites

The TGA graphs of Al/$K_2S_2O_8$ nanothermites with and without GO show that decomposition occurs mainly in three stages and is demonstrated in Figure 5a. First, the weight loss in nanothermite samples occurred in two mass reduction sub-steps at 270 °C and 310 °C. This weight loss is attributed to the thermal decomposition of $K_2S_2O_8$ to $K_2S_2O_7$ and O_2. Second, weight loss occurring in the temperature range of 420-610 °C is assigned to the major thermite reaction. The final decomposition step began at ~1050 °C and corresponded to the decomposition of K_2SO_4 to SO_2, O_2 and K.

The thermal decomposition of GO/Al/$K_2S_2O_8$ nanothermite is characterized by three endothermic and three exothermic peaks appearing in Figure 5b. The first endothermic peak is displayed at approximately 340 °C and is ascribed mainly to the $K_2S_2O_7$ phase change and decomposition of $K_2S_2O_8$ to $K_2S_2O_7$ and O_2 (small amount) [32]. The second endothermic peak appears at ~640 °C and corresponded to the melting of unreacted Al. The third endothermic peak characterized the melting of K_2SO_4 followed by decomposition to SO_2, O_2 and K [32]. On the other side, GO showed a non-negligible exothermic peak at 200 °C, suggesting the removal of the oxygenated group in GO and confirming TGA findings. The second exothermic peak mainly resulted from

the decomposition reaction of $K_2S_2O_8$ to $K_2S_2O_7$ and O_2. This reaction is highly exothermic in comparison with the other metallic oxidisers, which have an endothermic decomposition reaction. Nanothermite of GO/Al/$K_2S_2O_8$ had an exothermic peak at ~ 410 °C resulting in a 12 % weight loss and suggesting the thermite reaction occurrence. Inclusion of GO on Al/$K_2S_2O_8$ enhances the reactivity of the nanothermite due to the increasing heat released and the decreasing reaction onset temperature. The addition of GO improved the total energy output from GO/Al/$K_2S_2O_8$, however, it still had a lesser effect compared to GO/Al/$KClO_4$. The lesser effect of GO on GO/Al/$K_2S_2O_8$ can be illustrated by the capability of $K_2S_2O_8$ to oxidize nano-C in the mixed suspension before ignition [33, 34]. Therefore, the GO/Al/$K_2S_2O_8$ nanothermite loses the advantage of the high energy output from other suggested reaction paths, like (C-O, C-$KClO_4$) in GO/Al/$KClO_4$, in accelerating the main thermite reaction. So, the enhanced available energy of the GO/Al/$K_2S_2O_8$ nanothermite will be mainly directed to improving both the fuel-oxidizer contact and the reactant mass diffusion. The decomposition of the GO/Al/KIO_4 nanothermite and its reference sample is shown in Figure 6-6.

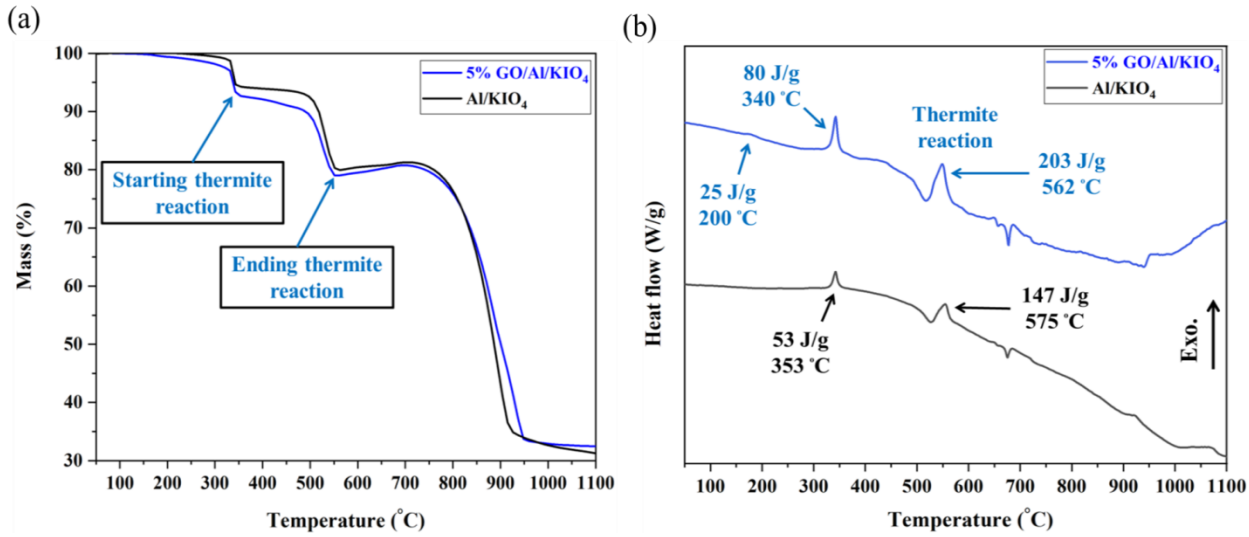

Figure 6-6 TGA/DSC curves for 5 % GO over Al/KIO_4 and reference nanothermites

Figure 6a clarifies that the GO/Al/KIO_4 nanothermite decomposes in two steps. First, KIO_4 decomposes to KIO_3 and O_2, which occurs at temperature 340 °C. Second, the decomposition step at temperature 550 °C represents the main thermite reaction with a weight loss of 15 %.

The thermal decomposition of the GO/Al/KIO_4 nanothermite is illustrated in Fig. 5b and exhibits three exothermic and two endothermic peaks. The exothermic peak appearing at a temperature of 340 °C is earmarked for the decomposition of KIO_4 to KIO_3 and releases oxygen. This temperature is less than the one reported in literature, [35] which can be ascribed to the effect of GO as EM by itself and its high surface area, which enhances the contact between the fuel and oxidiser. Although the decomposition of KIO_4 is exothermic (80 J/g), it is still less reactive than $K_2S_2O_8$ but more reactive than other metallic oxidisers. The endothermic peak displayed at temperature 530 °C is characterized by the decomposition of KIO_3 to potassium iodide (KI) and oxygen. The other two exothermic and endothermic peaks resulted from the decomposition of GO at 200 °C, the main thermite reaction at 550 °C and the melting of unreacted Al at 660 °C. It clearly appears in Fig. 6b that GO not only enhanced the reactivity of the Al/KIO_4 nanothermite by shifting the reaction onset temperature to a lower one, but also increased the energy released, which was calculated from the integration of the area under the peak. The heat released for the GO/Al/KIO_4 nanothermite increased by approximately 30 % compared to the reference one. Furthermore, the increasing percentage of the heat released in GO/Al/KIO_4 is less than that in the case of GO/Al/$KClO_4$. The high enthalpy of the side reaction (C-$KClO_4$), which was recorded at approximately 154 KJ/mol, is two times larger than (C-KIO_4), which has an enthalpy of reaction equal to 72 KJ/mol) [36], and is considered the main reason for the lower increase in the energy output of GO/Al/KIO_4 compared to GO/Al/$KClO_4$. Figure 6-7 demonstrates the TGA/DSC of GO/Al/$KMnO_4$ nanothermites.

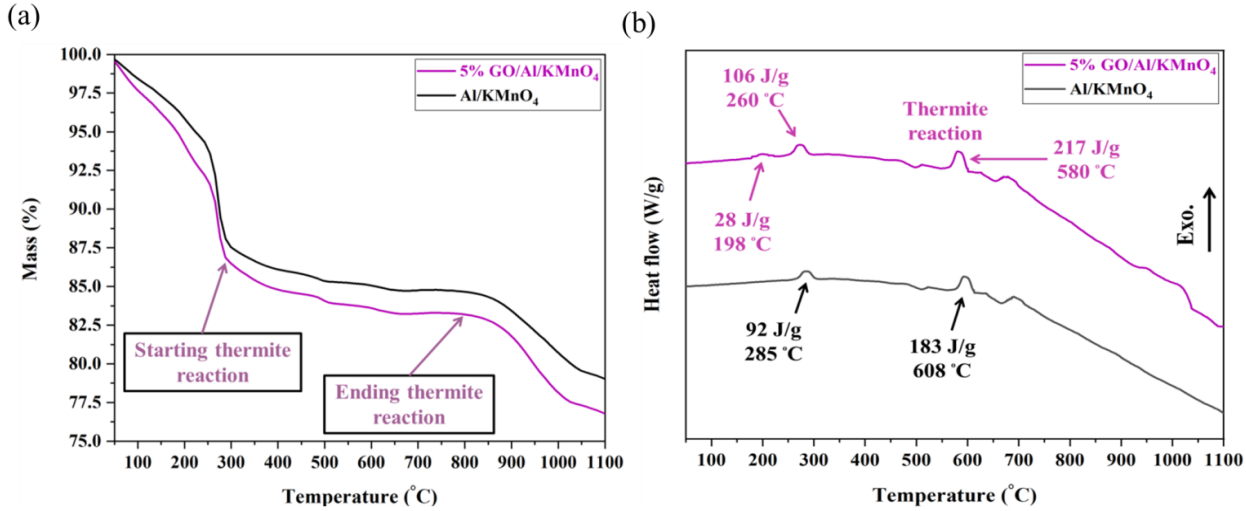

Figure 6-7 TGA/DSC curves for 5 % GO over Al/$KMnO_4$ and reference nanothermites

The mass loss of GO/Al/$KMnO_4$ is considered in two phases. The first phase is attributed to the decomposition of $KMnO_4$ at a temperature of 260 °C to K_2MnO_4 and O_2 accompanied by a weight loss of about 10 % [37]. In addition, further decomposition of K_2MnO_4 to K_3MnO_4 and O_2 occurs at 520 °C followed by the main thermite reaction as illustrated in Fig. 7a [38, 39].

Figure 7b indicates that the thermal decomposition of the GO/Al/$KMnO_4$ nanothermite has three exothermic peaks resulting from the decomposition of GO, $KMnO_4$ and the main thermite reaction. The reactivity of the GO/Al/$KMnO_4$ nanothermite is enhanced by the addition of GO and using n-Al. This appeared in the thermite exothermic peak in the DSC plot compared with the previous results reported by Chen Wei et al., which stated that the reaction of the micro Al size with the decomposition products of $KMnO_4$ will not occur until adding Mg as a secondary fuel to enhance micro Al sensitivity to react with $KMnO_4$ [40]. The other two endothermic peaks are characterized by the second decomposition step of K_2MnO_4 to K_3MnO_4 and O_2 and the melting of unreacted Al fuel. Thermal analysis for the decomposition of the GO/Al/NH_4NO_3 nanothermite and its reference sample is demonstrated in Figure 6-8.

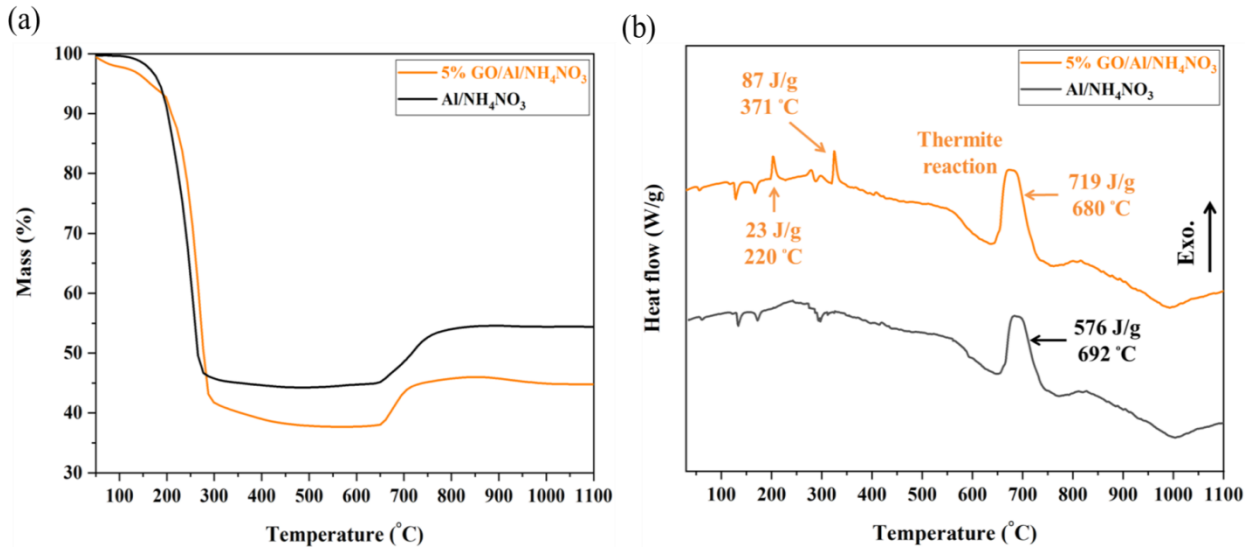

Figure 6-8 TGA/DSC curves for GO/Al/ NH_4NO_3 and its reference nanothermites

The thermal gravimetric analysis of GO/Al/NH_4NO_3 is reflected in two steps as shown in Fig. 8a. The first step is attributed to the decomposition of NH_4NO_3, within which several thermal events occur, begins with crystallographic transformation at 67 °C and ends with maximum rate of

decomposition at ~ 290 °C (~ 60 % mass loss). The second step is assigned to the main thermite reaction starting at 620 °C and ending at 750 °C with a 7 % mass gain.

Figure 8b demonstrates the DSC curve of GO/Al/NH_4NO_3 over the temperature range from 30 °C to 1100 °C, within which several thermal events occur. Four endothermic and three exothermic peaks can be identified during the course of heating GO/Al/NH_4NO_3 nanothermite and only one exothermic peak for the Al/NH_4NO_3. The unexpected small peaks at low temperature in DSC were likely resulted from the heat activated and insignificant atomic re-arrangement within the ternary mixtures. The first two endothermic peaks occur at 67 and 127 °C due to the crystallographic transformation IV → II and II → I, respectively. The third endothermic peak, corresponding to the melting point of ammonium nitrate, occurs near 170 °C, after which the decomposition starts. The fourth peak, corresponding to the maximum rate of decomposition, is reached at approximately 290 °C [41]. On the other side, the first exothermic peak is characterized by the decomposition of GO and appears at 200 °C. The second exothermic peak may be attributed to the intermediate reaction between the decomposition products of GO and Al and both first and second exothermic peaks do not appear in the Al/NH_4NO_3 reference sample. The third exothermic peak is assigned to the main thermite reaction between the decomposition products of NH_4NO_3 and Al fuel. So, we can observe that the inclusion of GO has a good catalytic effect on the performance of Al/NH_4NO_3 nanothermite. The effect of GO on the thermal decomposition of nanothermites based on metallic oxidizers (Fe_2O_3, CuO and WO_3) and n-Al is shown in Figure 6-9.

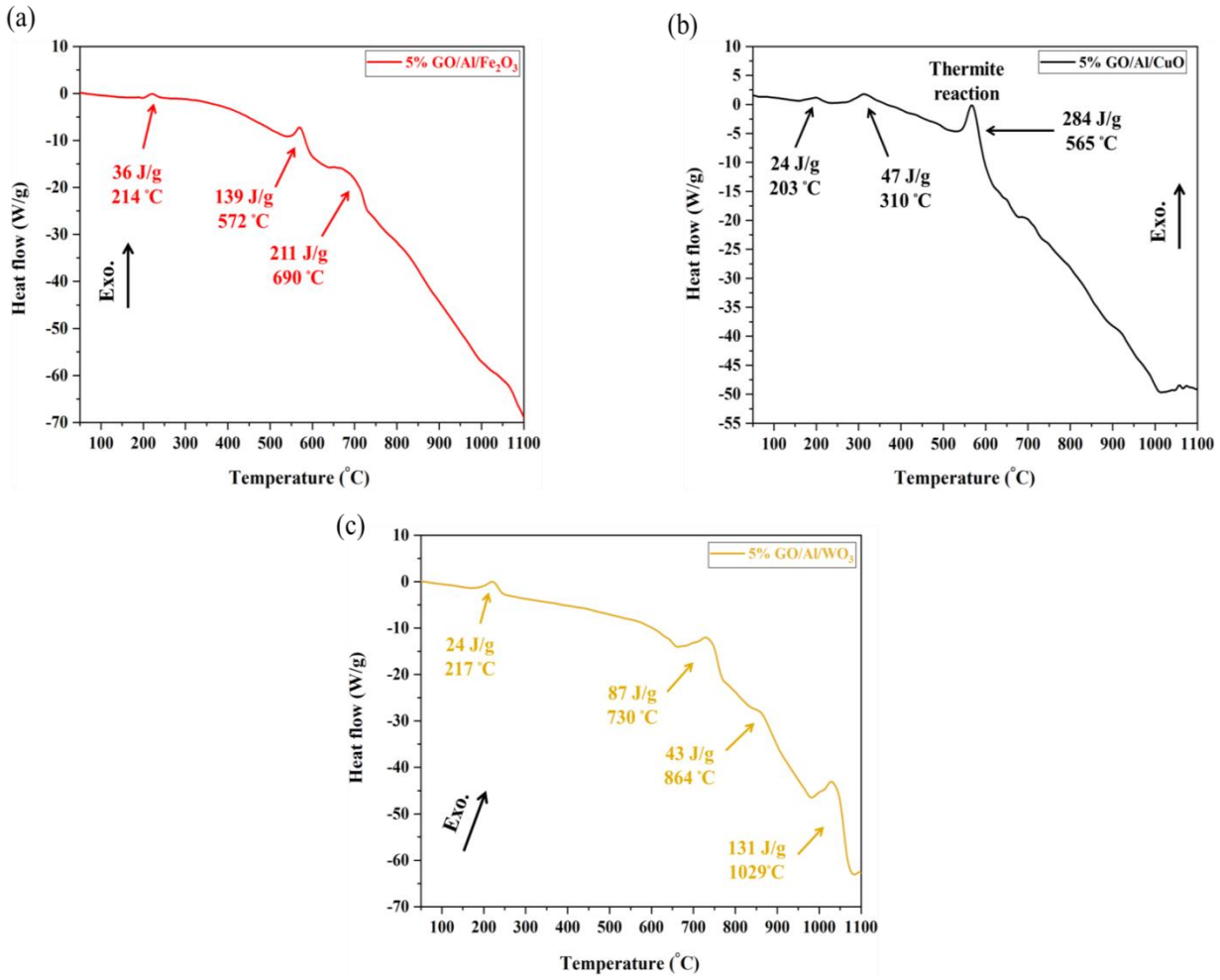

Figure 6-9 DSC (a) curve of GO/Al/Fe_2O_3, (b) GO/Al/CuO and (c) GO/Al/ WO_3

The thermal decomposition of GO/Al/ Fe_2O_3 occurs with two exothermic peaks as shown in Fig. 9a. Generally, the initial energy released was observed at a temperature of 550 °C in the first exothermic peak and a milder energy was released in the second exothermic hump, which represents the main thermite reaction at a temperature of 690 °C [25]. The effect of the addition of GO on Al/Fe_2O_3 is noted in enhancing the reactivity of Al/Fe_2O_3 by increasing the energy output in the first decomposition step and shifting the main thermite reaction to occur on the first stage and, consequently, increase the energy output.

Figure 9b illustrates the thermal decomposition of GO/Al/CuO with three remarkable exothermic peaks and one endothermic peak, which corresponds to the melting of unreacted Al. The first exothermic peak is characterized by the decomposition of GO at approximately 200 °C. The

second small exothermic peak at 300 – 350 °C is attributed to the moisture removal with heat treatment [42]. The third exothermic peak with a maximum peak temperature at 565 °C is assigned to the major thermite reaction of GO/Al/CuO. The heat released from GO/Al/CuO is 2.7 times greater than that of Al/CuO measured by Sharma et al [42]. The exothermic energy release of the GO/Al/CuO nanothermite increased and the reaction onset temperature decreased with the addition of GO due to increased intimate contact and effective heat transfer between the Al and CuO by the GO assisted oxidation of Al nanoparticles through oxygen liberation from GO decomposition.

Figure 9c shows that DSC curve of GO/Al/WO_3 is punctuated by four exothermic peaks and only one endothermic peak which is ascribed to the melting of Al. As mentioned before, the exothermic peak at 200 °C is assigned to the decomposition of GO. Three consecutive broad peaks after the melting of Al are described by the thermite reaction. Based on previous studies, the main thermite reaction of Al/WO_3 occurred at approximately 1000 °C and released most of thermite reaction heat [43]. Here, it is noted that the addition of GO enhanced the energy released in the first and second steps and decreased the energy output from the third peak, which means that ignition occurs at a lower temperature and overall reactivity will be enhanced.

6.4.3 Heat of combustion of nanothermites

The heat of combustion of all nanothermite samples was measured using a bomb calorimeter. Each test was performed five times and the average value of the heat of combustion was calculated. Sample mass for the first two tests was 0.1 g, then increased the sample mass to 0.3 g for the following two tests and the final test mass was 0.5 g. The energy of combustion was calculated according to standard operating procedures illustrated in reference [44]. The experimental values of the heat released are given in Table 2.

Table 6-2 Heat of combustion calculated from bomb calorimeter

Samples	**Average Heat of combustion (J/g)**	**Theoretical Heat of combustion (J/g)**
Al/$KClO_4$	3553 ± 197	10600 [34]
GO/Al/$KClO_4$	9614 ± 362	------
Al/$K_2S_2O_8$	2968 ± 125	5800 [34]
GO/Al/$K_2S_2O_8$	5470 ± 209	------
Al/KIO_4	3016 ± 143	6900 [34]
GO/Al/KIO_4	4680 ± 250	------
Al/$KMnO_4$	2383 ± 137	12230
GO/Al/$KMnO_4$	4598 ± 276	------
Al/NH_4NO_3	2995 ± 158	7775
GO/Al/NH_4NO_3	6270 ± 313	------
Al/Fe_2O_3	2153 ± 105	3989 [45, 46]
GO/Al/Fe_2O_3	3039 ± 182	------
Al/CuO	2435 ± 145	4072 [45, 46]
GO/Al/CuO	3814 ± 212	------
Al/WO_3	2192 ± 136	2902 [45, 46]
GO/Al/WO_3	2836 ± 165	------
Al/$KClO_4$	3620	10630
Al/I_2O_5	3680	6140
Al/$AgIO_3$	2670	5020
Al/$Ca(IO_3)_2$	2640	7810

Results demonstrated in Table 2 point out that the energy of combustion increased with the addition of GO. Again, this would be ascribed to the effect of GO on decreasing the diffusion distance between fuel and oxidiser, improving the dispersion of n-Al particles and preventing their agglomeration through the course of oxidizers. In addition to the exothermic decomposition of GO at 200 $^{\circ}$C, which consequently catalyzes the thermite reaction through C-O and C-oxidiser reaction pathways. So, GO acts as act as secondary fuel which adds more energy to the system, help in the completion of n-Al combustion and compensate the reduction of the active Al content due to the covering Al_2O_3 shell. Heat released by the GO/Al/$KClO_4$ nanothermite has the greatest value among those of the other samples, indicating that the combustion of Al in GO/Al/$KClO_4$ is more complete compared with those of other oxidizers.

Literature results reported in [47, 48] listed in Table 2 confirmed our observation that there is a big difference between theoretical and experimental values of heat of reaction. Furthermore, our measured value of heat of combustion for Al/$KClO_4$ comes with a great agreement with the literatured one which confirm the success of testing procedures and its reliability.

Alteration in heat of reaction between measured and theoretical values attributed to the fact that the latter is always calculated for Al metal, rather than Al nanoparticle which is totally different. Also, theoretical calculations do not simulate the real condition of the combustion process such inert Al_2O_3 passivation layer around the Al nanoparticles which act as diffusion barrier, heat sink and inhibiting oxygen from reacting with unreacted Al in the core of n-Al reducing the total energy liberated. Moreover, theoretical heat of reaction is calculated without taking into account the heats of the phase transitions (solid-solid. solid-liquid. or liquid-gas) occur over that temperature range and this leads to erroneously high heat of reaction [45, 46]. Finally, errors that may be occurred during the measurements such as thermometer reading errors can yield difference between theoretical and experimental heat of reaction.

6.4.4 Nanothermite reaction kinetics

To ensure safe processing, handling and storage of nanothermites, in addition to avoiding hazards associated with their thermal decomposition, stability and ignition, a kinetics evaluation should be carried out. Arrhenius parameters for the thermal decomposition reaction of nanothermite compositions were calculated using Kissinger’s method according to equation (1) [49].

$$\ln\frac{\beta}{T_p^2} = \ln\frac{A.R}{E} - \left(\frac{E}{R}\right)\frac{1}{T_p} \quad (1)$$

Where β is the heating rate of the DSC experiment; T_p is the maximum temperature of the exothermic decomposition peak at the differential heat rate of the DSC experiment; E, A and R the activation energy, the pre-exponential factor and the universal gas constant, respectively. Calculated value of activation energy was confirmed through Ozawa's method according to equation (2).

$$\log\beta = -0.4567\left(\frac{E}{R}\right)\frac{1}{T_P} \quad (2)$$

For each heating rate and nanothermite composition ln (β/T_p^2) was plotted against ($1/T_p$) as illustrated in Figure 6-10.

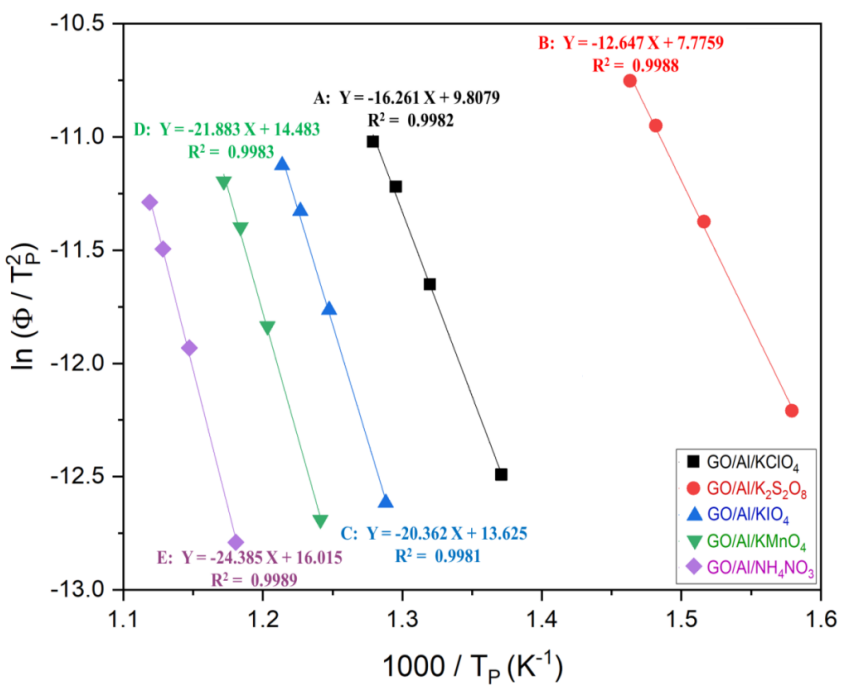

Figure 6-10 Data correlation line of ln (β/T_p^2) against ($1/T_p$) for nanothermite samples

Figure 10 demonstrates the relationship between ln (β/T_p^2) and ($1/T_p$) is a straight line obtained by linear regression through the data points. Activation energy and pre-exponential factors are calculated from the slope and intercept of the line for each composition. The results tabulated in Table 3 represent the kinetic parameters among all nanothermite samples.

Table 6-3 Kinetic parameters of nanothermite mixtures

Formulas	**E_a (Kissinger's method) kJ/mol**	**E_a (Ozawa's method) kJ/mol**	**A (S^{-1})**	**R^2**
GO/Al/$KClO_4$	135.197	140.485	295.579 x 10^6	0.9982
GO/Al/$K_2S_2O_8$	105.145	110.372	30.131 x 10^6	0.9988
GO/Al/KIO_4	169.292	173.616	168.302 x 10^8	0.9984
GO/Al/$KMnO_4$	181.938	186.106	426.580 x 10^8	0.9983
GO/Al/NH_4NO_3	202.734	206.532	219.959 x 10^9	0.9989

Results demonstrated in Table 3 show that the absolute values of the correlation coefficients of all nanothermites are greater than 0.99. Furthermore, the highest activation energy and pre-exponential factor achieved by a nanothermite is based on GO/Al/NH_4NO_3, while those based on GO/Al/$K_2S_2O_8$ represent the lowest one. Generally, nanothermites based on oxidizing salts have a lower activation energy compared with those based on metallic oxidizers, such as Al/Fe_2O_3, Al/Bi_2O_3, Al/MnO_3, Al/NiO, and Al/MnO_2, which were reported at 248, 222, 205, 217, and 342 kJ/mol respectively [15, 50, 51]. As well, the addition of GO could reduce the activation energy of nanothermites. For example, composition based on GO/Al/$KClO_4$ has an activation energy (135 kJ/mol), which is lower than all metallic oxides based nanothermites and even lower than this (Al/$KClO_4$) without GO, which recorded (145 kJ/mol) [30]. Reducing the activation energy of Al nanoparticle-based thermites can be illustrated as follows. Firstly, before the thermite reaction occurs, nanothermite components aggregate forming agglomerations. Then the thermal decomposition of GO happens with the liberation of oxygen through its oxygenated function groups, which could be disruptive to the aggregation of nanothermite constituents. To some extent, this process is equivalent to dispersing the nanothermite mixture again more even, just like a second mixing cycle. Besides, the amount of gaseous oxygen release will be good for the thermite exothermic reaction, which enhances the combustion process. Finally, according to the

TGA/DSC results, the process of most nanothermites' oxidizer thermal decomposition is exothermic, and the main thermite reaction comes afterward, which could be a kind of pre-ignition. Therefore, the activation energy of the system is reduced.

6.4.5 Nanothermite reaction mechanism

Although it is difficult to determine the reaction mechanisms of thermite formulations that have been developed because of their energetic nature, it is necessary to have a solid understanding of their reaction mechanisms in order to know the impact of nanothermite compositions on the ignition and reaction characteristics and, hence, control their combustion behaviour. Generally, whatever the type of oxidizer, thermite reaction mechanisms can be mainly classified into either condensed phase reaction (solid-solid reaction) or heterogeneous reaction (gas-solid reaction) mechanisms. The condensed phase reaction governs most thermite composites based on metallic oxidizers [52-55]. In this mechanism, the decomposition of the oxidizer to liberate oxygen will not occur and the reaction ensues at the interface between the two solid reactants (fuel and oxidizer) through direct contact and ion transfer. In the heterogeneous reaction mechanism, on the other hand, first the oxidizer decomposes to release oxygen, then gaseous oxygen migrates to n-Al particles and diffuses through the alumina shell until reaching the Al core where ignition takes place.

TGA/DSC will be used to identify the thermite reaction mechanism by correlating the activation energy and exothermic peaks. From TGA/DSC outputs, the relationship between the oxygen release temperature of different salt and metallic oxidizers and the onset temperature of the corresponding nano-Al-fueled thermites is demonstrated in Figure 6-11.

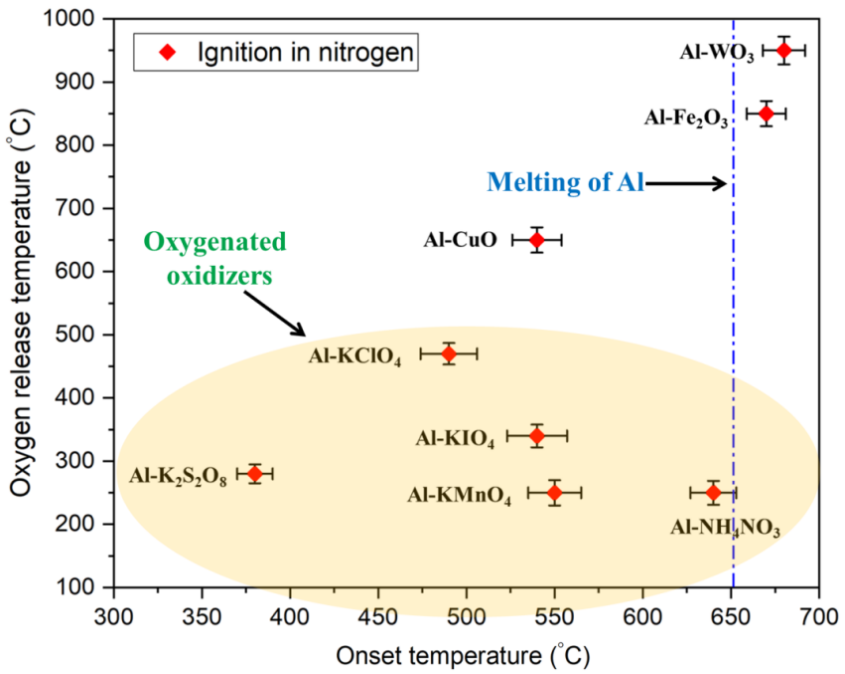

Figure 6-11 Relation between oxygen release temperature of different oxidizers and onset temperature of their nanothermites

Figure 11 illustrates that all of the oxidizing salts, in addition to CuO based nanothermites, have an onset temperature before the melting point of Al. These results indicate that the heterogeneous solid gas reaction is the dominant reaction mechanism and the oxygen release from oxidizers, in addition to the rate of Al diffusion outward from the alumina shell will be the rate determining steps of the reaction. In [34], the authors found two contradictive effects. On the one hand, the ignition of nanothermites based on Al and any type of salts ($KClO_4$, KNO_3, $K_2S_2O_8$, etc.) approximately occurred near the melting point of Al. On the other hand, the reaction onset temperature of those based on carbon as a fuel instead of Al rose close to the oxygen release temperature from the oxidizers. Thus, the addition of GO in the developed nanothermites illustrates the decrease in the activation energy and onset temperature due to the reactivity of carbon, which has no oxide shell and the fuel is directly accessible to the oxidizer. Furthermore, the presence of GO in the energetic composite decreases the dependence of the ignition mechanism on the Al diffusion rate and makes it more reliant on the oxygen release temperature. Also, GO shifted the onset temperature of both Al/Fe_2O_3 and Al/WO_3 nanothermites to a lower temperature in the direction of the solid gas reaction mechanism. The condensed phase reaction

mechanism, however, is their primary ignition mechanism where the ignition occurs at a temperature higher than the melting point of Al. Based on the above; the expected reaction mechanism is explained in Figure 6-12.

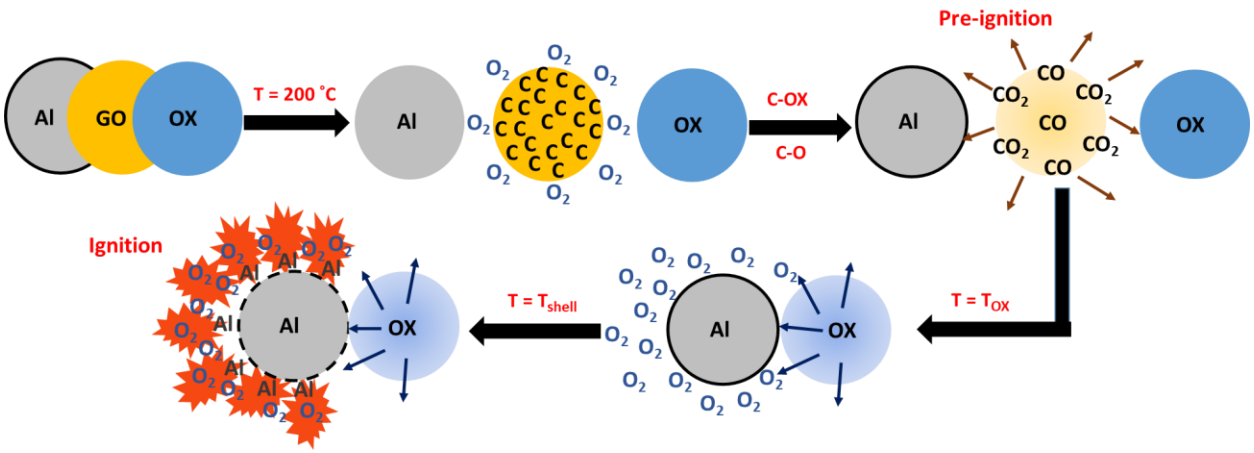

Figure 6-12 Suggested reaction mechanism of tertiary nanothermites

Here, we summarize the steps of the ignition process, which confirms the TGA/DSC findings and calculated activation energy results. First, the ignition process starts by the decomposition of GO at 200 °C with the liberation of oxygen. Then, the reaction between the nanothermite's oxidizer and carbon to form CO and CO_2 gaseous products occurs and releases energy. The formed CO and CO_2 play an important role in enhancing the gas-solid reaction mechanism and gas diffusion within the developed nanothermite composites. Moreover, they both improved the energy release as clarified in Equations (1&2) and resulted in less agglomerated reaction products [56, 57].

$$2Al_{(s)} + 3CO_{(g)} \rightarrow Al_2O_{3(s)} + 3C_{(s)} \quad 1251\ \frac{KJ}{mol} \tag{R1}$$

$$2Al_{(s)} + 3CO_{2(g)} \rightarrow Al_2O_{3(s)} + 3CO_{(g)} \quad 741\ \frac{KJ}{mol} \tag{R2}$$

Afterward when the temperature reached the oxidizer decomposition temperature (T_{OX}), decomposition occurred with the liberation of oxygen. Finally, the released oxygen diffused through the alumina shell and interacted with outwardly diffusing Al atoms to ignite the nanothermite composite. In the case of the GO/Al/$KClO_4$ nanothermite, $KClO_4$ melted prior to ignition and the melting of Al and hence, the initiation of the thermite happened by the interaction of bound oxygen in the molten $KClO_4$ and diffused Al in the alumina shell. Once the

ignition begins, the heat released from the reaction catalyzes the generation of gaseous oxygen, which will then be complete and be the dominant reaction mechanism.

6.5 Conclusions

In this paper, the thermal behavior reaction mechanism study and kinetic analysis of the tertiary nanothermite mixtures based on Al, GO and different salt and metallic oxidizers were performed using DSC, TGA and reaction bomb calorimetry. The findings of this study showed that the initial decomposition temperature of all prepared nanothermites shifted to a lower temperature compared to their reference formulations. Additionally, the heat of combustion significantly improved and the GO/Al/$KClO_4$ nanothermite achieved the highest value (9.6 kJ/g). This is in a good agreement with the TGA/DSC analysis and theoretical calculations. Based on the results of the TGA/DSC experiment, the thermite reactions between Al nanoparticles and different salts happened before the Al nanoparticles melted. Hence, the thermite reaction occurred in the solid phase for compositions based on oxidizing salts and the condensed phase reaction mechanism for those based on metallic ones. Finally, the kinetic parameters of nanostructure thermites were estimated by applying the Kissinger and Ozawa isoconversional method. The activation energy measured by the Ozawa method is slightly higher than that of the Kissinger method, but still has reference value to some extent. The possible reasons and mechanism of the effect of GO were analyzed. Due to the thermal decomposition, the nanothermite components are mixed more evenly without obvious agglomerations. Also, the process of GO thermal decomposition is exothermic, which could be a kind of pre-ignition. These results should provide references for formula design, safety, storage and handling of nanothermites from which a better performance in practical applications can be expected.

6.6 References

1. Trunov MA , Schoenitz M, Dreizin EL. Effect of polymorphic phase transformations in alumina layer on ignition of aluminium particles. Combust. Theory Model. 2006;10(4):603–623.

2. Rai A, Zhou L , Zachariah MR. Understanding the mechanism of aluminum nanoparticle oxidation. Combust. Theory Model. 2006;10(5):843–859.

3. Schoenitz M, Agboh O , Dreizin EL. Oxidation of aluminum powders at high heating rates. Thermochim. Acta. 2010;507-508:115–122

4. Chowdhury S, Piekiel N , Zhou L , Zachariah MR. Diffusive vs explosive reaction at the nanoscale. J. Phys. Chem. C. 2010;114(20):9191–9195.

5. Levitas VI, Son SF , Pantoya M. Melt dispersion mechanism for fast reaction of nanothermites. Appl. Phys. Lett. 2006;8:071909.

6. LeSergent L. Tailoring the Ignition and Reaction Properties of Cu_2O Thermite Nanolaminates, in Mechanical Engineering- Nanotechnology. 2018, Waterloo, Ontario, Canada. 1-97.

7. Kim SH, Zachariah MR. Enhancing the rate of energy release from nanoenergetic materials by electrostatically enhanced assembly. Adv. Mater. 2004;16(20):1821-1825.

8. Pantoya ML, Granier JJ. Combustion behavior of highly energetic thermites: Nano versus micron composites. Propellants Explos. Pyrotech. 2005;30(1):53-62.

9. Dreizin EL. Metal-based reactive nanomaterials. Progress in Energy and Combustion Science. 2009;35(2):141-167.

10. Jian G, Chowdhury S, Sullivan K. Nanothermite reactions: Is gas phase oxygen generation from the oxygen carrier an essential prerequisite to ignition? Combust. Flame. 2013;160(2):432-437.

11. Wu C, Chowdhury S, Jian G, Zhou L, Zachariah MR. Encapsulation of Perchlorate Salts within Metal Oxides for Application as Nanoenergetic Oxidizers,. Adv. Funct. Mater. 2012;22(1):78-85.

12. Kappagantula KS, Pantoya ML , Horn J. Tuning energetic material reactivity using surface functionalization of aluminum fuels. J. Phys. Chem. C. 2012;116:24469–24475.

13. Granier JJ , Pantoya ML. Laser ignition of nanocomposite thermites. Combust. Flame. 2004;138:373–383

14. Dean SW , Pantoya ML, Gash AE , Stacy SC , Hope LJ. Enhanced convective heat transfer in nongas generating nanoparticle thermites. J. Heat Transfer. 2010;132:111201

15. Wen JZ , Bohlouli-Zanjani G , Hu A, Nguyen NH , Persic J , Petre CF , Zhou YN. Characterization of thermochemical properties of Al nanoparticle and NiO nanowire composites. Nanoscale Res. Lett. 2013;8:184.

16. Sullivan KT , Chiou WA, Fiore R , Zachariah MR. In situ microscopy of rapidly heated nano-Al and nano-Al/WO_3 thermites. Appl. Phys. Lett. 2010;97(13):133104.

17. Sullivan KT , Wu C, Chowdhury S , Kelly ST , Hufnagel L, Fezzaa K , Zachariah ML. Reactive sintering: an important component in the combustion of nanocomposite thermites. Combust. Flame. 2012;159:2–15.

18. Balandin AA, Bao WZ, Calizo I, Teweldebrhan D, Miao F, Lau CN. Superior thermal conductivity of single layer graphene. Nano Lett. 2008;8:902–907.

19. Novoselov KS, Morozov SV, Jiang D, Katsnelson M, Grigorieva IV, Dubonos SF, Firsov AA. Two-dimensional gas of massless diracfermions in graphene. Nature. 2005;438:197–200.

20. Stankovich D, Dommett GHB, Kohlhaas KM, Zimney,Stach, Piner RD, Nguyen R. Graphene based composite materials. Nature. 2006;442:282–286.

21. Lee C, Kysar JW, Hone J. Measurement of the elastic properties andintrinsic strength of monolayer graphene. Science. 2008;321:385–388.

22. Qi-Long Y, Gozin M, Feng-Qi Z, Cohena A, Si-Ping P. Highly energetic compositions based on functionalized carbon nanomaterials. The Royal Society of Chemistry, Nanoscale. 2016;8:4799–4851.

23. Ferrari AC, Bonaccorso F, Fal'ko V. Science and technology roadmap for graphene, related two-dimensional crystals, and hybrid systems. Nanoscale. 2015;7:4598–4810.

24. Thiruvengadathan R, Basuray R, Balasubramanian B, Staley CS, Gangopadhyay K, Gangopadhyay S. A Versatile Self-Assembly Approach toward High Performance Nanoenergetic Composite Using Functionalized Graphene. Langmuir, American Chemical Society, 2014;30(22):6556-64.

25. Ning Y, Qin L, Haixia H, Longfei H, Zhao F, Hao F. Iron oxide/aluminum/graphene energetic nanocomposites synthesized by atomic layer deposition: Enhanced energy

release and reduced electrostatic ignition hazard. Applied Surface Science. 2017;408:51-59.

26. Zheng B, Shun M, Huachao Y, Jiajing Q, Junhong C, Jianhua Y, Kefa C. Green preparation of reduced grapheneoxide for sensing and energy storage applications. scientific reports. 2014;4:1-7.

27. Mokhtar MM, Hassaan MY, Morsy MS, Khalil MH. Thermally Reduced Graphene Oxide: Synthesis, Structural and Electrical Properties. Int J Nanoparticles Nanotech. 2017;3(1):1-9.

28. Vikas P, Tapan K R, Sarbajit B, Ganapati DY. Graphene oxide and functionalized multi walled carbon nanotubes as epoxy curing agents: a novelsynthetic approach to nanocomposites containing active nanostructured fillers. RSC Adv. 2014;4:49264–49272.

29. Peng-Gang R, Xu J, Tao C, Zhong-Ming L. Temperature dependence of graphene oxide reduced by hydrazine hydrate. Nanotechnology. 2011;22:1-8.

30. Manoochehr F, Behnejad H. A comparative study of thermal behaviors and kinetics analysis of the pyrotechnic compositions containing Mg and Al. J Therm Anal Calorim. 2015;120:1483–1492.

31. Kuibo Y, Yidong X, Hengchang B, Jun S, Zhiguo L, Litao S. Thermodynamic and Kinetic Analysis of Low-temperature Thermal Reduction of Graphene Oxide. cnNano-Micro Lett. 2011;3(1):51-55.

32. Zhou W, Li X, Liu L, Zachariah MR. Persulfate salt as an oxidizer for biocidal energetic nano-thermites. J. Mater. Chem. 2015;3(22):11838–11846.

33. Peng L, Wang T. Ultrasonic-assisted chemical oxidative cutting of multiwalled carbon nanotubes with ammonium persulfate in neutral media. Applied Physics A (Material Science and Processing). 2009;97:771–775.

34. Zhou W, DeLisio JB, Wang X, Zachariah MR. Reaction mechanisms of potassium oxysalts based energetic composites. Combust. Flame. 2017;177:1–9.

35. Jimmie C, James LS, Matthew MP, Maxwell JY, Jeffrey AC, Potential Biocides: Iodine-Producing Pyrotechnics. Propell. Explos. Pyrot. 2017;42:1-18.

36. Pauling L, General Chemistry, Dover Books on Chemistry. 2014.

37. Herbstein FH, Ron G, Weissman A. The thermal decomposition of potassium permanganate and related substances. Part I. Chemical aspects. J. Chem. Soc. A. 1971;1821-1826.

38. Brown ME, Kathryn CS, Michael WB. Isothermal DSC study of the thermal decomposition of potassium permanganate. Thermochimica Acta. 1985;89:27-37.

39. Becerra ME, Giraldo OH, López Suárez FE, Illán Gómez MJ, Bueno López A. Soot combustion manganese catalysts prepared by thermal decomposition of KMnO4. Applied Catalysis B: Environmental. 2011;102:260–266.

40. Chen W, Li P, Liu L, Chen B, Dai J, Wang L, Yuan Y, Li F. Ignition and Combustion of Super-Reactive Thermites of AlMg/KMnO4. Rare Metal Materials and Engineering. 2013;42(12):2458-2461.

41. Richard G, Dong-ke Z, Fiona B, Michael L. Amechanistic study into the reactions of ammonium nitrate with pyrite. Chemical Engineering Science. 2006;61:5781 – 5790.

42. Sharma M, Vimal S. Effect of carbon nanotube addition on the thermite reaction in the Al/CuO energetic nanocomposite, in Philosophical Magazine. 2017;1921–1938.

43. Yi W , Wei J., Zhipeng C, Weifan C, Chongwei A. Thermite reactions of Al/Cu core-shell nanocomposites with WO3. Thermochimica Acta. 2007;463:69–76.

44. Shoemaker DP, Garland CW, Steinfeld JI, Nibler JW. Experiment 7, in Experiments in Physical Chemistry. McGraw-Hill: New York, NY; 1981.pp.125-138.

45. Fischer SH., Grubelich MC. A survey of combustible metals, thermites, and intermetallics for pyrotechnic applications, in 32nd AIAA/ASME/SAE/ASEE Joint Propulsion Conference. Lake Buena Vista, Florida, USA; July 1996.

46. Fischer SH., Grubelich MC. Theoretical energy release of thermites, Intermetallics, and combustible metals, in 24th International Pyrotechnics Seminar. Monterey, CA. July 1998.

47. Cory WF, Pantoya ML, Martin L, Santanu C. Linking molecular level chemistry to macroscopic combustion behavior for nano-energetic materials with halogen containing oxides. The Journal of Chemical Physics. 2013;139:1-8.

48. Farley C. Reactions of Aluminum with Halogen Containing Oxides, in Mechanical Engineering. Texas Tech University: USA. 2013. pp. 74.

49. Kissniger HE. Reaction kinetics in differential thermal analysis. Anal. Chem.1957;29(6):1702.

50. Puszynski, JA. Processing and characterization of aluminum-based nanothermites. J Therm Anal Calorim. 2009;96:677–685.

51. Jiaxing S, Tao G, Miao Y, Wen D, Xiaonan Z, Fengli B, Jian T, Junyi H, Zhongshen Y. Thermal behavior and combustion of Al nanoparticles/ MnO2-nanorods nanothermites with addition of potassium perchlorate. RSC Advances. 2019;9:41319–41325.

52. Jacob RJ, Oritz-Montalvo DL, Overdeep KR,Weihs TP, Zachariah MR. Incomplete reactions in nanothermite composites. J. Appl. Phys. 2017;121:054307.

53. Sullivan KT, Chiou WA, Fiore R, Zachariah MR. In situ microscopy of rapidly heated nano-Al and nano-Al/WO3 thermites. Appl. Phys. Lett. 2012;97:133104.

54. Egan GC, LaGrange T, Zachariah MR. Time-resolved nanosecond imaging of nanoscale condensed phase reaction. J. Phys. Chem. 2015;119:2792-2797.

55. Jacob RJ, Jian G, Guerieri PM, Zachariah MR. Energy release pathways in nanothermites follow through the condensed state. Combust. Flame. 2015;162:258-264.

56. Sherif E, Fahd A, Hosam EM. Combustion characteristics of extruded double base propellant based on ammonium perchlorate/aluminum binary mixture. Fuel. 2017;208:296–304.

57. Elbasuney S, Gaber ZM, Radwan M, Mostafa SF. Stabilized super-thermite colloids: a new generation of advanced highly energetic materials. Appl Surf Sci. 2017;36:328-419.

CHAPTER 7 ARTICLE 3: SUPERIOR PERFORMANCE OF QUATERNARY NC/GO/AL/$KCLO_4$ NANOTHERMITE FOR HIGH SPEED IMPULSE SMALL-SCALE PROPULSION APPLICATIONS

Ahmed Fahd [a], Alex Baranovsky [b], Charles Dubois [a, *], Jamal Chaouki [a], John Wen [b]

[a] *Chemical Engineering Department, École Polytechnique de Montréal, Montréal, H3C 3A7 (Canada)*

[b] *Mechanical and Mechatronics Engineering Department, University of Waterloo, Ontario, N2L 3G1 (Canada)*

(This work was published online in Combustion and Flame Journal on May 24th, 2021)

(Note: Ahmad Fahd is the name I always use instead of Ahmad Emam in my all publications)

7.1 Abstract

Nanothermites are considered promising energetic materials and a key to develop new technologies in the field of energetics and propulsion. However, relatively low peak pressure, smaller thrust output, and incomplete combustion represent some of the potential problems associated with nanothermites. In this study to improve the combustion performance of nanothermites, varying quantities of nitrocellulose (NC) were introduced to produce the quaternary NC/GO/Al/$KClO_4$ nanothermite using facile electrospinning. The morphology of nanothermites was characterized by SEM-EDX which confirmed that the nanoparticles were homogeneously dispersed without agglomeration. The combustion behavior of the composites was evaluated by igniting the samples at different packing densities (%TMD) in open acrylic tubes within a reaction chamber and using a 3.5W continuous wave laser. High speed imaging captured the flame propagation and differential scanning calorimetry (DSC) was used to assess thermal behaviour and energy output. Finally, for propulsion characterization, a small-scale test motor (STM) with a converging/diverging nozzle was used to evaluate the combustion performance of the prepared samples. In general, thrust output, specific and volumetric impulses (I_{SP} and I_{SV}), and total heat released exhibit remarkable enhancement with the addition of NC.

Specifically, the total impulse (I_{FT}) and I_{SP} peaked at 5% NC/GO/Al/$KClO_4$ at ~ 50% TMD, with I_{FT} of 19.9 mN.s and I_{SP} of 203.2 s. These are improvements of over 50% compared to the sample without NC (13.4 mN.s and 137.4 s). The ignition delay time and the power required to ignite the NC-enriched mixture is increased, but a sufficiently fast response is maintained for practical applications. Thermal analysis implies that addition of NC introduced another step to the GO/Al/$KClO_4$ reaction: a gas− solid phase and liquid−liquid phase diffusion reaction, with the liquid−liquid phase reaction increasing with NC percentage. These results suggest that electrospinning is a simple technique for preparation of quaternary nanothermites that results in enhanced combustion performance and an improved suitability for small-scale propulsion applications.

7.2 INTRODUCTION

Energetic materials (EMs) have captured much attention due to their uses in both civilian and military fields such as micro and nano welding, pyrotechnics, and propulsion among others [1-4]. Developments in the field of micro electro mechanical systems (MEMS) increase the interest in the synthesis and development of new EMs to sufficiently meet the increasing demands in microscale energetic devices and miniature propulsion systems [5].

Nanothermites are a type of novel EMs that intentionally use nanoscale metallic fuels and oxidizers. Compared to traditional micron-scale thermite powders, nanothermites offer improvements in the reaction rate, heat release, pressure and thrust output by leveraging: large specific surface area, a decrease in the required activation energy, a fast energy release, and a high energy density [6, 7]. Despite their advantages over microthermites, nanothermites still suffer from relatively long ignition delays, slow combustion kinetics, particle agglomeration before ignition, and incomplete combustion that have limited their applicability [7-11]. In addition, classical EMs generally suffer from ignition difficulty and propagation process within small tubes and slots [12].

Nanothermites are classically defined as mixtures of metals and metallic oxides where at least one component is in the nanometer scale. Aluminum nanopowder (n-Al) is a key fuel material in nanothermites due to its high heat of oxidation, high density, low metallic latent heat of fusion, low toxicity, and compatibility with other reactants. For newly introduced nanothermites, this

definition is extended to include mixtures between n-Al and oxygenated or fluorinated oxidizers that can exchange the high electronegative atoms (O, S, F…) among the oxidizer and fuel during reaction and enhance gas generation [10, 13-16].

New nanothermite compositions aim to increase the generation of gas to mimic the behaviour of organic EMs. Oxygenated salts could represent the ideal alternative to metallic oxidizers to prepare nanothermites with high reactivity and superior combustion performance [17, 18]. They have higher atomic oxygen content compared to metal oxides or oxysalts and so are more suitable for gas generation and high burn rate applications [14, 19]. Moreover, the dissociation energies of nonmetal-oxygen bonds (Cl-O, I-O, etc.) in oxygenated salts are lower than those of metal-oxygen bonds (Cu-O, Fe-O, Bi-O, etc.). So, the increased oxygen mobility results in oxygen release at lower temperatures compared to metal oxides [20, 21].

Nanothermites based on oxygenated salts have a variety of practical uses in the field of solid propulsion and micro energetic systems. For example, an enriched mixture of Al and ammonium perchlorate (NH_4ClO_4) is used to propel the booster stage of the Ariane V rocket [22]. Pioneering studies by Armstrong et. al used pressure cell analysis to quantify the combustion velocity of aluminothermic compositions based on n-Al and ammonium perchlorate (NH_4ClO_4). They found that combustion velocity and pressure, respectively, increased from 25 mm/s at 0.14 MPa to 600 mm/s at 15 MPa as Al particle size decreased from 200 nm to 40 nm [23].

One proposed application of nanothermites is the development of micro thrusters for small attitude control, spacecraft station keeping, drag compensation, or orbital transformation [24, 25]. Studies performed on Al/CuO nanothermite at various densities (20-80% TMD) in a prototype microthruster showed high packing density resulted in lower thrust and longer burns (3-5 N, 1.5-3 ms) compared to higher thrust and shorter burns (75 N, 50 μs) at low packing density [23]. Specific impulse in both cases was relatively constant at around 20-25 s [26]. Sourgen et al. shifted a 40 mm projectile of 315 g by an angle of 3° compared to its initial position, within a supersonic air flow (Mach 3) in a wind tunnel [27]. For this purpose they used 160 mg of a gas generating nanothermite prepared from porous Cr_2O_3 loaded with RDX, mixed with an aluminium nanopowder [28]. Nanothermites have also been applied in microfluidic applications where nanothermite product gases were used to produce a controlled jet flow; this is widely useful for the expanding field of lab-on-a-chip devices [29].

The most critical specification requirements for any propulsion design are overall system mass and performance parameters, such as thrust and impulse [30, 31]. The force produced by a thruster is important in the design of a device because it directly influences the device dynamics. Transience in the thrust output is something that, if unaccounted for, can cause the device to become dynamically unstable and tumble. Thus, the thrust profile is important to characterize for a given propellant. Maximum and time-averaged thrust force values are useful to compare between different thruster configurations and propellant compositions. Likewise, impulse is used as a measure of the momentum that can be transferred to the device from the combustion of a propellant. Specific impulse is a particularly useful metric because it quantifies the momentum-transfer capability on a per-unit-weight basis, allowing for direct comparison between propellants. The combination of these performance metrics is important for the design of a thruster and their relevance to a designer will be case-dependent.

The use of oxygenated salt based nanothermites is one way to improve these performance metrics without introducing a mass penalty; thus, the overall specification of the propulsion system is improved. However, the novelty of these nanothermite fuels means that propulsion-specific characterization is limited in existing literature.

The goal of this work is to develop a nanothermite mixture with controllable combustion and tailored performance parameters for small-scale propulsion applications. We investigated quaternary nanothermites based on n-Al, potassium perchlorate ($KClO_4$), graphene oxide (GO) and nitrocellulose (NC). Electrospinning allows fine control over particle size with narrow particle size distribution, high mixture homogeneity, and low agglomeration. Since electrospinning is performed at ambient temperature/pressure, it allows the introduction of polymer binders into the mixtures that would be beneficial in our study to improve sample performance. The benefit of NC arises from its solubility in organic solvent to form collodion solution and interact with the raw particles at the solid/liquid interface. In addition, NC itself is an energetic material offering chemical reactivity and gas production, which may be useful in preventing further oxidation of Al powders during storage. Moreover, it might provide a way to enhance mechanical properties such as resilience [32, 33]. The mixtures used in this study were prepared by electrospinning and compared with samples prepared using the conventional mechanical mixing method.

The oxidizer $KClO_4$ was selected for this study due to its high oxygen content, strong oxidizing nature, and exothermic decomposition reaction [34, 35]. In addition, GO was used because of its large surface area, rich pore structure, and potential energetic nature; upon heating, GO undergoes violent exothermic decomposition due to the extensive oxygenic functional groups on the basal plane (phenol, hydroxyl, and epoxide) and at the edges (carboxylic) [36, 37]. NC is used as a gas generating binder within the nanothermite composite and adds energy to the system during the combustion process. Also, NC prevents reactive sintering of nanothermite components [32]. To evaluate the quaternary nanothermite compositions we first perform morphological and chemical characterizations by SEM coupled with EDX microscopy techniques. TGA/DSC is then used to evaluate the thermal behaviour of the composites and evaluate heat release. The thrust output, total impulse (I_{FT}), specific impulse (I_{SP}), volumetric impulse (I_{SV}), ignition delay time and normalized light intensity is assessed using a cylindrical test thruster and piezoelectric force transducer by igniting the sample using a laser ignition system. Finally, a nozzle is added to the test thruster to observe the feasibility of these mixtures in propulsion devices.

7.3 Materials and methods

7.3.1 Materials

Graphite flakes, phosphoric acid (H_3PO_4), sulphuric acid (H_2SO_4), hydrogen peroxide (H_2O_2), ethanol (99.9 %) and acetone (99.5 %) used in the preparation of GO and for dissolving NC were purchased from Sigma-Aldrich. $KClO_4$ and NC (12.6 % nitrogen content) were obtained from Defence Research and Development Canada. The as-purchased Al nanoparticles from US Research Nanomaterials Inc. have a spherical shape with an average particle size of 40 nm, a purity of more than 99.9 % metal basis, an active Al content of 80 wt. % (mass fraction) by thermogravimetric analysis, and a surface area of 30-50 m^2/g. Particles are assumed to be 80% Al (2.70 g/cm^3) and 20% Al_2O_3 (3.95 g/cm^3), leading to an average particle density of 2.88g/cm^3.

7.3.2 Synthesis of GO

Graphene oxide was synthesized using an improved Hummer method with graphite powder as the starting material [38]. Graphite (1 g) was mixed with 13 ml of 85 % H_3PO_4 and 120 ml of concentrated H_2SO_4 (98 %) in a 300 ml beaker, followed by the slow addition of 6 g of $KMnO_4$

in portions while mixing with a glass rod to inhibit any severe reactions that may result from rapid mixing. The mixture was left to cool and then mixed slowly with an overhead mechanical stirrer with a paddle rod (SS316L/PTFE) for 1-3 days until the mixture turned as viscous as honey and formed a mirror in the beaker's wall. After 3 days, the obtained products were slowly added in portions to 1.5 L of deionized water (DI) in a 2 L beaker with a stirrer mixing over an ice bath (~ 5 $^{\circ}$C). After one hour of mixing, hydrogen peroxide (~ 10 %) was added drop-by-drop to the mixture with continuous mixing until the mixture became yellow/orange in color. The GO dispersion was decanted 2-3 times with DI acidified with hydrochloric acid (HCl), each time minimizing the amount of residual liquid to remove most of the ionic impurities. Finally, GO was separated by centrifugation and rinsed with acetone.

7.3.3 Preparation of nanothermite compositions

Quaternary nanothermite compositions with NC as energetic binders were prepared using a modern electrospinning technique. NC was introduced to GO/Al/$KClO_4$ based tertiary nanothermite mixtures at mass fractions (2.5, 5, 7.5 and 10%), with the base GO/Al/$KClO_4$ mixture hereby referred to as the "reference sample". The mass content of GO was kept constant at 5 % in all formulations. The equivalence ratio (Φ) of a nanothermite mixture was calculated using the mass fractions of its fuel (n-Al) and oxidizer ($KClO_4$) components and was fixed to 0.8 in all the experiments. This value remains the same during the combustion measurement, because the influence of ambient air on the reaction under the applied condition is quite limited. A similar simplification was employed by others when the effect of NC enrichment was investigated [39-41].

Initially, tertiary nanothermites were prepared by dispersion of n-Al, $KClO_4$, and 5 % GO in acetone. The samples were then put in an ultrasonic bath for 30 minutes to ensure proper dispersion and form stable suspension. Meanwhile, an NC solution was prepared by measuring the required amount of NC according to its specific percentage in the quaternary composite and dissolved in a 2:1 volume ratio mixture of acetone: ethanol. Finally, the precursor solution was prepared by mixing the nanothermite suspension with the NC solution and magnetically stirring for an additional 6 h to ensure good homogeneity.

Electrospinning was performed by loading a syringe with the precursor and feeding at a pump rate of 3 mL/h. The surface tension at the precursor interface was overcome by carefully applying 19 kV between the syringe and substrate. The syringe and substrate were set 10 cm apart. As droplets travelled through this air gap, the solvents evaporated and nanothermite within an NC energetic binder was formed and the quaternary nanothermite NC/GO/Al/$KClO_4$ powder was collected from the substrate. A schematic diagram of the electrospinning process is presented in Figure 7-1.

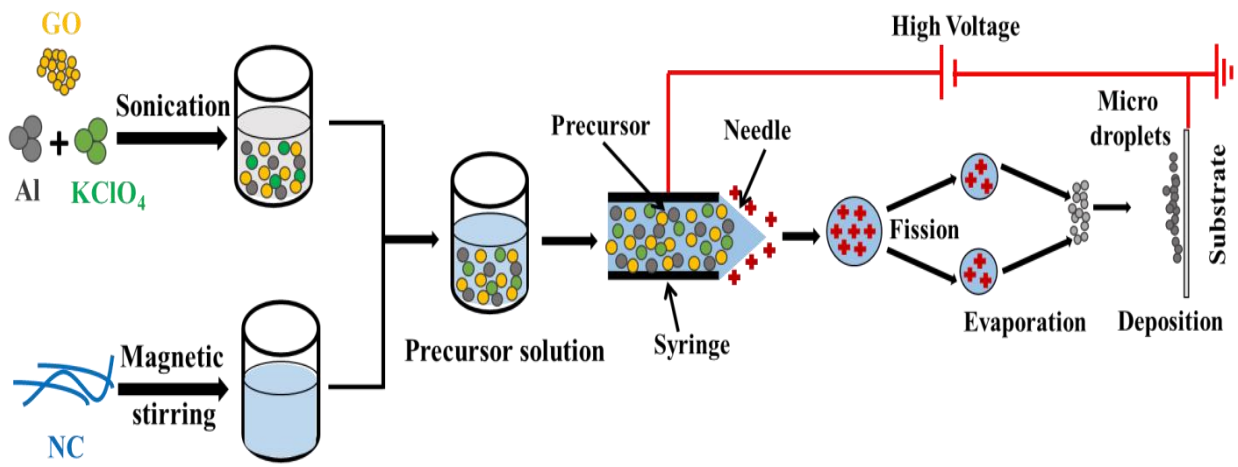

Figure 7-1 Schematic of electrospinning formation of quaternary NC/GO/Al/$KClO_4$ nanothermites

7.3.4 Nanothermite characterization

The morphology and homogeneity of the prepared samples were studied via SEM (FEI Quanta FEG 450 operated at 15 kV) coupled with EDX measurements. Laser ignition and high-speed imaging was used to evaluate the combustion performance of the prepared composites; a schematic is shown in Figure 7-2A. Schematic dimensions of the STMs used are illustrated in Figure 7-2B, C and D showing the nozzle and no-nozzle configurations, respectively; the nozzle used is a generic converging-diverging (CD) nozzle intended to accelerate exhaust gasses to a supersonic state.

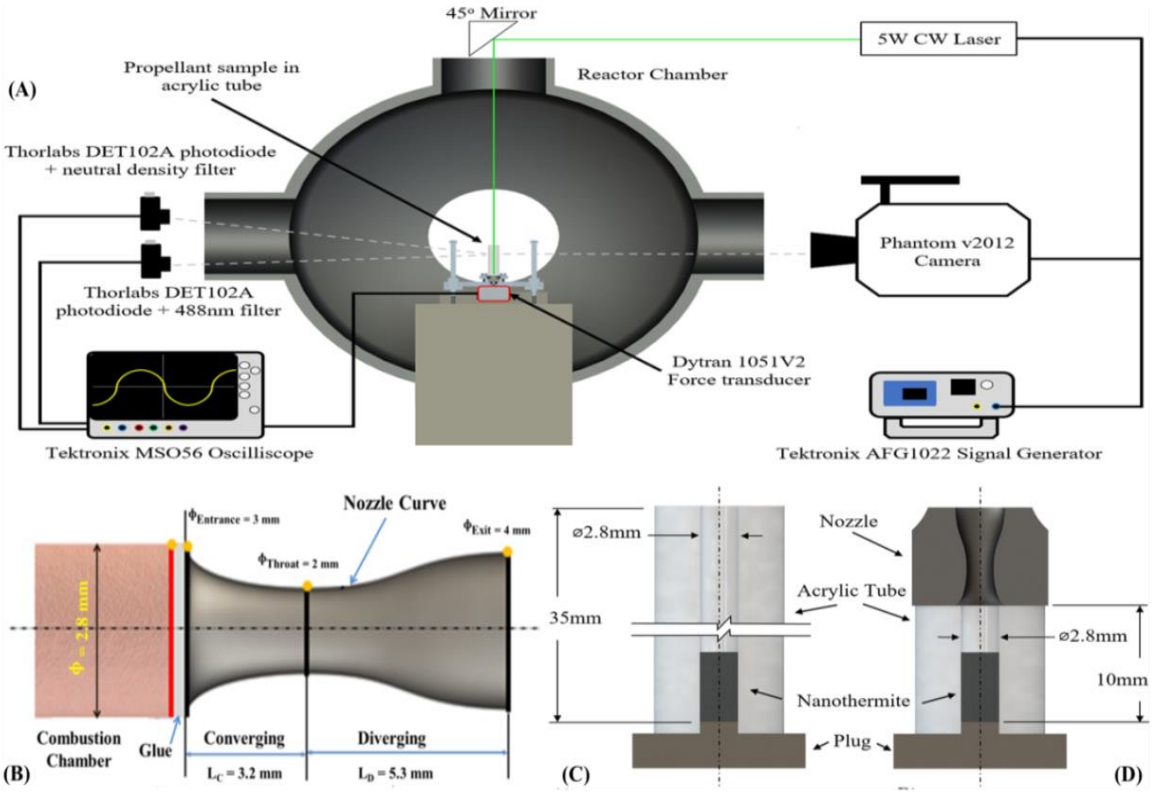

Figure 7-2 (A) Laser ignition and high-speed imaging set up (B) nozzle configuration (C) Dimension of open STM (D) Dimension of CD STM

A 5W continuous wave 532nm laser was used to ignite samples as shown in Figure 7-2. The combustion of the samples was recorded at 180,000 fps with 600 ns exposure time using a Phantom v2012 high-speed camera. A Dytran (1051V2) force transducer with a reference sensitivity of 22.43 mV/N was fixed underneath the sample to measure the thrust force. The force transducer characteristic frequencies for the STM configurations shown in Figure 2C and 2D are 4.9 kHz and 3.1 kHz, respectively. In processing the force data, band-stop filters were applied from these characteristic frequencies to 40 kHz to eliminate signal noise, depending on the configuration of the test. Two photodiodes (Thorlabs DET102A) were used to capture the light intensity output from the nanothermite sample. A neutral density filter (Thorlabs NDUV06B) was installed on one photodiode unit and a 488 nm wavelength filter (Thorlabs FLA488-10) on the other; 483nm being a characteristic wavelength for the AlO thermite reaction intermediary [42]. A Tektronix MSO56 oscilloscope was used to capture force and photodiode data at a sampling rate of 1MHz. Data recording and laser triggering was performed by a Tektronix

AFG1022 waveform generator using a standard TTL signal. All tests were carried out at normal atmospheric conditions.

Thermal behaviour and energy output of the prepared nanothermites were evaluated by measuring the heat flow as a function of temperature and integrating areas under exothermic peaks using a thermal analyzer (NETZSCH STA 449 F3). The measurements for the DSC samples were performed in a closed alumina pan (crucible), with 5 mg sample mass, under argon gas, at a heating rate of 10°C/min and argon flow rate of 40 mL/min.

7.4 Results and Discussion

Before the investigation of the combustion performance of different nanothermite compositions, the composition of prepared GO used in the experiment was checked by a CHNSO Elemental Analyzer EA3000 (EuroVector). The resulting elemental mass fractions are summarized in Table 1.

Table 7-1 Elemental composition of prepared GO samples expressed in mass fraction

Element	Mass fraction
C	0.4977 ± 0.0062
H	0.0174 ± 0.0011
O	0.4644 ± 0.0046
S	0.0205 ± 0.0015

The spatial homogeneity of components within the sample mixtures was ensured using SEM-EDX analysis. The results are shown in Figure 7-3 for a 5 % NC/GO/Al/$KClO_4$ mixture and are representative of the various electro-spun mixtures.

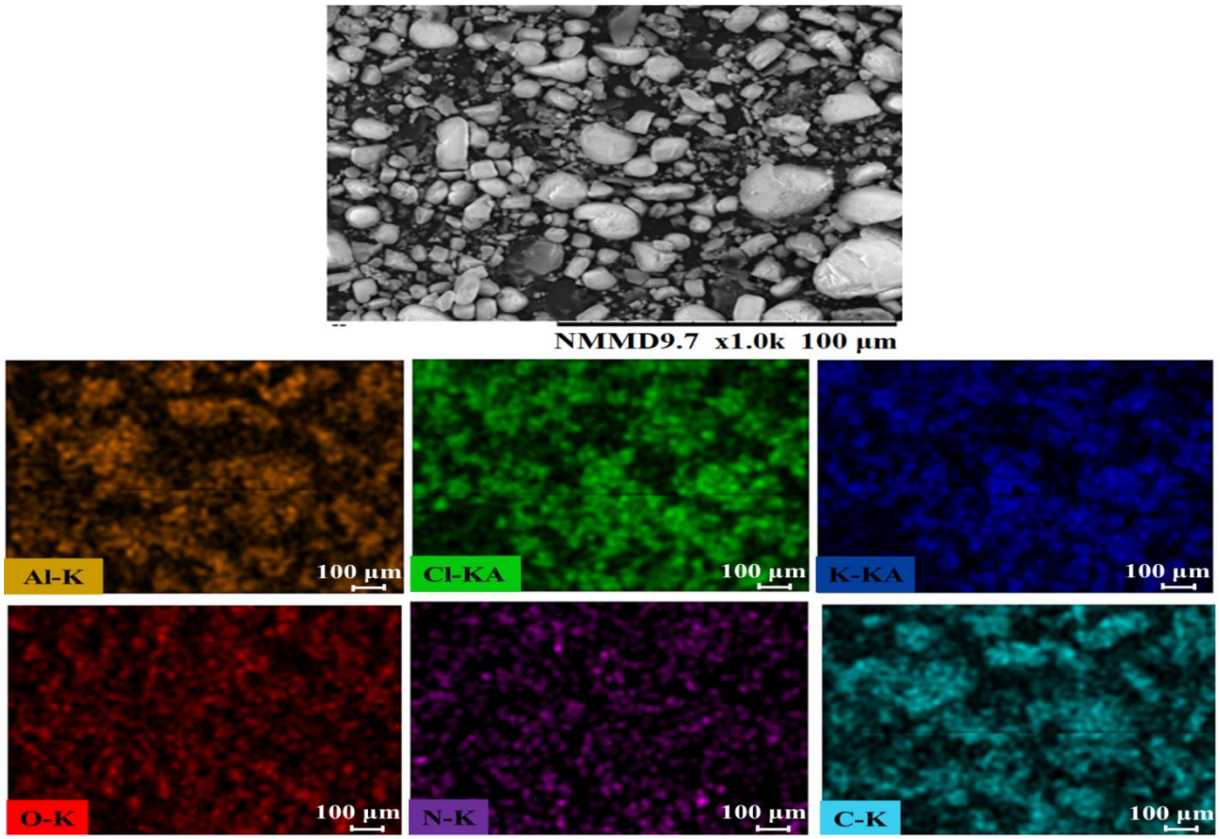

Figure 7-3 SEM image and EDX analysis of 5 % NC/GO/Al/KClO4 nanothermite

No major agglomerations of the fuel or the oxidizer are observable in Figure 7-3, which confirms adequate mixing and distribution of the particles. This demonstrates the benefit of electrospinning over mechanical mixing, since uniformity of reactants will result in improved combustion properties and reaction completeness.

7.4.1 Thermal behaviour and combustion mechanism

Thermal analysis was conducted to assess the outcome of NC addition on the reactivity and energy output of the prepared quaternary nanothermites. The thermograms of raw NC and different NC/nanothermite mixtures are shown in Figure 7-4.

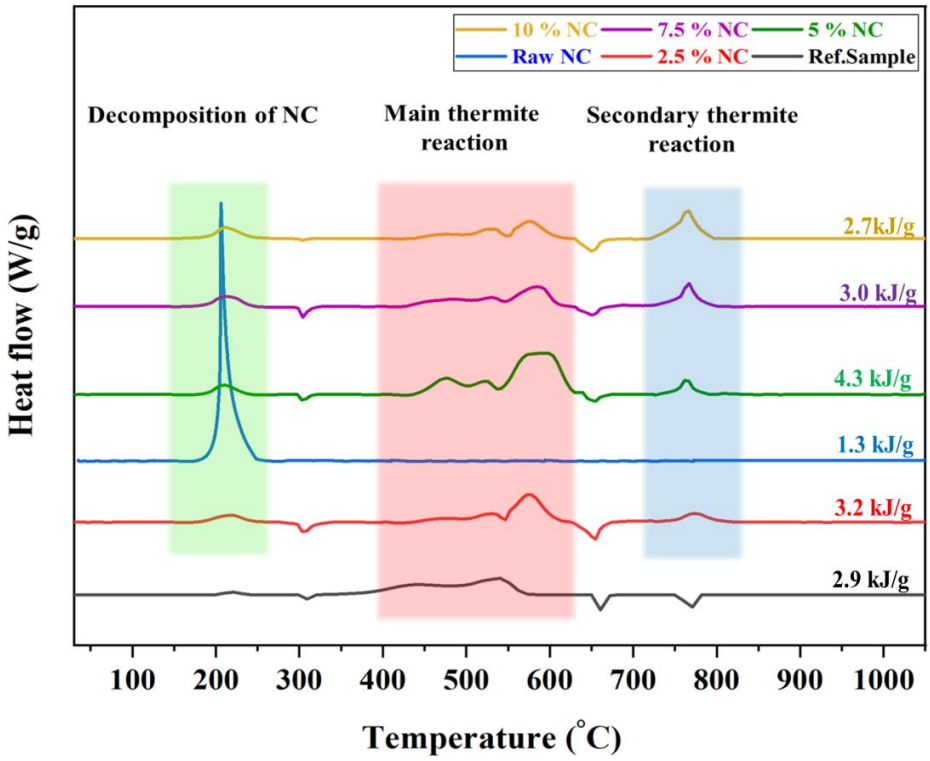

Figure 7-4 DSC curves of nanothermites with different NC content

Three distinctive exothermic regions are observed that characterize the thermal decomposition of the composite samples. The first exothermic peak occurs around 208 °C and is correlated with the exothermic decomposition of raw NC that yields many gaseous products including CO_2, CO, NO, N_2 and H_2O [32, 43]. The NC exothermic peak appears in all NC/nanothermite samples, assuring that NC is successfully incorporated into NC/GO/Al/$KClO_4$ without changing its exothermic behavior. The area under the first exothermic peak (energy release) increases with addition of NC.

The second exothermic region located between 400 °C and 630 °C is attributed to the main thermite reaction between Al and $KClO_4$ which occurs before the melting temperature of Al (660 °C) and has a peak temperature at 578 °C, thus suggesting that a gas-solid diffusion reaction is the controlling and dominant reaction mechanism. It is noticeable that this second exothermic region is the result of three consecutive exothermic peaks (as is clearly seen in 5% NC). The first and second exothermic peaks are assumed to be the pre-ignition reactions between NC and GO decomposition gases and nanothermite reactants according to reactions 1-5 [44, 45].

$$2Al_{(s)} + \frac{3}{2}O_{2\,(g)} \rightarrow Al_2O_{3(s)} + 1700\ kJ \quad (1)$$

$$2Al_{(s)} + 3CO_{(g)} \rightarrow Al_2O_{3(s)} + 3C + 1251\ kJ \quad (2)$$

$$2Al_{(s)} + 3H_2O_{(g)} \rightarrow Al_2O_{3(s)} + 3H_{2(g)} + 866\ kJ \quad (3)$$

$$2Al_{(s)} + 3CO_{2(g)} \rightarrow Al_2O_{3(s)} + 3CO + 741\ kJ \quad (4)$$

$$2Al_{(s)} + N_{2(g)} \rightarrow 2AlN_{(s)} + 346\ kJ \quad (5)$$

The third exothermic region (between 750 °C and 800 °C) appears only with the addition of NC, suggesting that addition of NC leads to a greater completion of the thermite reaction before reaching the melting temperature of Al. The condensed phase reaction mechanism (liquid−liquid reaction) is expected to be the controlling mechanism in the third region.

The gaseous NC oxidation products, CO and CO_2, may play a double role in the thermite reaction. During the initial stages, they involve more aluminum in the reaction, oxidizing it, and aid in the completion of the reaction in condensed phase after Al melts. However, at a NC content of more than 5%, it appears they begin to compete with Al for oxygen and escape from the crucible without reaction, thereby reducing the heat effect.

The presence of an endothermic peak at approximately 302 °C is ascribed to the phase change of $KClO_4$ from a rhombic to a cubic structure. The second and third endothermic peaks are assigned to the melting of the unreacted Al and KCl reaction product at 660 and 770 °C, respectively [46].

Energy output from the samples was evaluated by integrating the areas under exothermic peaks. The highest heat released is observed for the 5 % NC sample and it is 150% higher than the reference sample as seen in Figure 4. Improved heat release with the addition of NC can be ascribed to the following reasons. First, the DSC curves of the quaternary compositions differ from those of their components, which is evidenced by the decomposition of NC and the effects of its decomposition products on the thermite reaction. While addition of NC may affect the contacting intimacy of reactive components (here Al and $KClO_4$), additional chemical processes associated with NC can affect thermite reactions via: decomposing and production of carbon containing species, which may improve or hinder oxidation reaction; and subsequent temperature changes which may accelerate the oxidation rate. Second, a higher heat release is observed for 5

% of NC in the quaternary composition. Most likely when the NC content is less than 5%, its addition does not affect the intimacy of reactants significantly. Gaseous species from NC decomposition contributes to energy release via reactions 1-5, which is supported by the literature [47]. As a secondary factor suggested in the literature [48-50], pre-ignition of NC and its energy release may help break the alumina protective layer and enable the direct reaction between Al and $KClO_4$, as speculated in the broad second exothermic region between 550 °C and 650 °C in Figure 4. When the NC content is more than 5 %, addition of NC brings in a non-negligible influence on the contacting intimacy between Al and $KClO_4$, which promotes the phase separation and decreases both reaction rate and total energy release [32, 41, 51]. A proposed reaction mechanism of the prepared quaternary nanothermite compositions is illustrated in Figure 7-5.

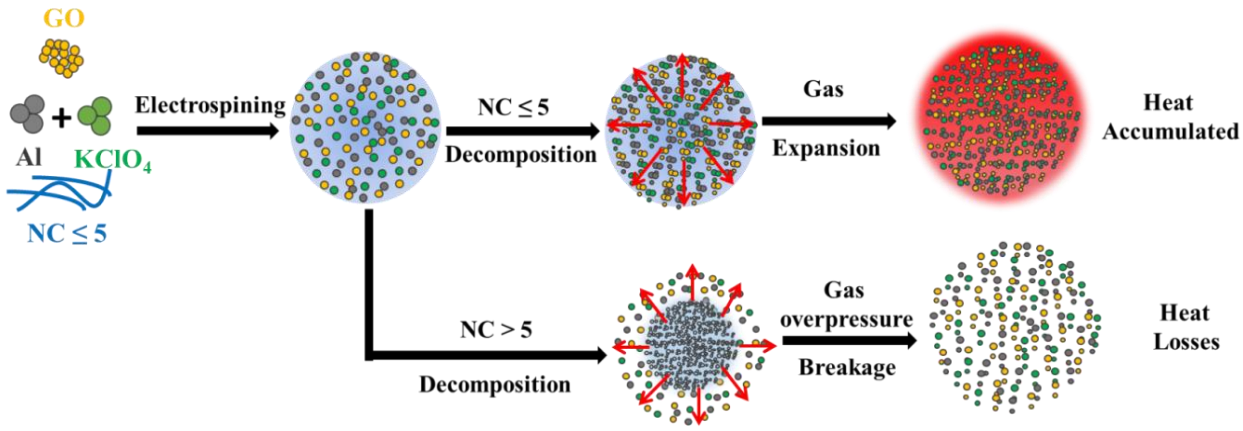

Figure 7-5 Suggested reaction mechanism of quaternary nanothermites

Addition of up to 5% NC produces high homogeneity and binding of nanothermite components which in turn greatly decreases the heat loss resulted from the isolated or aggregated reactants during thermite reaction. Also, NC helps accumulate the heat within the nanothermite mixture, promoting the mass transport as well as leading to self-propagating behavior [52]. Increasing the amount of NC above 5% NC causes overpressure within the nanothermite mixture as the NC decomposes and results in disintegration of nanothermite microstructure into smaller structures and hence the combustion characteristics are reduced [53].

To observe the effect of the gas release behavior of NC on nanothermite performance and correlate energy released to other combustion characteristics, samples were ignited at different packing densities in open acrylic tubes using a 3.5W continuous wave laser. High speed imaging

was used to capture the flame propagation, photodiodes were used to observe the optical flame intensity, and a piezoelectric force transducer measured thrust.

7.4.2 Thrust performance of quaternary nanothermites

In experimentation, the mechanically mixed samples exhibited partial ignition and sputtering combustion. The samples prepared by electrospinning were easily ignited by laser ignition and self-propagated. This indicates that the high homogeneity of reactants produced by electrospinning, as seen in Figure 7-3, results in improved ignition and combustion performance when compared to mechanically mixed NC-nanothermite compositions.

Measurements of thrust output, I_{FT}, I_{SP}, and I_{SV} are used to evaluate the success of the sample preparation method and determine the applicability of the quaternary mixtures. Thrust profiles of different quaternary NC/nanothermite composites are presented in Figure 7-6.

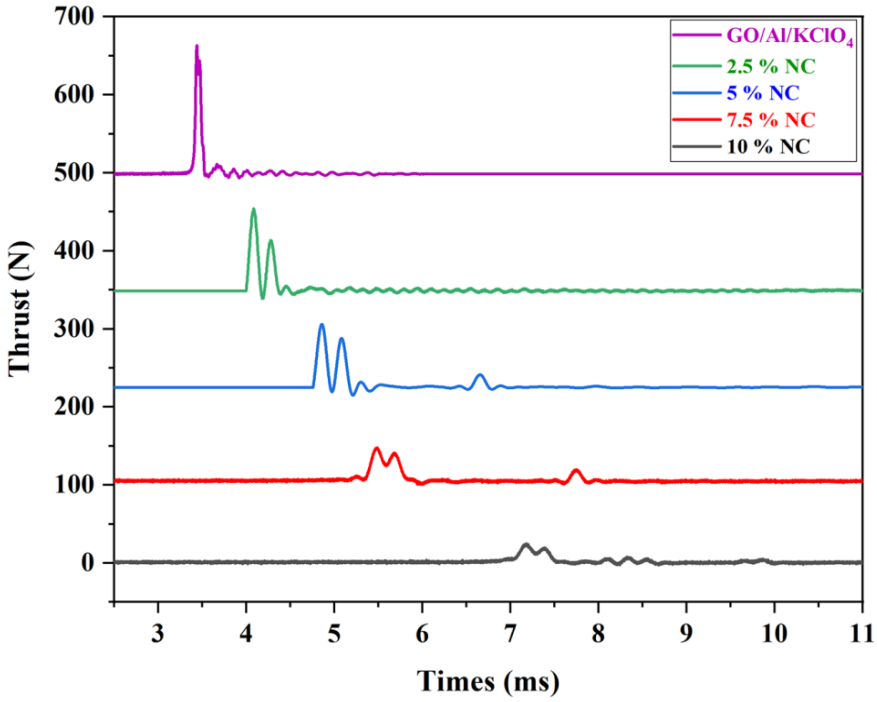

Figure 7-6 Thrust profiles for different NC/nanothermite samples at 20%TMD

Addition of NC in nanothermite impedes both combustion rate and energy release, as shown early in this work. Optimal selection of the NC and nanothermite ratio to achieve the highest thrust however depends on a balance between these two factors. Frist, combustion of pure

nitrocellulose can be accelerated by the pressurization which is resulted from a rapid energy release process such as thermite reactions. Secondly, combustion of nanothermite is usually decelerated by the pressurization due to its effect on transportation of gaseous intermediates and products, reported by Weismiller et al. [48]. According to Figure 7-6, a good balance exists for the NC 5% and 2.5% samples. The single peak with a higher trust value corresponding to the GO/Al/$KClO_4$ does not result in a large momentum change due to its very short combustion period.

It is noted that NC-enriched samples produce a characteristic two-peak shape, as observed in figure 6. As previously mentioned, filtering was performed on the data to eliminate noise from the data, but the oscillatory two-peak shape remained. In processing of the data, reducing the low-pass frequency limit would eliminate this oscillation but result in excessive smoothing and detail loss. From the high-speed videos, the oscillations presented in figure 6 could not be correlated to any trends in image intensity or structure formation, suggesting they are not related to the mixture itself, but an artifact of the experimental setup used. It is possible that acoustic interactions within the thruster cause the two-peak shape, but neither the high-speed video nor photodiode data provide further insights, so the cause remains unclear.

The burning period is calculated from the high-speed video by measuring the time difference between the frame where the distinct flame front first develops and the frame where the flame ceases to be observable (end of burning). Performance of the prepared nanothermites is further quantified through total, specific and volumetric impulses (I_{FT}, I_{SP} and I_{SV} respectively), which are calculated as follows [54]:

$$I_{FT} = \int_{t_i}^{t_e} F \ dt \tag{6}$$

$$I_{SP} = \frac{1}{W_t} \int_{t_i}^{t_e} F \ dt \tag{7}$$

$$I_{SV} = \frac{1}{V_t} \int_{t_i}^{t_e} F \ dt \tag{8}$$

where W_t, V_t, t_i and t_e are the nanothermite charge weight (N), volume of the nanothermite charge (mm^3), initial burning time (s), and ending burning time (s), respectively. Uncertainty of

measured and calculated values was determined by calculating standard deviation and then dividing by the number of measured samples as illustrated in equations (9) and (10).

$$\sigma = \sqrt{\frac{\sum_{i=1}^{n}(Reading_i - Average)^2}{n-1}} \tag{9}$$

$$U = \frac{\sigma}{\sqrt{n}} \tag{10}$$

where σ, U, and n are standard deviation, standard uncertainty, and number of measured samples, respectively. To increase the level of confidence to 95 %, the uncertainty values calculated in equation (10) are doubled to take into account two standard deviations of data from the mean [55, 56]. The effects of introducing NC into the sample on the propulsion characteristics (I_{FT}, I_{SP}, and I_{SV}) are presented in Table 2.

Table 7-2 Combustion characteristics of nanothermite samples

Nanothermite composition	**Average thrust (N)**	**High speed video burning period (ms)**	**Optical burning period (ms)**	**I_{FT} (mN.s)**	**I_{SP} (s)**	**I_{SV} (mN.s/mm^3)**
GO/Al/KP	54.1 ± 1.8	0.2 ± 0.1	0.3 ± 0.1	10.8 ± 0.2	110.2 ± 2.3	2.8 ± 0.1
2.5 % NC/GO/Al/$KClO_4$	8.0 ± 0.7	2.0 ± 0.2	1.8 ± 0.2	15.9 ± 0.3	162.4 ± 3.6	4.1 ± 0.2
5 % NC/GO/Al/$KClO_4$	6.8 ± 0.2	2.6 ± 0.2	2.4 ± 0.2	17.6 ± 0.2	179.2 ± 2.2	4.5 ± 0.2
7.5 % NC/GO/Al/$KClO_4$	4.3 ± 0.2	3.5 ± 0.3	3.1 ± 0.3	14.8 ± 0.3	149.7 ± 2.7	3.8 ± 0.2
10 % NC/GO/Al/$KClO_4$	2.9 ± 0.1	4.1 ± 0.4	3.6 ± 0.4	12.0 ± 0.2	122.0 ± 1.9	3.1 ± 0.1

The experimental measurements summarised in Table 7-2 show that NC addition increases I_{FT}, I_{SP}, and I_{SV} up to a point. Impulse values reach a maximum at 5 % NC composition where specific and volumetric impulses are approximately 35 % greater than the reference sample. The gases produced by NC decomposition may prevent nano-Al particles from sintering, maintaining

the large oxidation areas associated with nanoparticles thereby increasing completeness of the main thermite reaction. This produces more heat, which can be converted to kinetic energy and subsequently improve the overall momentum transfer capabilities, therefore increasing the measured impulses, I_{FT}, I_{SP} and I_{SV} presented in Table 7-2. In addition, these results highlight the performance benefits of $KClO_4$ as an oxidizer for nanothermites compared to metallic oxides. The quaternary samples presented in Table 2 have higher I_{SP} values than those of metal-oxide nanothermites such as Al/CuO and Al/Bi_2O_3 (26.7 and 59.4 s respectively) [41, 57]. This is due to the high oxidizing power, high reaction rate, low bond energy nonmetal-oxygen pair $KClO_4$ compared to the metal–oxygen pairs in CuO and Bi_2O_3 resulting in lower decomposition temperature and thus low oxygen release temperature [14, 19-21].

Increasing the NC content to 7.5% and 10% results in a decline of I_{FT}, I_{SP}, and I_{SV} compared to the 5% NC case. This agrees with the trends observed by DSC analysis in Figure 4. I_{FT}, I_{SP} and I_{SV} performance of the 7.5% and 10% samples was similar to the reference sample, albeit with lower average thrusts and increased burn durations. This small reduction in samples with NC content exceeding 5% is ascribed to the enlarged thermal diffusion barriers between the fuels and oxidizers, resultant reduced reaction rates, and subsequent lower mass flow rates.

To further correlate the effect of gas release behavior of NC on thrust performance to the energy released from thermal analysis, determine the ignition delay, and quantify energy output for the quaternary nanothermites, samples are ignited in an open acrylic tube test engine and recorded using a high-speed camera. From the resultant video, several selected images for each mixture during its combustion period are shown in Figure 7-7.

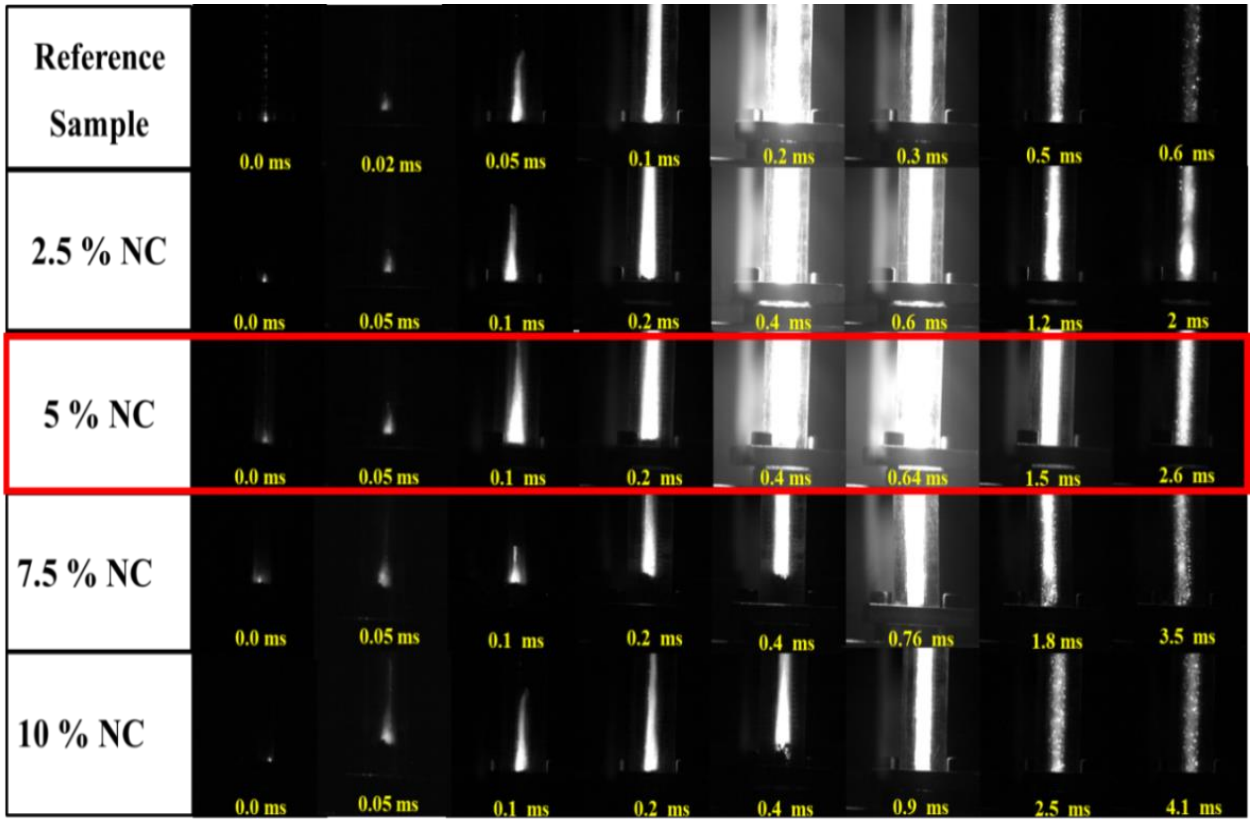

Figure 7-7 Snapshots of different nanothermite composites in open tube test engine

Before nanothermite ignition, the NC decomposes and releases gas products as shown in the second snapshot for each NC/nanothermite mixture in Figure 7-7 and confirmed by the blown up of very small amount of unreacted NC. As discussed alongside the results of thermal analysis, the gases released from NC at low temperature play an important role in the combustion enhancement of nanothermite composites. It is reasonable to conclude that NC serves as a low temperature gas generator to prevent the nanoparticles from sintering to larger particles before ignition, yielding enhanced reaction and improved energy output. In addition, more gas production may also promote the convective heat transfer during the combustion of the composites [58]. However, excessively increasing the amounts of NC in the nanothermite matrix can retard the combustion performance. Increasing NC content may increase the diffusion length scale of the reactive particles. Although NC is an energetic ingredient, its energy release rate is much lower than that of nanothermites [59, 60]. So, NC can be used as a compositional parameter to tune combustion performance of nanothermite mixtures as required by the given application.

The 5%NC sample exhibited the most luminous flame as shown in Figure 7-7, reinforcing the observed trend in Table 2 and Figure 4 where peak I_{SP}, I_{SV} and energy release occurred at 5%NC. Reduction in combustion performance of nanothermites (less violent and bright) occurs when the NC composition exceeds 5%, seen in Figure 7-7 as dimmer flames, is supported by findings from thrust and thermal analysis results presented in Figure 7-4, Figure 7-6 and Table 2.

Ignition delay is quantified from the high-speed video by measuring the time difference between the first frame where the laser spot is visible, and the first frame where a distinct flame front develops. In addition, light signals recorded via photodiodes during combustion are used to confirm and validate the high-speed video data. Variation of the light signals of nanothermite with different NC content is demonstrated in Figure 7-8A.

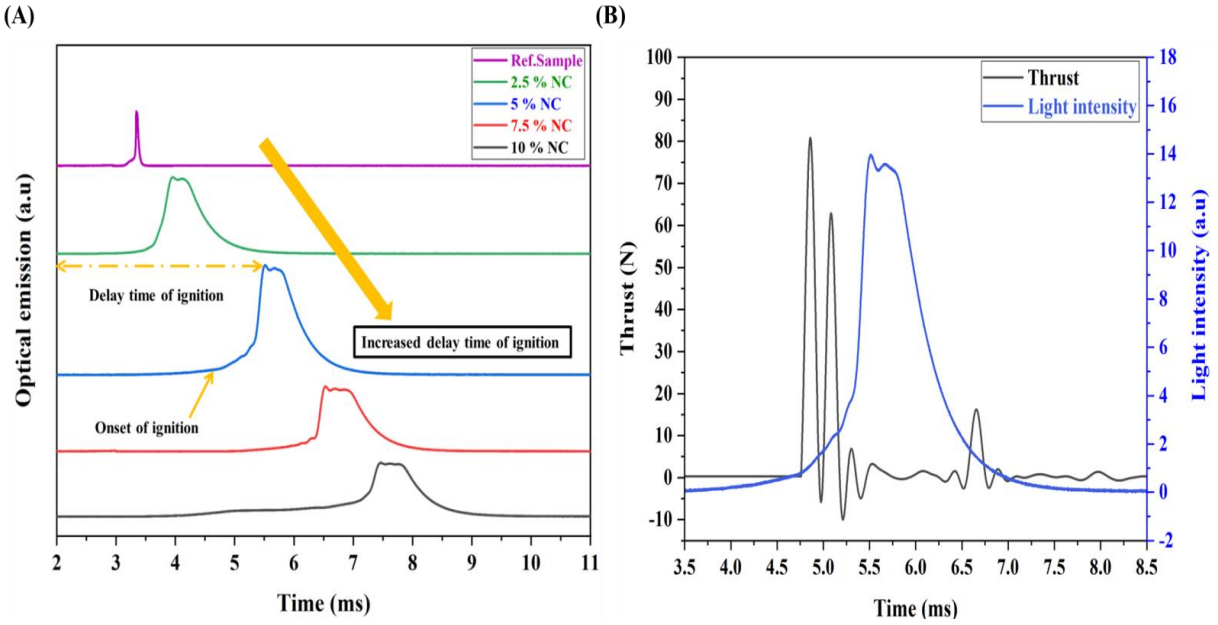

Figure 7-8 (A) Optical emissions of different nanothermite samples. (B) Combined optical signal and thrust curve for the 5% NC sample

Figure 7-8 shows that increasing the NC content in the quaternary nanothermite mixtures yields a gradual increase in the ignition delay; this is consistent with high-speed imaging results. Specifically, the 10 % NC sample delay time is more than twice the reference sample delay. The increase in ignition delay is likely due to the dissipation of some of the energy input resulting from the addition of NC, causing reduced temperature rise of the nanothermite base matrix. Figure 8B combines the optical signal and thrust curve for the 5 % NC sample and demonstrates

that optical energy and thrust overlapped, confirming the previous observed results. The maximum laser power for the setup and testing conditions is approximately 1.5 W for the used laser application time of 1 s. Table 7-3 collects values of the minimum amount of laser power required to ignite nanothermite samples and their onset and ignition delay.

Table 7-3 Ignition properties of nanothermite composites

Nanothermite composition	**Laser power input (W)**	**Energy required for ignition (mJ)**	**Onset ignition time (ms)**	**Delay time of ignition (ms)**
GO/Al/KP	0.30	1.00	3.15	3.34
2.5 % NC/GO/Al/$KClO_4$	0.38	1.51	3.56	3.97
5 % NC/GO/Al/$KClO_4$	0.45	2.48	4.88	5.52
7.5 % NC/GO/Al/$KClO_4$	0.68	4.47	5.81	6.57
10 % NC/GO/Al/$KClO_4$	1.20	8.96	6.58	7.47

Results demonstrated in Table 7-3 reveal that there is some correlation between thermal properties and laser ignition sensitivity. Nanothermite samples enriched with NC exhibit longer ignition delay time and thus require more laser energy input to ignite in comparison to the reference sample. The progressive increase in the ignition delay agrees with DSC results that show the increase in onset temperature of NC samples compared to the reference. In general, NC based quaternary nanothermites are less sensitive and thermally safer than those tertiary mixtures without NC due to the increased laser power required for ignition caused by NC addition [32].

The intensity of the sample combustion reaction can be evaluated by calculating the normalized time-averaged photodiode signal (integrating area under the curve) according to the following relation [61].

$$\overline{E_m} = \left(\frac{\int_{t_e}^{t_i} E\, dt}{(t_i - t_e)}\right)/m \qquad (11)$$

where E, t_i, t_e, m are: the photodiode signal (mV), initial combustion time (s), ending combustion time (s) and nanothermite mass charge (mg) respectively. Figure 7-9 shows the normalized time-averaged photodiode signal and different nanothermite mixtures.

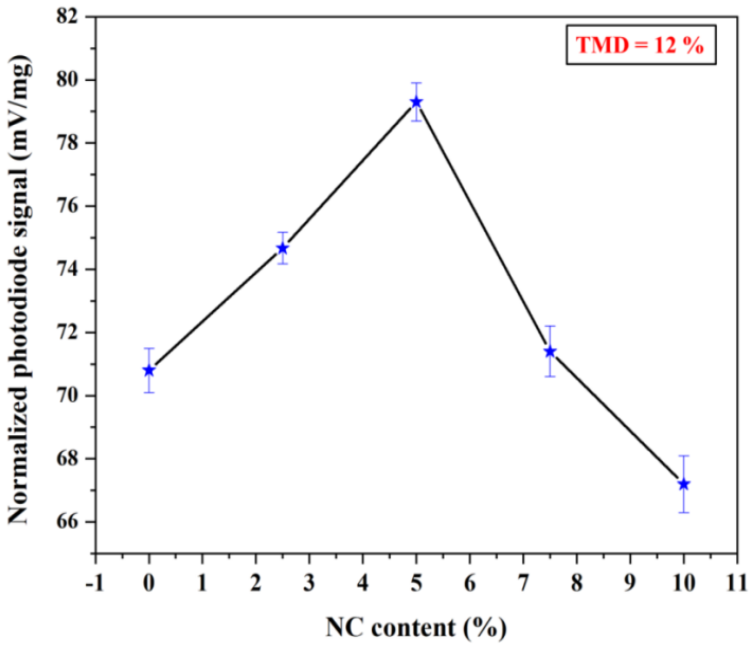

Figure 7-9 Normalized photodiode signal of different nanothermite samples

The specific optical energy release (normalized photodiode signal) increases linearly with the amount of NC and peaks at 5 % NC/GO/Al/$KClO_4$. Further NC addition results in a reduced normalized photodiode signal. This again supports the previous observation that 5 % NC quaternary mixtures perform better than the other samples tested. Improving the specific energy of the samples can be ascribed to the gas generation effect of NC which enhances the convective heat transfer during combustion of the composites and hinders the aggregation of nanothermite reactants [58]. Increasing NC content above 5 % hinders the combustion process due to increasing diffusion length between nano particle reactants [32]. To confirm the normalized photodiode output results and investigate the completion of combustion reaction, the light intensity of aluminum monoxide (AlO) reaction product is measured using a photodiode with a 488 nm wavelength filter to observe the 483nm characteristic emission wavelength. The captured AlO signals of nanothermites are shown in Figure 7-10.

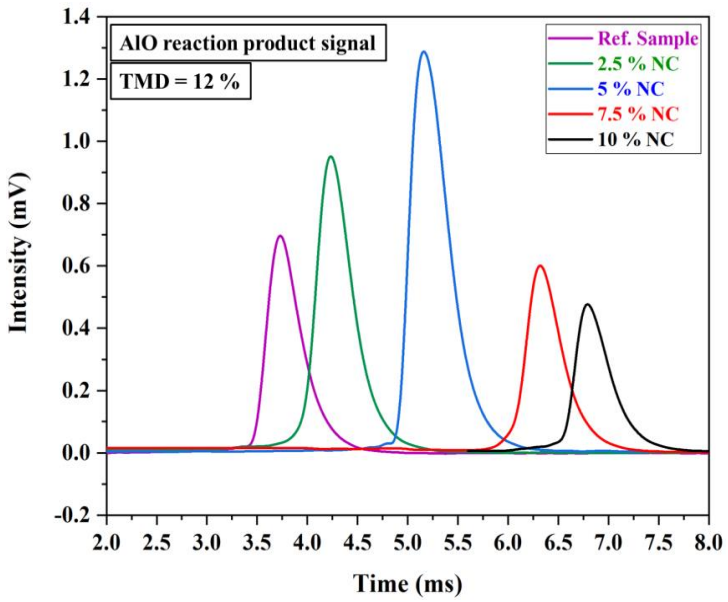

Figure 7-10 AlO photodiode signal of different nanothermite samples

The intensity of the AlO photodiode signal increases with the addition of NC with the largest intensity occurring at 5 % NC, supporting the findings observed in Figure 7-8A and Figure 7-9. AlO is the main gaseous reaction intermediate in the range of 1200-3300 °C, hence correlation between the amount of AlO formed during the reaction and measured by the intensity of photodiode signal can be used as indication of the completion of combustion reaction [62]. Higher light emission at around 488nm, the characteristic wavelength emitted by AlO [42], indicates a greater amount of AlO so the results presented in Figure 7-10 suggest a more complete nanothermite reaction in the 5 % NC case.

7.4.3 Effect of 5 % NC/GO/Al/KClO4 Bulk Density

The effect of bulk density on sample performance is important because it can be used as a tuning parameter of the nanothermite charge to tailor the fuel to a specific application. To describe the bulk density for powdered samples, sample density is compared to their theoretical maximum density (TMD). % TMD is defined as the ratio between the density of the nanothermite sample measured, based on the corresponding sample mass and volume, divided by the density calculated by the weighted average of the densities of each reactant in the composite [63]. Comparison between the measured sample density and TMD is expressed as a percentage, %TMD.

Thrust performance of 5 % NC/GO/Al/$KClO_4$ was evaluated from 20 to 63 %TMD using static thrust measurements as described in section 3.1. The samples were loaded into the small-scale test engine keeping mass constant (15 mg). So, to change the sample density, the sample volume was varied by pressing the nanothermite powder to achieve a desired %TMD. Variation of I_{SP} and I_{SV} at ranging densities is shown in Figure 7-11.

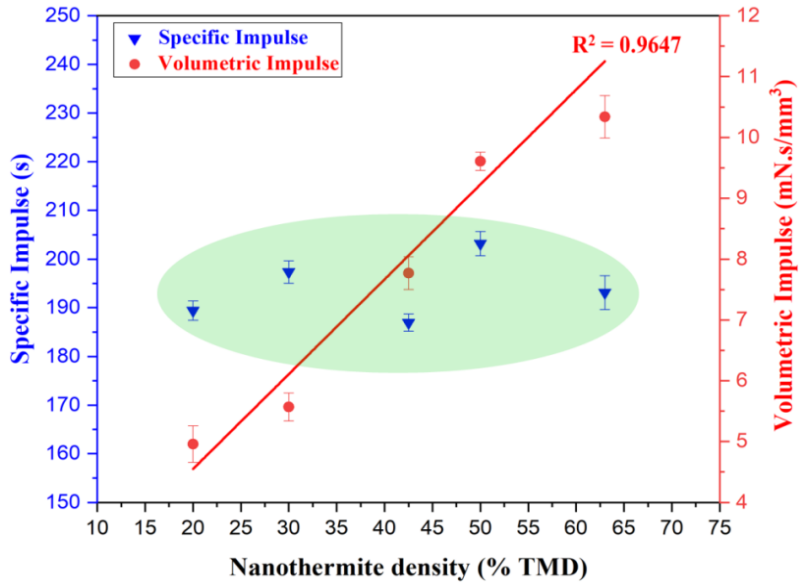

Figure 7-11 Specific and volumetric impulses of 5 % NC/GO/Al/KP with different %TMD

These results show that bulk density does not have significant influence on the values of I_{SP}; they range between 186-203 s. This observation agrees with the independence of I_{SP} and %TMD observed in Al/CuO and Al/Bi_2O_3 based thermite thrusters, as reported in [41, 57]. Moreover, the results indicate that low and high bulk density regimes have a comparable effect on both thrust output force and I_{SP}. In other words, the reactants seemed fully reacted and the specific energy release is nearly constant. Though bulk density does not affect I_{SP} greatly, I_{SV} increased linearly with %TMD. Since I_{SP} and I_{SV} are related by the density of the sample, and %TMD is a measure of density, a linear relation between %TMD and I_{SV} for a constant I_{SP} is expected. This is indeed the case, as seen in Figure 11, and agrees with previously observed trends for Al/CuO and Al/Bi_2O_3 based thermites [41]. This observation means that for applications where volume is a limiting factor, impulse is maximized by maximizing propellant charge density. The effect of bulk density on the combustion performance of the sample is important because it enables tunability of the nanothermite charge as necessary by application.

7.4.4 Performance of the nanothermites integrated in STM with a nozzle

To evaluate the nanothermite mixtures for small-scale propulsion applications, an STM with a CD nozzle as shown in Figure 2D was used. Limited data is available for these nanothermite compositions in small scale test engines prior to this study; the hope is that this research enables the development of next generation microthruster devices.

Time resolved thrust-force data for the reference, 2.5% and 5 %NC samples is presented in Figure 7-12. This figure shows the results obtained for 20% and 50%TMD packing densities as well as in nozzle and no-nozzle STM configurations.

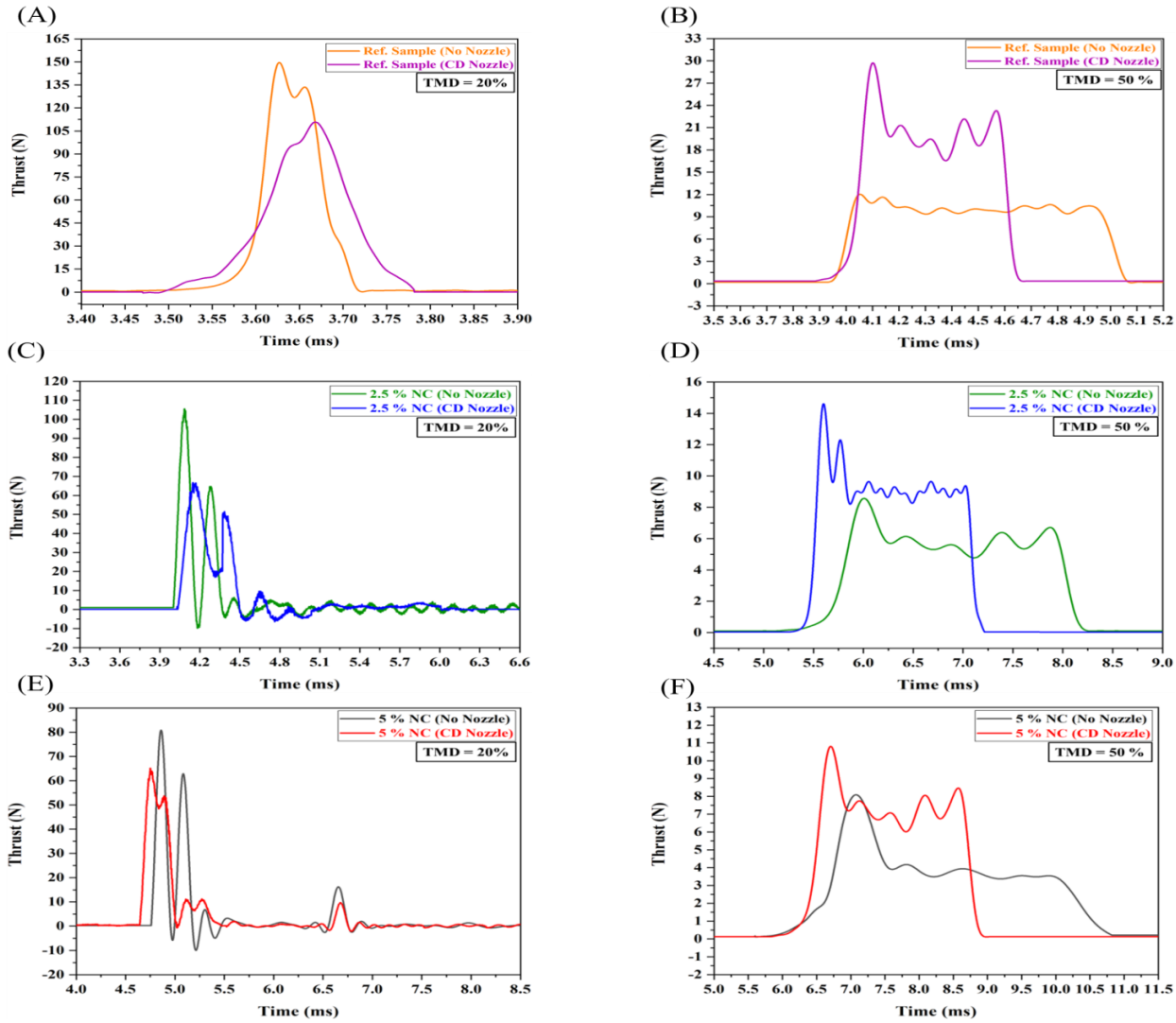

Figure 7-12 (A-F) Thrust/time curves for reference, 2.5 and 5 % NC nanothermites at 20 and 50 % TMD with and without nozzle, respectively

Figure 7-12 shows two different reaction regimes, slow and fast, for high- and low-density samples, respectively. For all nanothermite compositions, the low-density (20 % TMD, fast reaction regime) samples showed a reduced peak thrust force with the introduction of the CD nozzle but an increased combustion duration compared to the no-nozzle condition. The converse was true in the slow reaction regime for all the high density (50%TMD) samples. Combustion characteristics output from nanothermites within CD nozzle STM at fast and slow regimes are recorded in Table 7-4.

Table 7-4 Combustion characteristics of nanothermites within CD nozzle STM at 20 and 50 % TMD

Sample Composition	**Average Thrust (N)**	**Combustion Duration (ms)**	**I_{FT} (mN.s)**	**I_{SP} (s)**	**I_{SV} (mN.s/mm^3)**
Ref. Sample	43.8 ± 1.8	0.3 ± 0.1	12.3 ± 0.5	125.1 ± 4.7	3.1 ± 0.2
	14.7 ± 1.2	0.8 ± 0.1	12.2 ± 0.3	124.4 ± 2.4	3.1 ± 0.1
2.5% NC	7.4 ± 0.6	2.3 ± 0.3	17.1 ± 0.7	174.2 ± 5.6	4.9 ± 0.3
	6.7 ± 0.5	2.2 ± 0.2	15.3 ± 0.3	156.0 ± 2.3	3.9 ± 0.2
5% NC	6.0 ± 0.5	3.2 ± 0.3	19.0 ± 0.6	193.7 ± 3.8	4.9 ± 0.2
	5.5 ± 0.3	3.2 ± 0.2	17.7 ± 0.5	181.0 ± 4.1	4.6 ± 0.3
7.5% NC	3.8 ± 0.4	4.4 ± 0.5	16.5 ± 0.6	167.9 ± 3.9	4.2 ± 0.4
	3.9 ± 0.3	3.8 ± 0.4	14.9 ± 0.4	151.7 ± 2.4	3.8 ± 0.2
10% NC	2.4 ± 0.1	5.2 ± 0.4	12.6 ± 0.3	129.0 ± 2.2	3.2 ± 0.2
	2.3 ± 0.2	5.1 ± 0.5	11.8 ± 0.4	120.6 ± 1.7	3.0 ± 0.1

* Orange and gray colors represent 20 and 50 % TMD respectively.

Results in Table 7-4 exhibit higher I_{FT}, I_{SP}, and I_{SV} for samples ignited inside CD nozzle STMs in both fast and slow reaction regimes, compared to those tested in open STMs. This improvement in the performance is likely due to many factors including degree of confinement, mass flow of the exhaust gasses, and combustion stay-time [41, 64]. It is noted that, in Table 4, a slight reduction in the average thrust and extension of the combustion duration within CD nozzle STMs

occurs for the 20 % TMD samples. This can be attributed to the frictional forces between solid and liquid combustion products, as observed in Figure 7, along thruster walls. Additionally, the geometric nature of the CD nozzle may exacerbate these forces. For the 50 % TMD samples, the increase in thrust force and reduced combustion period are attributed to the acceleration of the exhaust flow through the nozzle and hence increasing the exhaust velocity at the nozzle exit [57, 64].

Moreover, in Table 7-4, total impulses in high packing density samples are consistently 6 to 10 % less than those with low packing density. This is attributed to decreased combustion rates and increased flow losses as the sample density is changed. Additionally, the combustion surface area in low packing density samples is higher than that in high packing density, so more grains burn simultaneously (i.e. more complete combustion). At high packing densities, pores and voids are reduced within the sample, eliminating convective pathways and causing conductive heat transfer to be the dominant mode. Combustion of high packing density samples is slower and more localized as a result, with the region surrounding the ignition spot ignited by the heat from the laser and a slow self-propagation of the flame from the ignition spot. The reduced heating rate may result in a lower reaction completeness, and as a result some grains exit without burning and some may remain as residue in the combustion chamber. Also, the high packing density and the short length of the motor, the residence time of the burning products cannot be the same which affects the efficiency of combustion. Furthermore, the theoretical relations and equations of impulse and thrust assume a fully gaseous phase product which, in the case of aluminothermic compositions, does not occur; there are some solid and liquid products that cause two-phase losses [65].

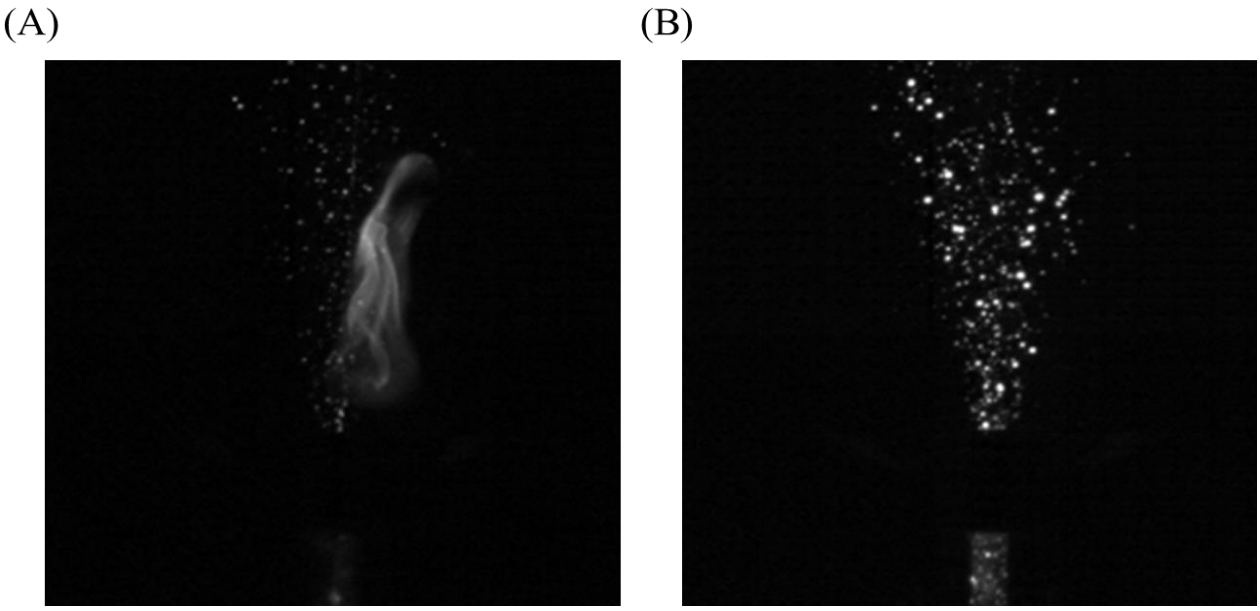

Figure 7-13 Snapshot at the end of combustion for 5 % NC sample at (A) low packing density and (B) high packing density

Two phase losses in high packing density samples are higher than low density samples due to the formation of more solid and liquid particles (size and quantity) as shown in Figure 7-13. Since the high-density samples produce more condensed phase products, the increase of two-phase losses supports the observed decrease in impulses presented in Table 7-4.

These results show that the effect of a generic CD nozzle on the combustion behaviour of nanothermites based on NC, Al and oxidizing salts ($KClO_4$) agrees with those based on some metallic oxidizers such as CuO as reported in [57]. In addition, the CD nozzle produces mixed effects depending on the sample density. To increase thrust for a high-density sample a CD nozzle may be used, but this is not the case for a low-density sample. Similarly, to improve combustion duration for a low-density sample a CD nozzle may be used, but this is not the case for a high-density sample. In addition, the generic nature of the used nozzle means that the results provide only a glimpse of the true capabilities of a well-designed thruster; a nozzle optimized for the Al/$KClO_4$ nanothermite charge is expected to produce much better results.

7.5 Conclusion

This study reports on the fabrication and performance characterization of quaternary nanothermites based on n-Al, $KClO_4$, GO and different quantities of NC to support future propulsion application demands. Electrospinning was introduced as a facile way to prepare quaternary nanothermite composites with well mixed components. Thermal behaviour of the mixtures was analysed and a mechanism for the effect of NC in the quaternary nanothermites was proposed. The prepared nanothermites ignited and self-propagated inside millimeter-scale STMs, a notable observation when compared with classical energetic materials that do not perform well in those conditions. These tests in open tube STMs showed increasing addition of NC to the base GO/Al/$KClO_4$ reference sample resulted in reduction of peak thrust forces and increases in both ignition delay and burn duration. As compared to the reference samples, improvements in the thrust output, I_{FT}, I_{SP}, and I_{SV} were achieved with the addition of up to 5 % NC; further addition of NC however reduced the performance. The enhancement in the performance and energy output of the prepared nanothermites is largely attributed the role of NC as an energetic binder that produces gas that aids in preventing reactive sintering. The introduction of a nozzle to the STMs resulted in reduced peak forces and increased burn times for all 20 % TMD samples while all 50 % TMD samples produced converse results. Other effects include improved impulses for the 20 % TMD samples and marginally reduced impulses for the 50 % TMD samples, with 5 % NC being the best performing composition across all sample densities. The thermite combustion process introduces multi-phase exhaust flows that result in two-phase losses, which may explain the nozzle STM results. Additionally, it is expected that refinement of the nozzle design may improve performance. Generally, tunable combustion parameters can be developed by the controlled addition of NC to oxygenated salt-based nanothermite mixtures. Further adjustment to the thermite can be performed by changing packing density and nozzle configuration to tailor performance case-specifically. The culmination of this information suggests that the considered quaternary nanothermites may be usefully applied in a wide range of micro-energetic applications.

7.6 Acknowledgement

Ahmed Fahd acknowledges the financial funding from the Egyptian government.

Baranovsky and Wen acknowledge the financial funding from the NSERC Discovery grant.

Charles Dubois acknowledges the financial funding from the NSERC Discovery grant.

7.7 References

[1] S.J. Widdis, K. Asante, D.L. Hitt, M.W. Cross, W.J. Varhue, M.R. McDevitt, A MEMS-based catalytic microreactor for a H_2O_2 monopropellant micropropulsion system, IEEE/ASME transactions on mechatronics, 18 (2013) 1250-1258.

[2] L.L. Wang, Z.A. Munir,Y.M. Maximov, Thermite reactions: their utilization in the synthesis and processing of materials, J. Mater. Sci. 28 (1993) 3693–3708.

[3] M.X. Zhou, J. Lu, R. Shen, K. Zhang, Nanostructured energetic composites: synthesis, ignition/combustion modeling, and applications, ACS Appl. Mater. Interfaces 6 (2014) 3058–3074.

[4] V.A. Arkhipov, A.G. Korotkikh, The influence of aluminum powder dispersity on composite solid propellants ignitability by laser radiation, Combust. Flame 159 (2012) 409-415.

[5] F.W. Ji Dai, C. Ru, J. Xu, C. Wang, W. Zhang, Y. Ye, R. Shen, Ammonium perchlorate as an effective additive for Enhancing the combustion and propulsion performance of Al/CuO nanothermites, J. Phys. Chem. C 122 (2018) 10240−10247.

[6] S.H. Kim, M.R. Zachariah, Enhancing the rate of energy release from nanoenergetic materials by electrostatically enhanced assembly, Adv. Mater. 16 (2004) 1821-1825.

[7] M.L. Pantoya, J.J. Granier, Combustion behavior of highly energetic thermites: Nano versus micron composites, Propellants Explos. Pyrotech. 30 (2005) 53-62.

[8] E.L. Dreizin, Metal-based reactive nanomaterials, Prog. Energy Combust. Sci. 35 (2009) 141-167.

[9] C.S. Jian, K. Sullivan, Nanothermite reactions: Is gas phase oxygen generation from the oxygen carrier an essential prerequisite to ignition? Combust. Flame 160 (2013) 432-437.

[10] K.S. Wu, S. Chowdhury, G. Jian, L. Zhou, M.R. Zachariah, Encapsulation of perchlorate salts within metal oxides for application as nanoenergetic oxidizers, Adv. Funct. Mater. 22 (2012) 78-85.

[11] K.S. Kappagantula, C. Farley, M.L. Pantoya, J. Horn, Tuning energetic material reactivity using surface functionalization of aluminum fuels, J. Phys. Chem. C. 116 (2012) 24469–24475.

[12] S.F. Son, B.W. Asay, T.J. Foley, R.A. Yetter, M.H. Wu, G.A. Risha, Combustion of nanoscale Al/MoO_3 thermite in microchannels, J. Propuls. Power 23 (2007) 715-721.

[13] G. Jian, J. Feng, R.J. Jacob, G.C. Egan, M.R. Zachariah, Superreactive nanoenergetic gas generators based on periodate salts, Angew. Chem. Int. 52 (2013) 9743–9746.

[14] W. Zhou, J.B. Delisio, X. Li, L. Liu, M.R. Zachariah, Persulfate salt as an oxidizer for biocidal energetic nano-thermites, J. Mater. Chem. 3 (2015) 11838–11846.

[15] W. Zhou, J.B. Delisio, X. Wang, M.R. Zachariah, Reaction mechanisms of potassium oxysalts based energetic composites, Combust. Flame 177 (2017) 1–9.

[16] X. Hu, J.B. Delisio, X. Li, W. Zhou, M.R. Zachariah, Direct deposit of highly reactive $Bi(IO_3)_3$– polyvinylidene fluoride biocidal energetic composite and its reactive properties, Adv.Eng. Mater. 19 (2017) 1-9.

[17] K.T. Sullivan, N.W. Piekiel, S. Chowdhury, C. Wu, M.R. Zachariah, C.E. Johnson, Ignition and combustion characteristics of nanoscale Al/$AgIO_3$: a potential energetic biocidal system, Combust. Sci. Technol. 183 (2010) 285-302.

[18] M. Comet, C. Martin, F. Schnell, D. Spitzer, Nanothermites: a short review. Factsheet for experimenters, present and future challenges, Propellants Explos. Pyrotech. 44 (2019) 18-36.

[19] G. Jian, J. Feng, R.J. Jacob, G.C Egan, M.R. Zachariah, Super-reactive nanoenergetic gas generators based on periodate salts, Angew. Chem. Int. 52 (2013) 9743-9746.

[20] Y.R. Luo, Comprehensive handbook of chemical bond energies. Boca Raton, Florida: 25 CRC Press, 2007.

[21] N.B. Stand, B.D. Darwent, Bond dissociation energies in simple molecules, Nat. Stand. Ref. Data Ser.,U.S.A, 1970, pp. 1-60.

[22] H. Fuzellier, M. Comet, "Étude synoptique des explosifs," Actual. Chimique 233 (2000) 4-11.

[23] B.W. Armstrong, B. Baschung, D.W. Booth, M. Samirant, Enhanced propellant combustion with nanoparticles, Nano Lett. 3 (2003) 253-255.

[24] M. Kabganian, M. Nabipour, F.F. Saberi, Design and implementation of attitude control algorithm of a satellite on a three-axis gimbal simulator, J Aerosp Eng. 229 (2015) 72–86.

[25] G. Mazoni, Y.L. Brama, Cubesat micropropulsion characterization in low earth orbit, Proceedings 29th annual AIAA/USU Conference on small satellites (2015).

[26] S.J. Apperson, Characterization and MEMS applications of nanothermite materials, Doctoral Faculty of the Graduate School, University of Missouri (2010).

[27] C. Baras, D. Spitzer, M. Comet, F. Ciszek, F. Sourgen, Piloting device of a missile or of a projectile, US8716640B2 (2014).

[28] M. Comet, B. Siegert, V. Pichot, P. Gibot, D. Spitzer, Preparation of explosive nanoparticles in a porous chromium(III) oxide matrix: a first attempt to control the reactivity of explosives, Nanotechnology 19 (2008) 285716.

[29] S. Suhard, P. Fau, B. Chaudret, S. S-Etienne, M. Mauzac, A-F. Mingotaud, G. A-Rodriguez, C. Rossi, M-F. Guimon, When energetic materials, PDMS-based elastomers, and microelectronic processes work together: fabrication of a disposable microactuator, Chem. Mater. 21 (2009) 1069–1076.

[30] S. Romero-Diez, J.M. Pearl, D.L. Hitt, M.R. McDevitt, P.C. Lee, A single-use microthruster concept for small satellite attitude control in formation-flying applications, Aerospace 119 (2018) 1-18.

[31] S.W. Jackson, Design of an air-breathing electric thruster for cubeSat applications, Master of Science, Department of Aerospace Engineering Science, University of Colorado (2017).

[32] Ji Dai, J. Xu, F. Wang, Y. Tai, Y. Shen, R. Shen, Y. Ye, Facile formation of nitrocellulose-coated Al/Bi_2O_3 nanothermites with excellent energy output and improved electrostatic discharge safety, Mater. Des. 143 (2018) 93–103.

[33] R. Li, H. Xu, H. Hu, G. Yang, J. Wang, J. Shen, Microstructured Al/Fe_2O_3/nitrocellulose energetic fibers realized by electrospinning, J. Energ. Mater. 32 (2014) 50–59.

[34] J.A. Conkling, C.J. Mocella, Chemistry of Pyrotechnics: Basic principles and theory, Taylor & Francis Group, Boca Raton, U.K., 2019.

[35] A. Fahd, S. Elbasuney, Certain ballistic performance and thermal properties evaluation for extruded modified double-base propellants, Cent Eur J Energetic Mater. 14 (2017) 296-304.

[36] A.C. Ferrari, V. Fal'ko, et al., Science and technology roadmap for graphene, related two-dimensional crystals, and hybrid systems, Nanoscale 7 (2015) 4598–4810.

[37] Q-L. Yan, M. Gozin, F-Q. Zhao, A. Cohena, S-P. Pang, Highly energetic compositions based on functionalized carbon nanomaterials, Nanoscale 8 (2016) 4799–4851.

[38] Z. Bo, X. Shuai, S. Mao, H. Yang, J. Qian, J. Chen, J. Yan, K. Cen, Green preparation of reduced grapheneoxide for sensing and energy storage applications, Sci. Rep. 4 (2014) 1-7.

[39] J.J. Granier, M.L. Pantoya, Laser ignition of nanocomposite thermites, Combust. Flame 138 (2004) 373–383.

[40] E. Lafontaine, M. Comet, Nanothermites, John Wiley & Sons, Inc., USA, 2016.

[41] C.S. Staley, R. Thiruvengadathan, S.J. Apperson, K. Gangopadhyay, S.M. Swaszek, P. Arsenal, R.J. Taylor, S. Charles, S. Gangopadhyay, Fast-impulse nanothermite solid-propellant miniaturized thrusters, J. Propuls. Power 29 (2013)1400-1409.

[42] C.G. Parigger, A.C. Woods, M.J. Witte, L.D. Swafford, D.M. Surmick, Measurement and analysis of atomic hydrogen and diatomic molecular AlO, C_2, CN, and TiO spectra following laser-induced optical breakdown, J. Vis. Exp. 84 (2014) 51250-51258.

[43] L. Huwei, F. Ruonong, Studies on thermal decomposition of nitrocellulose by pyrolysis-gas chromatography, J. Anal. Appl. Pyrolysis 14 (1988) 163–169.

[44] A. Fahd, S. Elbasuney, H. E. Mostafa, Combustion characteristics of extruded double base propellant based on ammonium perchlorate/aluminum binary mixture, Fuel 208 (2017) 296–304.

[45] P.P. Vadhe, R.B. Pawar, R.K. Sinha, S.N. Asthana, A.S. Rao, Cast aluminized explosives (review), Combust Explos Shock Waves 44 (2008) 461–477.

[46] M. Fathollahi, H. Behnejad, A comparative study of thermal behaviors and kinetics analysis of the pyrotechnic compositions containing Mg and Al, J Therm Anal Calorim. 120 (2015) 1483–1492.

[47] B. Asay, S. Son, J.R. Busse, D. Oschwald, Ignition characteristics of metastable intermolecular composites, Propellants Explos. Pyrotech. 29 (2004) 216–219.

[48] M.R.Weismiller, J.Y. Malchi, R.A.Yetter, T.J. Foley, "Dependence of flame propagation on pressure and pressurizing gas for an Al/CuO nanoscale thermite," Proc. Combust. Inst. 32 (2009) 1895-1903.

[49] J-E. Berthe, M. Comet, F. Schnell, Y. Suma, D. Spitzer, Propellants reactivity enhancement with nanothermites, Propellants Explos. Pyrotech. 41 (2016) 994-998.

[50] V.Y. Egorshev, V. Sinditskii, K.K. Yartsev, Combustion of high-density CuO/Al nanothermites at elevated pressures, In Proceeding of 2013 (10th) International Autumn Seminar on Propellants, Explosives and Pyrotechnics, Chengdu, China (2013)273-283.

[51] F.W. Chengbo Ru, J. Xu, J. Dai, Y. Shen, Y. Ye, P. Zhu, R. Shen, Superior performance of a MEMS-based solid propellant microthruster (SPM) array with nanothermites, Microsyst Technol. 23 (2017) 3161–3174.

[52] H. Wang, G. Jian, S. Yan, J.B. DeLisio, C. Huang, M.R. Zachariah, Electrospray formation of gelled nano-aluminum microspheres with superior reactivity, Appl. Mater. Interfaces 5 (2013) 6797–6801.

[53] H. Wang, G. Jian, G.C. Egan, M.R. Zachariah, Assembly and reactive properties of Al/CuO based nanothermite microparticles, Combust. Flame 161 (2014) 2203-2208.

[54] G.P. Sutton, O. Biblarz, Rocket propulsion elements, John Wiley & Sons, New York, 2001.

[55] S. Bell, A Beginner's guide to uncertainty of measurement. Teddington, Middlesex, United Kingdom, TW11 0LW, 2001.

[56] M.M. Selwanis, S. Kossa, M.K. Khalil, A.F. Nemnem, S. Wagdy, Uncertainty estimation for rotor vibration amplitude measuring system, 18th International Conference on Applied Mechanics and Mechanical Engineering (AMME Conference), Military Technical College, Kobry El-Kobbah, Cairo, Egypt, 2018.

[57] S.J. Apperson, A.V. Bezmelnitsyn, R. Thiruvengadathan, K. Gangopadhyay, S. Gangopadhyay, W.A. Balas, P.E. Anderson, S.M. Nicolich, Characterization of nanothermite material forsSolid-fuel microthruster applications, J. Propuls. Power 25 (2009) 1-6.

[58] B. Asay, S. Son, J.R. Busse, D.M. Oschwald, Ignition characteristics of metastable intermolecular composites, Propellants, Explos., Pyrotech. 29 (2004) 216-219.

[59] S. Yan, G. Jian, M.R. Zakariah, Electrospun nanofiber-based thermite textiles and their reactive properties, ACS Appl. Mater. Interfaces 4 (2012). 6432–6435.

[60] S. Jain, O. Yehia, L. Qiao, Flame speed enhancement of solid nitrocellulose monopropellant coupled with graphite at microscales, J. Appl. Phys. 119 (2016) 10–19.

[61] M. Saceleanu, N. Chaumeix, J.Z. Wen, Combustion characteristics of physically mixed 40 nm aluminum/copper oxide nanothermites using laser ignition, Front. Chem. 3 (2018) 1-10.

[62] V. Baijot, M.D. Rouhani, C. Rossi, A. Estève, Effect of temperature and O_2 pressure on the gaseous speciesproduced during combustion of aluminum, Chem. Phys. Lett. 649 (2016) 88–91.

[63] M.L. Pantoya, J.J. Granier, J.B. Henderson, Effect of bulk density on reaction propagation in nanothermites and micron thermites, J. Propuls. Power 25 (2009) 465-470.

[64] G.P. Sutton, Rocket propulsion elements, Wiley, New York, USA, 1986, pp. 27-41.

[65] Y.M. Timnat, Advanced chemical rocket propulsion, Academic Press Inc., Orlando, Florida, USA, 1987.

CHAPTER 8 ARTICLE 4: COMBUSTION CHARACTERISTICS OF EMOF/OXYGENATED SALTS NOVEL THERMITES FOR GREEN ENERGETIC APPLICATIONS

Ahmed Fahd [a,b‡], Mahmoud Y. Zorainy [a‡], Charles Dubois [*a], Daria. C. Boffito [a], Jamal Chaouki [a] and John Z. Wen [c]

[a] Chemical Engineering Department, École Polytechnique de Montréal, Montréal, H3C 3A7 (Canada)

Chemical Engineering Department, Military Technical College, Cairo, 11646 (Egypt)

[b] Mechanical and Mechatronics Engineering Department, University of Waterloo, Ontario, N2L 3G1 (Canada)

(Accepted for publication in Thermochimica Acta journal)

(Note: Ahmad Fahd is the name I always use instead of Ahmad Emam in my all publications)

8.1 Abstract

Metal-based thermites, especially those based on aluminum, have been recently included in materials for energetic applications such as pyrotechnics, propellants, and explosives. In parallel, several advances in the field of Metal-Organic Frameworks (MOFs) and Coordination Polymers (CPs) have as well paved the road for their use in developing novel energetic materials. In this context, we are introducing new thermites compositions with low ignition temperature, stable propulsive force, and high reactivity. These thermites are based on the $[Cu_4Na(Mtta)_5(CH_3CN)]_n$ (Mtta = 5-Methyl-1H-tetrazole) energetic metal-organic framework (EMOF-1) as a fuel instead of pure metals. We first report the synthesis of an energetic MOF via the microwave-assisted technique as a more rapid and greener method. The efficiency of composites based on EMOF-1 and Al together with various oxygenated salts were investigated. Multiple instruments are involved to characterize the morphology and the structure of EMOF-1 and the developed systems, such as SEM-EDX, FTIR, and XRD. The combustion behavior of the novel composites was evaluated by TGA/DSC, bomb calorimetry and laser ignition. Additionally, the apparent

kinetic parameters (activation energy & frequency factor) were calculated by the Kissinger and Ozawa approaches. The results revealed that the new thermite mixtures exhibit superior combustion characteristics of one and half to two-folds the average heat of combustion compared to aluminum-based ones, at almost half the ignition temperature. In this sense, the combustion reaction proceeds faster, easier (reduced activation energy), the ignition temperatures are noticeably lowered, the heat released has considerably improved and solid residue significantly decreased. In addition, they exhibited stable force with longer burning time. Among them, EMOF-1/KIO_4 thermite exhibits the highest heat release (4.7 kJ/g), while EMOF-1/NH4NO_3 thermite shows the lowest onset reaction temperature (224 $^{\circ}$C). EMOF-1/$KClO_4$ yields the highest average force (8.4 N), calculated pressure (1365 kPa), pressurization rate (0.32 kPa/μs) and the longest burning time assigned to EMOF-1/$K_2S_2O_8$ (40 ms).

8.2 Introduction

Energetic Materials (EMs) are widely used in many applications serving both the civilian and military fields. They have been used in micro- and nano-welding, material synthesis, ejection seats, safety air cushion, and power generation as civilian applications. On the other hand, regarding the military purposes, they have attracted much attention as application in pyrotechnics, micro-igniters, micro-thruster, bullets, propulsion, and hydrogen generation [1-4]. EMs can be classified according to their composition into monomolecular EMs (MEMs) or metastable intermolecular composites (MICs) materials. MEMs have the fuel and oxidizer components in the same molecule (e.g., nitrocellulose, nitroglycerine (NG), and trinitrotoluene (TNT)), while MICs are produced from mixing fuel (e.g., aluminum) and oxidizers (e.g., iron oxide or potassium perchlorate) as it is the case for red thermite (Al/Fe_2O_3) [5-10].

The advantage of using thermites, which is a synonym of MICs, comes from their high energy density (such as 16.5 and 20.8 kJ/cm^3 for Al/Fe_2O_3 and Al/CuO) [11] compared to MEMs (like 6.9 and 10.2 kJ/cm^3 for TNT and NG) [12] as a result of the high enthalpies of combustion and energy densities of the metallic fuels. However, the inherent problem of thermites is their slow rate of energy release in contrast with MEMs. In addition, they suffer from a relatively longer delay of ignition of metallic fuels that is usually accompanied by a delay in the diffusion of the oxidizer and/or the fuel through the passivation layer of the metal oxide[13-14]. Moreover, the

high electrostatic sensitivity, relatively elevated ignition temperature (~ 800 °C), lower peak pressures and excessive oxidation of nano-Al before combustion are undesirable characteristics [15-19]. Therefore, the output force by micro-scale devices would be limited because of the apparent lack of C-H-O-N elements in the thermite constituents and the decrease of the active Al content over time [20-21]. Hyper toxicity, hydrolytic instability, and other environmental hazards can result from using some of the primary components integrated into thermite mixtures such as NaN_3, and NH_4ClO_4, in addition to the resultant large quantity of thermite's solid residue [16, 22]. These risks have so far limited the military and civilian uses of thermites [23, 24]. Aluminum-free energetic thermites using high energy metal-organic frameworks (HE-MOFs) are a sound alternative to produce more environmentally friendly MICs with enhanced combustion properties [25, 26].

The superiority of EMOFs is owed to their higher heat of detonation, due to the high energy density nitrogen-rich organics such as imidazoles, triazoles, tetrazoles, triazines, tetrazines and their substituted derivatives [27]. Also, EMOFs undoubtedly have an excessive amount of released gases, fairly good stability, high specific surface area, controllable structure, and uniform pore size [28]. Commonly, there are three distinct types of EMOFs (1D, 2D, and 3D); each of them has its own energy storage and release characteristics. In most cases, 3D-EMOFs exhibit the best performance.

The EMOFs $[Cu(atrz)_3(NO_3)_2]_n$ (ATRZ-1) and $[Cu_4Na(Mtta)_5(CH_3CN)]_n$ (EMOF-1) exhibit heat of detonation of 3.62 and 2.37 kcal/g, respectively, which are higher than those of hexanitrohexaazaisowurtzitane (CL-20) (1.52 kcal/g) and octanitrocubane (ONC; about 1.8 kcal/g) [29]. Figure 8-1 illustrates the molecular structure of ATRZ-1 and EMOF-1.

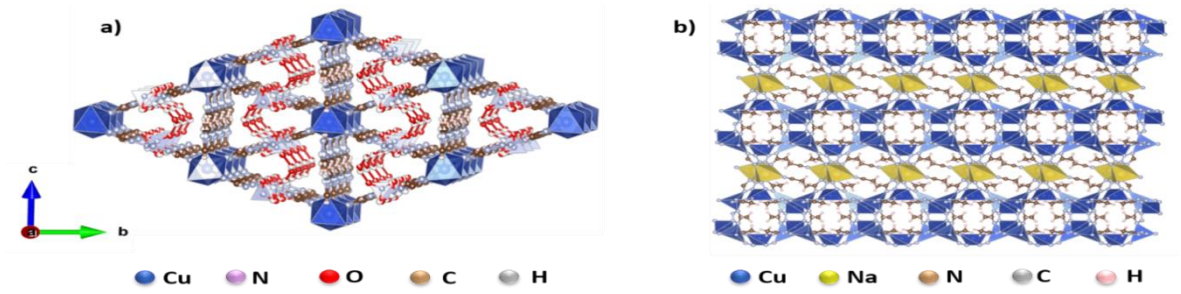

Figure 8-1 3D structure of (a) ATRZ-1 and (b) EMOF-1 viewed along the a-axis. (recreated from CCDC files "DIXNUV" and "TOXRIJ", respectively)

In general, the conventional solvothermal/hydrothermal technique is the most used method for the preparation of MOFs. However, other methods were also developed to fulfill other requirements within this field. Among these different synthesis methods characterized by shorter production times, there are the microwave-assisted, sonochemical, mechanochemical, and electrochemical methods [31, 31]. In particular, the solvent evaporation method and the vapor diffusion method require very long preparation times that may reach several weeks or months; nevertheless, they are still used in the synthesis of the highly sensitive energetic MOFs [32, 33]. Microwave-assisted synthesis is considered as one of the most promising non-conventional techniques for MOFs production as it reduces the overall processing time (up to 99.8%) and finely controls the energy consumption [34]. As well as being a timesaving and an energy-efficient technique, microwave technology gives the chance for controlling and modifying various MOF properties (particle size, morphology, and phase-selectivity) [34, 35].

The literature about thermites based on EMOFs is still scarce. Shenghua Li and his research group have reported a new thermite material with ATRZ-1, replacing Al as a fuel and either of perchlorates (NH_4ClO_4 and $KClO_4$) or periodates (KIO_4 and $NaIO_4$) as individual oxidizers. This specific type of thermites exhibited good results in both sensitivity and performance tests, as reported in Table 8-1 [36]. They concluded that thermites based on those EMOFs, and periodate salts show promise as a green secondary gas generator of reduced sensitivity [37].

Table 8-1 Sensitivity and combustion characteristics of ATRZ-1/thermite mixtures [36, 37]

Thermite mixture	**Impact sens. (J)**	**Frict. sens. (N)**	**ES. sens. (J)**	**Heat of combust. (kJ/g)**	**Max. press. (MPa)**	**Ign. temp.[a] (°C)**
ATRZ-1/NH_4ClO_4	4	118	0.69	3.84[a] (5.41[b])	6.90	242
ATRZ-1/$KClO_4$	8	110	0.16	1.70[a] (4.45[b])	5.70	227
ATRZ-1/KIO_4	9	32	0.19	2.05[a]	1.79	227
ATRZ-1/$NaIO_4$	10	8	0.13	2.63[a]	1.96	232

[a] Heat of combustion and ignition temperature measured by DSC.

[b] Heat of combustion measured by calorimetric bomb.

The goal of this work is to develop new thermite mixtures based on 3D EMOF as alternatives to Al and different types of oxygenated salts. Our work is original for several reasons: i) A new EMOF (EMOF-1) was prepared using microwaves instead of the solvothermal method reported before. The synthesis based on this method provided a shorter production time and smaller particle size. ii) EMOF-1 was selected as an alternative for Al fuel based on its structure as a bimetallic MOF and its energetic properties that would satisfy the intended purpose. iii) The oxygenated salts chosen in this study have a high oxygen content, strong oxidizing nature, and exothermic decomposition reaction. iv) The characterization of EMOF-1 and thermite compositions was conducted in two steps. Firstly, microscopy techniques (SEM coupled with EDX), PXRD and FTIR analyses characterized the morphological and chemical characteristics. Secondly, reactivity and performance are assessed by thermogravimetric analysis and differential scanning calorimetry (TGA/DSC), and oxygen bomb calorimeter. v) We compare the EMOFs with reference samples of Al-based thermites.

8.3 Materials and methods

8.3.1 Materials

In the synthesis of EMOF-1, copper(I) chloride (CuCl, 97%), sodium azide (NaN_3, ≥99.5%), and acetonitrile (CH_3CN, anhydrous 99.8%) as the main framework constituents were all purchased from Sigma-Aldrich (Canada), in addition to methanol and acetone as the washing liquids. These reagents were used without further purification.

Two types of oxidizers were included in the preparation of the thermite mixtures. The oxygenated salts including, potassium perchlorate ($KClO_4$, ≥99%) and ammonium nitrate (NH_4NO_3, ≥99%), were provided by Defence Research and Development Canada (DRDC). Potassium periodate (KIO_4, 99.8%) and potassium persulfate ($K_2S_2O_8$, ≥99%) were purchased from Sigma-Aldrich (Canada). Iron (III) oxide (Fe_2O_3, ≥96%) and copper (II) oxide (CuO, 98%), as metallic oxidizers, were also purchased from the same supplier and were only involved in the preparation of the reference samples with Al representing the well-known metal thermite mixtures. All oxidizers are fine powder in order of 5-10 μm according to their suppliers and used without further purification.

Al nanoparticles were obtained from the US Research Nanomaterials Inc., and were employed as purchased as the fuel for the reference samples. As specified by the manufacturer, the particles were of a spherical shape, an average particle size of 40 nm, and of purity of more than 99.9 % metal basis, an active Al content of 80 % (mass fraction) by thermogravimetric analysis. Their specific surface area was 30-50 m^2/g. Particles are assumed to be 80 % Al (2.70 g/cm^3) and 20 % Al_2O_3 (3.95 g/cm^3), leading to an average particle density of 2.88 g/cm^3.

8.3.2 Synthesis of EMOF-1

The 3D EMOF-1 was originally prepared following the hydrothermal route [38]. 5-methyl-1H-tetrazole (Mtta), as the nitrogen-containing organic ligand, was formed *in-situ* by the azide-alkyne Huisgen cycloaddition of CH_3CN and NaN_3 (Figure 8-2a), and catalyzed by the Cu^+ ions present [38, 39]. After the formation of the organic linker, it coordinates to the metal ions at high temperature, giving rise to the 3D structure of EMOF-1 (Figure 8-2b).

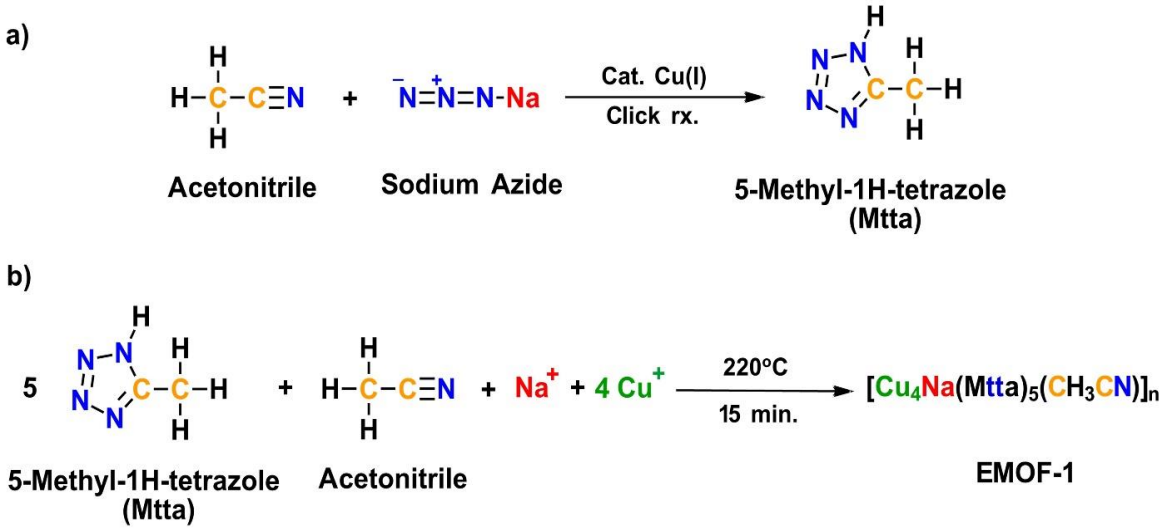

Figure 8-2 Stepwise synthesis of the energetic MOF (EMOF-1). a) Click reaction for the formation of the Mtta-linker, b) Coordination of the formed linker to the metal ions present in the reaction medium and the formation of the energetic MOF (EMOF-1)

Here, the microwave-assisted technique was utilized to synthesize EMOF-1 as follows: First, a mixture of 0.6 mmol (60 mg) CuCl, 1.5 mmol (99 mg) NaN_3, and 0.29 mol (15 ml) CH_3CN, was weighted into a 30 ml reaction vial (G30, Glass). Then, the mixture was stirred for 30 min, yielding a dark brown suspension. Afterwards, the vial was covered with a Teflon-lined cap and

placed in the microwave reactor (Anton Parr - Monowave 400). The mixture was held at 220°C for 15 min under stirring. The temperature was monitored via the embedded IR sensor along with the external Ruby thermometer accessory to control and minimize the variation in the temperature during the reaction. The synthesis scheme for EMOF-1 is illustrated in Figure S1 (Supporting information). The rapid heating of the reaction medium was applied through an initial MW pulse reaching the maximum power of 850W (Figure S2. Supporting information). At the specified temperature, the power delivered to the reactor chamber dropped and was kept almost constant with a slight fluctuation of 48 ± 2 W, maintaining the reaction temperature. The reaction proceeded under an autogenous pressure of nearly 20 bar, as indicated by the instrument pressure sensor (Figure S3. Supporting information). (The conditions at each step of the preparation process and synthesis scheme are available in the supporting information).

During the synthesis of EMOF-1, the initial dark brown suspension gradually turns into pale brown (beige), and the targeted block-like crystals of EMOF-1 can be observed (colorless solids). After the reaction, the resulting crystals were collected through centrifugation (10,000 rpm, 5 min), followed by subsequent washing with acetonitrile (×2), acetone (×2), and methanol (×3). The products were left to dry overnight in an oven at 100°C and were then preserved in a desiccator to avoid any moisture contact until use, as the structure was reported to be chemically stable in air but not water [38]. The solvothermal synthesis of EMOF-1 reported a 70% yield based on copper; [38] however, in our case of microwave synthesis, we obtained a comparable yield of 68%.

8.3.3 Preparation of thermite compositions

Thermite mixtures were prepared by weighing the EMOF-1 fuel and different oxidizers individually in a stoichiometric ratio, according to Table 2. The dispersion of the EMOF-1 with each oxidizer was conducted in acetone. The samples were then sonicated via a sonication probe for 30 min to ensure proper dispersion. Acetone was allowed to evaporate at 80 °C for 1 hour under continuous magnetic stirring to prevent agglomeration. Wet particles were fully dried in a vacuum desiccator for 12 h to drive off any remaining solvent. Finally, the dried powder was gently broken up with a spatula to remove any large clumps and until the consistency was that of a loose powder. Table 8-2 illustrates different thermite compositions and their reactions, which

account for the pathway for a majority of the products. This is also the pathway that will yield the most stable reaction products.

Table 8-2 Chemical composition and reaction of different nanothermite samples

Sample Name	Oxidant	Oxidant wt. %*	Fuel type, wt. %		Reaction
			EMOF-1	Al	
EMOF-1/$KClO_4$	$KClO_4$	63.91	36.09	0	$2Cu_4NaC_{12}N_{21}H_{18} + 18.75KClO_4 \rightarrow 8CuO + Na_2O + 18.75KCl + 18H_2O + 24CO_2 + 21N_2$
EMOF-1/KIO_4	KIO_4	74.61	25.39	0	$2Cu_4NaC_{12}N_{21}H_{18} + 18.75KIO_4 \rightarrow 8CuO + Na_2O + 18.75KI + 9H_2O + 24CO_2 + 21N_2$
EMOF-1/$K_2S_2O_8$	$K_2S_2O_8$	87.36	12.64	0	$Cu_4NaC_{12}N_{21}H_{18} + 18.75K_2S_2O_8 \rightarrow 4CuO + 0.5Na_2O + 18.75K_2SO_4 + 18.75\ SO_2 + 9H_2O + 12CO_2 + 10.5N_2$
EMOF-1/NH_4NO_3	NH_4NO_3	80.36	19.64	0	$Cu_4NaC_{12}N_{21}H_{18} + 37.5NH_4NO_3 \rightarrow 4CuO + 0.5Na_2O + 84H_2O + 12CO_2 + 48N_2$
Al/$KClO_4$	$KClO_4$	68.13	0	31.87	$8\ Al + 3\ KClO_4 \rightarrow 4\ Al_2O_3 + 3\ KCl$
Al/KIO_4	KIO_4	76.16	0	23.84	$8\ Al + 3\ KIO_4 \rightarrow 4\ Al_2O_3 + 3\ KI$
Al/$K_2S_2O_8$	$K_2S_2O_8$	88.25	0	11.75	$4\ Al + 3\ K_2S_2O_8 \rightarrow 2\ Al_2O_3 + 3\ K_2SO_4 + 3\ SO_2$
Al/NH_4NO_3	NH_4NO_3	81.64	0	18.35	$2\ Al + 3\ NH_4NO_3 \rightarrow Al_2O_3 + 3\ N_2 + 6\ H_2O$
Al/CuO	CuO	81.55	0	18.45	$2\ Al + 3\ CuO \rightarrow Al_2O_3 + 3Cu$
Al/Fe_2O_3	Fe_2O_3	74.73	0	25.27	$2\ Al + Fe_2O_3 \rightarrow Al_2O_3 + 3\ Fe$

*stoichiometric

8.3.4 Instrumentation

The morphology of EMOF-1 and thermite samples was studied by a FEI Quanta FEG 450 SEM operated at 15 kV coupled with EDX measurements. FTIR spectra were measured in the IR region of 400–4000 cm^{-1} with the help of the Perkin Elmer SP-65 FTIR spectrometer in an attenuated total reflectance (Miracle ATR) mode. Moreover, XRD patterns were recorded on a Panalytical 3050/60 Xpert-PRO using CuKα radiation. The simultaneous DSC/TGA was performed to measure the heat flow and weight loss characteristics as a function of temperature using a SDT Q600 thermal analyzer (TA Instruments). The measurements on all of the samples prepared in this work were carried out in argon under identical experimental conditions (heating rate of 10°C/min and argon flow rate of 100 ml/min). The heat of combustion of each sample was measured by the oxygen bomb calorimeter (model: Parr™ 1341 Plain Jacket Calorimeter). To assess the combustion propagation characteristcs of the thermites, a 5W continuous wave 532nm laser was used to ignite samples as shown in Figure S4 (Supporting information). The combustion of the samples was recorded at 180,000 fps with 600 ns exposure time using a Phantom v2012 high-speed camera. A Dytran (1051V2) force transducer with a reference sensitivity of 99.78 mV/lbf. was fixed underneath the sample to measure the output force. The force transducer characteristic frequency for the used STM configuration (Φ = 2.8 mm, L = 35 mm) is 4.9 kHz. In processing the force data, a band-stop filter was applied from this characteristic frequency up to 40 kHz to eliminate signal noise. A Tektronix MSO56 oscilloscope was used to capture force data at a sampling rate of 1MHz. Data recording and laser triggering was performed by a Tektronix AFG1022 waveform generator using a standard TTL signal. All tests were carried out at normal atmospheric conditions.

8.4 Results and discussions

8.4.1 Structural and chemical characterization

To verify the achievement of the EMOF-1 structure, multiple characterization techniques were used to determine the crystallographic data and the structural constituents of the products. PXRD for EMOF-1, shown in Figure S5 (Supporting information), was found to be identical to the simulated one from literature *(CCDC database identifier: TOXRIJ)* [38]. Besides, a slight shift was identified, indicating a smaller particle size of the crystals obtained using the microwave-

assisted technique [40]. Such a pattern indicates the formation of the reticular 3D bimetallic framework, built through the connection of two distinct one-dimensional metal-ligand chains.

First, the sodium azolate chain, in which the Na_2-$(azole)_2$ secondary building units (SBUs) are formed during the synthesis via the cycloaddition click chemistry protocol of joining small molecules of acetonitrile and sodium azide, yielding the 5-methyl-1H-tetrazole linker (Figure 8-3a) [41]. The creation of these conjugated molecules with a very low reaction rate usually requires high temperature and pressure otherwise, it can be catalyzed by copper, which, in our case, is one of the EMOF-1 constituents [38, 42]. A complex formation process takes place by the coordination of the copper ions to the nitrogen binding arms of the formed linkers, giving the other repeating beetle-like ribbon copper-ligand 1D chain (Figure 8-3b). The two chains are interconnected into the three-dimensional framework based on the μ_4-η^1:η^1:η^1:η^1 coordination mode of the Mtta ligand (Figure 8-3c) [38, 43]. The formation of this complex structure results in a thermostable compound with low sensitivity and high heat of detonation, as it supports the connection of metals to the nitrogen-rich heterocyclic compounds of high ring strain. The stability, and high nitrogen content, provides energetic N-N and N-C bonds [38, 44].

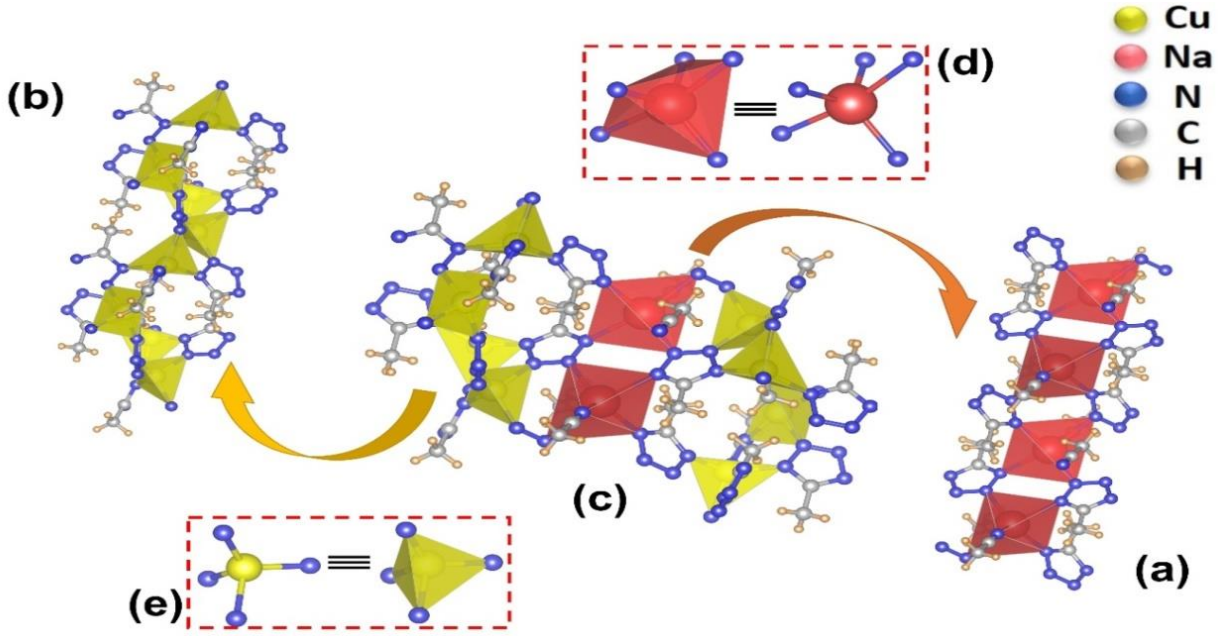

Figure 8-3 The detailed structure of EMOF-1, revealing a) Na azolate chains, b) Cu beetle-like chains, c) unit cell of EMOF-1, d) distorted hexagonal geometry of Na(I) centres, and e) tetrahedral geometry Cu(I) centres (according to the color code). [reproduced from CCDC file "*TOXRIJ*"]

The unit cell of EMOF-1 is shown in Figure 8-3c, in which the Na(I) centers adopt the distorted hexahedron geometry, binding with four nitrogen atoms of four different linker molecules and one acetonitrile molecule (Figure 8-3d). At the same way, the Cu(I) ions take the form of a tetrahedron coordinated with four Mtta molecules, whereby two of them are bonded to another two Cu(I) tetrahedra, and the other two are bonded to the Na(I) hexahedra (Figure 8-3e). The crystallographic data reveals an abundance ratio of copper to the sodium ions equal to 4:1 (Calc.), which was verified by the elemental analysis using SEM-EDX. The relative percentages of EMOF-1 constituents are given in Table 8-3, and the SEM images of EMOF-1 crystals are shown in Figure 8-4. The inset displays the stacked-layer topology of the MOF as a result of the chain connections.

Table 8-3 Relative percentage for EMOF-1 elemental analysis

Element	Atoms % (EDX)
N	57
Cu	17
Na	4
C	22

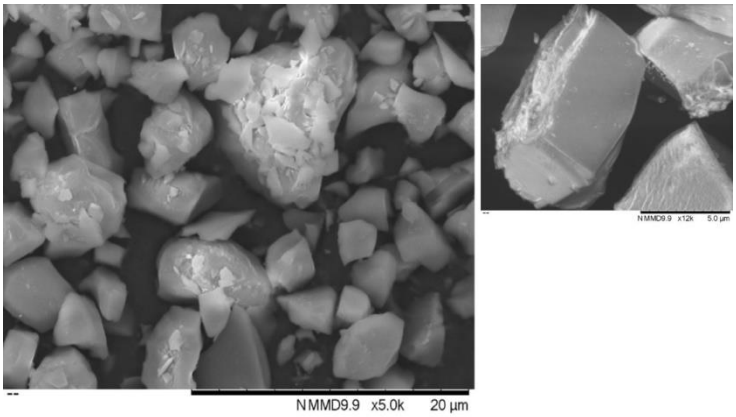

Figure 8-4 SEM images of the block-like crystals of EMOF-1. Side cross-section showing the built-up layers within the crystal (inset)

Furthermore, ATR-FTIR was used to confirm the formation of the Mtta ligand and its coordination with the metal ions (Figure 8-5). Aliphatic C-H symmetric and asymmetric stretching of methyl groups were recognized at 2924 and 2853 cm^{-1}, respectively, in addition to

the peaks around 1130 cm^{-1} corresponding to bending [45]. Three different modes for the carbon-nitrogen atoms were given with respect to the nature of bonding of these atoms within the structure. The C≡N bond stretch of acetonitrile was still recognized at 2248 cm^{-1}, besides the C=N and C-N absorption bands at 1625 and 1380 cm^{-1}, respectively [38, 43, 45].

Also, the peak at 1489 cm^{-1} related to the stretching vibrations of the C-C bonds was clearly noticed [43, 45]. These bands obviously confirm the formation of the Mtta linker with its conjugated triazine ring, as well as the presence of extra acetonitrile molecules that are connected to the Na(I) hexahedra. Finally, the sharp peak at 698 cm^{-1} characteristic of the metal-nitrogen bond vibrations proves the connection of the Cu(I) and Na(I) ions to the nitrogen-containing ligand [43].

The vibrational spectrum shows a characteristic broad peak at 3438 cm^{-1} that was not expected to appear, as it is attributed to the stretching of the N-H bonds of secondary amines, which is only found within the Mtta linker structure but not EMOF-1. All the nitrogen atoms found within the MOF after coordination are totally bonded to either carbon, nitrogen, or a metal atom, and the bond with the hydrogen does not appear anymore. However, comparing the spectrum with other MOFs' publications based on the same specific ligand, the same peak was found to appear even after the synthesis [38, 43]. Such a peak can belong to any unreacted secondary amine of the ligand's triazine ring or the O-H bonds related to any methanol residuals from the washing step [45].

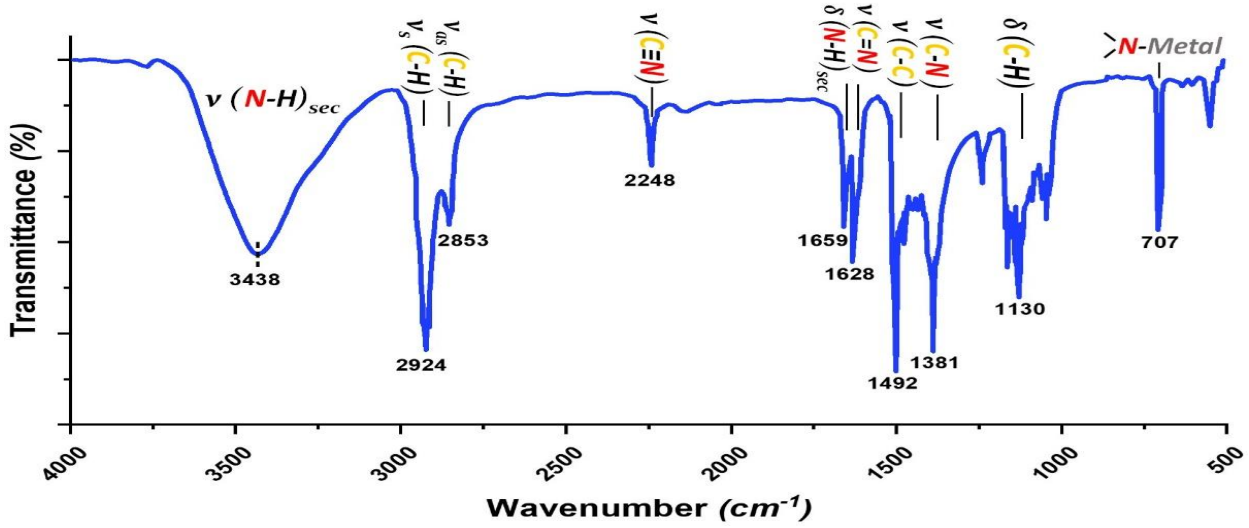

Figure 8-5 FTIR spectrum of EMOF-1

At this point, the achievement of EMOF-1, according to the previous study, was confirmed. Moving on to the thermite composites, different oxygenated salts were mixed with EMOF-1 by sonication according to the procedures discussed earlier in the method section. The homogenous distribution of the oxidizer throughout the whole sample was verified by the SEM-EDX analysis shown in Figure 8-6, in which the EMOF-1/KIO_4 was selected as a representative for the entirety of the samples.

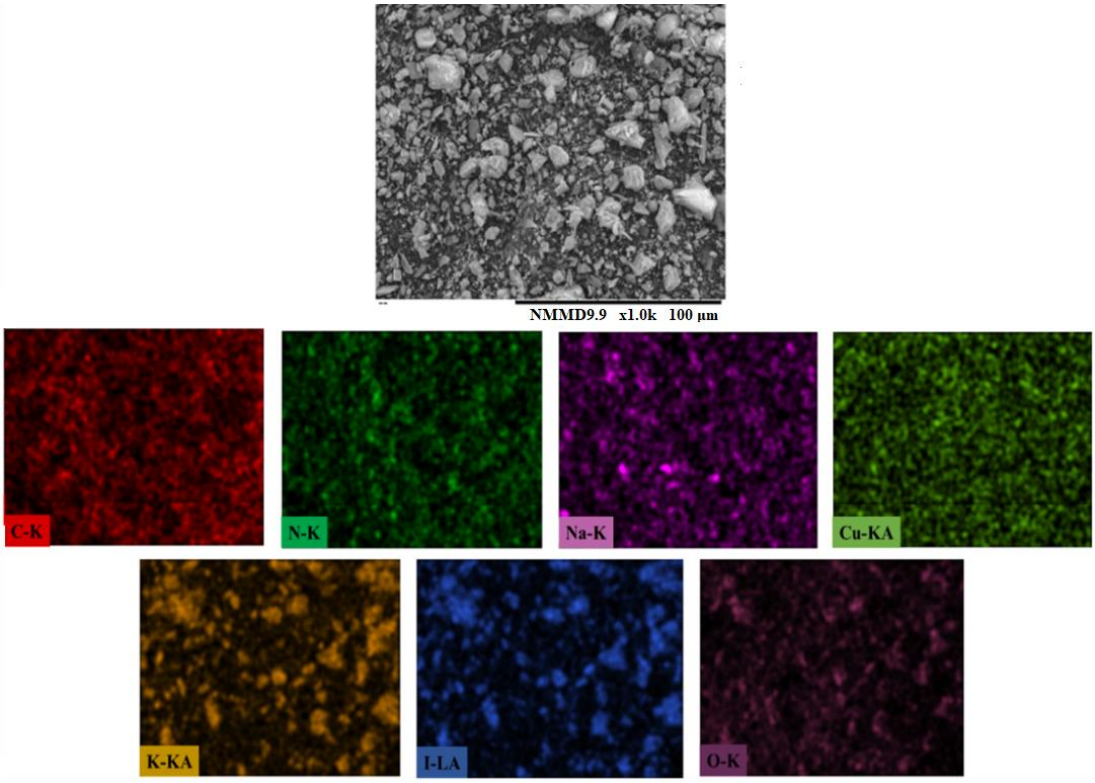

Figure 8-6 SEM images and EDX analysis of EMOF-1 and KIO4 thermite

As it can be seen, no agglomerations of the fuel or the oxidizer were noticed, which indicates the good mixing and distribution of the particles, thus validating the preparation method.

8.4.2 Thermal analysis

Simultaneous TGA/DSC was performed for EMOF-1 and different thermite compositions. Figure 7 illustrates the TGA/DSC thermogram of EMOF-1.

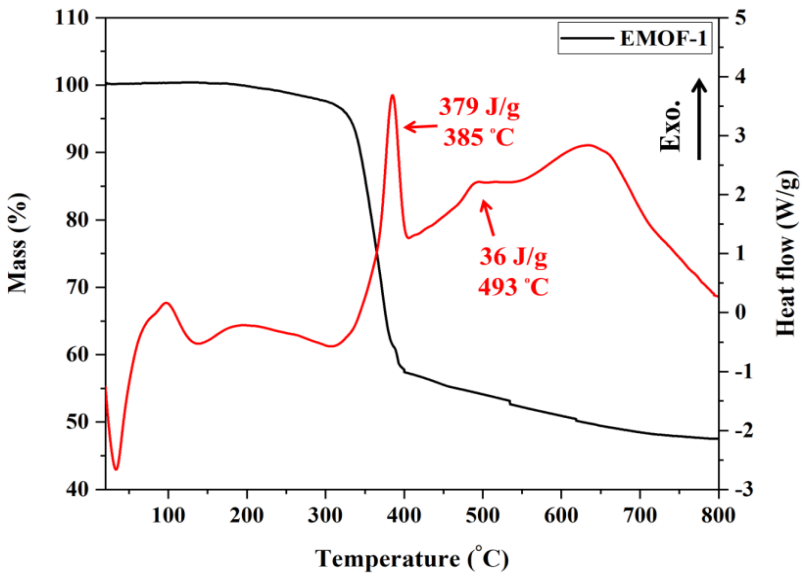

Fig. 7 TGA/DSC plots of pure EMOF-1

The thermal gravimetric analysis of E-MOF-1 develops in three steps (Figure 7). A first and steep weight loss is observed below 100 °C and ends at 315 °C, accompanied by a mass loss of about ~ 4.8 %. It is attributed to the thermal decomposition of one molecule of acetonitrile. A second weight loss from 335 to 415 °C is assigned to the breakdown of the major framework of EMOF-1. The third step is composed by two steep weight losses starting from 415 °C to 730 °C, yielding approximately 8 % mass loss and ascribed to the decomposition of the remaining EMOF-1. The thermal decomposition of EMOF-1 showed one major exothermic peak with an onset temperature of 310 °C and a maximum peak temperature at 385 °C, suggesting the collapse of the main framework of EMOF-1. The lower onset temperature of the prepared EMOF-1 (310 °C) compared to that of the hydrothermally prepared by Y. Fang et al. (335 °C) is ascribable to the effect of the microwave-assisted technique in improving the activity EMOF-1 [38]. The first endothermic peak at around 50 °C yields from the evaporation of solvent residuals absorbed inside the structure of the EMOF (acetone, methanol and acetonitrile). The small exothermic peak remarked at 104 °C corresponds to the first steep weight loss observed in TGA. The insignificant heat release accompanying the first small mass loss observed in the TGA corresponds to the first exothermic peak in DSC thermogram. The steep exothermic peak appears between 470 °C to 550 °C and is assigned to the decomposition of EMOF-1 residuals, which confirms the TGA data. The

thermal properties of all EMOF-1 based thermites were also explored using TGA/DSC, as demonstrated in Figure 8-7.

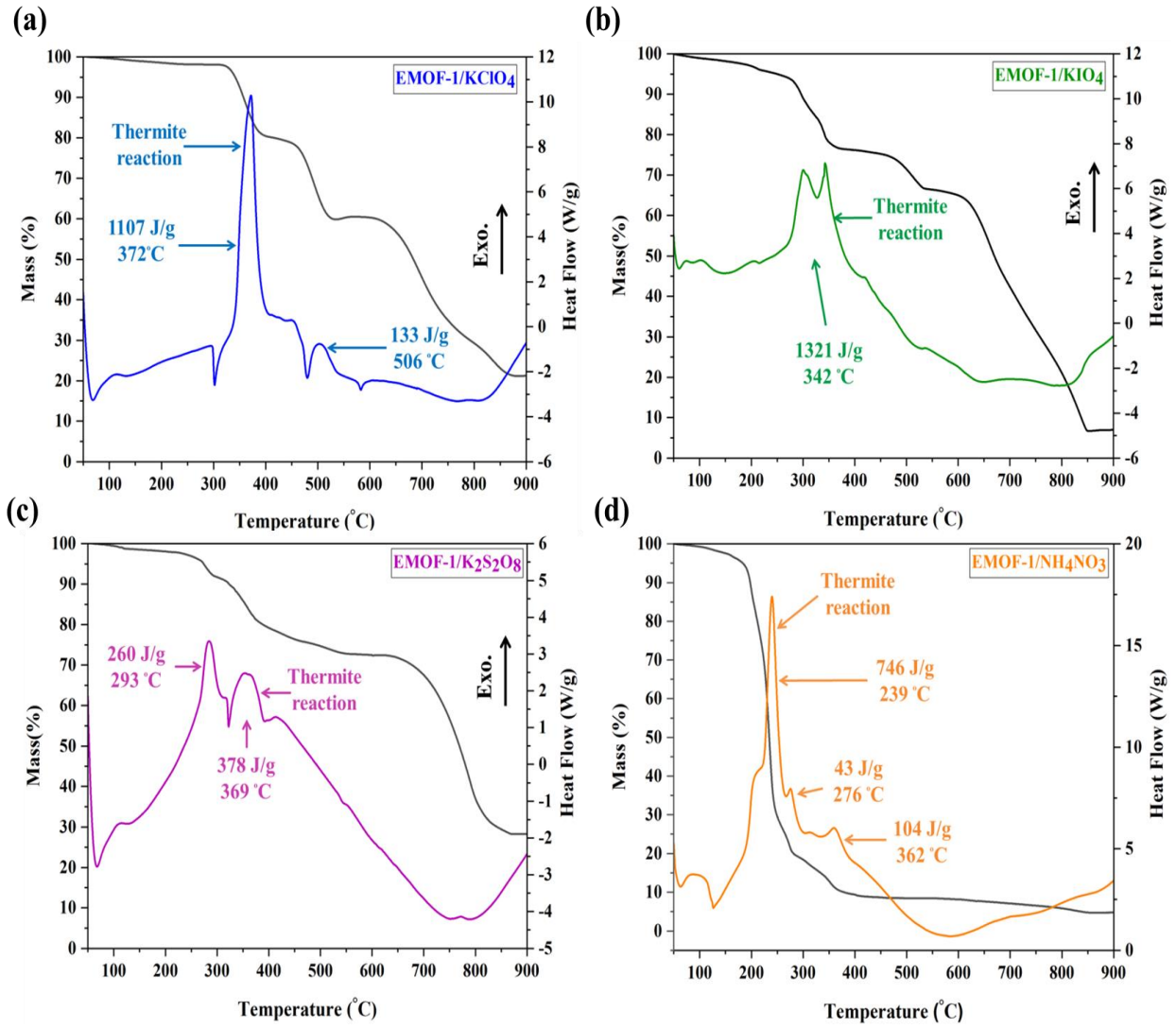

Figure 8-7 TGA/DSC curves of EMOF-1 based composites

All energetic composites based on EMOF-1 and different oxygenated salts reveal high heat release and low onset ignition temperature compared to their traditional thermites counterparts based on Al and either oxygenated or metallic oxidizers (see Table 4). The enthalpy of reaction of the thermites was calculated through the integration of the area underneath the exothermic peak. Moreover, the onset reaction temperature is usually determined from the DSC thermograms as the minimum temperature that can prompt the spontaneous exothermic reaction of a sample. Furthermore, the heat of combustion of all thermite samples was measured using a bomb

calorimeter. Each test was performed five times and the average value of the heat of combustion was calculated. The sample mass for the first two tests was 0.1 g, then we increased the sample mass to 0.3 g for the following two tests and finally to 0.5 g for the last two tests. The energy of combustion was calculated according to standard operating procedures illustrated in reference [46] (the procedure of calculating heat of combustion using calorimetric bomb is available in the supporting information). The experimental values of onset ignition temperature, heat released and heat of combustion of the prepared thermite samples are given in Table 8-4.

Table 8-4 Thermal characteristics of thermite samples

Sample Name	**Onset reaction temperature† (°C)**	**Heat released† (J/g)**	**Average Heat of combustion⁘ (kJ/g)**
EMOF-1/$KClO_4$	342	1240	4.5 ± 0.2
EMOF-1/KIO_4	318	1321	4.7 ± 0.3
EMOF-1/$K_2S_2O_8$	261	638	3.8 ± 0.2
EMOF-1/NH_4NO_3	224	893	4.1 ± 0.2
Al/$KClO_4$	647	840	3.5 ± 0.2
Al/KIO_4	637	678	3.1 ± 0.1
Al/$K_2S_2O_8$	617	597	2.9 ± 0.3
Al/NH_4NO_3	665	619	3.0 ± 0.1
Al/CuO	767	580	2.4 ± 0.2
Al/Fe_2O_3	1227	382	2.2 ± 0.2

† TGA/DSC

⁘ Calorimetric bomb

The results reported in Table 4 indicate that the heat of reaction of different thermite samples remarkably increased, and the onset reaction temperature decreased with the substitution of Al by EMOF-1, thus highlighting the importance of employing EMOF-1 as an energetic fuel. The best performing thermite mixture according to the heat released is EMOF-1/KIO_4, which is comparable to the one based on $KClO_4$ and recorded 1.5, 2, and 2 times higher energy than that of Al/KIO_4, Al/CuO and Al/Fe_2O_3 thermites, respectively. The lowest onset thermite reaction temperature was recorded by EMOF-1/NH_4NO_3 and this can be attributed to the powerful nature of NH_4NO_3 as an oxidizing agent that can release its oxygen fastly; hence the thermite reaction of the metal fuel in EMOF-1/NH_4NO_3 composite occurred in a single step as illustrated in Figure 10a. Generally, the substantial increase in energy release and reduction in onset reaction temperature achieved by EMOF-1 instead of Al is a direct result of the good compatibility between EMOF-1 and different oxygenated salts, which helps in the completion of the combustion reaction and produces environmentally friendly combustion products. Also, in the case of Al based thermites, the alumina shell decreases the diffusion process between the oxygen in the oxidizers and the Al core, which leads to an incomplete thermite reaction, while this barrier does not exist in EMOF based thermites where the oxidizer is in a direct contact with fuel. Additionally, the convergence of the initial decomposition temperature of EMOF-1 and the corresponding oxidizers enhances the reactivity and accelerates the complete combustion, hence improves the energy output.

The outstandingly high heat of combustion of these newly developed EMOF-1 based thermites could be ascribed to the following reasons. First, the superior energetic characteristics of EMOF-1 due to its high nitrogen content result from its tetrazole ligand, which possess the highest nitrogen content (82.34%) among analogues stable nitrogen-containing heterocyclic compounds [22]. Second, since the enthalpy of reaction of EMs increases with increasing the nitrogen content, the tetrazole will improve the heat formation of EMOF-1 as well the output heat of combustion of the prepared thermites [47]. Third, the potential average bond energies of C-N and N=N in the tetrazole heterocyclic molecule, which are 273 and 418 kJ/mol, respectively, will help improving the total heat of combustion of the composites [26]. Fourth, the high heat of detonation (9.88 kJ/g) of EMOF-1 resulting from the complicated structure motifs, nitrogen-rich heterocyclic ligand and strain energy in the 3D molecule, increases the heat of combustion [26,

38]. In short, strong structural reinforcement and extensive coordination networks, as well as the high nitrogen content of the Mtta ligand in the 3D framework, could be responsible for the high heat of combustion of the final thermite composite.

In addition, the ratio of the solid residue mass to the sample mass of thermite mixtures are 10.6 %, 7.3 %, 5.8 % and 4.2 % for thermites based on $KClO_4$, KIO_4, $K_2S_2O_8$ and NH_4NO_3 respectively. The developed thermite mixtures yield very low solid residue compared to the large quantity produced by the Al-based thermites such as 100 % and 80 % solid residue for Al/Fe_2O_3 and Al/CuO [36, 37]. Hence, EMOF-1 based thermites are higher activity, complete combustion and lower deleterious components and elements to meet environmental protection requirements.

Finally, the difference between heat of reactions measured by DSC and calorimetric bomb is explained by the fact that DSC measures heat released according to the slow transformation of thermites and maximum heat flux from the exothermic peak area. Hence, bomb calorimeter is considered the most accurate method to measure the heat of combustion from thermite mixtures and its output measurements values are more precise [48].

8.4.3 Reaction Kinetics

The determination of the kinetic parameters of energetic compositions is essential to assure safe processing, handling, and storage of thermites, besides avoiding any hazards associated with their thermal decomposition. Moreover, some of the thermite mixtures suffer from a difficult initiation process, such as Al/MnO_2, which is usually not easy to spark [49]. Hence, activation energy, which is defined as the minimum amount of energy required for the chemical reaction to proceed, can be used as a measurement tool for the likelihood of a chemical reaction to occur.

The Kissinger's method was used to quantify the activation energy and other Arrhenius parameters for the thermal decomposition reaction of EMOF-1 based thermites according to the following equation [50].

$$\ln\frac{\beta}{T_p^2} = \ln\frac{A.R}{E} - \left(\frac{E}{R}\right)\frac{1}{T_p}$$

where β is the heating rate of the DSC experiment; T_p is the maximum temperature of the exothermic decomposition peak at different heating rates (2, 5, 8 and 10 °C/min); E, A and R are

the activation energy, the pre-exponential factor, and the universal gas constant, respectively. The calculated value of the activation energy was confirmed through the Ozawa's method according to the following equation [51]:

$$\log \beta \cong \log \frac{AE}{R} - \log F(\alpha) - 0.4567 \left(\frac{\mathrm{E}}{\mathrm{R}}\right) \frac{1}{\mathrm{T_P}}$$

For each heating rate and thermite composition $\ln(\frac{\beta}{T_p^2})$ was plotted against (1/Tp), as illustrated in Figure 8-8.

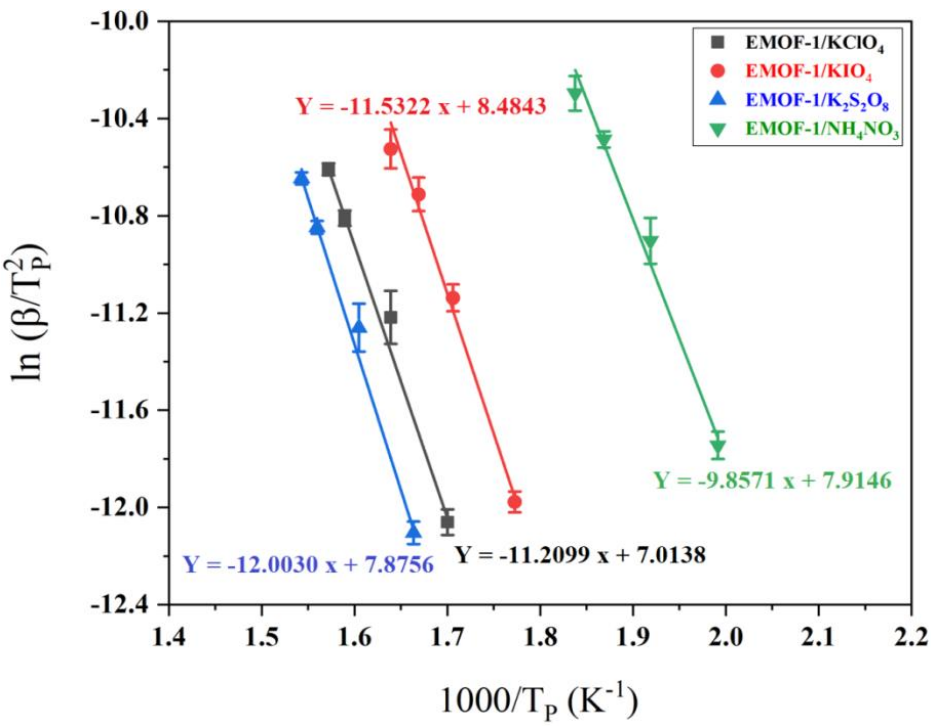

Figure 8-8 Data correlation line of ln $\ln(\frac{\beta}{T_p^2})$ against (1000/Tp) for nanothermite samples, error bars are taken as the uncertainties from linear fitting

It clearly appears from Figure 9 that the relationship between ln (β/T_p^2) and ($1/T_p$) is a straight line obtained by linear regression through the data point. Activation energy and pre-exponential factor are calculated from the slope and intercept of the line of each composition. The results tabulated in Table 8-5 represent the kinetic parameters among all nanothermite samples.

Table 8-5 Kinetic parameters of EMOF-1 based thermite compositions

Sample Name	**E_a (Kissinger's method) kJ/mol**	**E_a (Ozawa's method) kJ/mol**	**A (S^{-1})**	**R^2**
EMOF-1/$KClO_4$	93.20 ± 3.49	97.46 ± 7.28	$124.64 \pm 0.22 \times 10^5$	0.997
EMOF-1/KIO_4	95.88 ± 6.24	98.13 ± 6.92	$557.96 \pm 0.41 \times 10^5$	0.992
EMOF-1/$K_2S_2O_8$	99.79 ± 3.33	104.09 ± 6.74	$315.94 \pm 0.23 \times 10^5$	0.998
EMOF-1/NH_4NO_3	81.95 ± 5.32	83.53 ± 6.37	$269.78 \pm 0.33 \times 10^5$	0.992
EMOF-1 [38]	164	166	752×10^6	0.997
Al/$KClO_4$ [52]	143.68	-----	573.68×10^5	0.998
Al/CuO [53]	233.16	-----	161.08×10^7	0.969
Al/Fe_2O_3 [54]	248	-----	1.9×10^{13}	0.978

Results reported in Table 8-5 show that the linear correlation coefficients of all thermite compositions are very close to one, indicating that the model chosen well represent the experimental data. Furthermore, the derived activation energies of EMOF-1 based thermites are generally lower than those of traditional Al-based ones, such as 248, 222, and 205 kJ/mol for the Al/Fe_2O_3, Al/Bi_2O_3, and Al/MnO_3, respectively [54]. The lowest activation energy was achieved by EMOF-1/NH_4NO_3, followed by EMOF-1/$KClO_4$, EMOF-1/KIO4 and EMOF-1/$K_2S_2O_8$, respectively. This supports the results of the thermal analysis (Figure 8). The reduction of the activation energy thermites can be attributed to the good compatibility between EMOF-1 and different used oxygenated salts and the convergence of their initial decomposition temperature. In

addition, the high activity and the porous structure EMOF-1 enhance the diffusion process between the oxygen of the oxidizer and the unreacted solid fuel and consequently reduces the required energy to activate the reaction. Reducing the activation energy helps the initiation process of thermite at comparatively low energy and temperature. Moreover, EMOF-1 based thermites with reduced activation energy can be efficiently applied in nanostructured thermites explosives (NSTEX) mixtures, which can replace environmentally unfriendly primary explosives base on lead.

8.4.4 Combustion characteristics

Generally classical EMs suffer from difficulty of ignition and propagation within small tubes and slots [55]. Hence, to explore the reactivity of the developed thermites and figure out the full picture about their combustion characteristics, 12 mg of each sample was ignited inside an open acrylic tube (Φ = 2.8 mm, L = 35 mm) using the laser ignition system illustrated in Fig. S4 (Supporting information). The force against time profiles of the prepared composites are shown in Figure 8-9.

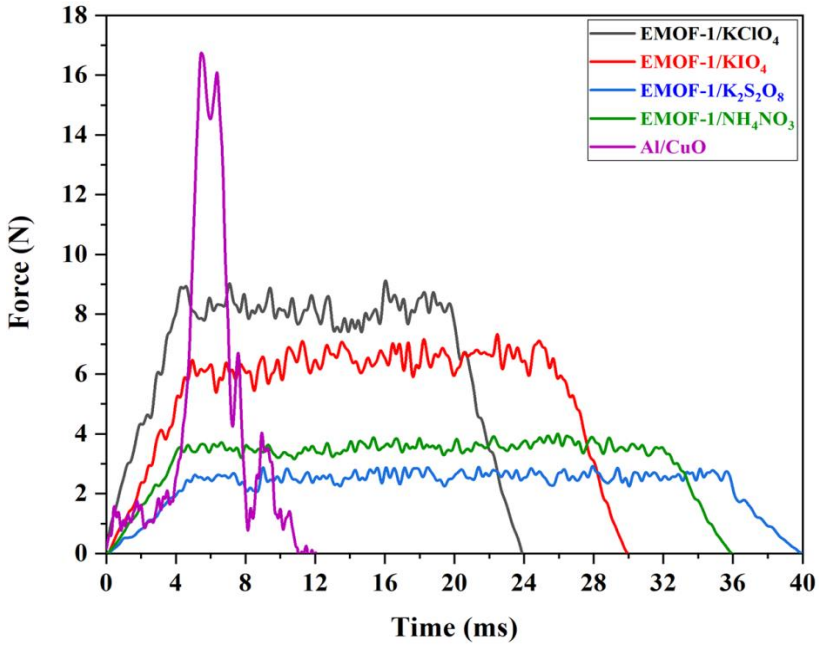

Figure 8-9 Force profiles for different EMOF-1 thermite samples

The prepared EMOF-1 mixtures ignited and self-propagated inside millimeter-scale open tubes, differently from classical energetic materials, which do not perform well in those conditions. This

indicates the good homogeneity of reactants and confirms the high reactivity of the composites illustrated earlier by the reduction of their activation energy. Force time profiles of all EMOF-1 based thermites showed a stable output force with average values equal to 8.4, 6.7, 2.7 and 3.8 N for EMOF-1, $KClO_4$, KIO_4, $K_2S_2O_8$ and NH_4NO_3, respectively. EMOF-1/KIO_4 and EMOF-A/$KClO_4$ have comparable work output; however EMOF-1/KIO_4 has a little a work output slightly higher than EMOF-1/$KClO_4$. More importantly, EMOF-1 based composites exhibit remarkable longer burn times (23, 30, 40 and 36 ms for EMOF-1, $KClO_4$, KIO_4, $K_2S_2O_8$ and NH_4NO_3 in that order) than Al/CuO, which recorded 11 ms (13 ms [37]). The relatively long burn times and stable output force for EMOF-1 based thermites can be ascribed to the following reasons. First, a high amount of gaseous products were produced from EMOF-1 decomposition due to its high C,H,O,N content. Second, EMOF-1 gases and its three-dimensionally ordered macroporous structure promote the convective heat transfer between the mixture during the combustion process and thus enhances complete reactions [47]. Third, the high heat released by EMOF-1 based composites could help in improving the diffusion process between the oxygen in the oxidizer and EMOF-1 as well. To better observe the combustion process and evaluate the energy output, the combustion processes of the samples were recorded using a high-speed camera. From the resultant video, several selected images for each mixture during combustion period are shown in Figure S7 (Supporting information).

Although snapshots of EMOF-1 with different oxidizers appear little blurred and foggy due to the adhesion of decomposition products with the combustion wall tube, EMOF-1/$KClO_4$ thermite exhibited the most luminous flame between the EMOF-1 mixtures as shown in Figure S7 (Supporting information). This result reinforces the observed trend in Figure 10, which showed the highest average force in the presence of $KClO_4$ as an oxidiser. The long duration of combustion observed for all prepared EMOF-1 based thermites will facilitate the production of sustained propulsive force. The culmination of this results concerning longer combustion time, stable average force, green combustion products and expected little solid residue suggests that the EMOF-1 based thermites synthesized in this study may be usefully applied in environmentally friendly gas generation applications.

To assess the possibility of using of EMOF-1 based energetic mixtures in gas generation applications, the average pressure output was estimated. In addition, average pressurization rate is

determined by calculating the ratio of the average pressure to the rise time. Approximately constant slopes in the time-force graphs indicate fixed pressurization rates. Calculated average pressure and pressurization rate for different EMOF-1 based energetic composites are shown in Figure 8-10.

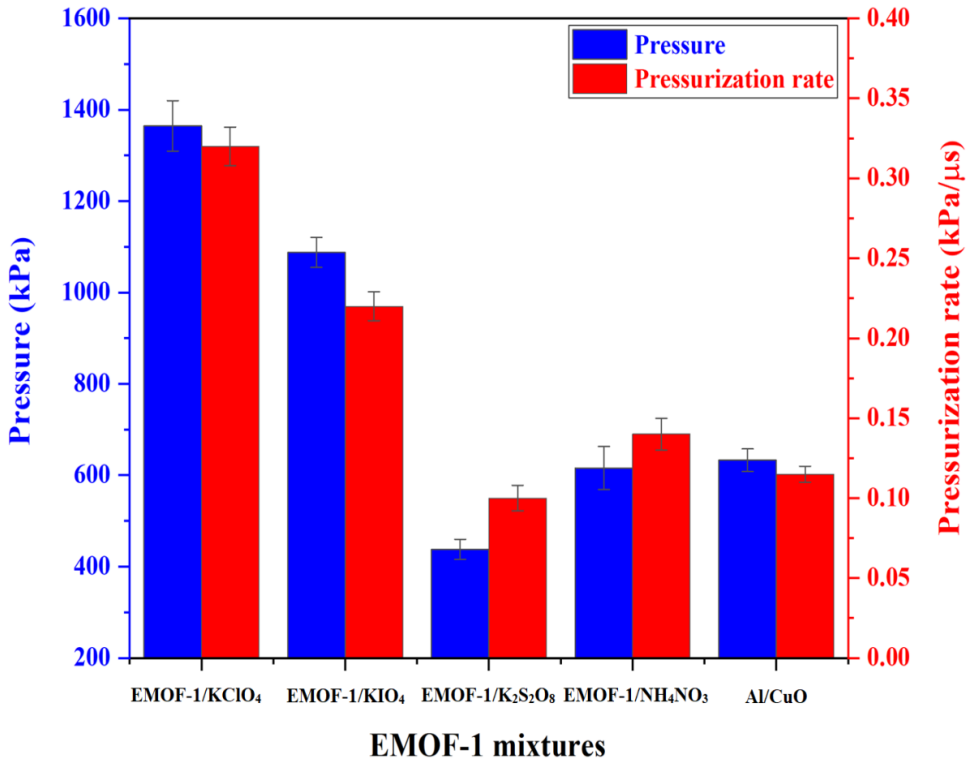

Figure 8-10 Comparison between pressure and pressurization rate for different EMOF-1 based energetic mixtures

Energetic mixtures based EMOF-1 show enhanced performance in terms of pressure and pressurization rate compared to the mixtures prepared by S. Kim et al. and based on sodium azide, micro Al and CuO [22]. The comparatively high pressure and pressurization rate is ascribed to the produced large decomposition gaseous species, which enhances advection and subsequently increases the heat transfer within the sample, which in turn promotes the fuel combustion. Moreover, the prepared EMOF-1 mixtures overcome the insufficient heat generated problems associated with the conventional gas generators such as tetrazole, sodium azide and nitroguanidine, which can cause serious malfunctions in gas-generating systems. In addition, the pressure output of the EMOF-1 composites is comparable to their analogues based on ATRZ-1

energetic MOF. The difference between the pressure output between composites based on EMOF-1 and those based on ATRZ-1 energetic MOF is attributed to the larger sample mass (i.e., 25 mg vs. 12 mg) that was employed in their testing system, which is approximately two times our mass sample [37, 56]. The pressure and pressurization rate exhibited by EMOF-1 based mixtures and different oxygenated salts suggest that the prepared energetic composites may be usefully applied in a wide range of gas generation applications.

8.5 Conclusions

In summary, this study reports on EMOF-1 as a good alternative energetic fuel for thermite mixtures with high combustion heat, suitable ignition temperature, and a large amount of gaseous products. We firstly synthesized EMOF-1 successfully using the microwave-assisted technique, which is more effective, faster, and gives a comparable yield to the solvothermal method. Then, we developed a novel type of thermites based on EMOF-1 instead of Al and integrated with different types of oxidizers by the conventional sonication mixing method. EMOF-1 significantly enhanced the combustion characteristics of the new advanced thermite composites. They exhibited higher heat of combustion, lower ignition temperature, reduced activation energy and lower solid residue than conventional thermites based on Al. While EMOF-1/KIO_4 composite has the best performance concerning heat released (4.7 kJ/g), EMOF-1/NH_4NO_3 recorded the lowest ignition temperature (224 $^{\circ}$C). The enhanced performance of EMOF-1 based mixtures correlated to the superior combustion characteristics of EMOF-1 as energetic fuel and the good compatibility with oxygenated salts. In addition, EMOF-1 based thermites ignited easily inside small tubes, and revealed stable propulsive force and longer combustion time compared to those traditional Al based ones. Finally, pressure and pressurization rate of EMOF-1 mixtures were estimated. Results suggest enhanced performance in terms of pressure and pressurization rate compared to composites based on Al. This is the first time the synthesis of thermites based on EMOF-1 is reported. It can be concluded that many advantages have been achieved with one shot. This manuscript shaded the light that thermite mixtures with tailored combustion performance and green combustion products can be developed via EMOF-1 as fuel. This work opens the route for more application of EMOFs in the future.

8.6 Acknowledgement

Ahmed Fahd and Mahmoud Y. Zorainy acknowledge the financial funding from the Egyptian government.

Charles Dubois acknowledges the financial funding from the NSERC Discovery grant

8.7 References

[1] S.J. Widdis, K. Asante, D.L. Hitt, M.W. Cross, W.J. Varhue, M.R. McDevitt, A MEMS-based catalytic microreactor for a H_2O_2 monopropellant micropropulsion system, IEEE/ASME transactions on mechatronics, 18 (2013) 1250-1258.

[2] Q. Zou, B. Lin, C. Zheng, Z. Hao, C. Zhai, T. Liu, J. Liang, F. Yan, W. Yang, C. Zhua, "Novel integrated techniques of drilling–slotting–separation-sealing for enhanced coal bed methane recovery in underground coal mines, J. Nat. Gas Sci. Eng. 26 (2015) 960-973.

[3] M.X. Zhou, J. Lu, R. Shen, K. Zhang, Nanostructured energetic composites: synthesis, ignition/combustion modeling, and applications, ACS Appl. Mater. Interfaces 6 (2014) 3058–3074.

[4] V.A. Arkhipov, A.G. Korotkikh, The influence of aluminum powder dispersity on composite solid propellants ignitability by laser radiation, Combust. Flame 159 (2012) 409-415.

[5] G.A. Rodriguez, S. Suhard, C. Rossi, D. Esteve, P. Fau, S.S-Etienne, A.F. Mingotaud, M. Mauzac, B. Chaudret, A microactuator based on the decomposition of an energetic material for disposable lab-on-chip applications: fabrication and test, J. Micromech. Microeng. 19 (2009) 015006-1 - 015006-8.

[6] L. Glavier, A. Nicollet, F. Jouot, B. Martin, J. Barberon, L. Renaud, C. Rossi, Nanothermite/RDX-based miniature device for impact ignition of high explosives, Propellants Explos. Pyrotech. 42 (2017) 308–317.

[7] P. Zhu , G. Hou, H. Wang, C. Xu, S. Zhao, R. Shen, Design, preparation, and performance of a planar ignitor inserted with pyroMEMS safe and arm device, J Microelectromech Syst. 27 (2018)1186-1192.

[8] A. Nicollet, G. Lahiner, A. Belisario, S. Souleille, M.D-Rouhani, A. Estève, C. Rossi, Investigation of Al/CuO multilayered thermite ignition, J. Appl. Phys. 121 (2017) 034503-1 - 034503-10.

[9] A. Nicollet, L. Salvagnac, V. Baijot, A. Estève, C. Rossi, Fast circuit breaker based on integration of Al/CuO nanothermites, Sens. Actuators, A 273 (2018) 249–255.

[10] A. Chaalane, C. Rossi, D. Esteve, The formulation and testing of new solid propellant mixture (DB + x%BP) for a new MEMS-based microthruster, Sens. Actuators, A 138 (2017) 161–166.

[11] S. Fischer, M. Grubelich, A survey of combustible metals, thermites, and intermetallics for pyrotechnic applications, in 32. AIAA/ASME/SAE/ASEE joint propulsion conference and exhibit, Orlando, FL (United States) (1996).

[12] R. Meyer, J. Köhler, A. Homburg, Explosives, Sixth ed., Wiley-VCH Verlag GmbH & Co. KGaA, Germany, 2007.

[13] E.L. Dreizin, Metal-based reactive nanomaterials, Prog. Energy Combust. Sci. 35 (2009) 141-167.

[14] M.L. Pantoya, J.J. Granier, Combustion behavior of highly energetic thermites: Nano versus micron composites, Propellants Explos. Pyrotech. 30 (2005) 53-62.

[15] G. Jian, J. Feng, R.J. Jacob, G.C. Egan, and M.R. Zachariah, Super-reactive nanoenergetic gas generators based on periodate salts, Angew. Chem. Int. Ed. 125 (2013) 9925-9928.

[16] K.S. Wu, S. Chowdhury, G. Jian, L. Zhou, M.R. Zachariah, Encapsulation of perchlorate salts within metal oxides for application as nanoenergetic oxidizers, Adv. Funct. Mater. 22 (2012) 78-85.

[17] C.S. Jian, K. Sullivan, Nanothermite reactions: Is gas phase oxygen generation from the oxygen carrier an essential prerequisite to ignition? Combust. Flame 160 (2013) 432-437.

[18] K.S. Kappagantula, C. Farley, M.L. Pantoya, J. Horn, Tuning energetic material reactivity using surface functionalization of aluminum fuels, J. Phys. Chem. C. 116 (2012) 24469–24475.

[19] J.J. Brege, C.E. Hamilton, C.A. Crouse, A.R. Barron, Ultrasmall copper nanoparticles from a hydrophobically immobilized surfactant template, Nano Lett. 9 (2009) 2239-2242.

[20] H.H. DiBiaso, B.A. English, M.G. Allen, Solid-phase conductive fuels for chemical microactuators, Sens. Actuator A Phy. 111 (2004) 260-266.

[21] W. Zhang, H. Peng, X. Gao, J. Ye, Z. Zhang, Y. Chao, An in situ chemical reaction approach to synthesize zinc picrate energetic thin film upon zinc oxide nanowires array, Surf Interface Anal. 44 (2012) 1203-1208.

[22] S.B. Kim, K.J. Kim, M.H. Cho, J.H. Kim, K.T. Kim, S.H. Kim, Micro-and nanoscale energetic materials as effective heat energy sources for enhanced gas generators, ACS Appl. Mater. Interfaces, 8 (2016) 9405-9412.

[23] V. Baev, C. Lvov, I. Shugalei, Influence of the Environment Internal Factors on Warm-blooded Organisms, Proc. Conf. Problems of Military and Emergency Medicine, SPbSPMA, St. Petersburg (in Russian), 1998, 62-63.

[24] M.B Talawar, R. Sivabalan, T. Mukundan, H. Muthurajan, A.K Sikder, B.R Gandhe, A. Subhananda Rao, Environmentally compatible next generation green energetic materials (GEMs), J. Hazard. Mater. 161 (2009) 589-607.

[25] Q. Zhang, J.M. Shreeve, Metal–organic frameworks as high explosives: a new concept for energetic materials, Angew. Chem. Int. Ed. 53 (2014) 2540-2542.

[26] S. Zhang, Q. Yang, X. Liu, X. Qu, Q. Wei, G. Xie, S. Chen, S.Gao, High-energy metal–organic frameworks (HE-MOFs): Synthesis, structure and energetic performance, Coord. Chem. Rev. 307 (2016) 292-312.

[27] C. Wang, D. Liu, W. Lin, Metal–organic frameworks as a tunable platform for designing functional molecular materials, J. Am. Chem. Soc. 135 (2013) 13222-13234.

[28] J. Zhang, J.M. Shreeve, 3D Nitrogen-rich metal–organic frameworks: opportunities for safer energetics, Dalton Trans. 45 (2016) 2363-2368.

[29] J.P. Agrawal, High Energy Materials: Propellants, Explosives and Pyrotechnics. Weinhein: Wiley-VCH, 2010.

[30] N. Stock, S. Biswas, Synthesis of metal-organic frameworks (MOFs): routes to various MOF topologies, morphologies, and composites, Chem. Rev. 112 (2012) 933-969.

[31] Y.R. Lee, J. Kim, and W.S. Ahn, Synthesis of metal-organic frameworks: A mini review, Korean J Chem. Eng. 30 (2013) 1667-1680.

[32] O.S. Bushuyev, G.R. Peterson, P. Brown, A. Maiti, R.H. Gee, B.L. Weeks, L.J. Hope-Weeks, Metal–organic frameworks (MOFs) as safer, structurally reinforced energetics, Chem. Eur. J. 19 (2013) 1706-1711.

[33] S. Li, Y. Wang, C. Qi, X. Zhao, J. Zhang, S. Zhang, S. Pang, 3D energetic metal–organic frameworks: synthesis and properties of high energy materials, Angew. Chem. Int. Ed. 52 (2013) 14031-14035.

[34] I. Thomas-Hillman, A. Laybourn, C. Dodds, S.W. Kingman, Realising the environmental benefits of metal–organic frameworks: recent advances in microwave synthesis, J. Mater. Chem. A. 6 (2018) 11564-11581.

[35] N.A. Khan, S.H. Jhung, Synthesis of metal-organic frameworks (MOFs) with microwave or ultrasound: Rapid reaction, phase-selectivity, and size reduction, Coord. Chem. Rev. 285 (2015) 11-23.

[36] J.Z. Hui Su, Y. Du, P. Zhang, S. Lia, T. Fang, S. Pang, New roles of metal–organic frameworks: Fuels for aluminum-free energetic thermites with low ignition temperatures, high peak pressures and high activity, Combust. Flame 191 (2018) 32–38.

[37] J.Z. Hui Su, Y. Du, P. Zhang, S. Lia, T. Fang, S. Pang, New roles for metal–organic frameworks: fuels for environmentally friendly composites, RSC Adv. 7 (2017) 11142–11148.

[38] Y. Feng, X. Liu, L. Duan, Q. Yang, Q. Wei, G. Xie, S. Chen, X. Yang, S. Gao, In situ synthesized 3D heterometallic metal–organic framework (MOF) as a high-energy-density material shows high heat of detonation, good thermostability and insensitivity, Dalton Trans. 44 (2015) 2333-2339.

[39] R. Varala, B.H. Babu, A Click Chemistry Approach to Tetrazoles: Recent Advances, in Molecular Docking, ed: Intech Open, 2018, pp. 52-75.

[40] C.F. Holder, R.E. Schaak, Tutorial on Powder X-ray Diffraction for Characterizing Nanoscale Materials, ACS Nano 13 (2019) 7359−7365.

[41] J. Roh, K. Vávrová, A. Hrabálek, Synthesis and functionalization of 5-substituted tetrazoles, Eur. J. Org. Chem. 31 (2012) 6101–6118.

[42] M.S. Singh, S. Chowdhury, S. Koley, Advances of azide-alkyne cycloaddition-click chemistry over the recent decade, Tetrahedron 72 (2016) 5257-5283.

[43] A. Mariyam, M. Shahid, I. Mantasha, M.S. Khan, M.S. Ahmad, Tetrazole Based Porous Metal Organic Framework (MOF): Topological Analysis and Dye Adsorption Properties, J Inorg Organomet Polym Mater. 30 (2020) 1935–1943.

[44] Q. Yang, J. Ge, Q. Gong, X. Song, J. Zhao, Q. Wei, G. Xie, S. Chen, S. Gao, Two energetic complexes incorporating 3, 5-dinitrobenzoic acid and azole ligands: microwave-assisted synthesis, favorable detonation properties, insensitivity and effects on the thermal decomposition of RDX, New J. Chem. 40 (2016) 7779-7786.

[45] J. Coates, Interpretation of Infrared Spectra, A Practical Approach. , In R.A. Meyers, M.L. McKelvy (Eds.), Encyclopedia of Analytical Chemistry : applications, theory and instrumentation, 2006.

[46] D.P. Shoemaker, C.W. Garland, Experiments in Physical Chemistry, fourth ed., New York: McGraw-Hill, 1981.

[47] H. Zhang , M. Zhang, P. Lin , V. Malgras, J. Tang, S.M. Alshehri, Y. Yamauchi , S. Du, J. Zhang, A Highly Energetic N-Rich Metal–Organic Framework as a New High-Energy-Density Material, Chem. Eur. J. 22 (2016) 1141 – 1145.

[47] W. Zhou, J.B. Delisio, X. Wang, M.R. Zachariah, Reaction mechanisms of potassium oxysalts based energetic composites, Combust. Flame 177 (2017) 1–9.

[48] E. Lafontaine, M. Comet, The Experimental Study of Nanothermites, In Nanothermites (Eds.), US: Wiley-ISTE Ltd, 2016, pp. 127-227.

[49] J. Song, T. Guo, W. Ding, M. Yao, F. Bei, X. Zhang, J. Huang, X. Fang, Study on thermal behavior and kinetics of Al/MnO2 poly (vinylidene fluorine) energetic nanocomposite assembled by electrospray, RSC Adv. 9 (2019) 25266-25273.

[50] H. E. Kissinger, Reaction kinetics in differential thermal analysis, Anal. Cheml. 29 (1957) 1702-1706.

[51] J.H. Flynn, The isoconversional method for determination of energy of activation at constant heating rates, correction for the Doyle approximation, J.Therm Anal Calorim. 27 (1983) 95-102.

[52] H.M. Fathollahi, H. Behnejad, A comparative study of thermal behaviors and kinetics analysis of the pyrotechnic compositions containing Mg and Al, J Therm Anal Calorim. 120 (2015) 1483–1492.

[53] J. Chen, T. Guo, W. Ding, J. Song, M. Yao, F. Bei, S. Li, Effect of CuO on the thermal kinetics and combustion properties of Al/MoO_3 thermite prepared by ball milling, Ceram. Int. 47 () 6500–16510.

[54] J. Puszynski, Processing and characterization of aluminum-based nanothermites, J. Therm. Anal. Calorim. 96 (2009) 677-685.

[55] S.F. Son, B.W. Asay, T.J. Foley, R.A. Yetter, M.H. Wu, G.A. Risha, Combustion of nanoscale Al/MoO3 thermite in microchannels, J. Propuls. Power 23 (2007) 715-721.

[56] G. Jian, J. Feng, R.J. Jacob, G.C. Egan, M.R. Zachariah, Superreactive nanoenergetic gas generators based on periodate salts, Angew. Chem. Int. 52 (2013) 9743–9746.

8.8 Supporting Information

- **Microwave synthesis of EMOF-1:**

  - Microwave reactor Model: Anton Paar Monowave 400.
  - Vial type: Glass vial G30.
  - Vial volume: 30 ml.
  - Filled volume: 15 ml.
  - Temperature control: Ruby thermometer + IR sensor

Table S 1 Procedures for EMOF-1 Microwave synthesis

Step	Program	Temp. (°C)	Time hh:mm:ss	Power (W) [limit]	Cooling	Stirrer speed (rpm)
1	Heat as fast as possible	220	----	850	Off	600
2	Hold	----	00:20:00	850	Off	600
3	Cool down	55	----	----	On	600

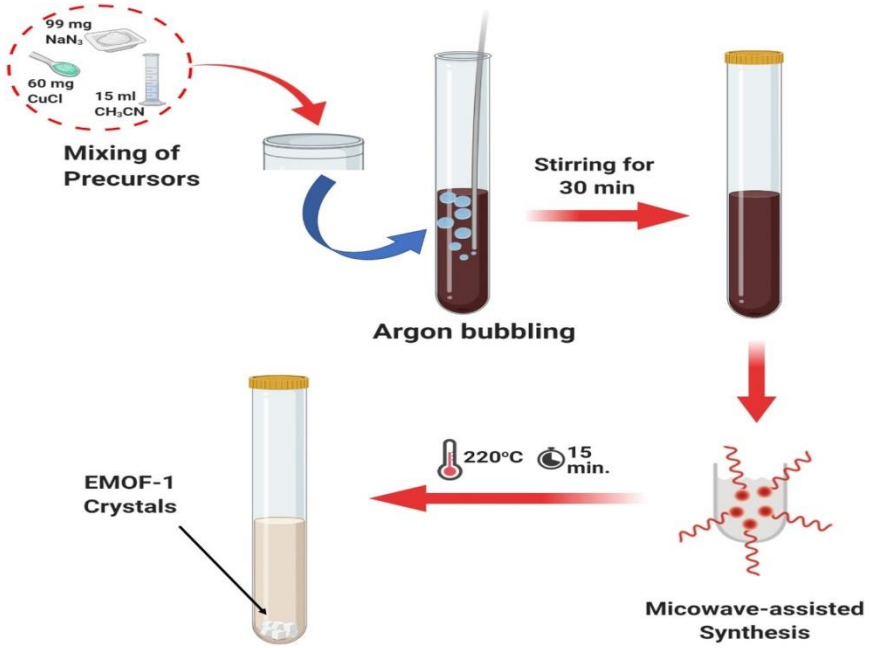

Figure S11 Synthesis scheme for EMOF-1 via the microwave-assisted technique

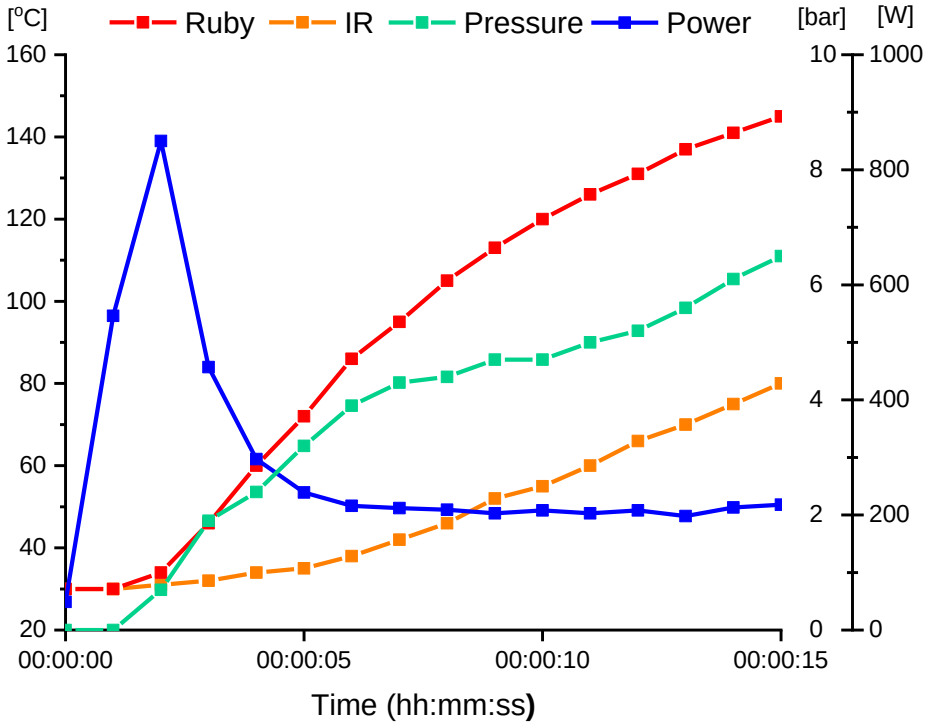

Figure S12 The initial pulse within the heating step of EMOF-1 preparation

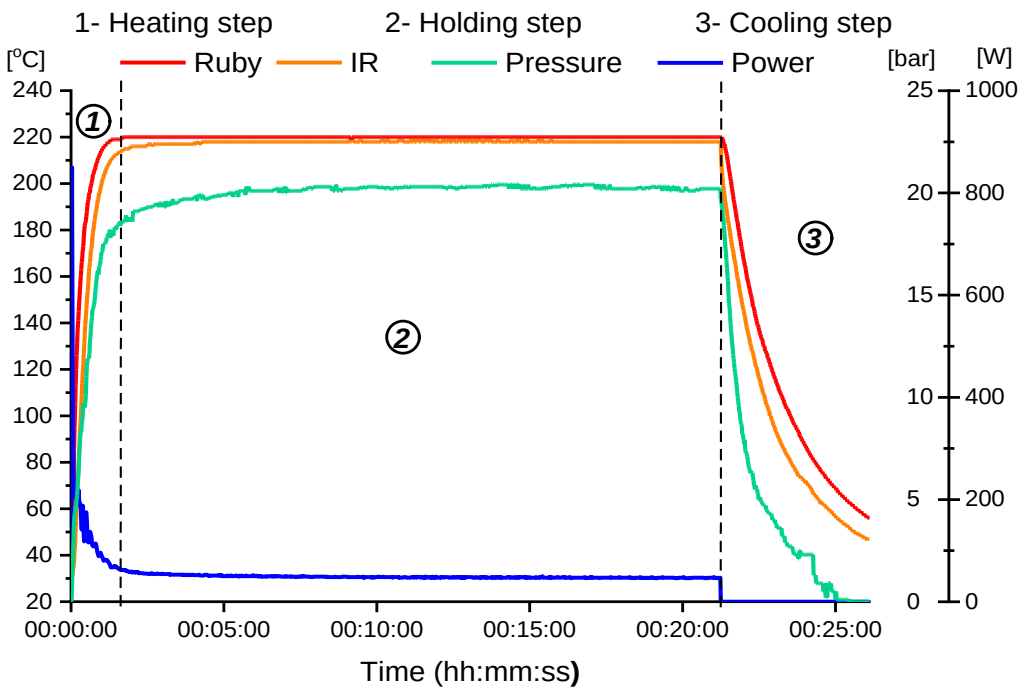

Figure S13 The whole microwave synthesis process for EMOF-1

- **<u>Laser ignition set up</u>**

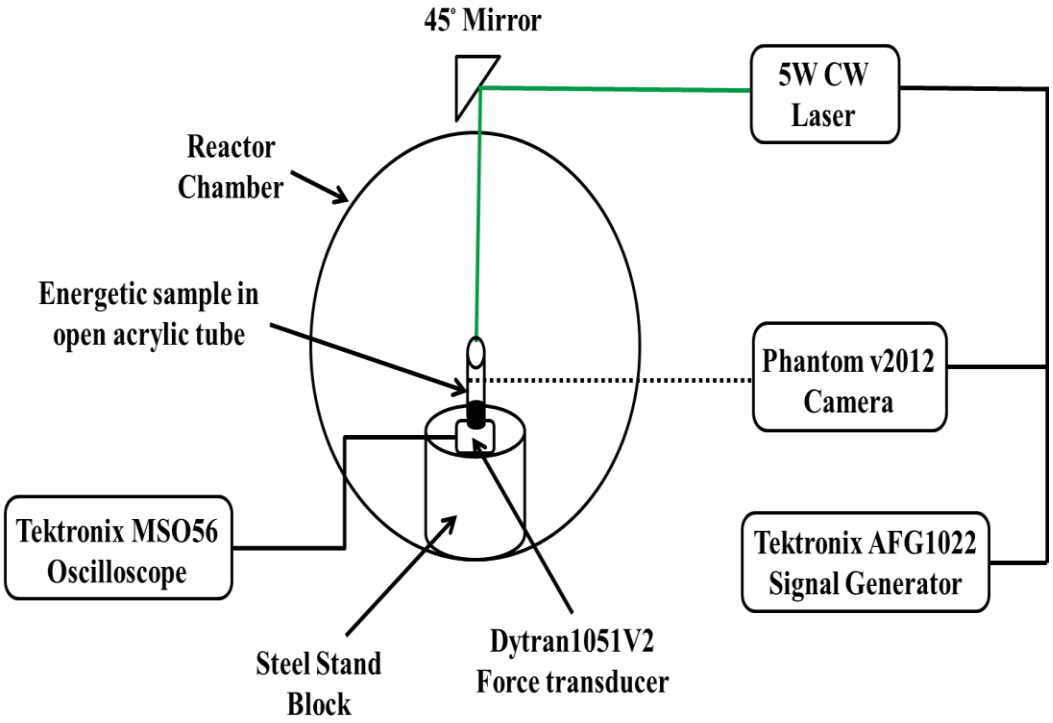

Figure S14 Block diagram of laser ignition and high-speed imaging set up

- **Powder XRD for the prepared and simulated samples**

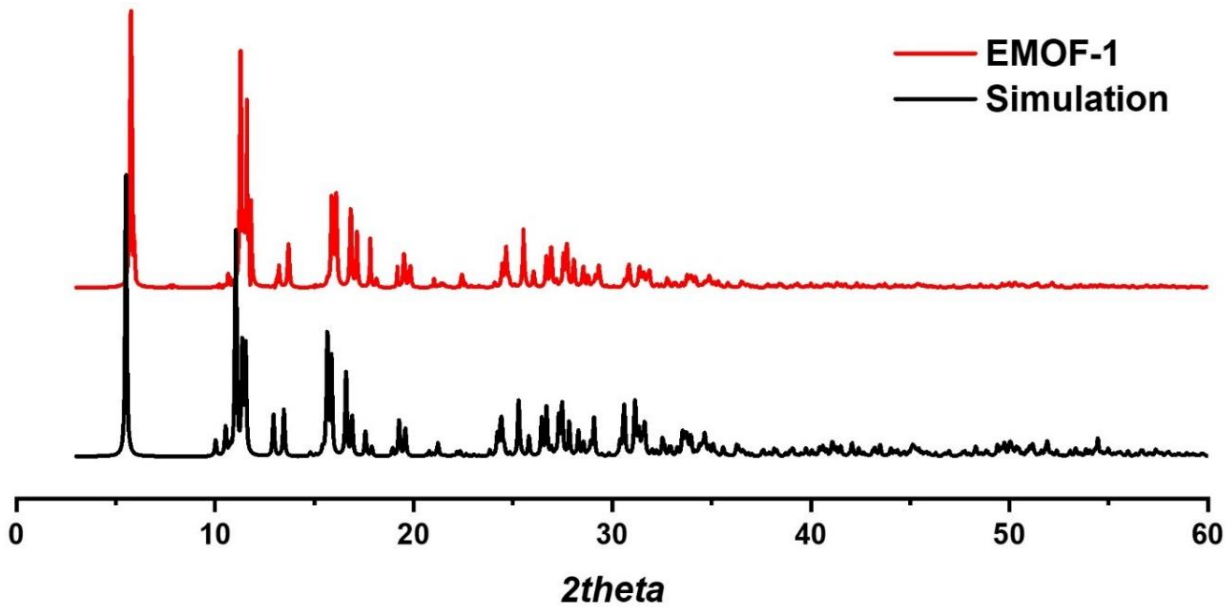

Figure S15 PXRD pattern for EMOF-1 compared to the simulated pattern

- **Heat of combustion using calorimetric bomb:**

Each test was performed five times and the average value of the heat of combustion was calculated. Sample mass for the first two tests was 0.1 g, then increased the sample mass to 0.3 g for the following two tests and the final test mass was 0.5. Energy of combustion was calculated according to the following equations (1) & (2).

$$Q = Q_{System} - Q_{Fuse\ wire} \quad (1)$$

$$Q_{System} = M * C_p * \Delta T \quad (2)$$

Where:

Q : Heat of combustion of each nanothermite sample (J).

S_{ystem} : Total heat of combustion (heat of combustion of the sample + heat of combustion of fuse wire) (J).

$Q_{Fuse\ wire}$: Heat of combustion of fuse wire (J), (calculated according to the used length in the test).

M : Mass of the test sample (g).

C_p : Specific heat capacity of water (J/g. °C).

ΔT : Temperature difference before and after ignition (°C).

Because determination of temperature difference is the most important parameter for calculation heat of combustion, so we need to minimize the errors caused by temperature drift before and after the ignition as much as we can to get accurate results. The temperature output for a representative bomb calorimetry experiment is shown in Figure S6.

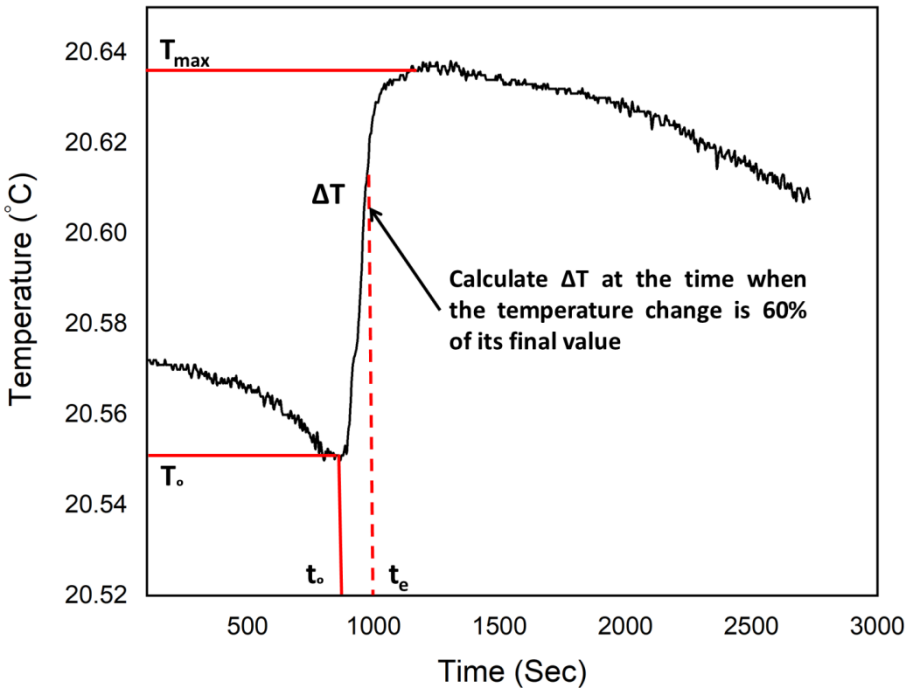

Figure S16 Temperature output of bomb calorimeter

In order to minimize the error in ΔT measurement, extrapolation procedures were performed on the lines before and after the complete reaction, while the first line is extrapolated forward, the other line is extrapolated backward. According to National

Institute of Standards and Technology (NIST), the accurate time to determine ΔT is the time which temperature corresponding to 60 % of its final value. Temperature difference calculated according to the following relation illustrated in equation 3.

$$\Delta T = (m_a t_e + b_a) - (m_b t_b + b_b) \quad (3)$$

Where t_e is the time at which temperature reaches 60 % of its final value, m_a and m_b represent the slope of the lines after and before ignition respectively and b_a, b_b are their corresponding intercepts. Average value of heat of combustion of all nanothermite compositions are tabulated in Table 4 in the main manuscript.

- **<u>Snapshots from high-speed camera</u>**

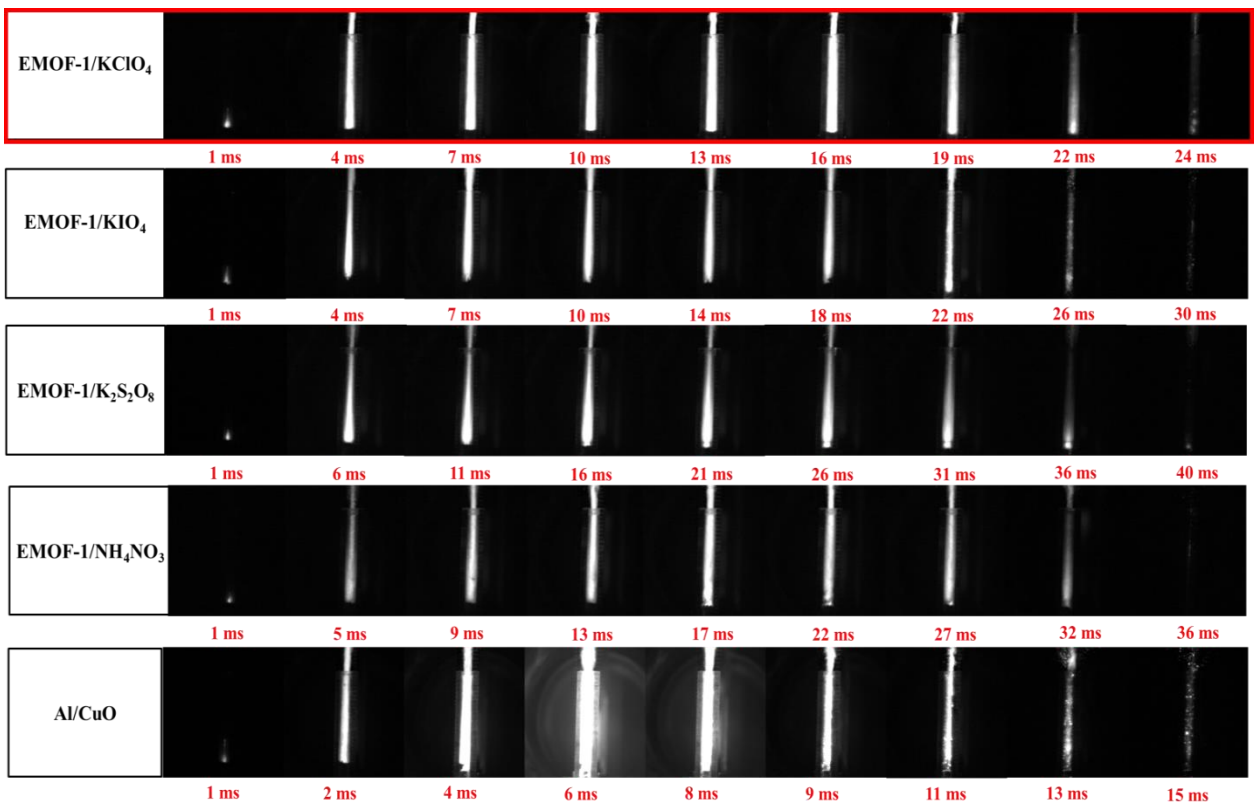

Figure 17 Snapshots for different EMOF-1 thermite samples

CHAPTER 9 GENERAL DISCUSSION

This work concerns the application of nanothermites as EMs in micro-energetic applications or additives in propulsion systems. As we mentioned earlier, reducing the particle sizes of thermite constituents improve their combustion performance considerably. Despite of their advantages over microthermites, nanothermites still suffer from particle agglomeration, excessive oxidation of nano-Al, which leads to incomplete combustion, high ignition temperature and low peak pressure. In addition, ignition and propagation process difficulties within small tubes and slots represent potential problems linked with nanothermites. These problems have been addressed in several previous studies that have proposed different ways to enhance the combustion properties of traditional nanothermites based n-Al and metallic oxides. In this PhD thesis, new promising nanothermite formulations for energetic applications are presented. These compositions are in contrast with more conventional nanothermites in which fuel and oxidizer are limited to Al and metal oxides. Instead, oxygenated salts were used as oxidizers due to their exothermic decomposition nature and high oxidizing power promoting the combustion processes. Besides, we added CNMs and particularly GO to get benefit from their large specific area and unique thermal, electrical and mechanical properties in enhancing the ignition and combustion properties of nanothermites. Furthermore, tunable combustion parameters developed by the controlled addition of NC to oxygenated salt based nanothermite mixtures, as it is useful in preventing sintering of n-Al, offering higher chemical reactivity and gas production. Finally, we proposed an EMOF-1 as good alternative energetic fuel for thermite mixtures with high combustion heat, suitable ignition temperature, and a large amount of gaseous products.

Ultrasonic mixing method was used to fabricate different samples of nanothermites based on either n-Al, oxygenated salts and CNMs or EMOF-1 and oxygenated oxidizers. In light of the findings of the review literature, this work was aimed at determining the effect of CNMs and equivalence ratios on the energetic performance of the new tertiary nanothermites. It should be noted that the tertiary mixtures showed significant new characteristics such as lower ignition temperature and higher heat of combustion enhancing the overall combustion characteristics, as a consequence of using oxygenated oxidizers instead of metallic ones, and also the features provided by the CNMS and special energetic nature of GO. The results confirmed that the ultrasonic mixing technique brings a good homogeneity to the prepared tertiary composites.

Nanothermite with 5% GO and equivalence ratio equals to 1.4 achieved the optimum combustion performance and this highlights the role of GO as an energetic reactant compared to other CNMs.

The comparative study conducted in the second part of this work showed the versatility of the prepared tertiary nanothermite mixtures. In fact, ultrasonication method proved to be a suitable technique to obtain new nanothermites with great reproducibility and ability to be scaled-up. In general, nanothermites based on oxidizing salts are more reactive than those with metallic oxides, as indicated in both theoretical and experimental data. Among them, the GO/Al/$KClO_4$ nanothermite exhibits the highest heat release (9614 J/g), while the GO/Al/$K_2S_2O_8$ nanothermite shows the lowest onset temperature and activation energy (380 $^{\circ}$C and 105 kJ/mol). In addition, solid phase reaction mechanism is the controlling mechanism for compositions based on oxidizing salts and the condensed phase reaction mechanism for those based on metallic ones. Reduction in the activation energy and shifting of reaction mechanism from condensed to solid phase in oxygenated salts based nanothermites, ascribed to the exothermic decomposition nature of GO and oxygenated salts, which could be a kind of pre-ignition enhancing mixing process and overall combustion properties.

One of the biggest challenges in the second part of the study was to examine the effect of CNMs on the laser ignition and thrust performance of various types of oxygenated salts/nanothermite mixtures inside tubes and slots. The limitations of measuring instruments, small size of the measured samples and tubes affect on the direct and easy measure of thrust and laser ignition characteristics of the prepared nanothermites. Hence, one of the objectives in the second part of the study was focused on optimization of the prerequisites of laser ignition and high-speed imaging characterization system such as the appropriate sample mass, length and diameter of the test tube, laser power and exposure time. In addition, we investigate the effect of chemical composition and packing density on the performance of the tertiary nanothermites inside small tubes with and without CD nozzle to simulate and predict the behaviour of microthruster. In short, thrust output, $I_{SP,}$ I_{SV} and normalized energy reveal notable improvement with the addition of CNMs. Results revealed two distinct reaction regimes (slow and fast) at low and high packing densities (20 and 55 % TMD). Total impulse and I_{SP} peaked 5% GO/Al/$KClO_4$ for both slow and fast reaction regimes and achieved improvements of over 95 % compared to the reference sample.

The third part of this work concerned the preparation of quaternary nanothermites by introducing various quantities of NC to the main tertiary nanothermite base using electrospining technique. The major difficulty found in this part was producing homogenous quaternary nanothermites because normal mixing method yields inappropriate homogeneity as we found in combustion performance tests. However, homogeneity problems were solved by changing the preparation method to electrospining, while significant efforts have been done to avoid safety hazards, adjusting operating parameters and producing composites with accepted homogeneity and consequently enhancing combustion properties. SEM-EDX results confirmed that the nanoparticles were homogeneously dispersed without agglomeration. The goal of this part of the work is to propose nanothermite mixtures with controllable combustion and tailored performance parameters for micro-propulsion and micro-energetic applications through assessment of thrust production and dynamic performance within a small tube attached to a nozzle with a throat of 2 mm. The nanothermite mixtures are packed at different densities and ignited using a 3.5 W continuous wave laser to observe combustion phenomena and thrust production. The exhaust plume of the mixtures is characterized using high-speed video and DSC determined the thermal behaviour and energy output. The addition of NC to the tertiary nanothermite base matrix resulted in a significant increase in total heat generated, owing to the inclusion of another stage (liquid-liquid phase) to the reaction, which aids in the completion of the combustion process. In comparison to conventional EMs, which do not perform well in millimeter-scale test motors, the generated quaternary nanothermites ignited successfully and self-propagated. At 5% NC and 50% TMD, I_{FT} and I_{SP} were 17.56 mN.s and 179.2 s, respectively. These are improvements of more than 50% over the non-NC samples (10.8 mN.s and 110.2 s). Fast and slow combustion regimes were observed for samples with low and high packing densities, respectively. Generally, tunable combustion parameters can be developed by the controlled addition of NC to oxygenated salt based nanothermite mixtures. Additional tuning in packing density and nozzle configuration can be performed to fit the required performance of certain energetic application specifically.

The fourth part of this work devoted to solve problems associated with n-Al using EMOF-1 as alternative fuel. We firstly synthesized EMOF-1 successfully using the microwave-assisted technique, which is more effective, faster, and gives a comparable yield to the traditional solvothermal method. From one side, SEM-EDX, FTIR, and XRD involved to ensure the

morphology and the structure of EMOF-1 and the developed composites. On the other side, TGA, DSC, bomb calorimetry and laser ignition system evaluated the combustion behavior of the achieved thermites. The apparent kinetic parameters were calculated using Kissinger and Ozawa approaches. The results revealed that the resulting new thermite mixtures exhibit superior combustion characteristics of two to three-folds the average heat of combustion compared to aluminum-based ones, at almost half the ignition temperature. EMOF-1/KIO_4 thermite composite has the best performance concerning heat released and ignition temperature and recorded 5.1 kJ/g and 314 $^{\circ}$C individually. In addition, EMOF-1 based thermites revealed stable propulsive force, longer combustion time and luminous flame compared to those traditional Al based ones. In general, tailored combustion performance and green combustion products can be developed via EMOF-1 as fuel and opens the route for more application of EMOFs in the future.

CHAPTER 10 CONCLUSIONS AND RECOMMENDATIONS

10.1 Conclusions

This research focused on the preparation and characterization of new nanothermites for their potential integration into propulsion systems such as microthrusters, gas generators, igniters and modified propellants. To do so, oxygenated salts were employed as alternative oxides to metallic ones with n-Al to form the base of nanothermite. Effects of CNMs and NC as energetic additives and polymer respectively on improving the combustion characteristics of nanothermites were evaluated. Finally, energetic MOFs were used as a nanothermite fuel instead of Al to overcome the problems associated with Al ignition, benefiting from energetic and large gas generation of MOFs in introducing new composite material for gas generation applications.

The first part of this work evaluated the effect of CNMs on the thermal behaviour and combustion properties of nanothermites based on n-Al and different types of oxygenated salts. The following conclusions can be drawn from the results:

1. Several CNMs integrated successfully in nanothermite compositions using a simple sonication process.
2. Onset reaction temperature of all prepared nanothermites shifted to a lower temperature compared to their reference formulations.
3. Controllable combustion performance and tailored energy release was achieved by the controlled addition of CNMs (type and amount) to oxygenated salt based nanothermite mixtures.
4. Ignition properties of ternary nanothermites based on oxygenated salts improved significantly due to increasing the reactivity, decreasing ignition temperature and activation energy compared to those mixtures based on metallic oxides
5. Nanothermite based on GO/Al/$KClO_4$ exhibits the highest heat release, while the GO/Al/$K_2S_2O_8$ nanothermite shows the lowest onset temperature and activation energy.

6. The CNMs, especially GO, were shown to be capable of improving sample combustion performance. Compared to the reference sample without GO, significant improvements in I_{FT}, I_{SP}, I_{SV}, and reduction in ignition delay were observed with the addition of GO.
7. The optimum addition value of GO is 5% with equivalence ratio 1.4.
8. Solid phase combustion mechanism is the controlling mechanism in the combustion reaction of ternary nanothermites based on oxygenated oxidizers and the condensed phase reaction mechanism for those based on metallic ones.
9. Oxygen release from oxidizers, in addition to the rate of Al diffusion outward from the alumina shell are the rate determining steps of the reaction.

The second phase of this research focused on the incorporation of NC as energetic binder in the ternary nanothermites. For this purpose, a facile electrospining technique was employed. The following findings are the main conclusions from this phase of the research:

1. Electrospinning introduced as a facile way to prepare quaternary nanothermite composites with well-mixed components.
2. Tunable combustion parameters developed by the controlled addition of NC to oxygenated salt based ternary nanothermite mixtures.
3. The prepared nanothermites ignited and self-propagated inside millimeter-scale STMs, which is contrary to classical EMs that has problems with ignition under the same conditions.
4. Increasing addition of NC more than 5% to the base ternary GO/Al/$KClO_4$ nanothermite reduced the peak thrust forces and increased both ignition delay and burn duration.
5. Significant improvements in the thrust output, I_{FT}, I_{SP}, and I_{SV} achieved with the addition of up to 5 % NC; further addition of NC however reduced the performance.
6. Two different reaction regimes (fast and slow) for high- and low-density samples were recognized.
7. The introduction of a nozzle to the STMs resulted in reduced peak forces and increased burn times for all 20%TMD samples while all 50%TMD samples produced converse

results. Other effects include improved impulses for the 20%TMD samples and marginally reduced impulses for the 50%TMD samples, with 5% NC being the best performing composition across all sample densities.

8. The fast reaction nature of low-density sample combustion is believed to introduce shock-based losses into the nozzle flow which, in combination with observed two-phase losses.

The third part of this research focused on introducing new energetic thermites with low ignition temperatures, stable propulsive force, and high reactivity using energetic MOF as alternative fuel of Al in a combination with different types of oxygenated salts. The following conclusions can be drawn from the results.

1. Microwave-assisted technique was presented as a more effective, faster, and gives a comparable yield to the solvothermal method in preparing EMOF-1.
2. Thermites based on EMOF-1 exhibited higher heat of combustion, lower ignition temperature, and reduced activation energy than those conventional thermites based on Al.
3. EMOF-1/KIO_4 composite has the best performance concerning heat released, while EMOF-1/NH_4NO_3 recorded the lowest ignition temperature.
4. EMOF-1 based thermites ignited easily inside small tubes, revealed stable propulsive force, longer combustion time, higher pressure and pressurization rate compared to those traditional Al based ones.

In short, this research provides benchmark information for optimizing the tertiary nanothermites design, use, storage and handling. In addition, it helps in creating a selection guide for the users to choose the appropriate composition fitting the targeted application. The map of energy output, combustion time, combustion properties, safety and application for different prepared samples is summarized in Figure 10-1.

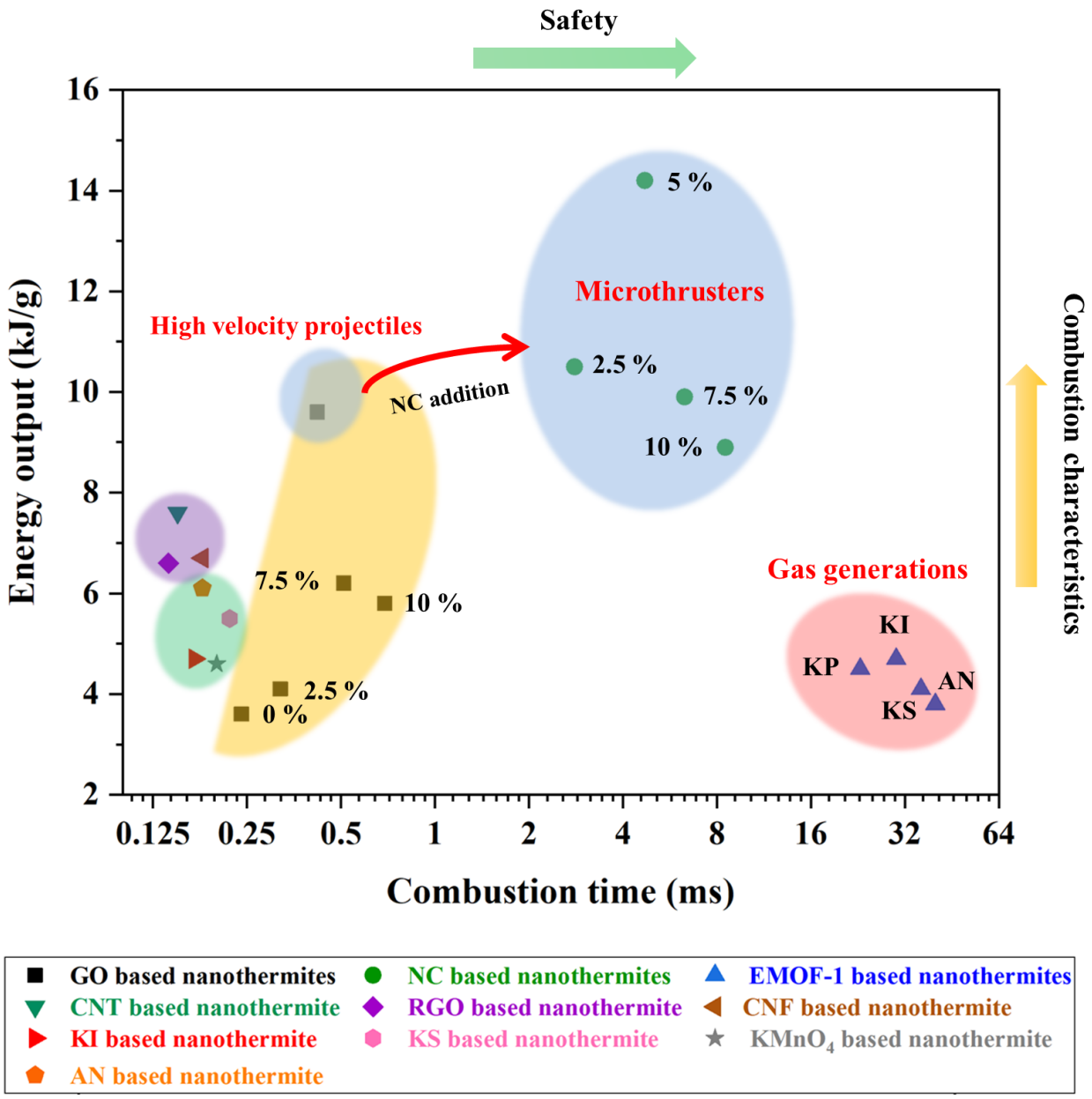

Figure 10-1 Map of combustion properties and applications of different thermite mixtures

10.2 Recommendations

This research provides insights about the development of new nanothermites mixtures with controllable and tailored combustion characteristics. However, there are some aspects that have not been explored in this research and are recommended in future studies:

1. In the first phase of this research, only Al as a fuel was utilized. Effect of CNMs on the combustion properties of ternary thermite composites based on another fuel like boron needs investigations and optimization. Moreover, combination between Al and boron can also be employed.
2. It would be greatly helpful to use other synthesis methods to try increasing the intimacy mixing between fuel and oxidizer.
3. Additional tuning in packing density and nozzle configuration can be performed to fit the required performance of certain energetic application specifically.
4. Integrate and evaluate the full performance of the prepared nanothermites in a full set of thrusters.
5. Investigation of the mechanism of reaction of EMOF-1 based thermites.
6. Assess the potential application of EMOF-1 based thermites as a gas generator by performing more tests such as inflation of the air bag by igniting the sample using a tungsten wire and trace the expansion of the airbag by the gaseous products of the combustion reactions of the composites.
7. Evaluate the effect of incorporation of nanothermite in propellant compositions on the burning rate behaviour.

BIBLIOGRAPHY

[1] S.J. Widdis, K. Asante, D.L. Hitt, M.W. Cross, W.J. Varhue, M.R. McDevitt, A MEMS-Based Catalytic Microreactor for a H2O2 Monopropellant Micropropulsion System, IEEE ASME Trans Mechatron. 18 (2013) 1250-1258.

[2] Q. Zou, B.L., C. Zheng, Z. Hao, C. Zhai, T. Liu, J. Liang, F. Yan, W. Yang, C. Zhu, Novel integrated techniques of drilling–slotting–separation-sealing for enhanced coal bed methane recovery in underground coal mines, J. Nat. Gas Sci. Eng. 18 (2015) 960–973.

[3] X. Zhou, M. Torabi, J. Lu, R. Shen, K. Zhang, Nanostructured Energetic Composites: Synthesis, Ignition/Combustion Modeling, and Applications, ACS Appl. Mater. Interfaces 6 (2014) 3058–3074.

[4] V.A. Arkhipov, A.G. Korotkikh, The influence of aluminum powder dispersity on composite solid propellants ignitability by laser radiation, Combust. Flame 159 (2012) 409-415.

[5] J. Dai, F. Wang, C. Ru, J. Xu, C. Wang, W. Zhang, Y. Ye, R. Shen, Ammonium Perchlorate as an Effective Additive for Enhancing the Combustion and Propulsion Performance of Al/CuO Nanothermites, J. Phys. Chem. C 122 (2018) 10240−10247.

[6] Y. Gan , L.Qiao, Combustion characteristics of fuel droplets with addition of nano and micron-sized aluminum particles, Combust. Flame 158 (2011) 354–368.

[7] L. Zhou, N. Piekiel, S. Chowdhury, M.R. Zachariah, Time-resolved mass spectrometry of the exothermic reaction between nanoaluminum and metal oxides: the role of oxygen release, J Phys Chem. 114 (2010) 14269–14275.

[8] M.A. Trunov , M. Schoenitz, X. Zhu , E.L. Dreizin, Effect of polymorphic phase transformations in Al_2O_3 film on oxidation kinetics of aluminum powders. Combust. Flame 140 (2005) 310–318.

[9] E.L. Dreizin, Metal-based reactive nanomaterials, Prog. Energy Combust. Sci. 35 (2009) 141-167.

[10] M.L. Pantoya, J.J. Granier, Combustion behavior of highly energetic thermites: Nano versus micron composites, Propellants Explos. Pyrotech. 30 (2005) 53-62.

[11] G. Jian, J. Feng, R.J. Jacob, G.C. Egan, M.R. Zachariah, Super-reactive nanoenergetic gas generators based on periodate salts. Angewandte Chemie. 52 (2013) 9925-9928.

[12] K.S. Wu, S. Chowdhury, G. Jian, L. Zhou, M.R. Zachariah, Encapsulation of perchlorate salts within metal oxides for application as nanoenergetic oxidizers, Adv. Funct. Mater. 22 (2012) 78-85.

[13] C.S. Jian, K. Sullivan, Nanothermite reactions: Is gas phase oxygen generation from the oxygen carrier an essential prerequisite to ignition? Combust. Flame 160 (2013) 432-437.

[14] K.S. Kappagantula, C. Farley, M.L. Pantoya, J. Horn, Tuning energetic material reactivity using surface functionalization of aluminum fuels, J. Phys. Chem. C. 116 (2012) 24469–24475.

[15] J.J. Brege, C.E. Hamilton, C.A. Crouse, A.R. Barron, Ultrasmall copper nanoparticles from a hydrophobically immobilized surfactant template. Nano letters 9 (2009) 2239-2242.

[16] H.H. DiBiaso, B.A. English, M.G. Allen, Solid-phase conductive fuels for chemical microactuators, Sens. Actuators, A 111 (2004) 260-266.

[17] W. Zhang, H. Peng, X. Gao, J. Ye, Z.Z.Y. Chao, An in situ chemical reaction approach to synthesize zinc picrate energetic thin film upon zinc oxide nanowires array, Surf. Interface Anal. 44 (2012) 1203–1208.

[18] S.B. Kim, K.J. Kim, M.H. Cho, J.H. Kim, K.T. Ki, S.H. Kim, Micro-and nanoscale energetic materials as effective heat energy sources for enhanced gas generators, ACS Appl. Mater. Interfaces 8 (2016) 9405–9412.

[19] V. Baev, C. Lvov, I. Shugalei, Influence of the Environment Internal Factors on Warm-blooded Organisms, in Proc. Conf. Problems of Military and Emergency Medicine. 1998.

[20] M.B. Talawar, R.Sivabalan, T.Mukundan, H.Muthurajan, A.K.Sikder, B.R.Gandhe, A.S. Rao, Environmentally compatible next generation green energetic materials (GEMs), J. Hazard. Mater. 161 (2009) 589-607.

[21] S.H. Kim, M.R. Zachariah, Enhancing the rate of energy release from nanoenergetic materials by electrostatically enhanced assembly, Adv. Mater. 16 (2004) 1821-1825.

[22] M.L. Pantoya, J.J. Granier, Combustion behavior of highly energetic thermites: Nano versus micron composites, Propellants Explos. Pyrotech. 30 (2005) 53-62.

[23] C.S. Jian, K. Sullivan, Nanothermite reactions: Is gas phase oxygen generation from the oxygen carrier an essential prerequisite to ignition? Combust. Flame 160 (2013) 432-437.

[24] K.S. Wu, S. Chowdhury, G. Jian, L. Zhou, M.R. Zachariah, Encapsulation of perchlorate salts within metal oxides for application as nanoenergetic oxidizers, Adv. Funct. Mater. 22 (2012) 78-85.

[25] K.S. Kappagantula, C. Farley, M.L. Pantoya, J. Horn, Tuning energetic material reactivity using surface functionalization of aluminum fuels, J. Phys. Chem. C. 116 (2012) 24469–24475.

[26] S.F. Son, B.W. Asay, T.J. Foley, R.A. Yetter, M.H. Wu, G.A. Risha, Combustion of nanoscale Al/MoO_3 thermite in microchannels, J. Propuls. Power 23 (2007) 715-721.

[27] G. Jian, J. Feng, R.J. Jacob, G.C. Egan, M.R. Zachariah, Superreactive nanoenergetic gas generators based on periodate salts, Angew. Chem. Int. 52 (2013) 9743–9746.

[28] W. Zhou, J.B. Delisio, X. Li, L. Liu, M.R. Zachariah, Persulfate salt as an oxidizer for biocidal energetic nano-thermites, J. Mater. Chem. 3 (2015) 11838–11846.

[29] W. Zhou, J.B. Delisio, X. Wang, M.R. Zachariah, Reaction mechanisms of potassium oxysalts based energetic composites, Combust. Flame 177 (2017) 1–9.

[30] X. Hu, J.B. Delisio, X. Li, W. Zhou, M.R. Zachariah, Direct deposit of highly reactive $Bi(IO_3)_3$– polyvinylidene fluoride biocidal energetic composite and its reactive properties, Adv.Eng. Mater. 19 (2017) 1-9.

[31] K.T. Sullivan, N.W. Piekiel, S. Chowdhury, C. Wu, M.R. Zachariah, C.E. Johnson, Ignition and combustion characteristics of nanoscale Al/$AgIO_3$: a potential energetic biocidal system, Combust. Sci. Technol. 183 (2010) 285-302.

[32] M. Comet, C. Martin, F. Schnell, D. Spitzer, Nanothermites: a short review. Factsheet for experimenters, present and future challenges, Propellants Explos. Pyrotech. 44 (2019) 18-36.

[33] G. Jian, J. Feng, R.J. Jacob, G.C Egan, M.R. Zachariah, Super-reactive nanoenergetic gas generators based on periodate salts, Angew. Chem. Int. 52 (2013) 9743-9746.

[34] Y.R. Luo, Comprehensive handbook of chemical bond energies. Boca Raton, Florida: 25 CRC Press, 2007.

[35] N.B. Stand, B.D. Darwent, Bond dissociation energies in simple molecules, Nat. Stand. Ref. Data Ser.,U.S.A, 1970, pp. 1-60.

[36] K-C. Huang, R.A. Couttenye, G.E. Hoag, Kinetics of heat-assisted persulfate oxidation of methyl tert-butyl ether (MTBE), Chemosphere, 49 (2002) 413-420.

[37] A. Tsitonaki, P. Petri, M. Crimi, H. MosbÆk, R.L. Siegrist, P.L. Bjerg, In Situ Chemical Oxidation of Contaminated Soil and Groundwater Using Persulfate: A Review, Environ. Sci. Technol. 40 (2010) 55-91.

[38] Qi-L. Yan, M. Gozin, F-Qi. Zhao, A. Cohena, Si-P. Pang, Highly energetic compositions based on functionalized carbon nanomaterials, Nanoscale 8 (2016) 4799–4851.

[39] A.C. Ferrari, V. Fal'ko, et al., Science and technology roadmap for graphene, related two-dimensional crystals, and hybrid systems, Nanoscale 7 (2015) 4598–4810.

[40] Ji Dai, J. Xu, F. Wang, Y. Tai, Y. Shen, R. Shen, Y. Ye, Facile formation of nitrocellulose-coated Al/Bi_2O_3 nanothermites with excellent energy output and improved electrostatic discharge safety, Mater. Des. 143 (2018) 93–103.

[41] R. Li, H. Xu, H. Hu, G. Yang, J. Wang, J. Shen, Microstructured Al/Fe_2O_3/nitrocellulose energetic fibers realized by electrospinning, J. Energ. Mater. 32 (2014) 50–59.

[42] Q. Zhang, J.M. Shreeve, Metal–organic frameworks as high explosives: a new concept for energetic materials, Angew. Chem. Int. Ed. 53 (2014) 2540-2542.

[43] S. Zhang, Q. Yang, X. Liu, X. Qu, Q. Wei, G. Xie, S. Chen, S.Gao, High-energy metal–organic frameworks (HE-MOFs): Synthesis, structure and energetic performance, Coord. Chem. Rev. 307 (2016) 292-312.

[44] C. Wang, D. Liu, W. Lin, Metal–organic frameworks as a tunable platform for designing functional molecular materials, J. Am. Chem. Soc. 135 (2013) 13222-13234.

[45] J. Zhang, J.M. Shreeve, 3D Nitrogen-rich metal–organic frameworks: opportunities for safer energetics, Dalton Trans. 45 (2016) 2363-2368.

[46] C. Rossi, Applications of Al Nanoparticles: Nanothermites, in Al-Based Energetic Nanomaterials :Design, Manufacturing, Properties and Applications, John Wiley & Sons, Inc: 111 River Street, Hoboken, NJ 07030, USA, (2015) 33-35.

[47] L. LeSergent, Tailoring the Ignition and Reaction Properties of Cu_2O Thermite Nanolaminates, in Mechanical Engineering- Nanotechnology, Waterloo: Waterloo, Ontario, Canada. (2018) 1-97.

[48] M. Comet, V. Pichot, B. Siegert, F. Schnell, F.Ciszek, D. Spitzer, Phosphorus-based nanothermites: A new generation of energetic materials. J. Phys. Chem. Solids 71 (2010) 64–68.

[49] D.A. Reese, D.M. Wright, S.F. Son , CuO/Al thermites for solid rocket motor ignition, J.Propul. Power 29 (2013) 1194-1199.

[50] D. Spitzer, M. Comet, C. Baras, V. Pichot, N. Piazzon, Energetic nano-materials: Opportunities for enhanced performances. J. Phys. Chem. Solids 71 (2010) 100–108.

[51] W.A. Trzciński, L. Maiz, Thermobaric and enhanced blast explosives properties and testing methods. Propellants Explos. Pyrotech. 40 (2015) 632-634.

[52] R.A. Yetter, G.A. Risha, S.F. Son, particle combustion and nanotechnology. Proc. Combust.Inst. 32 (2009) 1819-1838.

[53] S.H. FischerMark, M.C. Grubelich, A survey of combustible metals,thermites, and intermetallics for pyrotechnic applications, 32nd AIAA/ASME/SAE/ASEE Joint Propulsion Conference, Lake Buena Vista, FL,1996.

[54] N.H Yen, L.Y. Wang, Reactive metals in explosives. Propellants Explos Pyrotech. 37 (2012) 143–155.

[55] E. Lafontaine, M. Comet, Nanothermites, John Wiley & Sons, Inc., USA, 2016.

[56] K.T. Sullivan, G. Young, M.R. Zachariah, Enhanced reactivity of nano-B/Al/CuO MIC's, Combust. Flame 156 (2009) 302–309.

[57] K.S. Martirosyan, L. Wang, A. Vicent, D. Luss, Nanoenergetic Gas-Generators: Design and Performance. Propell. Explos. Pyrot. 34 (2009) 532-538.

[58] G.Young, K. Sullivan, M.R. Zachariah, K. Yu, Combustion characteristics of boron nanoparticles. Combust. Flame 156 (2009) 322-333.

[59] J.A. Conkling, C.J. Mocella, Chemistry of Pyrotechnics: Basic principles and theory, Taylor & Francis Group, Boca Raton, U.K., 2019.

[60] X. Zhou, D. Xu, Q. Zhang, J. Lu, K. Zhang, Facile green in situ synthesis of Mg/CuO core/shell nanoenergetic arrays with a superior heat-release property and long-term storage stability, ACS Appl. Mater. Interfaces 5 (2013) 7641–7646.

[61] G. Singla, K. Singh, O.P. Pandey, Structural and thermal properties of in-situ reduced WO_3 to W powder. Powder Technol. 237 (2013) 9-13.

[62] M.B. Karkevandi, R.E. Kahrizsangi, B.N. Tabrizi, Formation and stability of tungsten boride nanocomposites in WO_3–B_2O_3–Mg ternary system: Mechanochemical effects. Int J Refract Hard Met. 46 (2014) 117-124.

[63] Y. Millet, Corrosion resistance of titanium Corrosion of titanium and its alloys. Techniques de l'Ingénieur (2012) 1–15.

[64] P. Billik, G. Plescha, V. Brezová, L'.Kuchta, M.Valko, M.Mazú, Anatase TiO2 nanocrystals prepared by mechanochemical synthesis and their photochemical activity studied by EPR spectroscopy, J. Phys. Chem. Solids 68 (2007) 1112–1116.

[65] Y. Bertrand, R. Grebert, Fuse powder composition, US Patent 2468061 (1949).

[66] M. Comet, V. Pichot, B. Siegert, F. Schnell, F.Ciszek, D. Spitzer, Phosphorus-based nanothermites: A new generation of energetic materials. J. Phys. Chem. Solids 71 (2010) 64–68.

[67] N. Devis, Red phosphorus for use in screening smoke compositions, Pentagon Reports (1999).

[68] M. Comet, B. Sigert, F. Schnell, V. Pichot, F. Ciszek and D. Spitzer, Phosphorus-Based Nanothermites: A New Generation of Pyrotechnics Illustrated by the Example of n-CuO/Red P Mixtures, Propellants Explos. Pyrotech. 35 (2010) 220-225.

[69] M.X. Zhou, J. Lu, R. Shen, K. Zhang, Nanostructured energetic composites: synthesis, ignition/combustion modeling, and applications, ACS Appl. Mater. Interfaces 6 (2014) 3058–3074.

[70] H. Laucht, D. Kovalev, D. Clement, H. Bartuch, K. Ziegahn, Silicon initiator, from the idea to functional tests, in 7th International Symposium & Exhibition on Sophisticated Car Occupant Safety Systems, Karlsruhe, Germany (2004).

[71] C.R. Becker, S. Apperson, C.J. Morris, S. Gangopadhyay, L.J. Currano, W.A. Churaman, C.R. Stoldt, Galvanic porous silicon composites for high-velocity nanoenergetics, Nano. Lett. 11 (2011) 803–807.

[72] V.S. Parimi, S. Huang, X. Zheng, Enhancing ignition and combustion of micron-sized aluminum by adding porous silicon. Proc. Combust. Inst. 36 (2017) 2317–2324.

[73] H. Singh, S. Banerjee, Nanostructured Energetic Composites: An Emerging Paradigm, in Nano-Energetic Materials, S. Bhattacharya, A.K. Agarwal, T. Rajagopalan, Vinay K. Patel, Springer Nature Singapore Pte Ltd. (2019) 37-81.

[74] K.Park, A. Rai, D. Mukherjee, M.R. Zachariah, Size-resolved kinetic measurements of aluminium nanoparticle oxidation with single particle mass spectrometry. J Phys Chem. 109 (2005) 7290–7299.

[75] D.R. Pesiri, C. Aumann, L. Bilger, K.C. Walter, Industrial Scale Nano-Aluminum Powder Manufacturing, J. Pyro. 19 (2004) 19-31.

[76] C. E. Aumann, G. L. Skofronick, J. A. Martin, Oxidation behavior of aluminum nanopowders, J. Vac. Sci. Technol. 13(1995) 1178-1183.

[77] Y-S. Kwona, A.A. Gromov, J.I. Strokova, Passivation of the surface of aluminum nanopowders by protective coatings of the different chemical origin. Appl. Surf. Sci. 253 (2007) 5558-5564.

[78] A. Gromov, U.F. Barth, U. Teipel, Aluminium nanopowders produced by electrical explosion of wires and passived by non-inert coatings: Characterisation and reactivity with air and water, Power Technol. 64 (2006) 111-115.

[79] J.A. Puszynski, C.J. Bulian, J.J. Swiatkiewicz, Processing and Ignition Characteristics of Aluminum-Bismuth Trioxide Nanothermite System, J. Propul. Power 23 (2007) 698-706.

[80] D.S. Sundaram, V.Yang, V.E. Zarko, Combustion of Nano Aluminum Particles (Review). Combustion, Explosion, and Shock Waves 51 (2015) 173-196.

[81] V.I. Levitas , B.W. Asay , S.F. Son , M. Pantoya, Melt dispersion mechanism for fast reaction of nanothermites. Appl. Phys. Lett. 89 (2006) 1-4.

[82] V.M Boiko, S.V. Poplavski, Self-ignition and ignition of aluminum powders in shock waves. Shock Waves 11 (2002) 289-295.

[83] K.P. Brooks, M.W. Beckstead, Dynamics of aluminum combustion. J. Propuls. Power 11 (1995) 769-780.

[84] V.I. Rozenband, N.I. Vaganova, A strength model of heterogeneous ignition of metal particles, Combust. Flame 88 (1992) 113-118.

[85] A.V. Fedorov, Y.V. Kharlamova, Ignition of an aluminum particle. Combust Explos Shock Waves 39 (2003) 544-547.

[86] C. Wagner, Beitrag zur Theorie des Anlaufvorgangs, Z. Phys. Chem. B-Chem. E. B21 (1933) 25–41.

[87] N.F Mott, Oxidation of metals and the formation of protective films, Nature 145 (1940) 996-1000.

[88] N.F. Mott, The theory of the formation of protective oxide films on metals.-III, Trans. Faraday Soc. 43 (1947) 429-434.

[89] N. Cabrera, J. Terrien, J. Hamon, Sur l'oxydation de l'aluminium en atmosphère sèche, C. R. Acad. Sci. 224 (1947) 1558-1560.

[90] B.J. Henz, T. Hawa, M.R. Zahariah, On the role of built-in electric fields on the ignition of oxide coated nanoaluminum: Ion mobility versus Fickian diffusion, J. Appl. Phys. 107 (2010) 1-10.

[91] A. Rai , K. Park , L. Zhou, M.R. Zachariah, Understanding the mechanism of aluminium nanoparticle oxidation. Combust. Theory Model. 10 (2010) 843–859.

[92] G. Li, L. Niu, W. Hao, Y. Liu, C. Zhang, Atomistic insight into the microexplosion-accelerated oxidation process of molten aluminum nanoparticles, Combust. Flame 214 (2020) 238-250.

[93] S. Wang, Y. Yang, H. Yu, D.D. Dlott, Dynamical effects of the oxide layer in aluminum nanoenergetic materials. Propell. Explos. Pyrot. 30 (2005) 148-155.

[94] V.I. Levitas, B.W. Asay, S. Son, Mechanochemical mechanism for fast reaction of metastable intermolecular composites based on dispersion of liquid metal, J. Appl. Phys. 101 (2007) 1-20.

[95] V.I. Levitas, Burn time of aluminum nanoparticles: strong effect of the heating rate and melt-dispersion mechanism. Combust. Flame 156 (2009) 543-546.

[96] T. Campbell, R.K. Kalia, A. Nakano, P. Vashishta, S. Ogata, S. Rodgers, Dynamics of oxidation of aluminum nanoclusters using variable charge–molecular-dynamics simulations on parallel computers, Phys. Rev. Lett. 82 (1999) 4866–4869.

[97] T. Bazyn, H. Krier, N. Glumac, Combustion of nanoaluminum at elevated pressure and temperature behind reflected shock waves. Combust. Flame 145 (2006) 703-713.

[98] D. Prentice, M.L. Pantoya, A.E. Gash, Combustion Wave Speeds of Sol−Gel-Synthesized Tungsten Trioxide and Nano-Aluminum: The Effect of Impurities on Flame Propagation, Energy & Fuels 20 (2006) 2370-2376.

[99] B.C. Tappan, M.R. Dirmyer, G.A. Risha, Evidence of a kinetic isotope effect in nanoaluminum and water combustion. Angew. Chem. Int. Ed. 53 (2014) 9218-9221.

[100] S. H. Fischer, M. C. Grubelich, A survey of combustible metals, thermites, and intermetallics for pyrotechnic applications, in 32nd AIAA/ASME/SAE/ASEE Joint Propulsion Conference, Lake Buena Vista, FL, USA, (1996).

[101] M.R.Weismiller, J.Y. Malchi, J.G. Lee, R.A. Yetter, T.J. Foley, Effects of fuel and oxidizer particle dimensions on the propagation of aluminum containing thermites, Proc. Combust. Inst. 33 (2011) 1989–1996.

[102] J.A. Puszynski, C.J. Bulian, J.J. Swiatkiewicz, Processing and Ignition Characteristics of Aluminum-Bismuth Trioxide Nanothermite System. J. Propuls. Power 23 (2012) 698-708.

[103] J.A. Puszynski, C.J. Bulian, J.J. Swiatkiewicz, The Effect of Nanopowder Attributes on Reaction Mechanism and Ignition Sensitivity of Nanothermites, MRS Online Proceedings Library 896, 401 (2005).

[104] J.A. Puszynski, C.J. Bulian, J.J. Swiatkiewicz, The Effect of Nanopowder Attributes on Reaction Mechanism and Ignition Sensitivity of Nanothermites, MRS Online Proceedings Library 896, 401 (2005).

[105] V.E. Sanders, B.W. Asay, T.J. Foley, B.C. Tappan, A.N. Pacheco, S.F. Son, Reaction Propagation of Four Nanoscale Energetic Composites (Al/MoO_3, Al/WO_3, Al/CuO, and Bi_2O_3), J. Propul. Power 23 (2007) 707-714.

[106] A. Trebs, T.J. Foley, Semi-empirical model for reaction progress in nanothermite, J. Propul.Power 26 (2010) 772-775.

[107] H. Goldschmidt, Method of producing metals and alloys, 578868 A, US, (1897).

[108] H. Fuzellier, M. Comet, Étude synoptique des explosifs, Actual. Chimique 233 (2000) 4-11.

[109] B.W. Armstrong, B. Baschung, D.W. Booth, M. Samirant, Enhanced propellant combustion with nanoparticles, Nano Lett. 3 (2003) 253-255.

[110] A. Prakash, A.V. McCormick, M.R. Zachariah, Synthesis and Reactivity of a Super-Reactive Metastable Intermolecular Composite Formulation of Al/$KMnO_4$, Adv. Mater. 17 (2005) 900-903.

[111] A. Prakash, A.V. McCormick, M.R. Zachariah, Tuning the Reactivity of Energetic Nanoparticles by Creation of a Core-Shell Nanostructure, Nano Lett. 5 (2005) 1357-1360.

[112] A.M. Leung, E.N. Pearce, L.E. Braverman, Perchlorate, iodine and the thyroid, Best. Pract. Res. Cl. En. 24 (2010) 133-141.

[113] S. Kumar, A. Kumar, A. Bahuguna, V. Sharma, V. Krishnan, Two-dimensional carbon-based nanocomposites for photocatalytic energy generation and environmental remediation applications, Beilstein J. Nanotechnol. 8 (2017) 1571–1600.

[114] B.C. Brodie, On the atomic weight of graphite, Philos.Trans. R. Soc. 14 (1859) 249-259.

[115] W.S. Hummers, R.E. Offeman, Preparation of graphitic oxide, J. Am. Chem. Soc. 80 (1958) 1339.

[116] D.C. Marcano, D.V. Kosynkin, J.M. Berlin, A. Sinitskii, Z. Sun, A. Slesarev, Improved synthesis of graphene oxide, ACS Nano 4 (2010) 4806-4814.

[117] J. Chen, Y. Li, L. Huang, C. Li, G. Shi, High-yield preparation of graphene oxide from small graphite flakes via an improved Hummers method with a simple purification process, Carbon 81 (2015) 826-834.

[118] R. Li, J. Wang, J.P. Shen, C. Hua, G.C. Yang, Preparation and characterization of insensitive HMX/graphene oxide composites, Propellants, Explos., Pyrotech. 38 (2013) 798-804.

[119] N.K. Memon, A.W. McBain, S.F. Son, Graphene Oxide/Ammonium Perchlorate Composite Material for Use in Solid Propellants. J. Propuls. Power (2016) 1-5.

[120] R.Thiruvengadathan, S.W. Chung, S. Basuray, B. Balasubramanian, C. S. Staley, K. Gangopadhyay, S. Gangopadhyay, A Versatile Self-Assembly Approach toward High Performance Nanoenergetic Composite Using Functionalized Graphene, Langmuir 30 (2014) 6556−6564.

[121] N. Yan, L. Qin, H. Hao, L. Hui, F. Zhao, H. Feng, Iron oxide/aluminum/graphene energetic nanocomposites synthesized by atomic layer deposition: Enhanced energy release and reduced electrostatic ignition hazard, Appl. Surf. Sci. 408 (2017) 51-59.

[122] P-A. Liu, M-j. Wang, L. Wang, J. Wang, T. Wang, Effect of nano-metal oxide and nano-metal oxide/graphene composites on thermal decomposition of potassium perchlorate, Chem. pap. 73 (2019) 1489–1497.

[123] Y. Lan, M. Jin,Y. Luo, Preparation and characterization of graphene aerogel/Fe_2O_3/ammonium perchlorate nanostructured energetic composite, J. Sol-Gel Sci.Technol. 74 (2015) 161-167.

[124] Y-F. Lan, L. Yunjun, Preparation and characterization of graphene aerogel/ammonium nitrate nano composite energetic materials. J. Explos. Propellants 38 (2015) 15-18.

[125] L. Yu, H. Ren, X-Y. Guo, X-B. Jiang, Q-J. Jiao, A novel ε-HNIW-based insensitive high explosive incorporated with reduced graphene oxide, J.Therm Anal Calorim. 117 (2014) 1187-1199.

[126] X. Zhang, W.M. Hikal, Y. Zhang, S.K. Bhattacharia, L. Li, S. Panditrao, S. Wang, B.L. Weeks, Direct laser initiation and improved thermal stability of nitrocellulose/graphene oxide nanocomposites, Appl. Phys.Lett. 102 (2013) 141905-1 - 141905-5.

[127] H. Cai, L. Tian, B. Huang, G. Yang, D. Guan, H. Huang, 1,1-Diamino-2,2-dintroethene FOX-7, nanocrystals embedded in mesoporous carbon FDU-15. Microporous Mesoporous Mater. 170 (2013) 20-25.

[128] X-M. Qian, N. Deng, S-F. Wei, Z-Y. Li, Catalytic effect of carbon nanotubes on pyrotechnics, Chin. J. Energet. Mater. 17 (2009) 603-607.

[129] L-M. Liu, X-L. Kang, Y. Yi, H-F. Zhang, J-S. Luo, Y-J. Tang, Influence of CNTs on thermal behavior and light radiation properties of Zr/KClO4 pyrotechnics, Chin. J. Energet. Mater. 22 (2014) 75-79.

[130] D. Sylvain, B. Patric, G. Nicole, C. Sebastien, T. Serge, Flash-ignitable energetic material, US Patent, 20040040637A1 (2004).

[131] M. Sharma, S. Vimal, Effect of carbon nanotube addition on the thermite reaction in the Al/CuO energetic nanocomposite, Philos. Mag. (2017) 1921–1938.

[132] R. Guo, Y. Hu, R. Shen, Y. Ye, Electro-explosion performance of KNO3-filled carbon nanotubes initiator, J. Appl. Phys. 115 (2014) 174901-1 - 174901-5.

[133] C. Zhang, J. Li, Y-J. Li, Z.B. Zhang, Preparation and property studies of carbon nanotubes covalent modified BAMO-AMMO energetic binders, J.Energet Mater. 33 (2015) 305–314.

[134] I.G. Assovskiy, A.A. Berlin, Metallized carbon nanotubes, Int. J. Energ. Mater. Chem. Propul. 8 (2009) 281-289.

[135] C. Zhang, J. Li, Y. Luo, X. Zhang, B. Zhai, Preparation and properties of carbon nanotubes modified glycidyl azide polymer binder film, Polym. Mater. Sci. Eng. 29 (2013) 105-108.

[136] H.Y. Jeong, K.P. So, J.J. Bae, S.H. Chae, T.H. Ly, T.H. Kim, D.H. Keum, C.K. Kim, J.S. Hwang, Y.J. Choi, Y.H. Lee, Tailoring oxidation of Al particles morphologically controlled by carbon nanotubes, Energy 55 (2013) 1143-1151.

[137] Y. Liu, W. Jiang, J.-X. Liu, Y. Wang, G.-P. Liu, F-S. Li, Study of catalyzing thermal decomposition and combustion of AP/HTPB propellant with nano Cu/CNTs. Acta Armamentarii 29 (2008) 1029–1033.

[138] G-Y. Zeng, C-M. Lin, J-H. Zhou, Influences of Carbon Nanotubes on the Thermal Decomposition Behavior of HMX, Chin. J. Explos. Propellants 356 (2012) 55–57.

[139] K. Kappagantula, M.L. Pantoya, Experimentallymeasured thermal transport properties of aluminumpolytetrafluoroethylene nanocomposites with graphene and carbon nanotube additives, Int. J. Heat Mass Transfer 55 (2012) 817-824.

[140] J. Zhang , J.M. Shreeve, 3D nitrogen-rich metal–organic frameworks: opportuni- ties for safer energetics, Dalton Trans. 45 (2016) 2363–2368.

[141] M. Friedrich, J.C. Gálvez-Ruiz, T.M. Klapötke, P. Mayer, B. Weber, J.J. Weigand, BTA Copper Complexes. Inorg. Chem. 44 (2005) 8044–8052.

[142] G.H. Tao, D.A. Parrish, J.M. Shreeve, Nitrogen-Rich 5-(1-Methylhydrazinyl) tetrazole and its Copper and Silver Complexes, Inorg. Chem. 51 (2012) 5305–5312.

[143] B.D. Wu, Y.G. Bi, F.G. Li, L. Yang, Z.N. Zhou, J.G. Zhang, T.L. Zhang, A Novel Stable High-Nitrogen Energetic Compound: Copper(II) 1,2–Diaminopropane Azide. Anorg. Allg.Chem. 640 (2014) 224–228.

[144] S. Li, Y. Wang, C. Qi, X. Zhao, J. Zhang, S. Zhang, S. Pang, 3D energetic metal–organic frameworks: synthesis and properties of high energy materials, Angew. Chem. Int. Ed. 52 (2013) 14031-14035.

[145] Y. Feng, X. Liu, L. Duan, Q. Yang, Q. Wei, G. Xie, S. Chen, X. Yang, S. Gao, In situ synthesized 3D heterometallic metal–organic framework (MOF) as a high-energy-density material shows high heat of detonation, good thermostability and insensitivity, Dalton Trans. 44 (2015) 2333-2339.

[146] J.Z. Hui Su, Y. Du, P. Zhang, S. Lia, T. Fang, S. Pang, New roles of metal–organic frameworks: Fuels for aluminum-free energetic thermites with low ignition temperatures, high peak pressures and high activity, Combust. Flame 191 (2018) 32–38.

[147] J.Z. Hui Su, Y. Du, P. Zhang, S. Lia, T. Fang, S. Pang, New roles for metal–organic frameworks: fuels for environmentally friendly composites, RSC Adv. 7 (2017) 11142–11148.

[148] J.Y. Malchi , R.A. Yetter , T.J. Foley, S.F. Son, The effect of added Al_2O_3 on the propagation behavior of an Al/CuO nanoscale thermite, Combust. Sci. Technol. 180 (2008) 1278–1294.

[149] W.L. Perry, B.L. Smith, C.J. Bulian, J.R. Busse, C.S. Macomber, R.C. Dye, S.F. Son, Nano-scale tungsten oxides for metastable intermolecular composites, Propell. Explos. Pyrot. 29 (2004) 99-105.

[150] R. Thiruvengadathan, A. Bezmelnitsyn, S. Apperson, C. Staley, P. Redner, W. Balas, S. Nicolich, D. Kapoor, K. Gangopadhyay, S. Gangopadhyay, Combustion characteristics of novel hybrid nanoenergetic formulations, Combust. Flame 158 (2011) 964–978.

[151] R.H. Bouma, D. Meuken, R. Verbeek, M.M. Pacheco, L. Katgerman, Shear initiation of Al/MoO_3- based reactive materials, Propell. Explos. Pyrot. 32 (2007) 447–453.

[152] S.J. Apperson, Characterization and MEMS applications of nanothermite materials, Doctoral Faculty of the Graduate School, University of Missouri (2010).

[153] M. Comet, B. Siegert, V. Pichot, P. Gibot, D. Spitzer, Preparation of explosive nanoparticles in a porous chromium(III) oxide matrix: a first attempt to control the reactivity of explosives, Nanotechnology 19 (2008) 285716.

[154] C. Rossi, K. Zhang, D. Estève, P. Alphonse, P. Tailhades, C. Vahlas, Nanoenergetic Materials for MEMS: A Review, J Microelectromech Syst. 16 (2007) 919-931.

[155] M. Comet, C. Martin, F. Schnell, D. Spitzer, Nanothermite foams: From nanopowder to object. Chem. Eng. J. 316 (2017) 807–812.

[156] J.J. Berge , C.E. Hamilton , C.A. Crouse , A.R. Barron, Ultrasmall copper nanopar- ticles from a hydrophobically immobilized surfactant template, Nano Lett. 9 (2009) 2239–2242.

[157] H.H. DiBiaso , B.A. English , M.G. Allen, Solid-phase conductive fuels for chemical microactuators, Sens. Actuators A. 111 (2004) 260–266.

[158] W. Zhang , H. Peng , X. Gao , J. Ye , Z. Zhang , Y. Chao, An in situ chemical reac- tion approach to synthesize zinc picrate energetic thin film upon zinc oxide nanowires array, Surf. Interface Anal. 44 (2012) 1203–1208.

[159] V.I. Baev, C. Lvov, N. Shugalei, Influence of the Environment Internal Factors on Warm-blooded Organisms. in In Proceedings of the Problems of Military and Emergency Medicine, St. Petersburg, Russia (1998).

[160] M.B, Talawar, R. Sivabalan, T. Mukundan, H. Muthurajan, A.K. Sikder, B.R. Gandhe, A.S. Rao, Environmentally compatible next generation green energetic materials (GEMs). J. Hazard. Mater. 161 (2009) 589–607.

APPENDIX A ARTICLE 5: THRUST CHARACTERISTICS OF NANO-CARBON/AL/OXYGENATED SALT NANOTHERMITES FOR MICRO-ENERGETIC APPLICATIONS

Ahmed Fahd [a], Alex Baranovsky [b], Charles Dubois [a, *], Jamal Chaouki [a], John Z. Wen [b]

[a] Chemical Engineering Department, École Polytechnique de Montréal, Montréal, H3C 3A7 (Canada)

[b] Mechanical and Mechatronics Engineering Department, University of Waterloo, Ontario, N2L 3G1 (Canada)

(This work has been submitted to Applied Thermal Engineering)

(Note: Ahmad Fahd is the name I always use instead of Ahmad Emam in my all publications)

A.1 Abstract

Thrust performance and combustion propagation processes within small nozzles are important in determining practical aspects of nanothermite usage and key to exploring their applicability in compact-energetic systems. This study is devoted, via experimental and numerical means, to evaluating the thrust generating characteristics of nanothermite mixtures in a converging-diverging nozzle and an open tube. Mixtures are prepared using nano aluminum (n-Al), potassium perchlorate ($KClO_4$) and different types of carbon nano material (CNMs) additives such as graphene oxide, reduced graphene oxide, multi-walled carbon nano-tubes and carbon nanofibers. Oxidizing salts (KIO_4, $K_2S_2O_8$, $KMnO_4$ and NH_4NO_3) analogous to $KClO_4$ are also investigated. The nanothermite mixtures are packed at different densities and ignited using a 3.5 W continuous wave laser to observe combustion phenomena and thrust production. The exhaust plume of the reference sample (n-Al and $KClO_4$) is characterized using high-speed video and computational fluid dynamics (CFD) modeling. Thrust output, specific and volumetric impulse (I_{SP} and I_{SV}), and normalized energy are found to increase notably with addition of CNMs. Two distinct reaction regimes (fast and slow) are observed in combustion of low and high packing densities (20 and 55 TMD), respectively, and the total impulse (I_{FT}) and I_{SP} reaches a maximum in these both regimes when 5% GO/Al/$KClO_4$ is used. More specifically, I_{FT} and I_{SP} were

recorded as 7.95 mN.s and 135.20 s respectively at 20% TMD, which indicated an improvement of over 57 % in comparison to the reference sample without GO (5.05 mN.s and 85.88 s). This study suggests nanothermite mixtures with tailored combustion performance can be developed using oxidizing salts instead of metallic oxides and tuned by addition of small quantity of GO, introducing a new direction for micro-propulsion and micro-energetic applications.

A.2 Introduction

Demand for improved energetic materials (EMs) is increasing as propulsion technologies strive to be smaller, more efficient, and safer to use. Fields of active interest in novel EMs include civilian applications such as MEMS (micro-electromechanical systems) lab-on-a-chip devices as well as defence applications such as micro-thrusters and smart-projectiles. Nanothermites are solid-phase EM mixtures traditionally composed of metal and metal-oxide components at nanometric scale. However, nanothermites outperform standard micron-scale thermite powders in terms of reaction rate, heat release, pressure, and thrust [1, 2], they have limited utility due to their long ignitability and slow combustion dynamics [2, 6]. Furthermore, traditional EMs have a tough time igniting and propagating in small tubes [7].

A common family of nanothermites are those based on nano aluminum (n-Al) powders, traditionally mixed with metallic oxides. More novel formulations use combinations where atoms with high electronegativity (O, S, F, etc.) are exchanged between an oxidizer and a fuel, like in the case of $Al/KClO_4$ or $Al/K_2S_2O_8$ [5, 8, 9]. The preference of oxygenated salts over metal oxides or oxysalts comes from their higher atomic oxygen content which results in superior burn rates and gas generation capabilities [9, 10]. Moreover, the lower dissociation energies of non-metal-oxygen bonds (Cl-O, I-O, etc.) in oxygenated salts offer higher oxygen mobility that can lead to decomposition and oxygen release at lower temperatures when compared to metal-oxygen bonds (Cu-O, Fe-O, Bi-O, etc.) [11, 12]. Oxygenated salts produce intermediate radicals (e.g. hydroxyl radical, OH·) upon decomposition which in turn can produce other subsequent radicals and oxidants by initiating a chain of degradation reactions. As such, oxygenated salts have higher oxidation ability than oxidizers which undergo an electron capture based oxidation mechanism [13, 14].

Oxygenated salt-based nanothermites have a variety of practical uses in the field of solid propulsion and micro energetic systems. For example, ammonium perchlorate (AP, NH_4ClO_4)

and potassium perchlorate ($KClO_4$) are used alone or mixed with Al to improve the ballistic performance of modified double base propellant (MDB) for booster rocket motor applications such the Tow 2A anti-tank missile [15]. Elbasuney et al. used small scale test motors to evaluate the combustion characteristics of the developed samples. They found that NH_4ClO_4, $KClO_4$, and a binary mixture of NH_4ClO_4/Al increased burning rates (5.3%, 22% and 12% respectively), and increased the characteristic exhaust velocity (C^*) [15, 16]. Pressure-cell combustion tests of Al mixed with nano periodate salts (50-300 nm) such as sodium periodates ($NaIO_4$) and potassium periodates (KIO_4) generated pressurization rate (2.4–2.6 MPa/μs), considerably higher than those obtained with Al/CuO traditional nanothermite (0.06 MPa/μs) [10]. In addition, Al/ $NaIO_4$ and Al/ KIO_4 recorded ignition temperatures 880 and 950 K which are lower than that of Al/CuO (1040 K) [10].

One of the current applications of nanothermites is the development of miniature thrusters for small attitude control, spacecraft station keeping, drag compensation, orbital transformation, or course correction of high-velocity projectiles [17, 18]. Dai and colleagues used a 10×10 microthruster array with varying quantities of AP within an Al/CuO nanothermite base matrix. Their results showed that addition of 7.5wt-% AP to Al/CuO substantially improved specific impulse and heat energy (61 s and 1113 J/g) compared to their reference sample without AP (22 s and 792 J/g) [19]. Nanothermites can also be used in pyrotechnical micro electro mechanical systems (PyroMEMS) such as pyroswitches or circuit breakers in electrical systems, actuators, and safe-and-arm devices [20, 21]. A. Nicollet et al. exploited the powerful reaction capability of Al/CuO nanothermite to fabricate a miniature nanothermites-based circuit breaker for over current protection. The developed circuit breaker resulted in 0.57 ms response time with a 59 μs ignition delay, notably quicker than the 1 ms response time of traditional mechanical circuit breakers. In addition, the response time can be easily adjusted by varying the mass of nanothermite, as was demonstrated be Nicollet et al. by varying mass from 5.59 to 13.24 mg. The proposed circuit breakers can be used in energy storage, aerospace manufacturing, and parachute deployment systems [21].

Recently, graphene and its derivatives have been active fields of research in the improvement of nanothermites due to their large specific areas and unique thermal, electrical and mechanical properties [22-25]. Graphene oxide (GO) is an appropriate candidate for introduction into nanothermites due to its catalytic properties as well as relatively simple preparation methods [26].

GO itself is considered to be a potential EM, where upon heating, it can readily undergo violent exothermic decomposition due to the extensive oxygenic functional groups on the basal plane (phenol, hydroxyl, and epoxide) and along edges (carboxylic) [27].

The most critical requirements for any propulsion system design are: minimized overall system mass and maximized performance parameters such as thrust and impulse [28, 29]. By producing improved performance without incurring any associated mass increase, the overall propulsion design is improved. The use of oxygenated salt nanothermites is one way to improve performance without introducing a mass penalty, but the novelty of these compositions means that propulsion-specific characterization is limited in existing literature.

The goal of this work is to propose nanothermite mixtures with controllable combustion and tailored performance parameters for micro-propulsion and micro-energetic applications through assessment of thrust production and dynamic performance within a small tube attached to a nozzle with a throat of 2 mm. The test is done using small-scale test motors (STMs) in open-tube and converging-diverging (CD) nozzle configurations. The effects of chemical composition and packing density on the performance (I_{FT}, $I_{SP,}$ I_{SV} and normalized energy output) of nanothermites are investigated first using n-Al, potassium perchlorate ($KClO_4$) and varying quantities of GO. Then, other carbon nano materials are examined as additives to the base thermite mixture, including reduced graphene oxide (RGO), multi-walled carbon nano tubes (MWCNTs) and carbon nano fiber (CNF) to substitute GO. thrust performance of GO-enhanced nanothermites is compared to alternative oxidizers, such as potassium periodate (KIO_4), potassium persulphate ($K_2S_2O_8$), potassium permanganate ($KMnO_4$) and ammonium nitrate (NH_4NO_3). Computational fluid dynamics (CFD) modeling is utilized to reveal the velocity and temperature profiles of the nozzle plume and to calculate the thrust.

A.3 Materials and methods

A.3.1 Materials

Graphite flakes, phosphoric acid (H_3PO_4), sulphuric acid (H_2SO_4), hydrogen peroxide (H_2O_2), and acetone used in the preparation of GO were purchased from Sigma-Aldrich. $KClO_4$ and NH_4NO_3, were obtained from Defence Research and Development Canada. All other oxidizers, namely KIO_4, $K_2S_2O_8$ and $KMnO_4$ were purchased from Sigma-Aldrich. The as-purchased Al

nanoparticles from US Research Nanomaterials Inc. have a spherical shape with an average particle size of 40 nm, a purity of more than 99.9% metal basis, an active Al content of 80wt-% (mass fraction), a surface area of 30-50 m^2/g and bulk density of 2.7 g/cm^3 as specified by the manufacturer. MWCNT and CNF were purchased from Sigma-Aldrich. MWCNT has >98% carbon basis, O.D. × L 6-13 nm × 2.5-20μm and specific surface area of 216 m^2/g. CNF is graphitized platelets (conical) and has >98% carbon basis, and dimensions D × L 100 nm × 20-200μm.

A.3.2 Synthesis of GO and RGO

Graphene oxide was synthesized using an improved Hummer method with graphite powder as the starting material [30]. The detailed procedures of the GO and RGO preparation can be found in our previously published article [31]. The composition and heat of combustion of CNMs used in the experiment was checked by a CHNSO Elemental Analyzer EA3000 (EuroVector) and oxygen bomb calorimetry. The mass fraction (wt-%) of C, H, N, S and O and heat of combustion of each CNMs is summarized in Table A1.

Table A1 Elemental analysis and heat of combustion of CNMs

CNMs	**C (%)**	**H (%)**	**O (%)**	**N (%)**	**S (%)**	**Heat released (KJ/g)**
GO	49.77 ± 0.62	1.74 ± 0.11	46.44 ± 0.46	0.00	2.05 ± 0.15	34.35 ± 0.32
RGO	91.29 ± 1.18	1.89 ± 0.11	4.58 ± 0.36	0.00	2.24± 0.17	32.73 ± 0.36
MWCNTs	98.51 ± 0.42	0.24 ± 0.11	0.41 ± 0.14	0.84 ± 0.17	0.00	33.14 ± 0.42
CNF	98.17 ± 0.37	0.46 ± 0.08	0.65 ± 0.16	0.72 ± 0.26	0.00	32.88 ± 0.29

A.3.3 Preparation of nanothermite compositions

Nanothermite compositions were prepared by weighing the fuel (n-Al) and oxidizers individually based on the stoichiometric ratios presented in Table 2. The dispersion of n-Al with each oxidizer and GO (2.5, 5.0, 7.5, and 10 wt%) was conducted in acetone. The samples were then put in an ultrasonic bath for 30 min to ensure proper dispersion. Acetone was evaporated at 60 $^{\circ}$C for 1 hour with simultaneous mechanical stirring to prevent the re-agglomeration of nanoparticles. Wet

particles were then fully dried in a vacuum desiccator for 12h to drive off any remaining acetone. Finally, the dried powder was gently broken up with a spatula to remove any large clumps and until the consistency was that of a loose powder. For comparison purposes, other CNMs (RGO, MWCNTs and CNFs) and oxidizers (KIO_4, $K_2S_2O_8$, $KMnO_4$ and NH_4NO_3) were used as alternatives to GO and $KClO_4$ respectively. Different nanothermite compositions and their reactions are shown in Table A2.

Table A2 Chemical composition of different nanothermite samples

Oxidizer type	**Oxidizer (wt. %)**	**Al (wt. %)**	**CNMs type**	**CNMs (wt. %)**	**Thermite reaction**
$KClO_4$	65.80	34.20	GO	0.00	$8Al + 3KClO_4 \rightarrow 4Al_2O_3 + 3KCl$
$KClO_4$	64.15	33.35	GO	2.50	$8Al + 3KClO_4 \rightarrow 4Al_2O_3 + 3KCl$
$KClO_4$	62.51	32.49	GO	5.00	$8Al + 3KClO_4 \rightarrow 4Al_2O_3 + 3KCl$
$KClO_4$	60.86	31.64	GO	7.50	$8Al + 3KClO_4 \rightarrow 4Al_2O_3 + 3KCl$
$KClO_4$	59.22	30.78	GO	10.00	$8Al + 3KClO_4 \rightarrow 4Al_2O_3 + 3KCl$
$KClO_4$	64.72	30.28	RGO	5.00	$8Al + 3KClO_4 \rightarrow 4Al_2O_3 + 3KCl$
$KClO_4$	64.72	30.28	CNT	5.00	$8Al + 3KClO_4 \rightarrow 4Al_2O_3 + 3KCl$
$KClO_4$	64.72	30.28	CNF	5.00	$8Al + 3KClO_4 \rightarrow 4Al_2O_3 + 3KCl$
KIO_4	72.35	22.65	GO	5.00	$8Al + 3KIO_4 \rightarrow 4Al_2O_3 + 3KI$
$K_2S_2O_8$	83.84	11.16	GO	5.00	$4Al + 3K_2S_2O_8 \rightarrow 2Al_2O_3 + 3K_2SO_4 + 3SO_2$
$KMnO_4$	81.14	13.86	GO	5.00	$2Al + 2KMnO_4 \rightarrow 5Al_2O_3 + 3K_2O + 6MnO$
NH_4NO_3	77.56	17.44	GO	5.00	$2Al + 3NH_4NO_3 \rightarrow Al_2O_3 + 3N_2 + 6H_2O$

A.4 Instrumentation

Laser ignition and high-speed imaging was used to evaluate the combustion performance of the prepared composites; a schematic is shown in Figure 1 (A). Schematic dimensions of the STMs used are illustrated in Figure A1 (B), (C) and (D) showing the nozzle and no-nozzle configurations; the nozzle used is a generic converging-diverging (CD) design intended to accelerate exhaust gasses to a supersonic state [32].

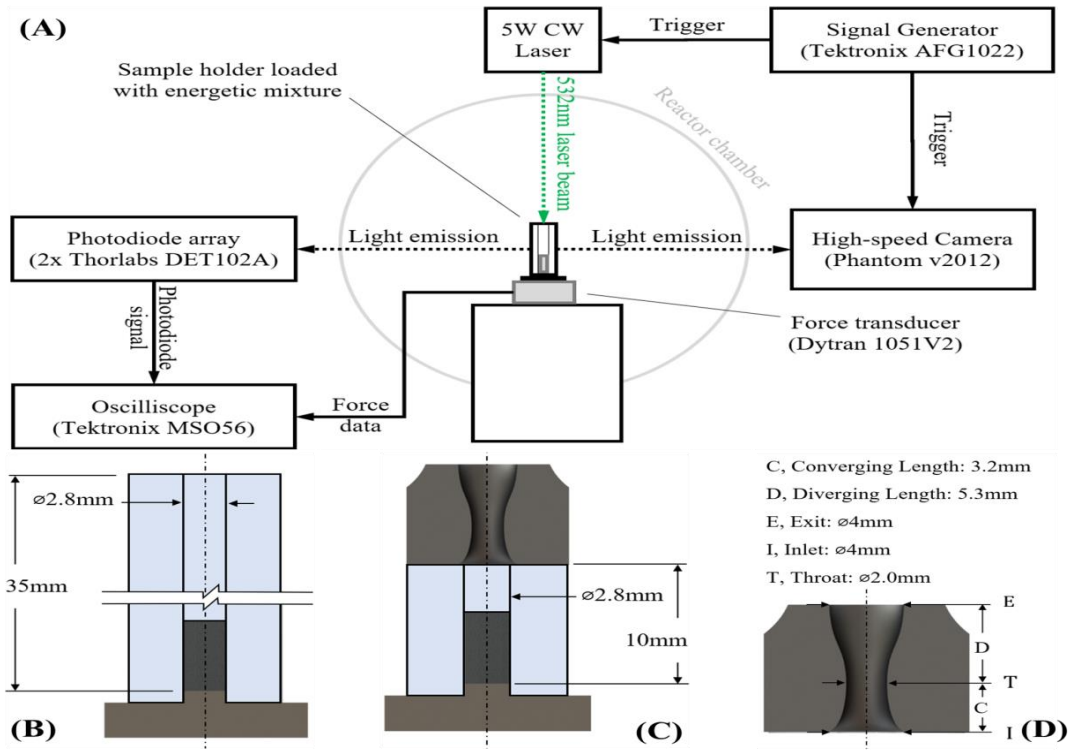

Figure A1 Schematic diagram of experimental setup showing: laser ignition and high-speed imaging set up (A), no-nozzle STM configuration (B), CD nozzle STM configuration (C), and converging diverging nozzle geometry (D)

A 5W continuous wave 532nm laser was used to ignite samples. The combustion of the samples was recorded at 180,000 fps with 600 ns exposure time using a Phantom v2012 high-speed camera. A Dytran (1051V2) force transducer with a reference sensitivity of 22.43 mV/N was fixed underneath the sample to measure the thrust force. Two photodiodes (Thorlabs DET102A) were used to capture the light intensity output from the nanothermite sample. A neutral density filter (Thorlabs NDUV06B) was installed on one photodiode unit and a 488 nm wavelength filter (Thorlabs FLA488-10) on the other; 483nm being a characteristic wavelength for the AlO thermite reaction intermediary [33]. A Tektronix MSO56 oscilloscope was used to capture force and photodiode data at a sampling rate of 1MHz. Data recording and laser triggering was performed by a Tektronix AFG1022 waveform generator using a standard TTL signal. All tests were carried out at normal atmospheric conditions.

A.5 Numerical Modeling

The development of supersonic flow within the converging-diverging nozzle, produced by combustion of a nanothermite pellet, was numerically investigated using a finite element method (FEM) software [34]. The conservation equations for mass, momentum and energy of the high-speed compressible flow were solved in a 2D-axisymmetric domain with the Spalart-Allmaras turbulence model chosen for its simplicity. Thermodynamic and transport properties of the fluid (i.e., ideal-gas air) were evaluated by the material library within the software. While the nozzle geometry shown in Figure A1 (D) was directly used, to keep the back pressure constant, the computational domain includes a large reservoir surrounding nozzle and open tube outlets. Dependence of the solution on the mesh size was evaluated using the adapted mesh function detailed in the software. The domain geometry is presented in Figure A2, along with the boundary and initial conditions.

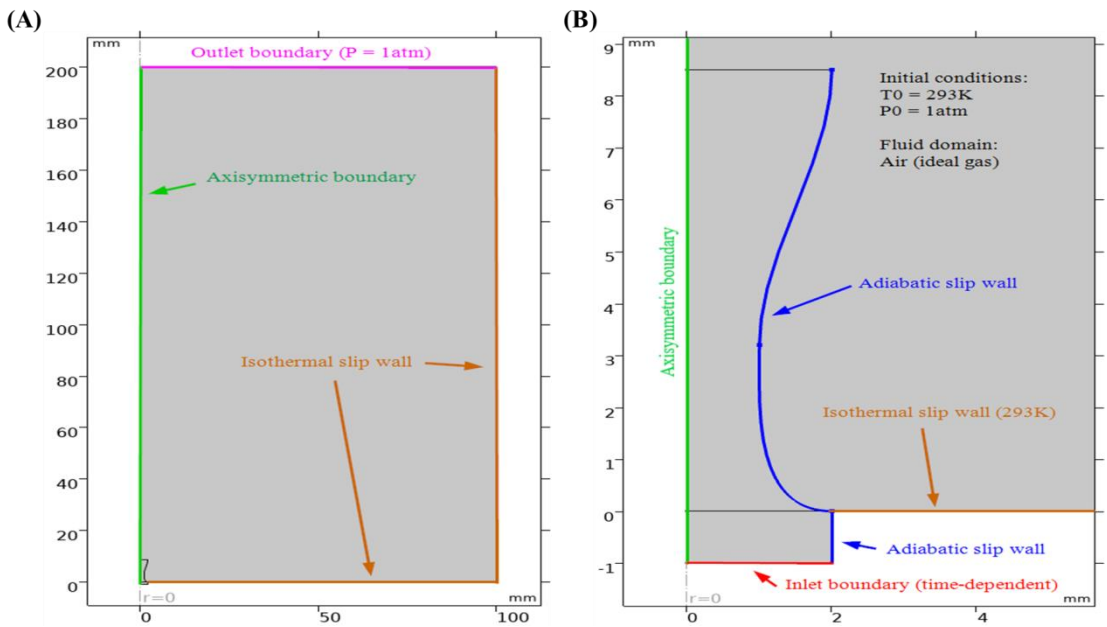

Figure A2 Schematic diagram of 2D-axisymmetric domain used for modelling showing: A) reservoir boundary conditions, and B) nozzle-area boundary and initial conditions

Combustion of the reference sample (Al/ $KClO_4$) was modeled using the ICT code [35, 36] under the assumption that reactants were perfectly mixed. This code solves the adiabatic combustion of a heterogeneous mixture and simulates the final product composition, temperature, and pressure. Note that with the stoichiometric ratio of one, the reactants produce gaseous products which

include 19 mol% of oxygen containing gases, 11mol% of AlO and 23mol% of KCl. Due to the complexity of gas mixture during the combustion process, the working fluid was modelled as an ideal gas. Table A3 lists the values of the specified parameters at the nozzle inlet.

Table A3 Modeling parameters at the inlet of the nozzle based on ICT calculation

Pressure (bar)	**Temperature (K)**	**Average gas density (kg/m^3)**	**Mass flow rate (g/s)**	**Average mole weight (g/mol)**
112.88	3762.23	22.02	61.55	60.99
Average specific heat (J /mol. Gases* K)	**Ratio of specific heats**	**Mach number**	**Speed of sound (m/s)**	**Average flow velocity (m/s)**
49.153	1.20	0.32	695.10	222.43

The ICT code cannot account for the effects of the packing density on the combustion products and their thermodynamic properties. To investigate the qualitative trend of the transient thrust production with reduced energy release from a burning pellet with varying packing density, three simulation cases were run on the CD nozzle and two simulation cases were run on the straight open tube. This largely simplified approach uses the estimated mass flow rate at the inlet based on the following assumptions: i) the reference sample has high a CHON content, resulting in a reduced amount of solid phase residual and negligible effects of gas diffusion through the condense phase and ii) the combustion behavior of the pellet is similar to a porous propellant grain, with the generation of gas regressing linearly with time and increasing linearly with porosity. The initial conditions were set to room temperature and atmospheric pressure.

A.6 Results and Discussion

A.6.1 Effect of chemical composition

The combustion characteristics, particularly thrust output and specific impulse, are the most important parameters that need to be measured to evaluate the propellant performance of a nanothermite mixture. They are highly dependent on the chemical composition of mixtures and allow us to predict performance, thereby determining the appropriate application for the prepared samples. Static thrust data was collected from different samples in the open-tube test engine

shown in Figure A1 (B). The comparative performance of various CNMs and oxidizers mixtures is shown in Figure A3.

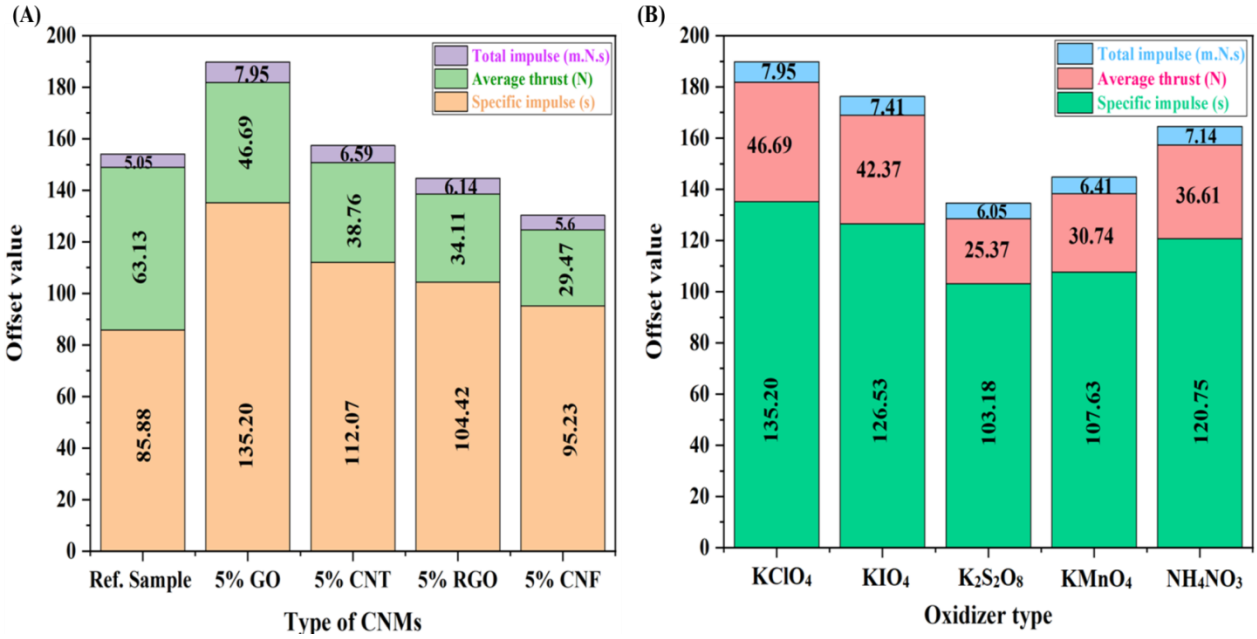

Figure A3 Comparative plots for nanothermites based on: (A) Al/KClO4 with various CNM additives (B) Al based mixtures with different oxidizers; all enriched with 5%GO content

Figure A3 (A) shows that addition of CNMs improves performance of nanothermite mixtures in terms of total and specific impulses. Adding CNT, RGO, and CNF to Al/$KClO_4$ nanothermite increased the total and specific impulses by 31%, 22% and 11% respectively. This enhancement can be attributed to the highly conductive thermo-electric properties and large specific areas of CNMs which facilitate the uniform mixing of n-Al and $KClO_4$ [26]. Furthermore, CNMs may act as secondary fuels which add energy to the system, help in the completion of n-Al combustion, and compensate for the reduction of active Al content due to the Al_2O_3 shell. These effects combine to increase the total and specific impulses compared to the base thermite mixture.

Figure 3 (B) shows the combustion characteristics of nanothermite composites based on n-Al and various types of oxygenated salts. These results show that nanothermites based on oxygenated salts have higher I_{SP} than those with metallic oxides such as Al/CuO (26.7s) and Al/Bi_2O_3 (59.4s) as previously reported in literature [37, 38]. Oxygenated salt-based nanothermites produce large I_{sp} due to the high oxidizing power, high reaction rate, lower bond energy, and low oxygen release temperature of nonmetal-oxygen pairs compared to the metal–oxygen bonds in metal oxides [9-12]. GO/Al/$KClO_4$ nanothermite displayed the highest I_{FT} and I_{SP} due to the high

enthalpy of C-$KClO_4$ (154 kJ/mol) and C-KIO_4 (72 kJ/mol) side reactions [39]. The reduced performance of the GO/Al/$K_2S_2O_8$ mixture with respect to the others may stem from the oxidation of nano-C by $K_2S_2O_8$ in the mixed suspension before ignition [40, 41]. Therefore, the GO/Al/$K_2S_2O_8$ nanothermite does not have the same proposed high energy output reaction paths, like C-O and C-$KClO_4$ in GO/Al/$KClO_4$, which may aid in completion of the main thermite reaction.

For the highest performing mixture, GO/Al/$KClO_4$, GO quantity was varied to observe compositional effects on the thrust performance. The resultant thrust profiles are presented in Figure A4.

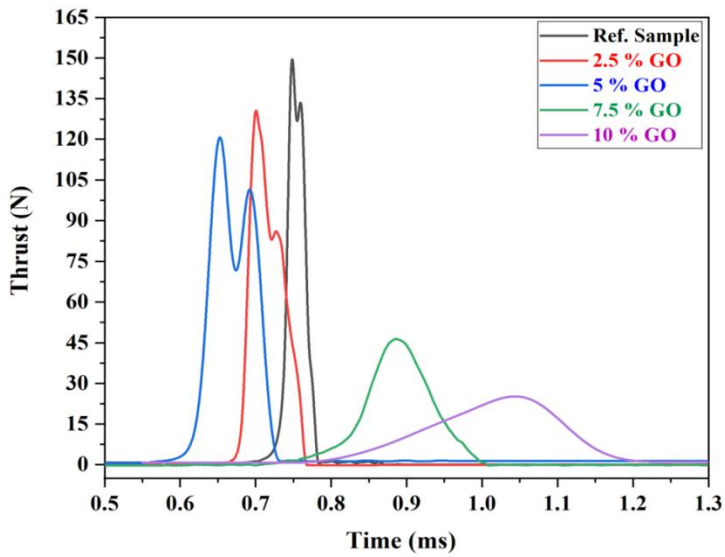

Figure A4 Thrust profiles for different GO/nanothermite samples at 20 %TMD

The reference sample (Al/$KClO_4$) exhibits a relatively narrow thrusting duration (~0.1 ms) which can be correlated to the high oxidizing power and exothermic decomposition nature of $KClO_4$. Moreover, the reference sample shows two peaks, the first of which may be caused by either the shock release from the exit of the STM or heterogeneous combustion of the sample.

Adding GO into the mixture brings about three major effects. First, the peak thrust value is decreased (15% reduction for 2.5% GO sample, 80% for 10% GO sample), largely due to the reduced energy release which is caused by the separation of the oxidant and the metal as well as potential GO-oxidizer side reactions that detract from the main thermite reaction. Second, the thrust delay time decreases with 2.5% and 5% GO samples, while the 7.5% and 10% GO samples

show a similar or marginally increased delay compared to the reference sample. Thirdly, the thrusting duration increases with the GO content from 0.1 ms for the reference sample to about 0.5 ms for the 10% GO sample. It is apparent from this figure that addition of up to 5 % GO yields two peaks; the first peak was from the exothermic decomposition of GO, $KClO_4$ and preignition reactions between GO decomposition products and nanothermite reactants, while the second came from the main thermite reaction [31]. Besides, addition of up to 5 % GO content produces slightly decreased thrust peaks compared to the reference sample and improving the total performance through improving the contact between reactive particles and the heat transfer pathway. Though increasing the amount of GO over 7.5% significantly reduces the peak thrust and slightly increased the ignition delay time, it helped in sustaining a more uniform burning process. To analyze the combined effects of thrust forces and combustion duration, impulse is quantified through total impulse (I_{FT}), specific impulse (I_{SP}), and volumetric impulse (I_{SV}). These are calculated as follows:

$$I_{FT} = \int_{t_i}^{t_e} F \ dt \tag{1}$$

$$I_{SP} = \frac{1}{W_t} \int_{t_i}^{t_e} F \ dt \tag{2}$$

$$I_{SV} = \frac{1}{V_t} \int_{t_i}^{t_e} F \ dt \tag{3}$$

where: W_t, V_t, t_i and t_e are the nanothermite weight (N), volume of the nanothermite charge (mm^3), initial combustion time (s), and ending combustion time (s) respectively. The effect of GO quantity on the sample propulsion characteristics (I_{FT}, I_{SP} and I_{SV}) are presented in Table A4.

Table A4 Combustion characteristics of nanothermite samples at 20 %TMD

Nanothermite composition	**Average thrust (N)**	**Combustion duration (ms)**	**Total impulse (mN.s)**	**Specific impulse (s)**	**Volumetric impulse ($mN.s/mm^3$)**
Al/ $KClO_4$	63.13 ± 2.38	0.08 ± 0.01	5.05 ± 0.14	85.88 ± 2.27	1.29 ± 0.07
2.5 % GO/Al/$KClO_4$	56.82 ± 1.87	0.11 ± 0.01	6.25 ± 0.19	106.29 ± 2.94	1.60 ± 0.11
5 % GO/Al/$KClO_4$	46.69 ± 2.13	0.16 ± 0.02	7.95 ± 0.23	135.20 ± 2.61	2.04 ± 0.10
7.5 % GO/Al/$KClO_4$	19.13 ± 1.24	0.30 ± 0.04	5.74 ± 0.17	97.62 ± 1.86	1.47 ± 0.08
10 % GO/Al/$KClO_4$	12.04 ± 1.13	0.45 ± 0.03	5.42 ± 0.21	92.18 ± 2.15	1.39 ± 0.05

The measurements summarised in Table A4 show that GO addition has a positive impact in both I_{SP} and I_{SV} up to a point. Impulse values reach a maximum at 5% GO composition where specific and volumetric impulses show over 50% improvement compared to the reference sample. The increase in I_{SP} and I_{SV} values is attributed to the role and effect of GO in improving both the fuel-oxidizer contact and mass-diffusion of the reactants. GO acts as a substrate, increasing the dispersion of n-Al and effectively reducing its aggregation within the $KClO_4$ matrix. Consequently, uniform mixing of n-Al metal fuel and $KClO_4$ oxidant occurs and more complete combustion is expected [42-44]. Furthermore, the decomposition of GO gives rise to reactions between C and nanothermite reactants (C-O, C-$KClO_4$ and C-Al) which are likely prominent reaction pathways in the early stages of combustion [45]. These promote completion of the main thermite reactions (Al-$KClO_4$ and Al-O) and this is a proposed explanation for the observed increase in the combustion time [31]. Also, the exothermic decomposition nature of the $KClO_4$ and GO introduce pre-ignition reactions which may help in cracking the alumina (Al_2O_3) shell layer and improving the diffusion process of both free oxygen and the molten Al core in a melt-dispersion mechanism [41]. However, excessive GO content (more than 5%) in nanothermites gives $KClO_4$ the chance to grow directly on GO nano sheets, causing separation of the oxidizer and metal fuel and a reduction of thrust from the thermite reaction [44-46]. Interestingly, the reduction in thrust with the addition of GO (more than 5%) is compensated by sustained, but lower, thrust over a longer combustion time such that impulse is still increased compared to the reference sample. Ignition delay of nanothermite mixtures is determined using light signals recorded via photodiodes during sample combustion, measuring the delay between laser spot activation (t = 0s) and the first maxima of the photodiode signal. In addition, high-speed video is used to support ignition delay results by measuring the time difference between the first frame where the laser spot is visible and the first frame where a distinct flame front develops. Variation of the light emission of nanothermite mixtures with different GO content is shown in Figure A5.

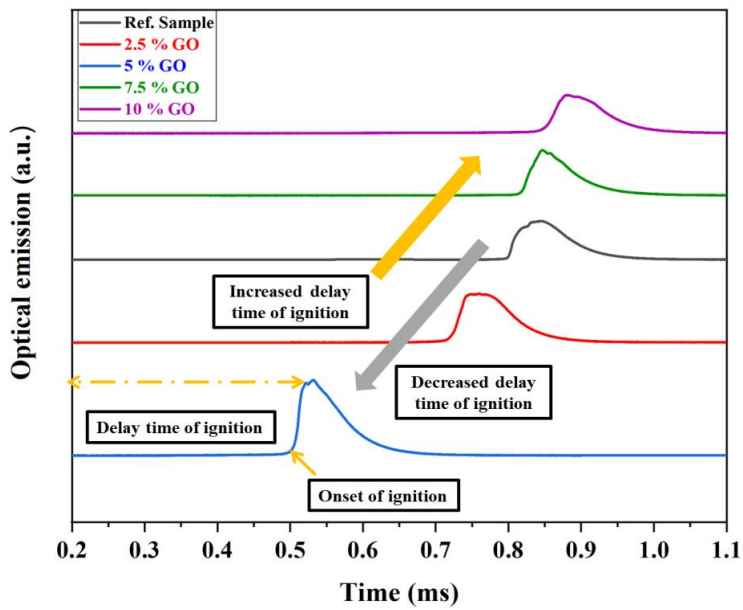

Figure A5 Optical emissions of different GO/nanothermite samples

Addition of GO to the nanothermite mixtures yields two distinct effects on ignition delay; reduction for samples below 5% GO and increase for samples above 5% GO. Addition of up to 5% GO decreases the ignition delay time by approximately 11% and 40% for 2.5% and 5% GO respectively. This is because GO absorbs laser light upon illumination and undergoes exothermic reactions, generating heat and radicals from GO decomposition reactions, which facilitate the ignition and combustion of nanothermite [47]. The presence of GO causes fast local ignition of the nanothermite mixture by the photo-thermal effect. Increasing the amount of GO above 5% GO increases the ignition delay from the reference sample by up to ~50ms (for 10% GO sample). This suggests that increasing the quantity of GO more than 5% in the GO/nanothermite matrix is detrimental to the photo-thermal effect due to environmental heat dissipation through the rapid heat transfer of aggregated GO.

Table A5 collects values of the minimum laser power required ignite loose-packed GO/nanothermite samples, their onset time, ignition delay, and specific energy release. Specific energy release of the sample combustion reaction can be evaluated by calculating the normalized time-averaged photodiode signal (integrating area under the curve) according to the following equation.

$$\overline{E_n} = \left(\frac{\int_{t_e}^{t_i} E\, dt}{(t_i - t_e)}\right)/m \qquad (6)$$

where E, t_i, t_e, m are the photodiode signal (mV), initial combustion time (s), ending combustion time (s) and nanothermite mass charge (mg) respectively.

Table A5 Ignition properties of nanothermite composites

Nanothermite composition	**Laser power input (W)**	**Onset ignition time (ms)**	**Delay time of ignition (ms)**	**Normalized photodiode signal (mV/mg)**
Al/ $KClO_4$	0.53	0.80	0.85	57.55
2.5 % GO/Al/$KClO_4$	0.41	0.72	0.76	64.93
5 % GO/Al/$KClO_4$	0.30	0.50	0.52	70.80
7.5 % GO/Al/$KClO_4$	0.68	0.81	0.85	62.41
10 % GO/Al/$KClO_4$	0.74	0.84	0.89	56.76

Specific energy release (normalized photodiode signal) increases with the amount of GO up to 5% composition; further addition of GO results in reduced normalized photodiode signal. This again supports the observation that 5% GO mixture performs better than the other samples tested. Improving the specific energy of the samples can be accredited to the catalytic effect of GO on the dissociation of oxygen molecules, providing a direct diffusion pathway for the dissociated oxygen atoms to reach and react with Al, thus accelerating the oxidation of Al during the combustion process [48]. The catalytic effect of GO occurs when heat and gaseous products are released at relatively low temperature (200°C) by decomposition and oxidation reactions [49, 50]. Additionally the GO decomposition gases can enhance the convective heat transfer during combustion of the composites and hinder the aggregation of nanothermite reactants [51]. Finally, the observed trends are confirmed by the AlO light signals captured by photodiode with a 488 nm wavelength filter (Thorlabs FLA488-10), shown in Figure A6.

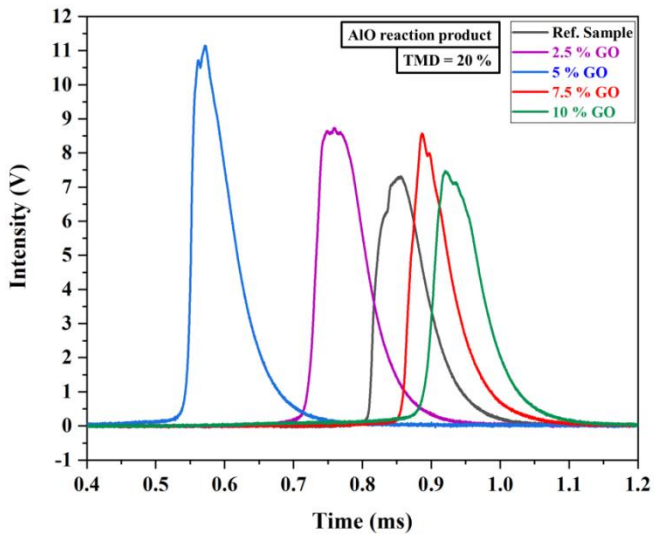

Figure A6 AlO photodiode signal of different nanothermite samples

The intensity of the AlO photodiode signal increases with the addition of GO, with the largest intensity occurring at 5% GO, supporting the findings observed in Figure A3 and Figure A4. AlO is the main gaseous reaction intermediate in the range of 1200-3300 °C, hence correlation between the amount of AlO formed during the reaction, as measured by the intensity of a photodiode signal filtered at 488nm, can be used as indication of the completion of combustion [52]. The agreement of the AlO data signal and values in Table A5 therefore suggests that the 5% GO sample has greatest impulse performance due to a maximization of combustion completion [33].

A.6.2 Effect of nanothermites packing density

To describe the bulk density for powder samples, the theoretical maximum density (TMD) is defined as the theoretical density of the powdered materials if they could be combined into a single monolithic solid. Comparison between the measured sample density and TMD is expressed as a percentage, %TMD and calculated according to the following equation.

$$\% \text{ TMD} = \frac{\rho_{\text{measured}}}{\rho_{\text{calculated}}} \tag{4}$$

Here, $\rho_{measured}$ is the density of the nanothermite sample based on the corresponding sample mass and volume, whereas $\rho_{calculated}$ is the density calculated by the weighted average of the densities of each reactant in the composite [53]. Variation of I_{SP} with different TMD percentages for all GO/nanothermite samples is shown in Figure A7.

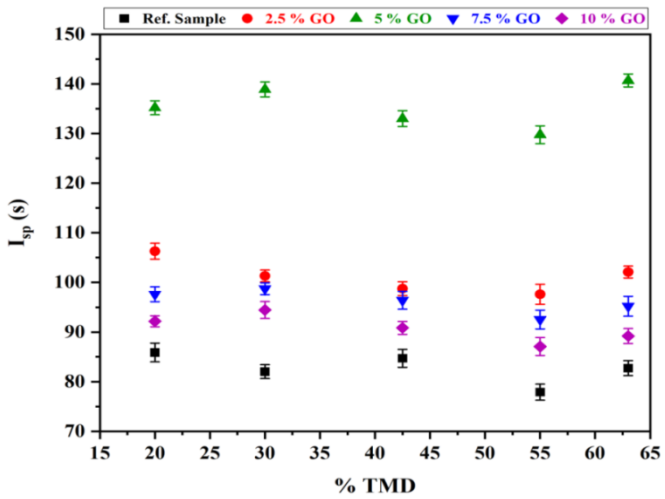

Figure A7 Specific impulse plotted against powdered sample density (%TMD) for Al/KClO4 based nanothermites

Figure A7 shows that the bulk density does not have a significant influence on I_{SP} and that no distinguishable correlation can be observed between the specific impulse and %TMD. The I_{SP} values for all GO/nanothermite composites indicate that mass-based thrust efficiency is almost constant at different packing densities. This finding agrees with other works that have studied the effects of packing pressure on specific impulse in energetic nanothermite mixtures [32].

More interestingly, two distinct reaction regimes were detected while varying the packing density as illustrated in Figure A8.

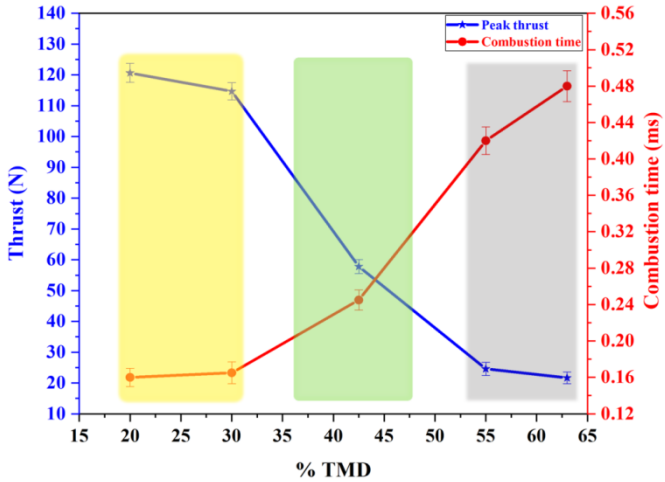

Figure A8 Peak thrust and combustion duration of 5% GO/Al/KClO4 with different %TMD showing fast reaction regime (yellow), transitional regime (green), and slow reaction regime (gray)

Figure A8 shows that low-density samples produced high peak thrust for short combustion durations whereas high-density samples produced low peak thrust but for long combustion times. In between the extremes, at 42.5%TMD, the sample thrust and combustion time were between high and low packing density results. It is apparent in Figure 8 that there are three distinct regimes: fast reaction regime at low packing density less than 32.5%TMD (yellow region), slow reaction regime at high packing density exceeding 55%TMD (gray region), and a transitional regime (green region) in between. It is likely that the low-density samples undergo supersonic combustion: supersonic combustion behaviour of low-density nanothermites has been observed in other studies using open-ended combustion tubes [37, 54]. So, fast reaction behaviour may be correlated to the rapid discharge of combustion products caused by reflected wave of the combustion front (supersonic combustion performance). Additionally, in open STMs combustion is controlled by convective heat transfer so, at low packing density, pores within the sample allow hot gas propagation into the fuel grain and thus heat transfer into the sample from the flame front via convection. Removing these pores by compressing thermite into a pellet (reducing volume but keeping constant mass) reduces the convective pathways, so the role of convective mechanisms on the flame propagation is reduced and conduction becomes dominant.

To observe the time-resolved thrust behaviour of samples in the slow reaction regime, thrust traces are plotted for Al-$KClO_4$ samples with varying GO quantities at 55%TMD in Figure A9.

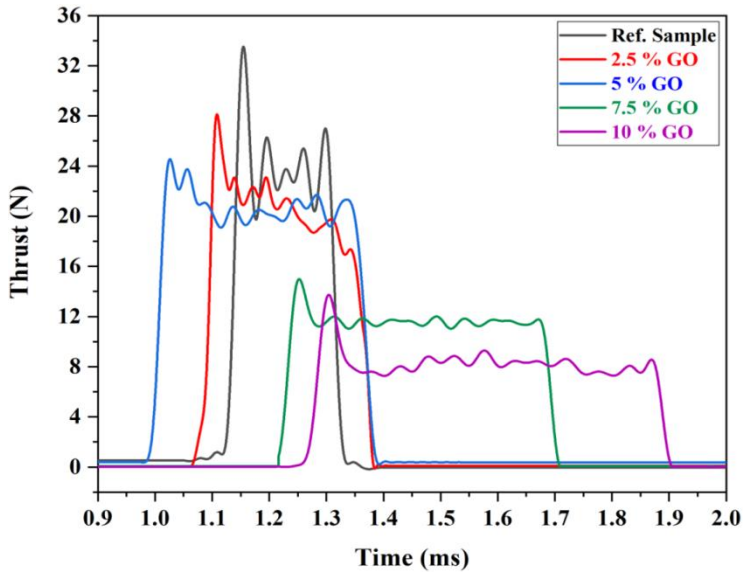

Figure A9 Thrust profiles for different GO/nanothermite samples at 55 %TMD

For combustion of highly porous media (low-density), unsteady reaction rates can lead to unstable energy release and gas production. However, in the slow reaction regime (high packing density), the behaviour is analogous to a stable burning stage of a typical propellant grain where thrust force and combustion rates are relatively constant throughout the combustion period, albeit over a very short period [55]. The shift in the flame propagation mode can be another possible explanation for the fast and slow reaction regimes observed in Figure A8 [56]. Combustion characteristics output from GO/nanothermites at slow regime (55%TMD) are summarized in Table A6.

Table A6 Combustion characteristics of nanothermite samples at 55 %TMD

Nanothermite composition	**Average thrust (N)**	**Combustion duration (ms)**	**Total impulse (mN.s)**	**Specific impulse (s)**	**Volumetric impulse ($mN.s/mm^3$)**
Al/ $KClO_4$	19.08 ± 1.47	0.24 ± 0.02	4.58 ± 0.16	77.89 ± 1.61	1.17 ± 0.06
2.5 % GO/Al/$KClO_4$	17.94 ± 0.81	0.32 ± 0.03	5.74 ± 0.21	97.62 ± 2.25	1.47 ± 0.11
5 % GO/Al/$KClO_4$	18.17 ± 0.74	0.42 ± 0.03	7.63 ± 0.27	129.76 ± 2.13	1.96 ± 0.14
7.5 % GO/Al/$KClO_4$	10.67 ± 0.68	0.51 ± 0.05	5.44 ± 0.14	92.52 ± 1.57	1.39 ± 0.09
10 % GO/Al/$KClO_4$	7.42 ± 0.52	0.69 ± 0.04	5.12 ± 0.18	87.07 ± 1.84	1.31 ± 0.10

A.6.3 Effect of convergent-divergent nozzle

Limited data is available for these nanothermite compositions in small scale test engines, so an STM with a generic converging-diverging (CD) nozzle, as shown in Figure A1(C) was used to evaluate the in-device performance of the prepared nanothermites. It is intended that the captured thrust data serves as a baseline for future propulsion system designs and refinements. Time resolved thrust-force data for different GO/nanothermite composites for slow and fast reaction regimes (20 and 55%TMD) in CD nozzle and no-nozzle STM configurations are presented in Figure A10 (A) and (B) respectively.

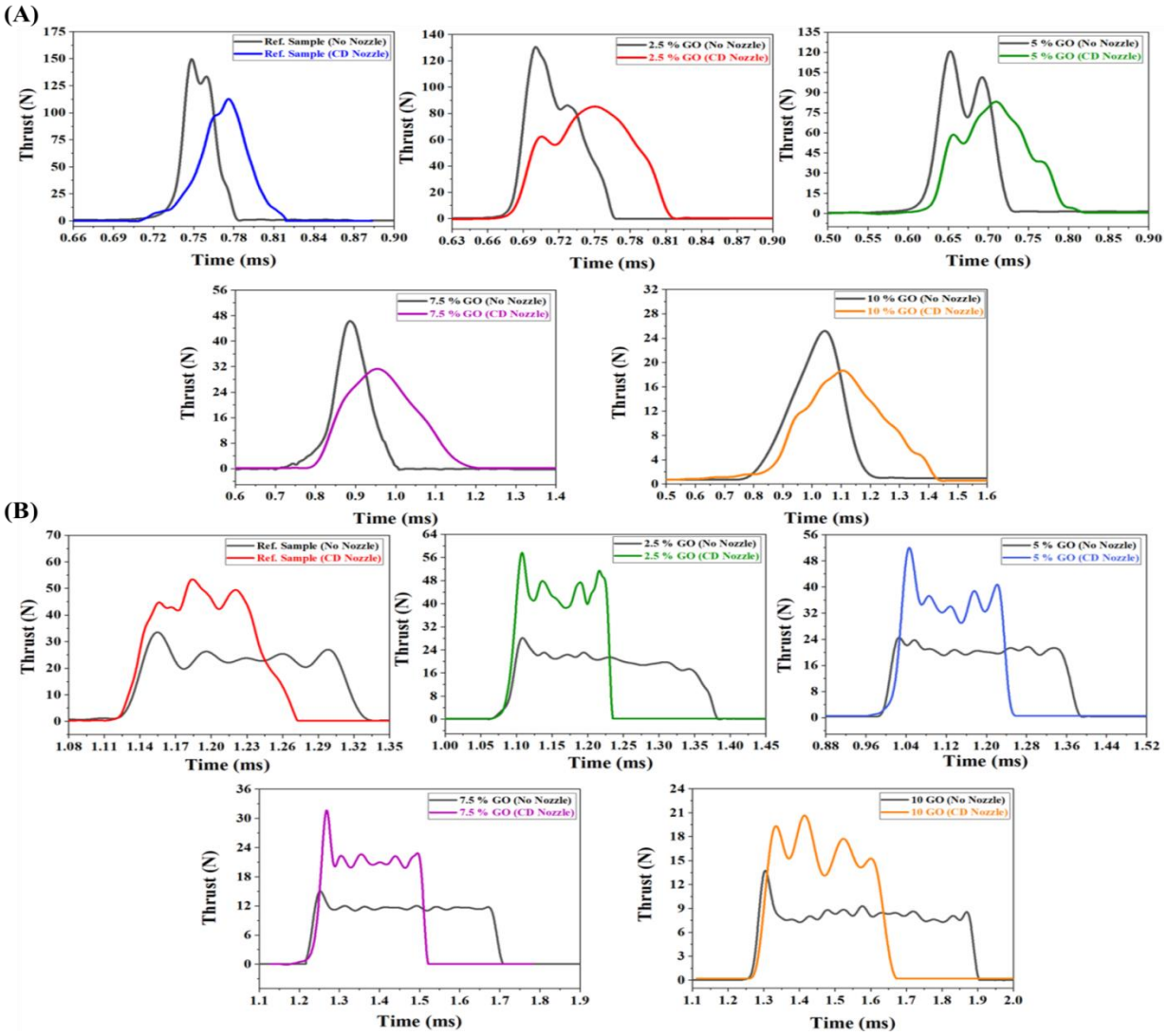

Figure A10 Thrust-time curves for different GO/nanothermite samples at (A) 20 %TMD (B) 55 %TMD with and without CD nozzle

Introducing a CD nozzle has an opposite effect on the performance of GO/nanothermite samples depending on the packing density. Comparison with open-tube configurations shows that the CD nozzle significantly increased the thrust amplitude and reduced the combustion duration for slow reaction regime samples (55%TMD); contrary effects were observed for all low-density (20%TMD) samples though to a lesser degree. To observe the quantitative effects of the CD nozzle, combustion characteristics of GO/nanocomposites within the CD nozzle STM at high and low packing densities are presented in Table A7.

Table A7 Thrust performance of GO/nanothermites within CD nozzle STM at 20 & 55 %TMD

Sample Composition	Average Thrust (N)	Combustion Duration (ms)	Total Impulse (mN.s)	Specific Impulse (s)	Volumetric Impulse (mN.s/mm^3)
Al/$KClO_4$	49.27 ± 3.17	0.11 ± 0.01	5.42 ± 0.18	92.18 ± 2.34	1.39 ± 0.11
	34.40 ± 2.54	0.15 ± 0.02	5.16 ± 0.10	87.76 ± 1.93	1.32 ± 0.09
2.5 % GO/Al/$KClO_4$	42.56 ± 2.73	0.16 ± 0.03	6.81 ± 0.21	115.82 ± 1.86	1.75 ± 0.14
	29.57 ± 1.31	0.21 ± 0.03	6.21 ± 0.19	105.61 ± 2.44	1.59 ± 0.13
5 % GO/Al/$KClO_4$	39.86 ± 1.68	0.22 ± 0.02	8.77 ± 0.15	149.15 ± 2.91	2.25 ± 0.21
	27.97 ± 0.67	0.29 ± 0.03	8.11 ± 0.28	137.93 ± 2.37	2.08 ± 0.19
7.5 % GO/Al/$KClO_4$	15.07 ± 0.84	0.42 ± 0.06	6.33 ± 0.23	107.65 ± 1.94	1.62 ± 0.17
	18.34 ± 1.21	0.32 ± 0.03	5.87 ± 0.15	99.83 ± 1.68	1.51 ± 0.15
10 % GO/Al/$KClO_4$	9.29 ± 0.68	0.65 ± 0.05	6.04 ± 0.13	102.72 ± 1.67	1.55 ± 0.12
	13.61 ± 0.78	0.41 ± 0.04	5.58 ± 0.11	94.90 ± 1.58	1.43 ± 0.12

* Orange and gray colors represent 20 and 55 % TMD respectively

The effect of a CD nozzle on the thruster performance is mixed, depending primarily on packing density. As can be seen in Figure 10 (A) and Table 7, peak thrust is reduced and combustion time increases for 20%TMD samples with the introduction of a CD nozzle. This trend is true for all low-density samples, regardless of GO content. For low packing density, the total, specific, and volumetric impulses are increased with the addition of the CD nozzle. This indicates a propulsion efficiency gain in the low-density samples, although performance is contrary to what is expected from a CD nozzle (reduced thrust, increased combustion duration). Meanwhile, the results in Figure A10 (B) show a trend that is expected for the addition of a CD nozzle (increased thrust, reduced duration), although unlike the low-density samples, the net effect is a reduced specific impulse compared to 55% samples in Table A6 and Table A7.

To investigate the effect of the CD nozzle at different packing densities, we need to consider the definition of thrust. Thrust is defined by equation (5) [57].

$$F = \dot{m}V_2 + (P_2 - P_{amb})A_2 \tag{5}$$

The first term is the momentum force, corresponding to product the gaseous mass flow rate ($\dot{m}$) and its exhaust velocity (V_2) relative to the STM. The second term represents the pressure thrust; it consists of the product of the cross-sectional area at the nozzle exit (A_2) and the difference between the exhaust gas pressure at the exit and the ambient fluid pressure ($P_2 - P_{amb}$) [57, 58]. Most nozzle designs aim to achieve fully expanded nozzle flow, so that the pressure at nozzle exit is equal to ambient pressure thereby making momentum force the dominant component of overall thrust.

In the slow reaction regime, the increase in thrust force is expected since the nozzle is implemented to convert energy from the combustion process into momentum force by increasing exhaust velocity. The reduction in combustion time is a result of increased burn rate due to geometric confinement of the solid propellant [37, 57]. A high-density sample in the open tube configuration burns without geometric acceleration of the exhaust, so the total thrust will have a larger pressure force component but the pressurization rate is low due to slow burn rate. However, when a low-density sample (fast reaction regime) is used in the open-tube configuration, the rapid burn rate should result in high pressurization and a large, rapid impulse of pressure-induced thrust. This form of combustion is not suited well to a nozzle-configuration engine.

The ideal nozzle, as stated by Sutton, assumes that combustible materials and reaction products are homogenous, combustion products are in gaseous state with adiabatic, steady, and continuous flow with no friction forces and neglected boundary effects. We can certainly say these conditions are not met with our sample behaviour. Due to the small dimensions of the STM used in this work, friction forces and boundary effects cannot be neglected [7, 37]. Also, low-density nanothermites can generate shock waves and so uniformity and continuity cannot be assumed with GO/nanothermites samples, especially as it is likely that a shock wave travels through the nozzle as combustion evolves [54, 59]. It can be seen from the force data in Figure A4 and Figure A10 (A) that the low-density sample never reaches a steady state, reducing the usefulness of the CD nozzle. For the low-density samples, where reaction rates are increased, the deviations from ideal conditions are likely amplified and so attenuation in thrust force in the fast reaction regime are expected within the CD nozzle STM.

The effect of GO on the ignition and flame evolution of oxygenated-salt nanothermite composites is presented in Figure A11, as obtained from high-speed imaging.

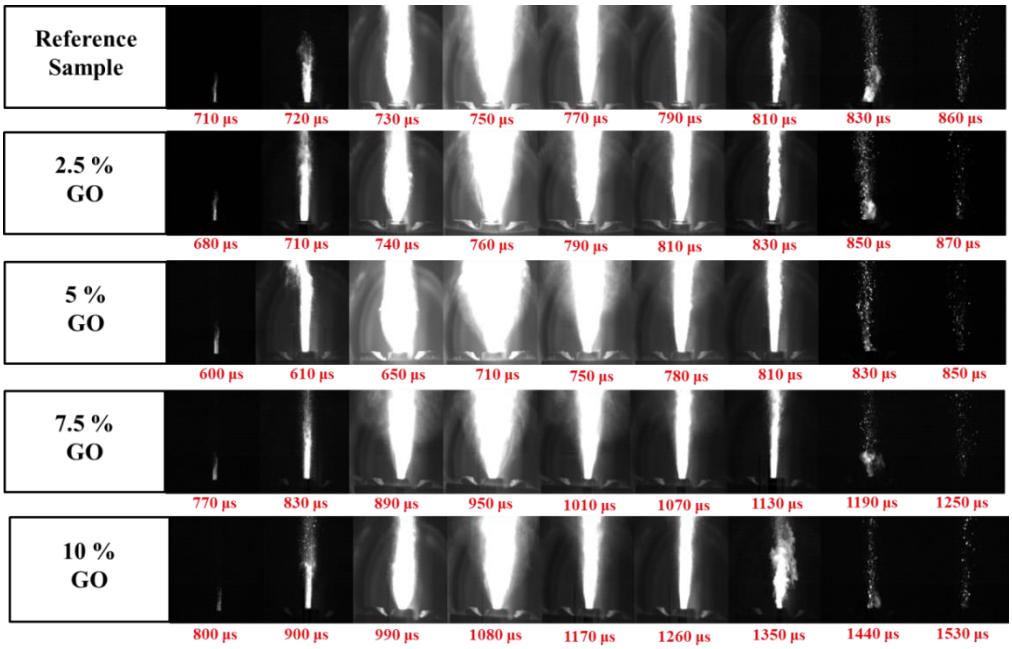

Figure A11 Snapshots of different GO/nanothermite composites in CD STM at 20 %TMD

All the prepared samples readily ignited by laser heating and sustained combustion. All samples were accompanied by bright flames (as seen in Figure A11) indicating high combustion capability [47, 60]. The images shown in Figure A11 support a trend first observed in Table 4; the improvement in nanothermite thrust performance with the addition of GO up to 5%. This trend is observed in Figure 11 as the 5% GO sample can be seen to have the largest plume at 720 µs. The enhancement of the GO/nanothermite sample is attributed to the energetic nature of GO and its ability to increase the intimate mixing between fuel and oxidizer through its cross-linked porous framework structure [47]. Further addition of GO shows a reduced plume size and intensity, as observed in Figure A11, once again supporting the observed trend in Table A7.

We can observe solid and liquid combustion products ejected within the exhaust plume in Figure A11, such as at 830µs for the 5% GO sample. Therefore, frictional force occurs between solid and liquid products and thruster walls introducing significant two phase losses [61]. Meanwhile, the CD nozzle likely moves the STMs away from ideal nozzle conditions. This is yet another possible contribution to the reduced thrust observed for low-density samples in Figure 10 and

Table 7 when used in the CD nozzle STM. Similarly, this is likely a contributing factor to the reduction of I_{sp} in high-density samples in Table A6.

The shape change of the flame from 80 to 200 is visible in the experimental images (730-810) shown in Figure A11. The exit speed of product gasses reached between 1800-2000 m/s which is double that of nanothermite based on metallic oxides, which recorded ~1000 m/s as previously reported in literature [62, 64]. This result supports the higher impulse of the prepared ternary nanothermite and highlights the advantage of using oxygenated salts as alternatives of metallic oxides in propulsion applications.

A.7 Revealing velocity and temperature fields by CFD modeling

The high-speed flow through the CD nozzle and resultant plume were modelled using CFD code. Three mass flow rates at the inlet of the CD nozzle were used: 61.55 mg/ms for the ICT calculated value, 42.41 mg/ms for the 20%TMD sample, and 30.37 mg/ms for the 55%TMD sample. Figure A12 shows the simulated profile of the Mach number magnitude within and above the CD nozzle, which is produced by the 20%TMD sample.

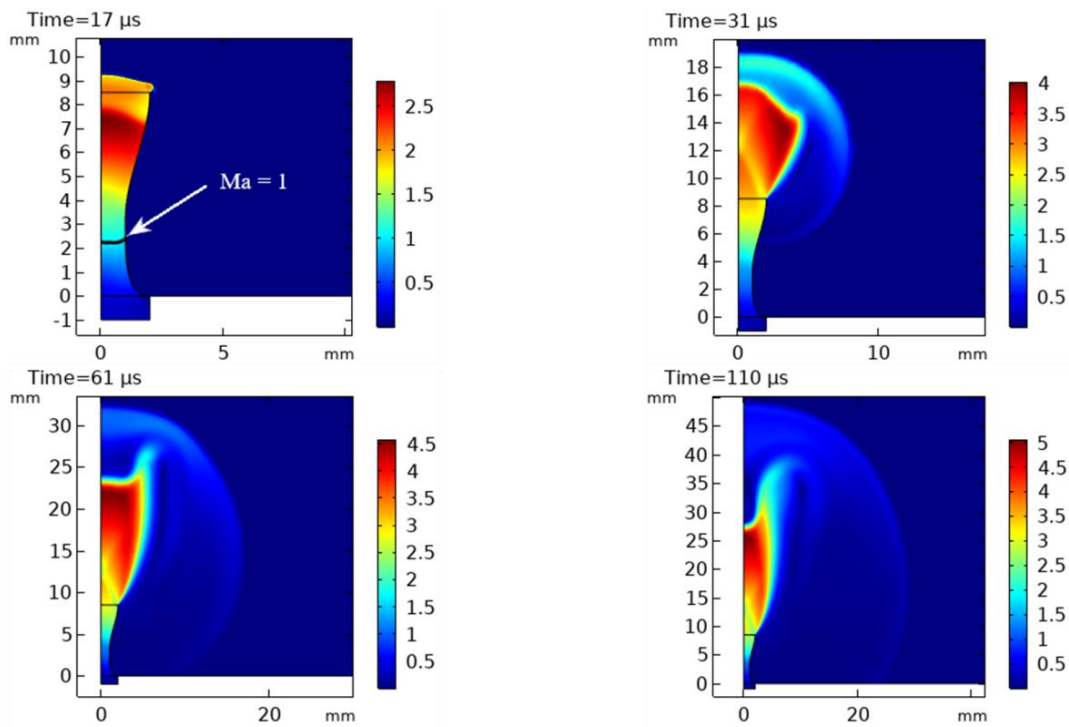

Figure A12 Velocity profile at different moments for the reference sample with 20 %TMD

Three key observations about the nozzle plume can be made in Figure 12. First, a sonic interface (Ma = 1) is formed at the throat of the CD nozzle as expected (17 μs profile), and its location remains unchanged during the simulation time. Secondly, the design of the CD nozzle is not optimal and thus leads to the formation of an under-expanded plume. So, for the environmental conditions used in testing, the thrust produced by this nozzle can be improved by increasing the degree of expansion at the outlet. Thirdly, transition of the plume shape is visible, analogous to the experimental results presented in Figure A11. At 17 μs, the high-speed flow reaches the nozzle outlet, accompanied with the rapid increase of the thrust. At 31 μs, the shape of the plume is bell-like, characterized by the maximum value at the center line of the nozzle. At 61 μs the shape of the plume evolves into an inversed-bell with the minimum value of the velocity magnitude existing at the center line. At 110 μs, the inversed-bell shape can be seen to transition into a typical jet-plume. Eventually the width of the plume in the radial direction decreases and leads to the extinction of the flame.

The temperature profiles of these high-speed flows were also simulated. Figure A13 shows the simulated profile of the temperature field within and above the CD nozzle, which is produced by the 20%TMD sample. While the peak temperature of the combustion exhaust remains about 3800K near the nozzle inlet, the plume temperature still reaches about 1500K to 2000K in all these images. The transition of the plume shape is clearly visible with increasing time, changing from a bell shape to an inverse bell, as observed in Figure A12.

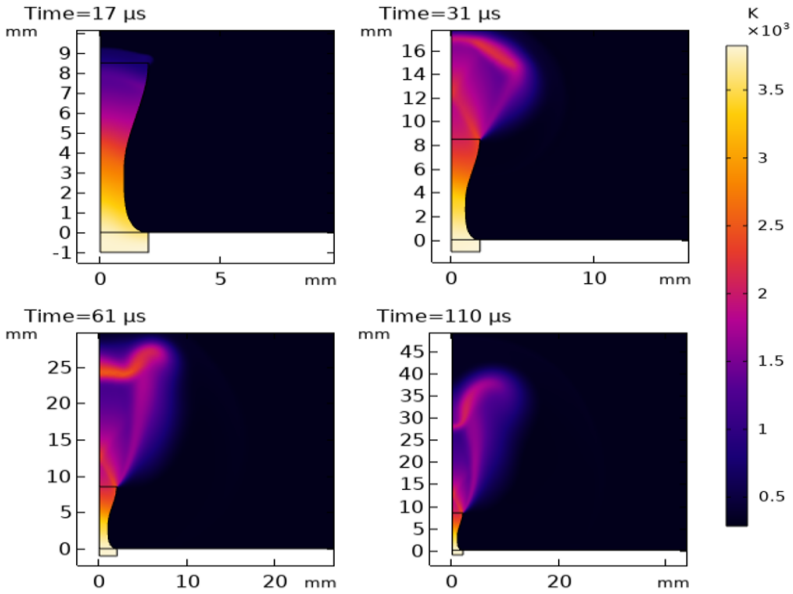

Figure A13 Temperature profile at different moments for the reference sample with 20 %TMD

Two mass flow rates at the inlet of the open tube were used to calculate the velocity and temperature fields: 42.41 mg/ms for the 20%TMD sample and 30.37 mg/ms for the 55%TMD sample. develops.

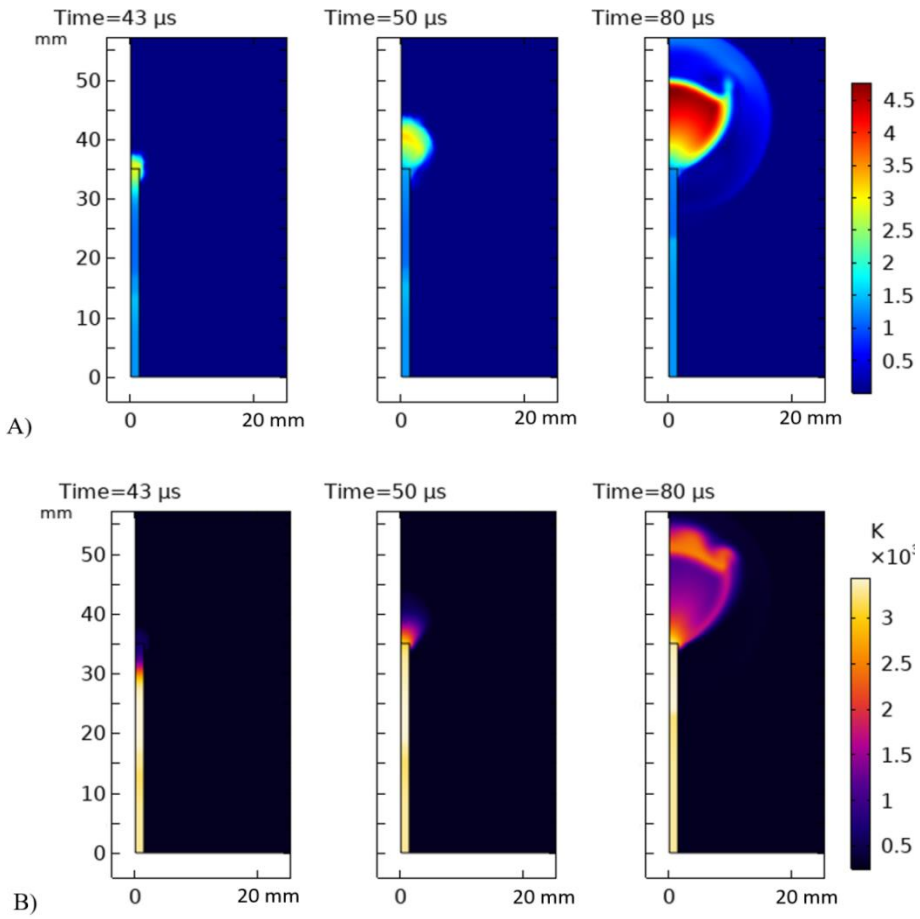

Figure A14 shows the simulated temperature and velocity profiles from the open tube for the reference sample with 20%TMD. Flow within the tube is supersonic throughout, but the Mach number at the tube outlet decreases substantially with time. When the flow first reaches the outlet at 43 μs, the Mach number at the outlet is 2.8. At 50 μs, the outlet Mach number drops to 1.4, and then to 1.3 as the plume evolves at 80 μs. These results suggest that momentum thrust should maximize when the flow first reaches the tube exit and stabilize as the exhaust plume develops.

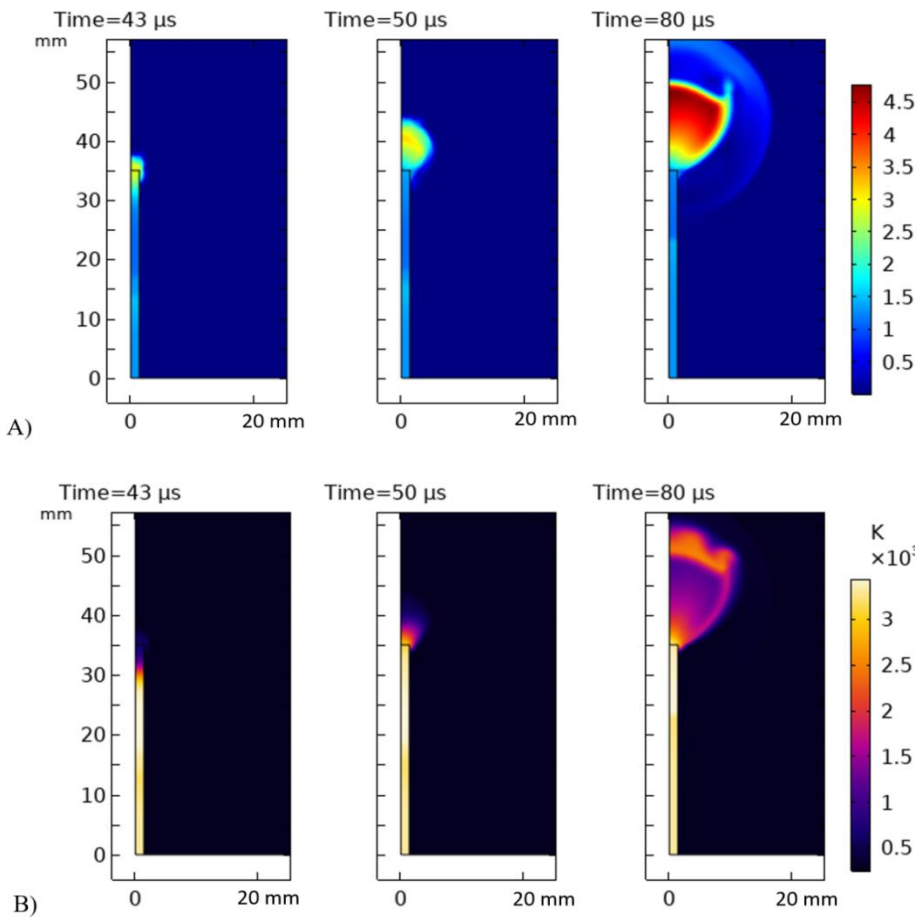

Figure A14 Temperature and velocity profiles of the plume from the open tube at different moments for the reference sample with 20 %TMD: a) - c): temperature; d) - f): velocity

By comparing the numerical results for the open-tube and CD cases we can see that the Mach number at the outlet is generally higher for the CD case throughout. Temperature at the outlet is lower in the CD case than in the open-tube case. These observations suggest that pressure forces contribute to thrust production in the open tube case more than in the CD case. Performing a force balance at the nozzle outlet, the momentum and pressure forces are summed throughout the simulation time to obtain force profiles for the given simulation cases as shown in Figure A15.

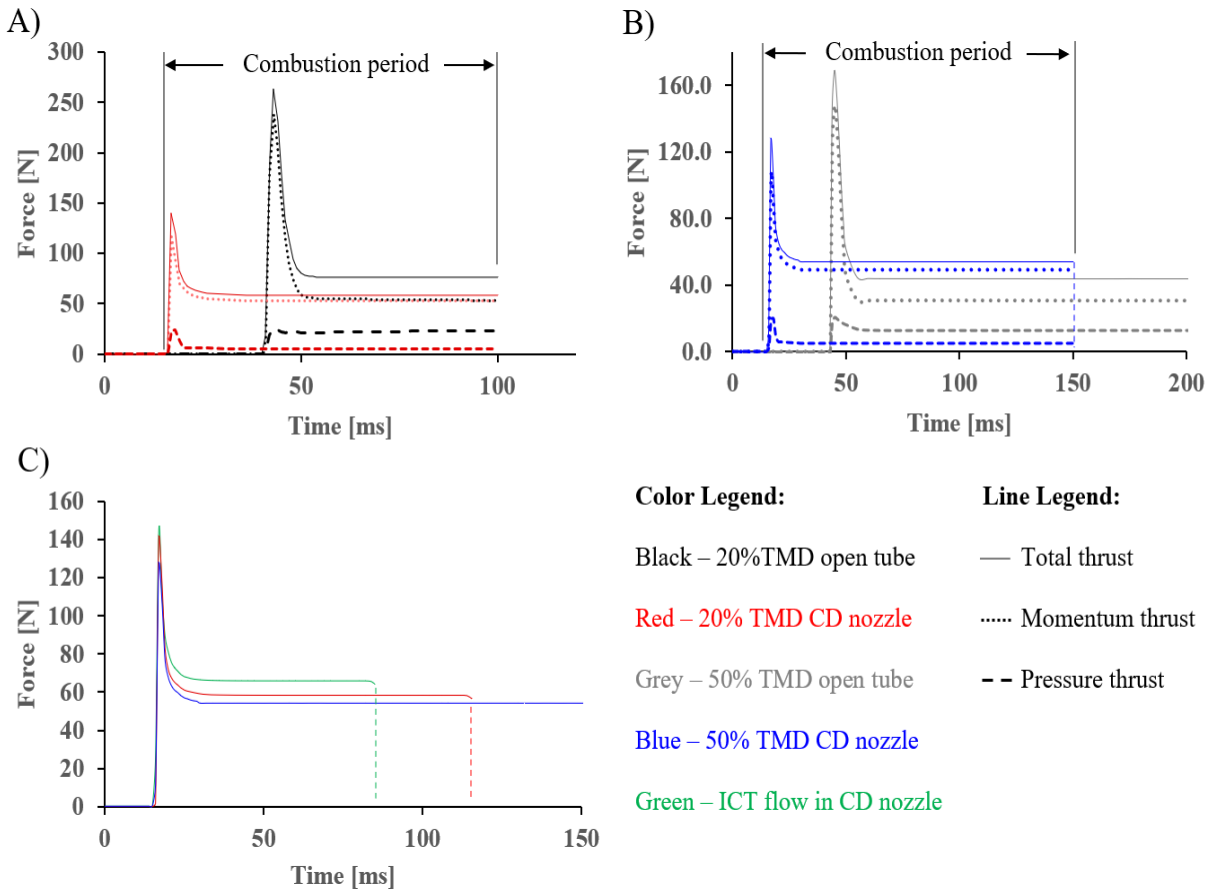

Figure A15 Simulated thrust-time profiles of the Al/KClO4 nanothermite (reference) sample with different nozzle geometries: A) 20%TMD; B) 55%TMD and C): the CD nozzle with varying TMDs

All profiles in Figure A15 show the same characteristic shape with a large peak followed by a period of steady force. In both 20 and 50%TMD cases, the open tube test showed greater delay in force production because the length of the open tube is greater than that of the CD nozzle, as can be seen in Figure A1. The momentum component of thrust dominates in the CD cases shown in Figure A15 (A) and Figure A15 (B), whereas pressure force contribution remains substantial in the open tube tests. This result is expected, as the CD nozzle is implemented specifically to convert heat and pressure into thrust. The results also suggest that, regardless of packing density, pressure force in the open-tube case makes up 25-30% of thrust, and that the peak force observed is produced mostly by momentum force.

The force is generally over-predicted in the model when compared to experimental results, but there is agreement in magnitude. Like the experimental results shown in Figure A11, the open

tube cases seen in Figure A15 (A) and Figure A15 (B) generate higher peak forces than the CD nozzle cases. In the 20%TMD case, the steady-state force output is greater in the open tube configuration; the opposite is true for the 50%TMD case. This observation agrees with the experimental data presented for 55%TMD samples in Figure A10 (B), where the quasi-steady force is increased with the addition of a CD nozzle. The similarity between experimental and numerical results for the high-density (~50%TMD) cases also extends to the magnitude of steady-state forces as well as general profile shape, albeit experimental results do not show the same peaks that are observed in the model. These similarities are not observed with the low-density (~20%TMD) cases, since there is no steady force production in the experimental results seen in Figure A10 (A). This is likely a limitation of the idealized assumptions used to model the flow domain and mass-flow due to combustion.

Considering only the CD nozzle case shown in Figure A15 (C), it is seen that the highest forces are produced when mass flow is maximised; mass flow increases with decreasing %TMD. This agrees with the results presented in Table A7, where average force is higher for 20%TMD samples. This suggests that the nozzle is not mass-flow choked and, for the given nozzle geometry, packing density should be minimized if output force is to be maximized.

The simulation supports the experimental investigations for the 20%TMD, open-tube reference ($Al/KClO_4$) sample with results of 86.3 N, 0.06 ms, 5.2 mN.s, 105.6 s, and 0.38 mN.s/mm^3 for average thrust, combustion time, I_{FT}, I_{SP} and I_{SV} respectively. These results agree with the experiments within approximately 25 % error. So, the model can be used with an understanding of its limitations for further investigation of the important physical characteristics of the developed ternary nanothermites. This will subsequently help develop engineering applications for these new composites.

A.8 Conclusion

In this study, we have examined the effect of CNMs on the laser ignition and thrust performance of various types of oxygenated-salts/nanothermite mixtures and demonstrated non-metallic oxidisers as good alternative energetic oxidants for thermite mixtures with high combustion performance. CNMs were successfully integrated on nanothermite compositions using a simple ultrasonic mixing method. Prepared nanothermites were ignited in both an open tube and a CD nozzle STM at different packing densities to assess the practicality of these mixtures for

propulsion applications. All prepared nanothermites ignited successfully and combusted self-sufficiently inside the STMs. The CNMs, especially GO, were shown to be capable of improving sample combustion performance. Compared to the reference sample, significant improvements in I_{FT}, I_{SP}, I_{SV}, and reduction in ignition delay were observed with the addition of up to 5% GO. The improved combustion properties of the GO/Al/$KClO_4$ compositions are proposed to be resultant of the catalytic nature of GO in facilitating uniform mixing of n-Al and $KClO_4$, in addition to its effect as an energetic reactant acting as a secondary fuel and adding energy to the system. Additionally, two different reaction regimes (fast and slow) are recognized as result of the sample packing density. The introduction of a CD nozzle is shown to have two opposing effects on thrust output in fast and slow reaction regimes where it reduces thrust output but increased impulse in fast regime samples but increases thrust and reduced impulse in slow regime samples. Deviations from ideal nozzle design conditions suggest that a nozzle may hinder performance in fast reaction regimes. This study shows that energetic composites with tailored and controlled thrust performance can be developed via CNMs/n-Al/oxygenated-salt nanothermites and enables development of more focussed future propulsion applications.

A.9 References

[1] S.H. Kim, M.R. Zachariah, Enhancing the rate of energy release from nanoenergetic materials by electrostatically enhanced assembly, Adv. Mater. 16 (2004) 1821-1825.

[2] M.L. Pantoya, J.J. Granier, Combustion behavior of highly energetic thermites: Nano versus micron composites, Propellants Explos. Pyrotech. 30 (2005) 53-62.

[3] E.L. Dreizin, Metal-based reactive nanomaterials, Prog. Energy Combust. Sci. 35 (2009) 141-167.

[4] C.S. Jian, K. Sullivan, Nanothermite reactions: Is gas phase oxygen generation from the oxygen carrier an essential prerequisite to ignition? Combust. Flame 160 (2013) 432-437.

[5] K.S. Wu, S. Chowdhury, G. Jian, L. Zhou, M.R. Zachariah, Encapsulation of perchlorate salts within metal oxides for application as nanoenergetic oxidizers, Adv. Funct. Mater. 22 (2012) 78-85.

[6] K.S. Kappagantula, C. Farley, M.L. Pantoya, J. Horn, Tuning energetic material reactivity using surface functionalization of aluminum fuels, J. Phys. Chem. C. 116 (2012) 24469–24475.

[7] S.F. Son, B.W. Asay, T.J. Foley, R.A. Yetter, M.H. Wu, G.A. Risha, Combustion of nanoscale Al/MoO_3 thermite in microchannels, J. Propuls. Power 23 (2007) 715-721.

[8] M. Comet, C. Martin, F. Schnell, D. Spitzer, Nanothermites: a short review. Factsheet for experimenters, present and future challenges, Propellants Explos. Pyrotech. 44 (2019) 18-36.

[9] W. Zhou, J.B. Delisio, X. Li, L. Liu, M.R. Zachariah, Persulfate salt as an oxidizer for biocidal energetic nano-thermites, J. Mater. Chem. 3 (2015) 11838–11846.

[10] G. Jian, J. Feng, R.J. Jacob, G.C Egan, M.R. Zachariah, Super-reactive nanoenergetic gas generators based on periodate salts, Angew. Chem. Int. 52 (2013) 9743-9746.

[11] Y.R. Luo, Comprehensive handbook of chemical bond energies. Boca Raton, Florida: 25 CRC Press, 2007.

[12] N.B. Stand, B.D. Darwent, Bond dissociation energies in simple molecules, Nat. Stand. Ref. Data Ser.,U.S.A, 1970, pp. 1-60.

[13] K-C. Huang, R.A. Couttenye, G.E. Hoag, Kinetics of heat-assisted persulfate oxidation of methyl tert-butyl ether (MTBE), Chemosphere, 49 (2002) 413-420.

[14] A. Tsitonaki, P. Petri, M. Crimi, H. MosbÆk, R.L. Siegrist, P.L. Bjerg, In Situ Chemical Oxidation of Contaminated Soil and Groundwater Using Persulfate: A Review, Environ. Sci. Technol. 40 (2010) 55-91.

[15] A. Fahd, S. Elbasuney, H.E. Mostafa, Combustion characteristics of extruded double base propellant based on ammonium perchlorate/aluminum binary mixture, Fuel 208 (2017) 296–304.

[16] A. Fahd, S. Elbasuney, H.E. Mostafa, Certain ballistic performance and thermal properties evaluation for extruded modified double-base propellants, Cent Eur J Energetic Mater 14 (2017) 296-304.

[17] M. Kabganian, M. Nabipour, F.F. Saberi, Design and implementation of attitude control algorithm of a satellite on a three-axis gimbal simulator, J Aerosp Eng. 229 (2015) 72–86.

[18] G. Mazoni, Y.L. Brama, Cubesat micropropulsion characterization in low earth orbit, Proceedings 29th annual AIAA/USU Conference on small satellites, 2015.

[19] J. Dai, F. Wang, C. Ru, J. Xu, C. Wang, W. Zhang, Y. Ye, R. Shen, Ammonium perchlorate as an effective additive for enhancing the combustion and propulsion performance of Al/CuO nanothermites," J. Phys. Chem. C 122 (2018) 10240−10247.

[20] P. Zhu , G. Hou, H. Wang, C. Xu, S. Zhao, R. Shen, Design, preparation, and performance of a planar ignitor inserted with pyroMEMS safe and arm device," J Microelectromech Syst. 27 (2018) 1186-1192.

[21] A. Nicollet, L. Salvagnac, V. Baijot, A. Estève, C. Rossi, Fast circuit breaker based on integration of Al/CuO nanothermites," Sens. Actuators, A 273 (2018) 249–255.

[22] A.A. Balandin, S. Ghosh, W.Z. Bao, I. Calizo, D. Teweldebrhan, F. Miao, C.N. Lau, Superior thermal conductivity of single layer graphene, Nano Lett. 8 (2008) 902–907.

[23] K.S. Novoselov, A. K. Geim, S.V. Morozov, D. Jiang, M.I. Katsnelson, I.V.Grigorieva, S.V. Dubonos, A.A. Firsov, Two-dimensional gas of massless diracfermions in graphene, Nature 438 (2005) 197–200.

[24] S. Stankovich, D.A. Dikin, G.H.B. Dommett, K.M. Kohlhaas, E.J. Zimney, E.A.Stach, R.D. Piner, S.T. Nguyen, R.S. Ruoff, Graphene based composite materials, Nature 442 (2006) 282–286.

[25] C. Lee, X. Wei, J.W. Kysar, J. Hone, Measurement of the elastic properties andintrinsic strength of monolayer graphene, Science 321 (2008) 385–388.

[26] Qi-L. Yan, M. Gozin, F-Qi. Zhao, A. Cohena, Si-P. Pang, Highly energetic compositions based on functionalized carbon nanomaterials, Nanoscale 8 (2016) 4799–4851.

[27] A.C. Ferrari, V. Fal'ko, et al., Science and technology roadmap for graphene, related two-dimensional crystals, and hybrid systems, Nanoscale 7 (2015) 4598–4810.

[28] S. Romero-Diez, J.M. Pearl, D.L. Hitt, M.R. McDevitt, P.C. Lee, A single-use microthruster concept for small satellite attitude control in formation-flying applications, Aerospace 119 (2018) 1-18.

[29] S.W. Jackson, Design of an air-breathing electric thruster for cubeSat applications, Master of Science, Department of Aerospace Engineering Science, University of Colorado, 2017.

[30] Z. Bo, X. Shuai, S. Mao, H. Yang, J. Qian, J. Chen, J. Yan, K. Cen, Green preparation of reduced grapheneoxide for sensing and energy storage applications, Sci. Rep. 4 (2014) 1-7.

[31] A. Fahd, C. Dubois, Jamal Chaouki, J.Z. Wen, E. Youssef, Synthesis and Characterization of Tertiary Nanothermite CNMs/Al/$KClO_4$ with Enhanced Combustion Characteristics, Propellants Explos. Pyrotech. 46 (2021) 995-1005

[32] A. Fahd, A. Baranovsky, C. Dubois, J. Chaouki, J. Wen, Superior performance of quaternary NC/GO/Al/$KClO_4$ nanothermite for high speed impulse small-scale propulsion applications, Combust. Flame (2021).

[33] C.G. Parigger, A.C. Woods, M.J. Witte, L.D. Swafford, D.M. Surmick, Measurement and analysis of atomic hydrogen and diatomic molecular AlO, C_2, CN, and TiO spectra following laser-induced optical breakdown, J. Vis. Exp. 84 (2014) 51250-51258.

[34] COMSOL Multiphysics® v. 5.6. www.comsol.com. COMSOL AB, Stockholm, Sweden.

[35] H. Bathelt, F. Volk, The ICT-Thermodynamic Code (ICT-Code),Proceddings 27th International Annual Conference of ICT, Fraunhofer-Institut für Chemische Technologie (ICT), Pfinztal/Berghausen, Germany (1996).

[36] S. Kelzenberg, P.B. Kempa, S. Wurster, M. Herrmann, T.S. Fischer, New version of the ICT-Thermodynamic Code, in energetic materials. Particles, Processing, Applications, Proceddings 45th International Annual Conference of ICT, Fraunhofer-Institut für Chemische Technologie (ICT), Pfinztal, Karlsruhe, Germany, (2014) 95.1–95.9.

[37] S.J. Apperson, A.V. Bezmelnitsyn, R. Thiruvengadathan, K. Gangopadhyay, S. Gangopadhyay, W.A. Balas, P.E. Anderson, S.M. Nicolich, Characterization of nanothermite material fors solid-fuel microthruster applications, J. Propuls. Power 25 (2009) 1-6.

[38] C.S. Staley, R. Thiruvengadathan, S.J. Apperson, K. Gangopadhyay, S.M. Swaszek, P. Arsenal, R.J. Taylor, S. Charles, S. Gangopadhyay, Fast-impulse nanothermite solid-propellant miniaturized thrusters, J. Propuls. Power 29 (2013)1400-1409.

[39] L. Pauling, General Chemistry, Dover Books on Chemistry, Courier Corporation, North Chelmsford, USA, 2014.

[40] P. Liu, T. Wang, Ultrasonic-assisted chemical oxidative cutting of multiwalled carbon nanotubes with ammonium persulfate in neutral media, Appl Phys A. 97 (2009) 771–775.

[41] W. Zhou, J.B. Delisio, X. Wang, M.R. Zachariah, Reaction mechanisms of potassium oxysalts based energetic composites, Combust. Flame 177 (2017) 1–9.

[42] N. Li, Z. Geng, M. Cao, L. Ren, X. Zhao, B. Liu, Y. Tian, C. Hu, Well dispersed ultrafine Mn_3O_4 nanoparticles on graphene as a promising catalys tfor the thermal decomposition of ammonium perchlorate, Carbon 54 (2013) 124–132.

[43] A. Dey, J. Athar, P. Varma, H. Prasant, A.K. Sikder, S. Chattopadhya, Graphene-iron oxide nanocomposite (GINC): an efficient catalyst forammonium perchlorate (AP) decomposition and burn rate enhancer for APbased composite propellant, RSC Adv. 5 (2015) 1950–1960.

[44] N. Yan, L. Qin, H. Hao, L. Hui, F. Zhao, H. Feng, Iron oxide/aluminum/graphene energetic nanocomposites synthesized by atomic layer deposition: Enhanced energy release and reduced electrostatic ignition hazard, Appl. Surf. Sci. 408 (2017) 51-59.

[45] R.Thiruvengadathan, S.W. Chung, S. Basuray, B. Balasubramanian, C. S. Staley, K. Gangopadhyay, S. Gangopadhyay, A Versatile Self-Assembly Approach toward High Performance Nanoenergetic Composite Using Functionalized Graphene, Langmuir 30 (2014) 6556−6564.

[46] N.W. Piekiel, K.T. Sullivan, S. Chowdhury, M.R. Zachariah, The role of metal oxides in nanothermite reactions: Evidence of condensed phase initiation, DTIC Document, 2010.

[47] C. Liu , X. Li, R. Li, Q. Yang, H. Zhang, B. Yang, G. Yang, Laser ignited combustion of graphene oxide/nitrocellulose membranes for solid propellant micro thruster and solar water distillation, Carbon 166 (2020) 138-147.

[48] J.L. Gottfried, E. J. Bukowski, Laser-shocked energetic materials with metal additives: Evaluation of chemistry and detonation performance, Appl. Opt. 56 (2017) B47−B57.

[49] Y. Jiang, S. Deng, S. Hong, J. Zhao, S. Huang, C.C. Wu, J.L. Gottfried, K. Nomura, Y. Li, S. Tiwari, R.K. Kalia, P. Vashishta, A. Nakano, X. Zhen, Energetic performance of optically activated aluminum/graphene oxide composites, ACS Nano 12 (2018) 11366-11375.

[50] Y. Jiang, S. Deng, S. Hong, S. Tiwari, H. Chen, K. Nomura, R.K. Kalia, A. Nakano, P. Vashishta, M.R. Zachariah, X. Zheng, Synergistically chemical and thermal coupling between graphene oxide and graphene fluoride for enhancing aluminum combustion, ACS Appl Mater Interfaces 12 (2020) 7451-7458.

[51] B. Asay, S. Son, J.R. Busse, D. Oschwald, Ignition characteristics of metastable intermolecular composites, Propellants Explos. Pyrotech. 29 (2004) 216–219.

[52] V. Baijot, M.D. Rouhani, C. Rossi, A. Estève, Effect of temperature and O_2 pressure on the gaseous speciesproduced during combustion of aluminum, Chem. Phys. Lett. 649 (2016) 88–91.

[53] M.L. Pantoya, J.J. Granier, J.B. Henderson, Effect of bulk density on reaction propagation in nanothermites and micron thermites, J. Propuls. Power 25 (2009) 465-470.

[54] C.J. Bulian, S. Smith, J.A. Puszynski, Experimental and modeling studies of self-sustaining reactions nbtween nanopowders," In 2006 AIChE Annual Meeting (AIChE Annual Meeting, Conference Proceedings), San Francisco, CA, United States, 2006.

[55] G.P. Sutton, Definitions and Fundamentals, In: Rocket propulsion elements, Wiley, New York, USA, 1986, pp. 27-45.

[56] D. Prentice, M. Pantoya, A. Gash, Combustion wave speeds of sol−gel-synthesized tungsten trioxide and nano-aluminum: the effect of impurities on flame propagation, Energy & Fuels 20 (2006) 2370-2376.

[57] G.P. Sutton, Chemical rocket propellant performance analysis. In: Rocket propulsion elements, Wiley, New York, USA, 1986, pp. 160-197.

[58] A. Fahd, Fabrication and Characterization of Advanced Double Base Solid Rocket Propellant, PhD Paper based thesis, Chemical Engineering Department, Military Technical College, Cairo, Egypt, 2016.

[59] D. Prentice, M. Pantoya, A. Gash, Combustion wave speeds of sol−gel-synthesized tungsten trioxide and nano-aluminum: the effect of impurities on flame propagation, Energy & Fuels 20 (2006) 2370-2376.

[60] Ji Dai, J. Xu, F. Wang, Y. Tai, Y. Shen, R. Shen, Y. Ye, Facile formation of nitrocellulose-coated Al/Bi_2O_3 nanothermites with excellent energy output and improved electrostatic discharge safety, Mater. Des. 143 (2018) 93–103.

[61] Y.M. Timnat, Advanced chemical rocket propulsion, Academic Press Inc., Orlando, Florida, USA, 1987.

[62] M.R.Weismiller, J.Y. Malchi, R.A.Yetter, T.J.Foley, Dependence of flame propagation on pressure and pressurizing gas for an Al/CuO nanoscale thermite, Proc Combust Inst. 32 (2009) 1895-1903.

[63] J.J. Granier , M.L. Pantoya, Laser ignition of nanocomposite thermites, Combust. Flame 138 (2004) 373–383.

[64] V.E. Sanders, B.W. Asay, T.J. Foley, B.C. Tappan, A.N. Pacheco, S.F. Son, Reaction propagation of four nanoscale energetic composites (Al/MoO_3, Al/WO_3, Al/CuO, and Bi_2O_3), J. Propul. Power 23 (2007) 707–714.